Project No. 11-3023

Self-Sustaining Thorium Boiling Water Reactors

Reactor Concepts

Dr. Ehud Greenspan
University of California-Berkeley

In collaboration with:
Massachusetts Institute of Technology
University of Michigan
Brookhaven National Laboratory

Brian Robinson, Federal POC
Temitope Taiwo, Technical POC

NEUP Nuclear Energy University Programs
U.S. Department of Energy

NEUP Project # 11-3023

September 2011 to December 2014

Self-sustaining thorium boiling water reactors

Summary Report

Ehud Greenspan, Phillip M. Gorman, Sandra Bogetic, Jeffrey E. Seifried, Guanheng Zhang, Christopher R. Varela, Massimiliano Fratoni and Jasmina L. Vujic
UC Berkeley, gehud@nuc.berkeley.edu
Thomas Downar, Andrew Hall, Andrew Ward, Michael Jarrett, Aaron Wysocki and Yunlin Xu
University of Michigan, downar@umich.edu
Mujid Kazimi, Koroush Shirvan and Alexander Mieloszyk
MIT, kazimi@MIT.EDU
Michael Todosow, Nicholas Brown and Lap Cheng
BNL, todosowm@bnl.gov

28 February 2015

Table of Contents

Executive Summary

The primary objectives of this project are to:

- Perform a pre-conceptual design of a core for an alternative to the Hitachi proposed fuel-self-sustaining RBWR-AC, to be referred to as a RBWR-Th. The use of thorium fuel is expected to assure negative void coefficient of reactivity (versus positive of the RBWR-AC) and improve reactor safety.
- Perform a pre-conceptual design of an alternative core to the Hitachi proposed LWR TRU transmuting RBWR-TB2, to be referred to as the RBWR-TR. In addition to improved safety, use of thorium for the fertile fuel is expected to improve the TRU transmutation effectiveness.
- Compare the RBWR-Th and RBWR-TR performance against that of the Hitachi RBWR core designs and sodium cooled fast reactor counterparts – the ARR and ABR.
- Perform a viability assessment of the thorium-based RBWR design concepts to be identified along with their associated fuel cycle, a technology gap analysis, and a technology development roadmap.

A description of the work performed and of the results obtained is provided in this Overview Report and, in more detail, in the Attachments. The major findings of the study are summarized below:

RBWR-Th

- It is not possible to design a self-sustaining thorium-fueled RBWR core (RBWR-Th) to have an acceptable shutdown margin without significant degradation in the core performance. This is due to the large negative void coefficient of reactivity of such a core.
- By adding 25% to 35% depleted uranium to the thorium feed fuel it is possible to reduce the RBWR-Th negative void coefficient of reactivity to a desirable level and achieve an adequate shutdown margin. This also improves stability. Thus, it is possible to design RBWR cores to be fuel-self-sustaining using ~70% thorium (Th) and ~30% depleted uranium (DU) feed fuel with all trans-fertile isotopes recycled unlimited number of times. The coolant void reactivity coefficient can be optimized by adjusting the feed DU/Th ratio.
- Due to limited relevant experimental data available, there is a very large uncertainty in the correlations for predicting the coolant void fraction and the critical power. The thermal-hydraulic correlations used by Hitachi for designing their RBWR cores differ significantly from the correlations we arrived at (MIT recommended correlations) by re-evaluating the limited available experimental data.
- The optimal fuel-self-sustaining RBWR-Th core design strongly depends on the thermal-hydraulic correlations used. Using the most conservative MIT recommended correlations the RBWR-Th, core power needs be down-rated to ~80% of the ABWR's and its HM inventory is undesirably large. No power down-rating is required when using the Hitachi assumed correlations. The following conclusions that refer to the fuel-self-sustaining RBWR-Th pertain to the design based on the T-H correlations used by Hitachi.

- The peak cladding temperature (PCT) of the RBWR-Th design with Hitachi correlations during an all pump trip accident – that is expected to be one of the most limiting design basis accidents, is lower than of an ABWR, mainly due to the significantly lower peak LHGR of the RBWR-Th. The RBWR-AC features a higher PCT than an ABWR.
- Potential issues regarding unstable behavior of the RBWR-Th core design with Hitachi correlations during transients need be investigated more carefully.
- Under Chapter 15 licensing safety analysis the RBWR-Th with HITACHI used correlation is expected to perform better or similar in all categories compared to an ABWR.
- The attainable burnup may be limited by fuel performance more than by the neutronics. The constraining phenomenon identified is hydrogen pickup by the Zircaloy-2 cladding that at high fast neutron fluences induced by the harder neutron spectrum experiences an acceleration in corrosion and hydrogen pickup and, hence, cladding embrittlement rates. It may be possible to alleviate the hydrogen pickup by using improved cladding material such as Ziron -- a high iron low nickel zirconium alloy under development by GNF. Maintaining the fuel integrity of the RBWR-AC core is even more challenging due to its significantly higher LHGR.

RBWR-TR

- It is possible to design RBWR cores to transmute TRU from LWR UNF (RBWR-TR) using thorium as the fertile fuel. No depleted uranium need be added to the thorium feed fuel (as was the case for the RBWR-Th). The "Fission Efficiency" of the optimal design is close to 50%; that is, approximately half of the core fissions are fissions of TRU; the rest are fissions of primarily ^{233}U.
- The optimal RBWR-TR design features nearly 3 times the coolant mass flow rate and, therefore nearly 1/3 exit quality than the RBWR-TB2 Hitachi counterpart. Both cores feature significantly larger P/D ratio than their fuel-self-sustaining RBWR cores. As a result the RBWR-TR design is not subjected to as large uncertainties in the thermal-hydraulic correlations as the other RBWR cores; a single set of correlations was used for the RBWR-TR core design.
- The peak cladding temperature (PCT) during an all pump trip accident – that is expected to be one of the most limiting design basis accidents, is lower than of an ABWR, mainly due to the significantly lower peak LHGR of the RBWR-TR. The RBWR-TB2 resulted in PCT higher than an ABWR.
- The RBWR-TR burner design exhibited higher levels of stability compared to the ABWR and its stability performance is expected to be satisfactory. This is not the case for the RBWR-TB2.
- Under Chapter 15 licensing safety analysis the RBWR-TR is expected to perform better or similar in all categories compared to an ABWR.
- The attainable burnup may be limited by fuel performance more than by neutronics. The constraining phenomena are hydrogen pickup by the Zircaloy-2 cladding that at high fast neutron fluences induced by the harder neutron spectrum experiences an acceleration in corrosion and hydrogen pickup and, hence, cladding embrittlement rates. It may be possible to alleviate the

hydrogen pickup by using improved cladding material such as Ziron -- a high iron low nickel zirconium alloy under development by GNF.

Additional comparison vs Hitachi RBWR core designs

- Relative to Hitachi RBWR-AC, the RBWR-Th core design based on the T-H correlations used by Hitachi is simpler and features larger safety margins. The RBWR-Th core does not need an internal blanket, its seed is longer, its peak LHGR is smaller and its axial distribution is smoother and more stable with burnup, and no absorber is loaded in the upper reflector.
- Likewise for the RBWR-TR versus the Hitachi RBWR-TB2 core designs.
- Relative to Hitachi RBWR-TB2[1], the RBWR-TR core features nearly 3 times the coolant mass flow rate and, therefore nearly 1/3 exit quality and softer seed neutron spectrum; ~20% higher HM loading; ~20% lower average and less than 50% peak burnup; less than half peak linear heat generation rate; ~20% higher TRU incineration per GWeY; slightly higher fuel cycle cost; slightly higher activity of the waste streams; approximately 40% plutonium recycling; similar fissile plutonium fraction and nearly twice ^{238}Pu fraction and specific decay heat in the Pu in the discharged fuel. On the other hand, the RBWR-Th discharged fuel contains also significant amounts of ^{233}U; the ^{233}U/U ratio in the recycled fuel is ~15%.

Comparison vs SFR core designs

- Relative to the ARR, the fuel self-sustaining RBWR-Th core designed using the T-H correlations used by Hitachi features less than half the core power density and specific power; ~70% of the discharge burnup and ~70% higher rate of HM reprocessing and TRF discharge per unit of electricity generated; their discharged plutonium contains a somewhat smaller fraction of fissile isotopes and more than 4 times ^{238}Pu fraction; nearly 4 times Pu specific decay heat; and higher radioactivity and radiotoxicity of the waste streams.
- Compared to the reference CR=0.5 metal-fuelled ABR, the RBWR-TR burns slightly more TRU from LWR UNF per unit of electricity generated but, similarly to the RBWR-TB2, has roughly one third of the discharge burnup, power density, and specific power. It requires a larger reprocessing capacity, but can operate in longer cycles with a comparable reactivity swing.
- Relative to the reference ABR and RBWR-TB2 designs, the fuel discharged from the RBWR-TR core contains significantly less Pu of significantly smaller fissile fraction and significantly higher ^{238}Pu fraction. However, the RBWR-TR also discharges significant amount of U over 60% of which is fissile.
- Due, primarily, to their lower average discharged burnup, the fuel cycle cost of all RBWRs will be higher than that of the SFR of comparable conversion ratio, but the capital cost of the RBWRs is expected to be lower and their technology is more mature and mostly familiar to the nuclear industry and NRC.

[1] Hitachi is now in the process of redesigning their RBWR-TB2 core design as our project team indicated to them that it features a too low margin on critical power and too high peak burnup and fast neutron fluence for their fuel to survive. The comparison with the RBWR-TR core will, most likely, have to be revised.

Technical gaps

- The uncertainties in the thermal-hydraulic correlations for predicting the void fraction distribution and the critical power in the RBWR cores are too large. New experiments need be planned, executed and analyzed before RBWR cores could be reliably designed and licensed.
- The fast neutron fluence the RBWR fuel will be exposed to is significantly higher than of typical BWR cores. Improved cladding materials need be developed and certified for use in RBWR core conditions. The RBWR fuel need also undergo irradiation experiments up to somewhat above the peak design burnup before this fuel could be licensed.
- The design of the RBWR fuel assemblies and control rods greatly differs from that of standard BWR and these fuel assemblies are subjected to highly different coolant flow conditions. Integral testing of complete fuel assemblies and control rods is required. Such experiments should also establish the axial variation of the water density in the bypass channels between the fuel assemblies.
- Commercial thorium-based fuel reprocessing and recycling capability will have to be developed.
- The economic viability of the RBWRs need be thoroughly compared against that of the SFR counterparts that are design to perform the same functions. This comparison need to include capital and O&M costs in addition to investment in required R&D towards commercialization.

Additional accomplishments of the project

- Development of the following new computational capabilities:
    - An improved 3-D core simulator – SERPENT/PARCS/PATHS – that can accurately account for strong axial heterogeneity. This is advancing state-of-art – it is the first code system to enable 3-D cross section generation that is required for accurate capture of axial heterogeneities and axial leakage.
    - An effective Monte-Carlo based assembly level equilibrium search capability – MocDown – MCNP5.1/ORIGEN2.2/PATHS. MocDown is particularly useful for tradeoff studies and search for promising fuel assemblies designs as it uses problem-independent cross sections and accurately accounts for all spatial heterogeneities while consistently accounting for the coupling between the neutronics, depletion, and thermal-hydraulics.
    - Fuel performance analysis capability for thoria-based fuel rods that accounts for the special operating conditions of RBWR cores – notably tertiary fuel thermal conductivity model (e.g. Th, U, Pu oxides). The fuel performance capability has been extended to cover the high fluence of high energy neutrons all RBWR core structural materials are exposed to.
- A total of 20 researchers, mostly students and postdoctoral scholars, participated in this project. The students acquired valuable experience from this highly multidisciplinary project.
- A total of 22 papers were published in Journals and Conference Proceedings. See list following the list of references to this Overview paper.

- A special session about the RBWR technology was organized at the ICAPP-2014. It consisted of 1 paper from Hitachi, one paper from Cambridge (UK), and 5 papers from our project.

1. Introduction

This report summarizes the R&D performed from September 2011 through 2014 related to the design and analysis of a number of Reduced moderation Boiling Water Reactor (RBWR) cores. The work was performed by a team consisting of research groups from the University of California, Berkeley; University of Michigan, Ann Arbor; MIT and BNL. It has been funded by the NEUP contract NEUP 11-3023 – "Self-sustaining thorium boiling water reactors".

The primary objective of the NEUP 11-3023 project was to evaluate the feasibility of improving the design and performance of a couple of RBWR cores proposed by Hitachi by feeding them with thorium as the primary fertile fuel instead of the depleted uranium used by Hitachi. The Hitachi designed cores used as the reference for this project are [1-3]: (1) the RBWR-AC – a fuel-self-sustaining core design, and the RBWR-TB2 – a burner core for LWR TRU. Hitachi designed these cores to fit within the ABWR pressure vessel and is suggesting these cores to perform functions traditionally assigned to Sodium cooled Fast Reactors (SFR) – breeding and transmutation.

This Overview paper is structured as follows: Section 2 describes the Hitachi RBWR-AC and RBWR-TB2 core designs and discusses the rationale for moving from depleted uranium to thorium for the primary fertile fuel. Section 3 briefly describes the computational methods developed or improved for this project and their verification. A detailed account of the methods developed can be found in the 1st, 2nd, 3rd and 4th Attachments. Section 4 and 5 summarize the feasibility of designing, respectively, the fuel-self-sustaining RBWR-Th cores and the TRU transmuting RBWR-TR cores and describes the optimal core preliminary designs arrived at. Details about the designs and analyses are provided in the 5th and 6th Attachments. The 7th Attachment presents information, beyond that provided in Attachments 5 and 6, about the safety and stability of the thorium-based RBWR cores in comparison with the reference Hitachi designed RBWR cores. Comparisons of the performance and fuel cycle characteristics of the different RBWR core designs against those of their sodium cooled counterparts and of the Hitachi RBWR designs are summarized in Section 7 and detailed in the 8th Attachment. Section 8 provides a brief assessment of the technology maturity of the RBWR and their fuel cycle and a suggested roadmap for their development. Details are given in the 9th Attachment. Section 9 summarizes the findings, conclusions and accomplishments of the NEUP RBWR projects.

2. The RBWR cores

2.1. Hitachi designs

Hitachi is proposing the reduced moderation BWR, to which it refers as the Resource-renewable BWR (RBWR), for achieving the same functions traditionally assigned to Sodium-cooled Fast Reactors (SFR) – either fuel sustainability or transmutation of trans-uranium (TRU) elements from LWR Used Nuclear Fuel (UNF) – using the more mature BWR technologies [1-3]. These functions are achieved by designing the cores to have a significantly harder neutron spectrum than conventional BWR cores; that is, to have

reduced moderation. All the Hitachi RBWR core designs use fuel assemblies of same transverse dimensions and can fit within the Advanced BWR (ABWR) pressure vessel. They are designed to recycle their fuel unlimited number of times. The RBWR core design and performance characteristics addressed in this and the Attachments pertain to the equilibrium core composition that is reached after a large enough number of fuel recycles. Of the several RBWR cores designed by Hitachi [1-3] we have focused on two: the RBWR-AC and the RBWR-TB2. Presented below is only a brief summary of the Hitachi core design and performance. Details can be found in References 3 and 5. The value of all the performance characteristics reported in this section are those reported by Hitachi.

The RBWR-AC is a break-even core designed to burn depleted uranium by maintaining a net TRU Inventory Ratio of 1.0. It is the RBWR counterpart of the ARR – The Advanced sodium cooled Recycling Reactor. The RBWR-TB2 core is designed to transmute TRU from LWR UNF. Its makeup fuel is TRU from LWR UNF and depleted uranium. All the actinides discharged from its core are recycled back (excluding recycling losses). The RBWR-TB2 is the counterpart of the ABR – The Advanced sodium cooled Burner Reactor.

Fig. 1 shows the reactor pressure vessel (RPV) of the RBWR. The common plant specifications of the RBWR and the latest commercial BWR, the ABWR, are listed in Table 1. The rated thermal power, electric power, pressure vessel diameter and core pressure are identical for both reactor plants. Fig. 2 shows a horizontal cross-sectional view of the RBWR core configuration. The RBWR core is composed of 720 hexagonal fuel assemblies (or bundles) and 223 Y-type control rods. These differ greatly in shape (as well as intra-assembly and axial dimensions) from the square shape assemblies and cross shape control rods of the ABWR. The axial layout of the Hitachi RBWR cores is of a parfait shape -- an internal blanket of depleted uranium oxide is placed between an upper and lower short seed sections that are loaded with the TRU oxides. Depleted uranium oxide blanket sections are located also between the seed sections and the axial reflectors.

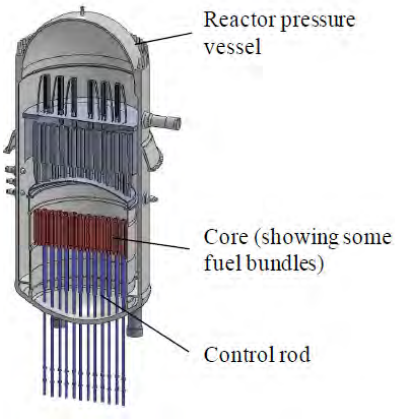

Figure 1 RBWR reactor vessel layout [3]

Item	RBWR	ABWR
Thermal power (MWt)	3926	3926
Electric power (MWe)	1356	1356
RPV diameter (m)	7.1	7.1
Core pressure (MPa)	7.2	7.2
Number of fuel bundles	720	872
Fuel lattice type	Hexagonal	Square
Lattice pitch (mm)	199	155
Number of control rods	223	205
Control rod type	Y-type	Cruciform

Table 1 RBWR vs ABWR plant characteristics [3]

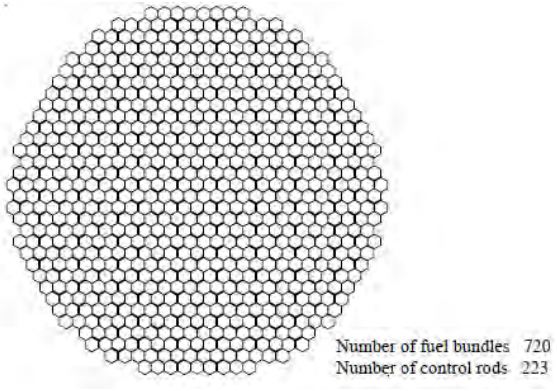

Figure 2 RBWR core layout; horizontal [3]

2.1.1. RBWR-AC

The axial fuel bundle configuration of the RBWR-AC is shown in Fig. 3. In this parfait-like core, a 52 cm long internal blanket is in between 19.3 cm lower and 28 cm upper fissile zones, and lower and upper blankets are 28 cm and 7 cm long. This very uncommon axial segregation of seed and blanket fuel was dictated by the requirement to achieve negative void reactivity coefficient; it enhances the negative contribution of neutron leakage to the void reactivity effect to the extent required to compensate for the large positive contribution of spectrum hardening to the void reactivity effect. An additional design feature used by Hitachi to enhance the axial neutron leakage probability upon coolant voiding is the placement of an absorber zone in the upper and lower reflectors. The upper neutron absorber zone is composed of B_4C pellets in sealed tubes, 7.7 mm in outer diameter, located between the fuel rod plenums. Each upper neutron absorber rod is 50 cm long and the distance between the upper end of the fuel zone and the lower end of the neutron absorber rod is 30 cm. The lower neutron absorber zone is composed of B_4C pellets inside the fuel cladding. The length of the lower neutron absorber zone is 7 cm.

Figure 4 shows a horizontal cross-sectional view of the RBWR-AC fuel bundle and its fissile Pu enrichment radial distribution. The fuel bundle lattice pitch is 19.92 cm on the sides with control blade and 19.47 cm on the side without it. The channel box of the fuel bundle is hexagonal with an inner width of 18.91 cm and wall thickness is 2.4 mm. The blade is 6.5 mm thick and the gap between the blade outer surface and the bundle channel box is 1.6 mm on each side. The gap between channel boxes on the side without the control blades is 0.8 mm. The fuel rod gap and pitch are 1.3 and 11.4 mm, respectively. Both the upper and lower fissile zones utilize five different fissile Pu concentrations aimed at minimizing the pin-wise power peaking. The bundle-average fissile plutonium enrichment is 15.7 wt% for the upper fissile zone (Fig. 4 (a)) and 20.1 wt% for the lower fissile zone (Fig. 4 (b)). The axial enrichment variation is intended to shape the axial power to meet the thermal-hydraulic constraints and provide negative void coefficient of reactivity.

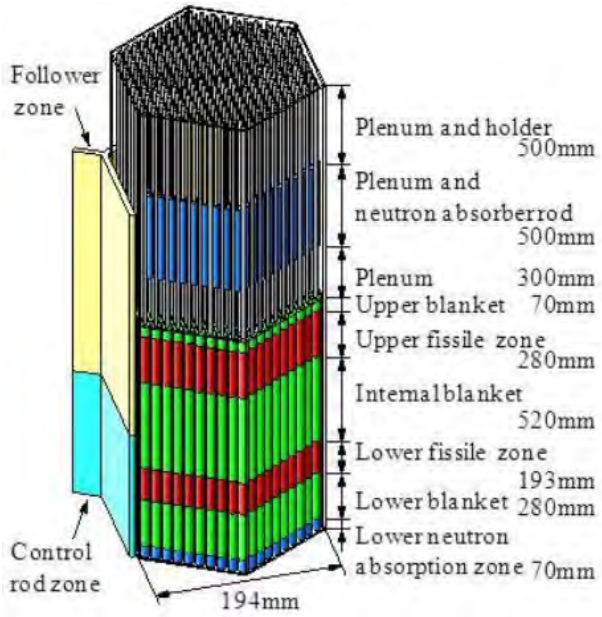

Figure 3 Isometric view of the RBWR-AC fuel bundle and control blade [3]

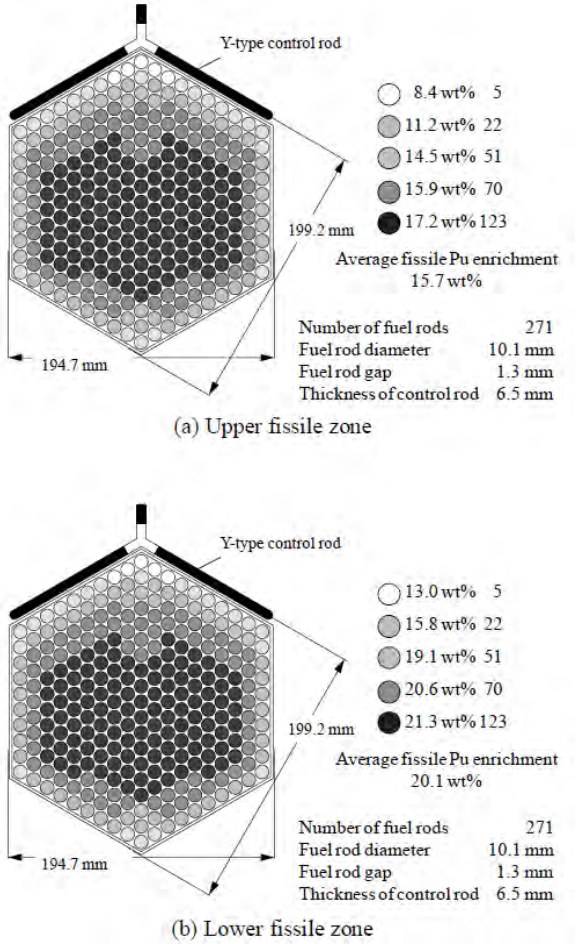

Figure 4 Radial arrangement of the RBWR-AC fuel pins [3]

Selected design and performance characteristics of the RBWR-AC equilibrium core are summarized in Table 1. The coolant flow rate is 2.6×10^4 t/h at a sub-cooling temperature of 5 K at the entrance and has a steam quality of 35 % at the core exit. The void fraction of core coolant is about 30 % at the bottom of the lower fissile zone due to heating in the lower blanket. It reaches 80 % at the top of the core. Figure 5 compares the void fraction axial variation with that of the ABWR. A breeding ratio of 1.01 is achievable with a core average burnup of 45 GWd/t. The peak burnup is more than double the average. The core radial power peaking factor is about 1.25 and the axial power peaking factor is about 1.8 including the blanket zones. Hitachi is estimating that the maximum linear heat generating rate of this core is 47 kW/m;[2] a minimum critical power ratio of 1.3; and a void reactivity coefficient of - 2.4×10^{-4} $\Delta k/k/\%$void.

[2] Recent analysis by the University of Michigan collaborators came up with a peak LHGR of 75 kW/m

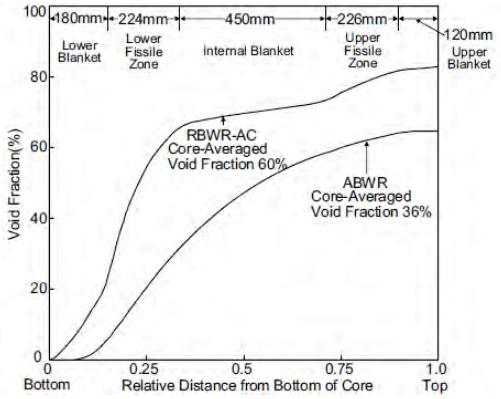

Figure 5. Void fraction axial distribution in the RBWR-AC (not updated design) versus the ABWR [2]

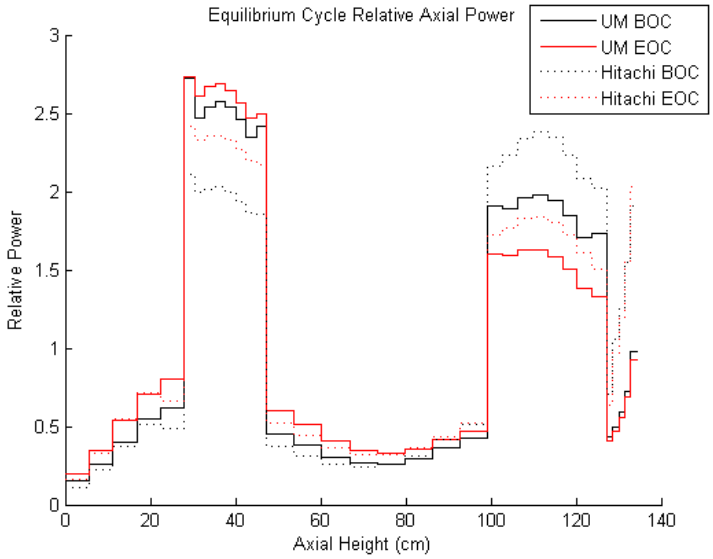

Figure 6. RBWR-AC axial power profile as calculated by UM and by Hitachi.

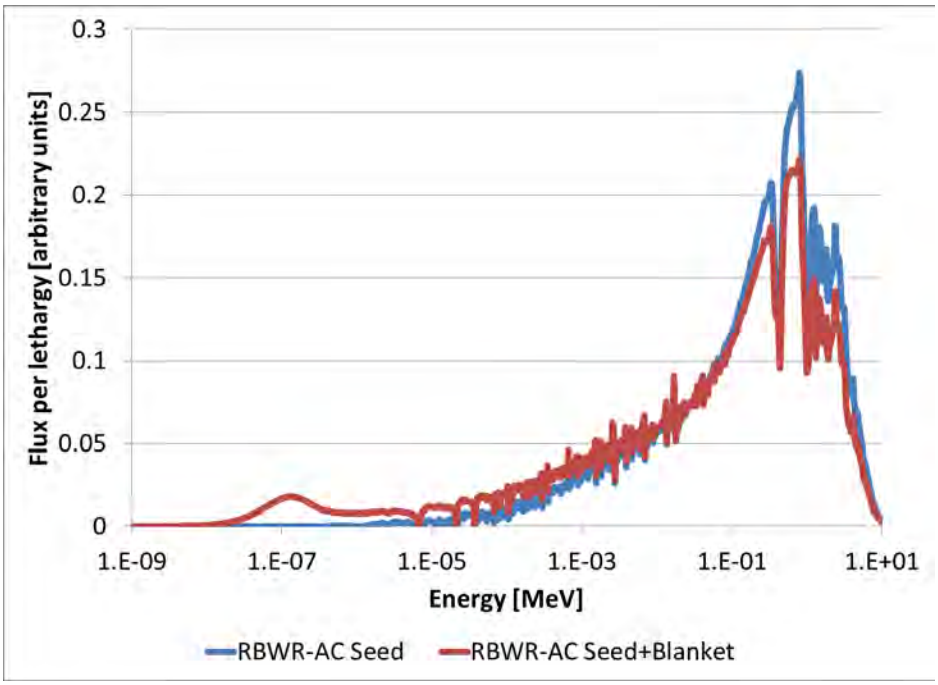

Figure 7. RBWR-AC flux spectrum for a fresh fuel assembly.

Table 2 Selected Design and Performance Characteristics of the RBWR-AC and RBWR-TB2 [3] Versus the ABWR

Item	ABWR	RBWR-AC	RBWR-TB2
Core height (mm)	3810	1343	1025
Fuel rod diameter (mm)	10.3	10.1	7.2
Fuel rod pitch (mm)	12.95	11.4	9.4
Fuel rod gap (mm)	0.082*	1.3	2.2
Pellet diameter (mm)	8.82	8.7	6.0
Number of fuel rods	92	271	397
Coolant flow rate (t/h)	$5.22 \cdot 10^4$	$2.6 \cdot 10^4$	$2.4 \cdot 10^4$
Core exit quality (%)	14.5	35	36
Void fraction (%)		53	56
Pressure drop (MPa)	0.25	0.14	0.06
HM inventory (t)		144	76
Puf/HM in fissile zone (wt%)	-	15.7/20.1	25
Burnup (GWd/t)	50	45	65
MLHGR (kW/m)	44	47[3]	47
MCPR	1.3	1.28	1.28
Void reactivity coefficient (Δk/k/%void)		$-2.4 \cdot 10^{-4}$	$-4 \cdot 10^{-4}$
Breeding ratio	-	1.01	-
TRU fission efficiency (%)	22	-	45

*assumed same as PWR

[3] Recent analysis by the University of Michigan collaborators came up with a peak LHGR of 75 kW/m and 55 KW/m for, respectively, the RBWR-AC and RBWR-TB2

2.1.2. RBWR-TB2

The RBWR-TB2 is designed to burn TRU from LWR spent fuel during the period in which LWR are being operated as base load power plants. It is the RBWR counterpart to the sodium cooled Advanced Burner Reactors (ABR) extensively examined in the US [6] and in other countries for the same purpose. The layout of the RBWR-TB2 fuel bundles, including axial reflectors and absorbers, is shown in Figs. 6 and 7. The length of the upper and lower fissile zones is, respectively, 22.4 and 22.1 cm. The length of the upper and central blanket zones, made of depleted uranium oxide, is 2 and 56 cm, respectively. The RBWR-TB2 does not have a lower blanket because breeding of fissile plutonium is to be minimized in order to maximize the TRU transmutation effectiveness. Although breeding significant amount of plutonium, the central blanket must be incorporated in order to achieve negative void coefficient of reactivity.

The RBWR-TB2 also has neutron absorber zones above and below the active core. The upper neutron absorber zone has the same structure as that of the RBWR-AC. The number of neutron absorber rods in the lower neutron absorber zone is 19; it was determined so as to keep the void reactivity coefficient negative.

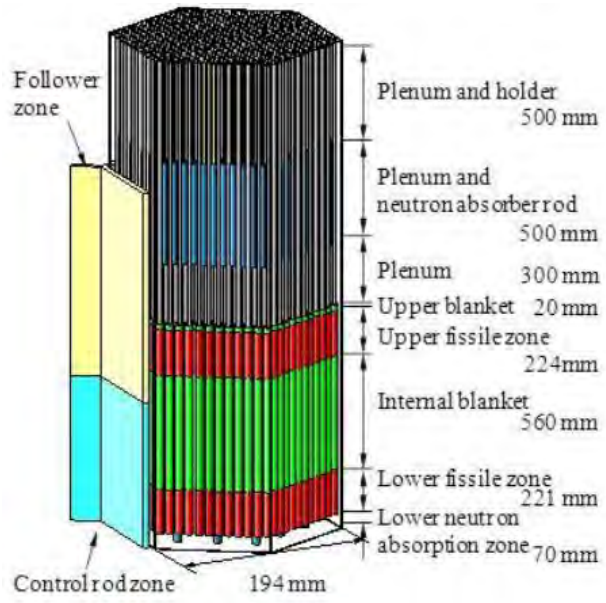

Figure 8. Isometric view of the RBWR-TB2 fuel bundle and control blade [3]

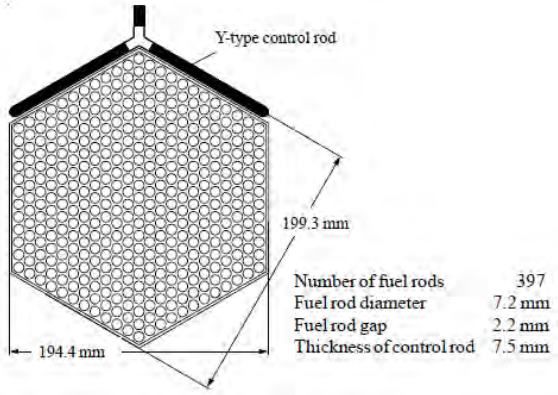

Figure 9. Radial arrangement of the RBWR-TB2 fuel pins [3]

The fuel bundle of the RBWR-TB2 is composed of uniform fissile plutonium enrichment of 25 wt%. The lattice pitch of the fuel bundles is 19.93 cm on the side with the control rod and 19.44 cm on the side without it. The channel box of the fuel bundle is hexagonal with an inner width of 18.96 cm and its

thickness is 2 mm. The control rod is 7.5 mm thick and the gap between the rod outer surface and the channel box is 1.6 mm on each side. The gap between channel boxes on the side without the control rod is 0.8 mm. Geometries of the channel boxes and the control rods are slightly different from those of the RBWR-AC. However, since the center positions of the control rods are same in the RBWR-AC and RBWR-TB2, both cores can fit within the same reactor pressure vessel.

The fuel rod diameter and gap of the RBWR-TB2 are 7.2 mm and 2.2 mm, respectively; these values result in a larger moderator to fuel volume ratio and a softer neutron energy spectrum than those of the RBWR-AC.

The main RBWR-TB2 equilibrium core specifications and performance characteristics are summarized in Table 2. The core coolant flow is 2.4×10^4 t/h at a sub-cooling of 10 K at the entrance and has a steam quality of 36 % at the core exit. The loading pattern of fuel bundles in the equilibrium core is similar to that of the RBWR-AC. The maximum linear heat generation rate is 47[4] kW/m and the MCPR is estimate to be 1.28. The void reactivity coefficient is estimated to be -4×10^{-4} Δk/k/%void.

The fission efficiency of TRU in the RBWR-TB2 is 45 %. Hitachi defines the "fission efficiency" as the fraction of the total number of fissions throughout the fuel residence time that is due to the TRU initially loaded; the rest of the fissions are of the TRU bred in the TB2 and with a small contribution from direct fissions of the depleted uranium. This value corresponds to about twice the production efficiency of TRUs, 22 %, in the ABWR. Hitachi defines the production efficiency of TRU as the net increase in TRU divided by the total amount of fissioned actinides through the fuel residence time in the core. Since the electricity output of the RBWR-TB2 is the same as that of the ABWR, this means that a single RBWR-TB2 can get rid of (i.e., fission) all the TRU that will accumulate in a couple of ABWRs of same power; that is, the support ratio of the RBWR-TB2 is 2.

2.2. Independent evaluation of the Hitachi designs

In 2007 the Electric Power Research Institute (EPRI) organized a team from three universities – University of Michigan (Ann Arbor), University of California (Berkeley) and MIT, to perform an independent evaluation of the Hitachi RBWR core designs and performance. The first phase of this work, performed from May 2007 through December 2007, had a limited scope and was based on design specifications and analysis results provided by Hitachi to EPRI. The second phase - from August 2008 through September 2009, involved a more detailed analysis of the RBWR–TB2 and RBWR–AC. The RBWR designs were then updated by Hitachi and EPRI was requested to conduct a more complete "Phase III" evaluation. The methodology used for this evaluation and the obtained results are provided in the Phase III summary report [5]. Following are excerpts from the Summary and Conclusions section of this report:

- The recent RBWR-AC and RBWR-TB2 designs were reviewed by teams from three universities using largely independent methods, with periodic joint review of the analyses with Hitachi. The analyses

[4] Recent analysis by the University of Michigan collaborators came up with a peak LHGR of 55 kW/m

collectively indicate that the two designs appear to be able to achieve their objectives… However, there are several areas of the current design that require further attention:

- There appears to be considerable uncertainty in the void coefficient calculation and it is not certain that the void coefficient is negative at all times; in particular for the RBWR-TB2 core. In general, the values of the coefficients calculated by the three universities are different than those predicted by Hitachi.[5]
- The two correlations for critical power prediction that were derived in Japan from the experiments on a small hexagonal fuel assembly with the similar axial power distribution as of the Hitachi RBWR design do not agree fully with each other, leading to uncertainty about the margin to Critical Power.
- In general the current design appears to be very sensitive to small design variations and to perturbations in operating conditions, which could make the core more difficult to safely operate than current BWRs.
- The upper and lower fissile zones of the core appear to be neutronically weakly coupled, which could introduce control issues.
- Information about the behavior of the zircaloy cladding in hard spectrum light water reactors is practically non-existent. There are indications in the literature that the corrosion rate of the cladding may be accelerated under the harder neutron spectrum.
- The linear heat generation rate distribution in the fissile regions will lead to significantly higher power gradients than in traditional BWRs. This effect may lead to a migration of some of the fission products to the cooler regions at the interface with the blanket. This may accelerate the chemical pellet-clad interaction at those interfaces.
- The higher power density in the fuel will lead to higher burnup in the fissile zones, with associated fuel swelling and fission gas release. This may lead to higher cladding strains at those locations than desirable (1% strain is typically desired in LWRs).
- Additional R&D work is recommended to address the above issues.

2.3. The incentive for thorium-based RBWR

Most of the concerns regarding the Hitachi RBWR core designs listed in the previous sub-section derive from the use of a couple of very short seed sections – their combined length is less than 50 cm, with a depleted uranium blanket in between. In comparison, the ABWR active core height is in the vicinity of 4 m and does not have an internal blanket. The highly heterogeneous design of the Hitachi RBWR core was dictated by the need to have the leakage component of reactivity feedback due to coolant voiding larger in absolute magnitude than the spectrum hardening component so that the net reactivity effect of coolant voiding will be negative. Instead of enhancing the negative leakage reactivity feedback we have proposed [7, 8] to reduce the magnitude of the large positive spectral component by using thorium instead of ^{238}U as the primary fertile fuel.

[5] In a more recent (2014) evaluation the University of Michigan researchers found, using more advanced computational capability, that the void coefficients of the latest Hitachi designs of RBWR cores are actually negative.

As ^{232}Th has a significantly smaller fast fission cross section than ^{238}U and as the η(^{233}U) increase with neutron energy is significantly smaller than that of ^{239}Pu and most other TRU in the relevant high energy range (See Figure 10), it is most likely possible to design a Th-based high void fraction water cooled core to have negative void reactivity coefficients without having to resort to short seed segments, internal blankets and parasitic absorbers in the axial reflectors. Relative to the Hitachi RBWR cores the thorium-based RBWR cores are expected to have a significantly longer seed and thereby significantly lower peak linear heat generation rate and larger safety margins, more axially stable power distribution and significantly smaller peak-to-average discharge burnup. The latter feature is due to the significantly smaller blanket-to-seed volume ratio. As indicated in the previous sub-section, there are concerns that the Hitachi RBWR fuel will not be able to maintain its integrity up to the peak burnups and corresponding fast neutron fluences it is designed to have. Figure 11 schematically compares the expected axial structure and dimensions of the thorium-based versus uranium-based self-sustaining fuel rods. The fission gas plenum extending above the active core in the upper reflector is of a smaller diameter than the fuel rod in order to reduce the coolant pressure drop and, in case of Hitachi, to provide space for thin absorber pins that are interspersed in-between.

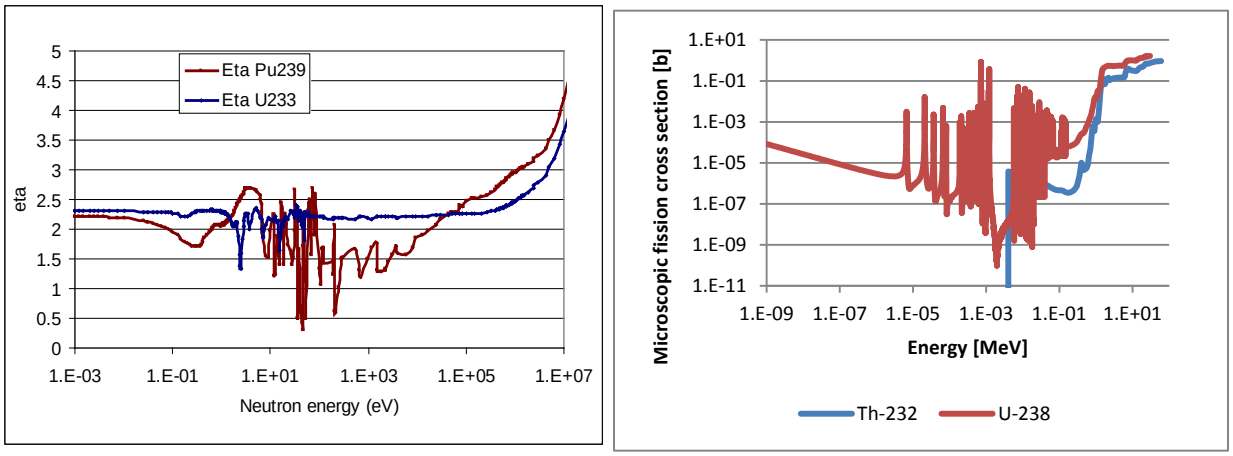

Fig. 10 η of ^{233}U and ^{239}Pu (left) and fission cross section of ^{232}Th and ^{238}U [20] (right)

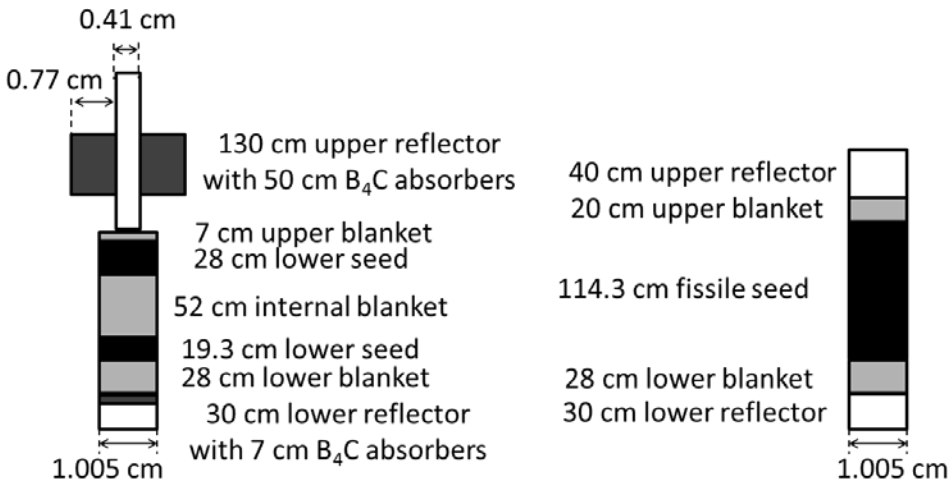

Fig. 11 Schematic axial layout of the self-sustaining thorium-based RBWR fuel pin (right) versus the RBWR-AC fuel pin (left). The thorium-based fuel pin shown uses the same T/H correlations as the Hitachi RBWR-AC.

The idea of using thorium as the primary fertile material in LWR had been extensively investigated over many decades [9-19 is a partial list of references] but, primarily, for PWRs. The closest design arrived at in the past to a thorium fueled LWR breeder are the "seed-and blanket" designs in which the seed fuel rods (that contained most of the ^{233}U) and the blanket fuel rods (containing primarily Th) were radially segregated. As a result, there is a significant variation of the pin-wise radial power distribution over the cycle which complicates the core design and safety. In earlier designs of the LWBR, [9, 10], the seed fuel assemblies had to be axially moved for controlling reactivity in order to achieve breeding. No such complications are needed for implementing the designs proposed for the RBWR cores; these cores feature no movable fuel parts and no radial segregation of seed and blanket fuel and, therefore, are not subjected to radial power shift over the cycle and flow/power mismatch.

The potential of using thorium in a tight lattice BWR has been recognized before. In particular, in [15] the authors provide a comprehensive overview of the properties of the ^{233}U-Th systems for BWR in tight lattices using a 2-D single pin/assembly unit cells modeled with the lattice code Helios. The main conclusion of the work in [15] is that Th-based fuels for BWR in intermediate spectra require a higher fissile content than ^{238}U-based fuels to achieve the same cycle length, but generally feature a higher conversion ratio. However, a configuration that could achieve a conversion ratio as high as 1 was not found in [9] that was limited to 2-D analysis. Nevertheless, it was recommended in [15] that Th-based fuels in tight lattice BWR will be further investigated using 3-D simulations.

2.4. The Thorium-based RBWR core designs

Three thorium-based RBWR cores were designed in this project -- two fuel-self-sustaining; denoted as RBWR-Th; and one TRU burner denoted as the RBWR-TR core. One of the RBWR-Th cores is designed using the conservative thermal-hydraulics correlations arrived at in this project [as described in Section 3.5 and Attachment 4] and the other is designed using the more optimistic correlations used by Hitachi for the design of their RBWR cores. It is expected that these two RBWR-Th cores will bracket the

performance of the actual core. Only one set of T-H correlations was used for the RBWR-TR core design as the P/D ratio of these cores was sufficiently large and the average quality sufficiently small that the RELAP correlation for void fraction prediction and the MIT-modified CISE4 (M-CISE) correlation for critical power prediction were deemed reasonable [see Section 3.5 and Attachment 4]. As detailed in Attachment 6, the presented design for the RBWR-TR has a positive void coefficient; however, it is possible to design a core with a slightly negative void coefficient and also have at least as high a TRU transmutation efficiency as the RBWR-TB2. Such a design will have a slightly smaller burnup and cycle length than the presented design. Such a design is currently being pursued.

Table 3 summarizes selected design and performance characteristics of the three RBWR cores designed in this project and of the two Hitachi designed RBWR cores used as a reference. Figure 12 compares the neutron flux spectra averaged over the seed (driver) region of these cores while Figure 13 compares these cores spectra of the fission inducing neutrons; the latter more clearly displays the spectral difference between the examined cores.

Table 3. A brief summary of the 5 designs considered, as well as some key characteristics.

Parameter	Units	RBWR-AC	RBWR-Th Y-CISE/LPG	RBWR-Th H-CISE/RELAP	RBWR-TB2	RBWR-TR
Makeup fuel	-	DU	Th+DU	Th+DU	DU+TRU	Th+TRU
	MW	3926	3200	3926	3926	3926
Core flow rate	t/hr	2.60E+04	1.99E+04	2.29E+04	2.40E+04	6.26E+04
MCPR	-	1.28	1.3	1.25	1.4	1.59
Exit quality	%	35.0	13.8	12.4	36.0	13.2
Pressure drop	MPa	0.14	0.29	0.13	0.06	0.15
Upper blanket length	cm	7	25	20	2	15
Upper seed length	cm	28	300	114.3	22	100
Internal blanket length	cm	52	-	-	56	-
Lower seed length	cm	19.3	-	-	22.1	-
Lower blanket length	cm	28	20	28	7	15
Fuel pin OD	cm	1.005	0.74	1.005	0.724	0.705
Fuel pin pitch	cm	1.135	0.799	1.135	0.941	0.944
Fuel pin P/D	-	1.13	1.08	1.13	1.3	1.34
Pins per assembly	-	271	547	271	397	397
Average burnup	GWd/t	45	50	49	65	55
TRU efficiency	%	-	-	-	45	48
Cycle length	EFPD	380	1110	413	304	313
Maximum LHGR	W/cm	472	45	261	470	189
Void coefficient (BOEC/EOEC)	pcm/% void	-24/-14	-4/-2	-4/-2	-42/-35	+2/+4[6]

[6] A positive VCR is not acceptable. However, our tradeoff study indicates that it it is possible to design a core with a slightly negative void coefficient and also have at least as high a TRU transmutation efficiency as the RBWR-TB2.

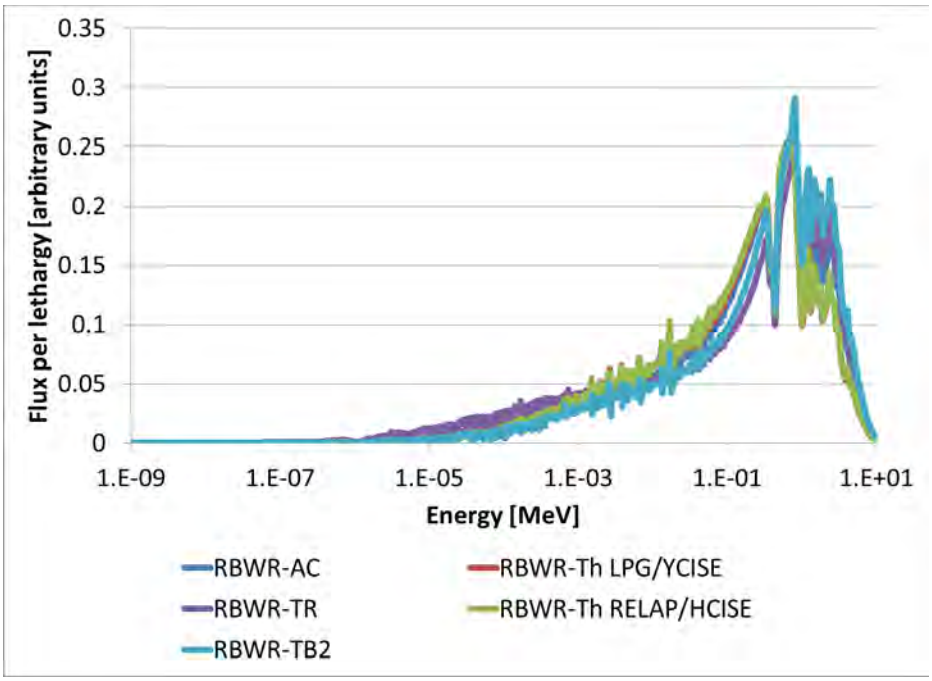

Fig. 12. Seed average neutron flux spectra of the RBWR cores

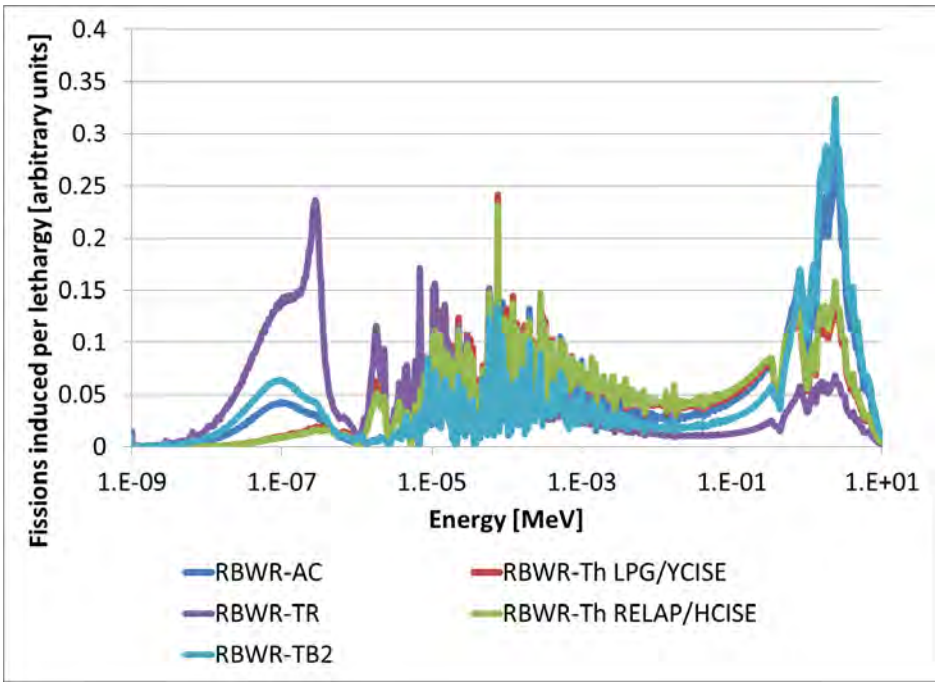

Figure 13. Spectra of neutrons that induce fission in each of the RBWR cores

3. Development of computational methods for RBWR type cores

All RBWR cores feature strong axial heterogeneity due to the strongly declining water density with elevation and, in case of the RBWR-AC and -TB2, also incorporation of a blanket fuel section in between

relatively short seed sections. The RBWR cores differ from conventional BWR cores in other ways as well – they feature significantly tighter lattices (in hexagonal array), significantly higher void fraction and higher fissile fuel loading. All these differences make the RBWR core spectrum significantly harder than that of conventional BWR. Moreover, the spectrum varies significantly with elevation. In addition, the RBWR cores feature extremely strong coupling between thermal hydraulics (axial water density distribution) and neutronics (axial power shape). As a result, thermal-hydraulic correlations, core design methodologies and fuel performance evaluation methodologies developed for BWR core design are not applicable for RBWR core design. Consequently, the first undertaking of this project was the development of computational capability that will enable reliable simulation of RBWR core performance. A large fraction of the effort invested in this project has been devoted to the accomplishment of this objective. This effort is briefly summarized below. The new computational capability developed in this project advances the state of the art and will be valuable for many future projects and the nuclear industry.

Section 3.1 and Attachment 1 describe the deterministic 3-D core simulator developed. Section 3.2 and Attachment 2 describe the Monte-Carlo assembly unit cell code developed; it is the primary design tool for the RBWR cores. Section 3.3 describes the coupled neutronics – thermal hydraulics code system developed for the RBWR transient analysis as part of a companion RBWR-related NEUP project [33]. Section 3.4 and Attachment 3 describe the fuel performance analysis code developed for thoria-based fuel that is subjected to high fluence of fast neutrons in high void boiling water. Section 3.5 and Attachment 4 describe the void fraction and critical power correlations developed for this project and compare them against the correlations used by Hitachi for the RBWR core designs.

3.1 3-D core simulator

A 3-D core simulator was developed to accurately model the strongly axially non-uniform RBWR cores. It consists of a 3-step approach which includes 3-D fuel assembly unit cell calculations, cross section generation and processing followed by coupled neutronics-TH 3-D core simulation. The primary innovation of this core simulator is the use of a 3-D Monte-Carlo code, Serpent, for generating the homogenized group constants for use in the PARCS nodal diffusion code. Serpent replaces the 2-D lattice codes, such as Helios, that were used for the group constants generation. The 2-D lattice codes, commonly used throughout the industry, were found inadequate for accurately capturing the strong axial variation in the neutron spectrum and strong axial neutron leakage of the RBWR cores. The overall structure of the 3-D core simulator is shown in Figure 14. The three modules on left (pink shaded boxes) are used for pre-processing while the PARCS and PATHS modules are used, in a coupled mode, to search for the equilibrium core composition and for quantifying the performance characteristics of this core.

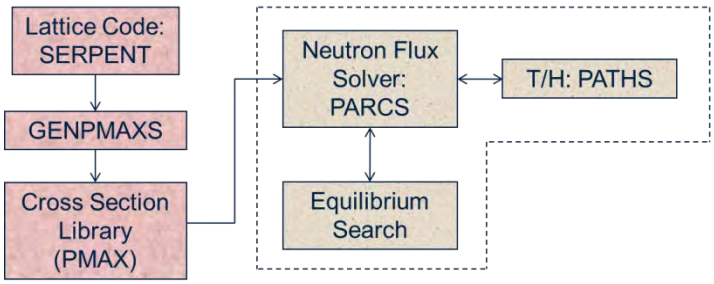

Figure 14. Structure of 3-D simulator developed for RBWR core design

The Monte Carlo code Serpent is used for 3-D modeling of the RBWR fuel assembly unit cell. Through the use of the SerpentXS code [24], developed at MIT, multiple Serpent calculations are performed to generate the multi-group constants for different burnups and different branch cases necessary to bound the core state over its life. The second portion of the core simulator involves the GenPMAXS [25] code which processes the raw data and creates the cross section files (PMAX) used in the coupled code simulation. This portion of the code also produces the axial discontinuity factors (ZDFs) which correct for steep changes in the flux at material interfaces – such as between seed and blanket zones. All the above constitute the pre-processing phase. The actual core simulation phase is performed by the coupled PARCS and PATHS modules. PARCS [26] is a 3D nodal diffusion code capable of solving hexagonal geometries. It uses a triangular polynomial expansion method (TPEN) to solve the 2D direction while coupling to a 1D NEM solver to calculate the axial solution. PATHS is a drift flux thermal-hydraulics code that solves the mass, momentum and energy equations using a specified correlation for the void fraction. This code provides the thermal-hydraulic feedback within PARCS for steady-state simulations and search for the equilibrium cycle. Details about the 3D core simulator developed and its validation are given in Attachment 1.

3.2 Monte-Carlo based coupled neutronics – TH – depletion analysis capability

The generation of the group constants required for the application of the PARCS-based core simulator is a time consuming process that is not practical to apply for a tradeoff study that requires covering many permutations of design variables. A more practical design tool, called MocDown, was developed for the tradeoff studies. MocDown couples the neutron transport MCNP5.1.60 [21] with transmutation code ORIGEN2.2 [22] and with the thermal-hydraulics code PATHS [23] as schematically illustrated in Figure 2. For a given beginning of cycle (BOC) newly loaded unit cell composition MocDown first iterates between the neutronics and T-H calculations until the axial power shape and axial coolant density are consistent. Then MCNP5.1 generates effective one group cross sections and total neutron flux for each depletion zone in the assembly. ORIGEN2.2 uses these effective one-group parameters to perform depletion calculations up to a specified fuel residence time and the end of cycle core average multiplication constant is estimated for a core of a specified number of batches. Efficient algorithms are built into the MocDown code system to accelerate the convergence to a critical equilibrium core composition. Details, including code validation, are given in Attachment 2.

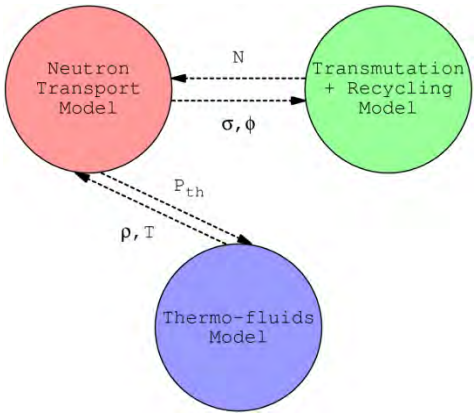

Figure 15. Structure of the MocDown computational capability developed for the RBWR core tradeoff studies. Neutron transport is performed with MCNP5.1.60, while thermo-fluids is performed in PATHS and depletion is done in ORIGEN2.2.

3.3 Stability and safety analysis capability

Any BWR type system is susceptible to two phase flow oscillations of the density wave type. The MIT in-house stability code, STAB, was used to analyze the RBWR-Th response to three modes of instability: Single channel thermal hydraulics, out-of-phase coupled neutronics-thermal hydraulics regional stability and in-phase coupled neutronics-thermal hydraulics global stability. STAB is a frequency domain code that models the entire core with three different radial power regions and uses point kinetics parameters from full core neutronic calculations to inform the core response under coupled neutronics-thermal hydraulic response [27].

The TRACE version 5785 patch 3 was obtained from the NRC [28]. The TRACE input deck for an ABWR of the University of Michigan was used as a reference for developing a TRACE input for simulating the RBWR-Th [29]. The reference ABWR model consists of 18 separate thermal-hydraulic channels with no neutronic feedback modeling. The RBWR core modeling was greatly refined by modeling the 720 separate assemblies in the vessel to allow accurate prediction of the core response to transients. The control system was connected to the hydraulic components for proper transient simulations. The steam separators and safety relief valves of an ABWR were also added to the TRACE model as they are critical for performing reliable transient simulations. All four steam lines and ten internal reactor pumps of the ABWR are explicitly modeled. The two critical power correlations recommended for RBWR (See Section 3.5) were added to the TRACE model to enable reliable simulation of various transients. Details are provided in Reference [34].

3.4 Fuel performance analysis capability

The RBWR-Th and RBWR–TR cores use a mixed oxide fuel in which ThO_2 is the most abundant constituent, though relevant amounts of UO_2 and PuO_2 are also present. The thermo-physical properties of ThO_2-based fuels differ greatly from those of the UO_2 and MOX fuel of a typical BWR and are not incorporated in presently available fuel performance analysis codes. Also, the RBWR fuel is subjected to

a significantly harder neutron spectrum and higher neutron fluence. The harder neutron spectrum and higher fluence are known to cause Zircaloy-2 to experience accelerated oxidization and hydrogen pickup. Presently available fuel performance codes are not applicable for reliable analysis of these phenomena.

To provide fuel performance analysis capability for the RBWR-Th and RBWR-TR, modifications, detailed in Attachment 3, were made to the steady state fuel performance code FRAPCON-MIT. Based on the NRC steady state fuel performance code, FRAPCON-3.4, FRAPCON-MIT has been developed to allow the assessment of advanced LWR fuel concepts, including $(ThU)O_2$ fueled PWRs. To accommodate the use of $(ThUPu)O_2$ fuel in the RBWR, several fuel properties were augmented, including the fuel thermal conductivity, thermal expansion, and melting temperature. Notably, a new thermal conductivity model was developed to account for the effect mixing on phonon and electronic heat transfer mechanisms.

Other behavioral models, such as Fission Gas Release (FGR), were able to use previous modifications for $(ThU)O_2$ fueled PWRs. The radial fission rate distribution model was able to make use of a previously developed model to include Th breeding isotopics. However, the much harder neutron spectrum of the RBWR dictated the modification of the applied capture and fission cross sections. This modification made use of data generated by a Monte Carlo neutronic simulation.

Due to its dependence on fuel burnup rather than cladding fluence, the FRAPCON-3.4 Zircaloy-2 hydrogen pickup model was determined to be ill fit for describing RBWR-Th cladding behavior. To remedy this, a hydrogen pickup model that is based on cladding corrosion and fast neutron fluence was applied. This model accounted for the known accelerated hydrogen uptake observed in BWRs and also allowed for the investigation of hypothetical advanced claddings that could delay such accelerated behavior. Additionally, the high axial temperature and hydrogen pickup gradients at the blanket-seed interfaces are expected to drive axial hydrogen migration. This motivated the development of a model to simulate hydrogen transport and precipitation in the cladding.

In evaluating the acceptability of RBWR-Th and RBWR-TR fuel performance several limiting criteria were applied. First the fuel is not allowed to reach its melting temperature, which is approximately 3400K for all the cases considered. Second, the cladding strain must be limited to a maximum value of 1% to prevent excessive deformation of the coolant channel. Third, in order to prevent the risk of cladding lift-off, the plenum gas pressure is not allowed to exceed that of the coolant, which is the same as that of an ABWR (7.14 MPa). Lastly, the allowable Equivalent Cladding Reacted (ECR) during transients and LOCA events is limited based on the hydrogen content in the cladding, as shown in Equation 1, because of concerns surrounding hydrogen induced cladding embrittlement. Because Reactivity Insertion Accidents (RIAs) are not considered to be design basis accidents for the ABWR [30], with which the RBWR shares its safety systems, hydrogen based RIA limits are not imposed on the RBWR-Th or RBWR-TR.

$$\mathrm{ECR}_{\mathrm{Allowed}} = \begin{cases} 18 - 0.03\mathrm{H}; & \mathrm{H} < 400 \\ 18 - 0.01\mathrm{H}; & 400 \leq \mathrm{H} < 600 \\ 0; & 600 \leq \mathrm{H} \end{cases} \quad (1)$$

Details about the fuel performance capability developed are provided in Attachment 3.

3.5 Thermal hydraulic correlations for tight lattice high void cores

Reliable determination of the coolant void axial distribution and the margin to Critical Power (CP) of the RBWR cores requires use of flow correlations that are accurate for the tight-lattice, high void fraction flow regime of such cores. The fuel length, boiling length, mass flux, void fraction and hydraulic diameters of the RBWR-Th breeder designs are very different from traditional BWRs. In the RBWR analysis by Hitachi, a standard drift-flux BWR void fraction correlation was used along with a modified CISE-4 (common CP correlation for hexagonal and square assemblies), based on experiments with triangular high quality experiments performed by Bettis Atomic Power Laboratory (BAPL) in early 1970s [31]. Experiments with small assemblies of RBWR fuel rod pitch and diameter, operating conditions and "pancake" axial power shape were performed by the Japan Atomic Energy Agency (JAEA) in the 2000s, post Hitachi analysis of the RBWR [32]. These experiments, that included both void fraction and CP measurements, result in correlations showing smaller void fraction and smaller CP than predicted by the correlations Hitachi used for their RBWR core designs. Two new correlations that account for all the experimental data available in the open literature were developed in our work: the Modified LPG void fraction and MIT Modified CISE CP correlations.

For prediction of void fraction, the Modified LPG correlation tends to result in about 10% lower void fraction values than the Hitachi (or standard RELAP or EPRI) correlations. This results in a softer neutron spectrum and reduces the burnup that can be achieved with a fuel self-sustaining core. It is noted that the correlation validation pedigree is only based on few data points as future experimental data is required.

For prediction of the Minimum CP Ratio (MCPR), the MIT modified CISE correlation results in a value of at least 0.2 ΔMCPR lower than the Hitachi correlation for RBWR type reactors. Due to the wide spread of CP predictions of experimental data from 7 different geometries and over 100 data points an additional 0.2 is recommended for safety margin to be added to the steady state limit of 1.3. This will require significant derating of the power (the parameter most sensitive to CP prediction), if the conservative MIT-CISE correlation is used along with a MCPR limit of 1.5. The range of data used for validation of MIT-CISE correlation were narrowed to the expected steady state operating conditions of RBWR. The scatter in the data was considerably reduced and a new modified CISE correlation Y-CISE, was derived to be used with MCPR limit of 1.3. Both the new correlation and Hitachi used correlations were used for the RBWR-Th breeder design, yielding to two very different configurations. Since the RBWR-Th burner design operating conditions are similar to ABWR, the Hitachi void fraction correlation and MIT-CISE correlation were used in its design as they were assumed to be valid for such conditions.

Details can be found in Attachment 4.

4. Feasibility of fuel-self-sustaining RBWR-Th cores

4.1 Study strategy

This task searches for feasible designs for the RBWR-Th core -- a reduced-moderation BWR which is fuel-self-sustaining. Except for the initial fuel loading, it is charged with only fertile fuel and discharges only

fission products, recycling all actinides. The RBWR-Th is a variant of the RBWR-AC core proposed by Hitachi, which arranges its fuel in a hexagonal tight-lattice, has a high outlet void fraction, axially segregates seed and blanket regions, and fits within the ABWR pressure vessel. The RBWR-Th shares these characteristics but replaces depleted uranium with thorium as the primary fertile fuel, eliminates the internal blanket while elongating the seed region, and eliminates absorbers from the axial reflectors.

The search for acceptable fuel self-sustaining core designs was done in four stages: The first stage consisted of a thorough tradeoff study, performed using the MocDown code system (Section 3.2), that searched for the combination of design variables that will meet the following design constraints:

1. charge only fertile material,
2. recycle all trans-fertile (TRF) material,
3. maintain a fissile inventory ratio (FIR) of unity at equilibrium,
4. fit within an ABWR pressure vessel,
5. use the Hitachi RBWR assembly dimensions,
6. provide the full ABWR thermal power,
7. operate on a cycle length of at least 12 months,
8. have a pressure drop through core ≤ 0.3 MPa,
9. possess negative coefficients of reactivity for fuel temperature, coolant void, and power,
10. maintain criticality,
11. avoid coolant dryout (MCPR ≥ 1.3),
12. suppress density wave oscillations (DR ≤ 0.8), and
13. have sufficient shutdown margin to shut down the core at any time in the cycle.

The design variables of this tradeoff studies include the seed region length, axial blanket region lengths, axial isotopic charge distribution, coolant mass flow rate, atom fraction of depleted uranium (DU) in the seed makeup, fuel pin pitch-to-diameter ratio, number of pins per assembly, core power (when nominal ABWR power could not be reached), depletion time, void fraction correlation and CPR correlation (a couple of options for each of the latter two variables), bypass water density, and control blades follower material. The performance of the RBWR-Th core was found to be particularly sensitive to the pitch-to-diameter ratio and to modeling assumptions.

In the second stage of the design process, the results of the tradeoff studies guided the search for two bounding core designs -- one corresponding to the conservative thermal-hydraulic correlations arrived at in this project (Section 3.5) while the other corresponding to the correlations used by Hitachi. The MocDown code system (Section 3.2) was used for this search. Using the thermal hydraulic correlations used by Hitachi, similar performance to the RBWR-AC was attained while using a single significantly longer seed and significantly lower peak linear heat generation rate than of the Hitachi RBWR-AC. However, using the more conservative assumptions developed in this project the RBWR-Th core power had to be reduced to 81.5% of the nominal, and the core volume had to be significantly increased – both trends are economically undesirable. Also performed in the 2nd stage is a search for the optimal radial enrichment within the fuel assembly that will provide an acceptable peak-to-average pin power. This was found essential due to the otherwise high power peaking in the fuel pins in proximity to the control blade channels.

The third stage involved application of the SERPENT/PARCS/PATHS 3-D core simulator (Sec. 3.1) to search for the control rods insertion pattern and insertion height that will maintain k_{eff} at 1.0 throughout the cycle and to search for the resulting equilibrium core composition. This analysis starts with the optimal assembly design identified in Stage 2 but more accurately accounts for the radial power distribution, fuel shuffling and excess reactivity control. It provides more accurate values of the attainable discharge burnup, reactivity coefficients, control rod reactivity worth, shutdown margin and all other core-wise performance characteristics. A summary of the designs arrived at is given in Section 4.2.

The 4th stage was to perform transient and stability analyses on the RBWR cores identified in Stage 3 using the PARCS/TRACE code system described in Sec. 3.3. However, since the results from the 3-D core simulator were obtained late in the project, only simplified safety analyses based off the assembly model and using bounding values for void coefficients were performed. The results are summarized in Section 4.3.

In parallel with the safety analyses, a fuel performance analysis was performed on the RBWR core design arrived at in Stage 2 using the methodology described in Section 3.4. It was found that, unfortunately, with the presently available cladding materials it appears impossible to reach the neutronically attainable burnup without exceeding the maximum permissible hydrogen concentration. It is hoped that improved cladding materials that will not restrict the attainable burnup will eventually be developed. Details are provided in Section 4.4.

4.2 RBWR-Th core designs

The initially considered fuel cycle assumed recycling of all the trans-thorium elements produced in the seed and in the blankets into the seed and adding thorium for the makeup fuel. However, the resulting void coefficient of reactivity was found too negative to enable achieving sufficient shutdown margin at cold zero power conditions. In order to overcome this difficulty depleted uranium (DU) was added to the makeup fuel. The fraction of DU was adjusted so as to yield the desirable void coefficient of reactivity; a larger fraction results in a less negative or more positive void reactivity worth. The optimal DU weight fraction was found to be in the vicinity of 30%. No DU is added to the blanket fuel. All the trans-uranium and trans-thorium elements are recycled into the seed.

Table 4 summarizes the design characteristics of the two “bracketing” RBWR-Th core designs arrived at – one using the MIT recommended thermal-hydraulic correlations and the other using the correlations Hitachi used for the design of their RBWR cores, and compares them with those of the Hitachi RBWR-AC core. Table 5 similarly summarizes and compares the cores performance characteristics and Table 6 the discharge fuel isotopics.

Table 4 RBWR-Th versus RBWR-AC design information

Parameter	Units	RBWR-AC	RBWR-ThM	RBWR-ThH
Core thermal power	MWth	3926	3200	3926
Core electric power	MWe	1356	1104	1356

Parameter	Units	RBWR-AC	RBWR-ThM	RBWR-ThH
# of assemblies	#	720	720	720
Core HM mass (BOEC)	t	140	354	153
Core TRF mass (BOEC)	t	16.7	48.9	18.9
TRF/HM core avg at BOEC	w/o	11.9%	13.8%	12.4%
Specific power	MWe/t	10	3	9
Assembly area	cm^2	338	338	338
Core flow rate	kg/s	7222	5285	6358
Outlet quality	%	35.0%	38.7%	39.5%
Core volume	m^3	32	84	40
Power density	Wth/cm^3	123	38	99
Upper blanket length	cm	7	25	20
Upper seed length	cm	28	300	114.3
Internal blanket length	cm	52	-	-
Lower seed length	cm	19.3	-	-
Lower blanket length	cm	28	20	28
Total fuel length	cm	134.3	345	162.3
Active fuel length	cm	47.3	300	114.3
Fuel pin OD	cm	1.005	0.740	1.005
Fuel pin pitch	cm	1.135	0.799	1.135
Fuel pin P/D	-	1.13	1.08	1.13
Hydraulic diameter	cm	0.41	0.22	0.41
Heated diameter	cm	0.44	0.23	0.44
Pins per assembly	-	271	547	271

Table 5 RBWR-Th versus RBWR-AC performance metrics

Metric	Units	RBWR-AC	RBWR-Th YCISE/LPG	RBWR-Th H-CISE/RELAP
Pressure Drop	MPa	0.14	0.29	0.13
Maximum LHGR	Wth/cm	472	45	261
# of batches	#	5	5	5
Average discharge burnup	GWd/t	45	50.1	48.8
Fuel residence time	EFPD	1651	5124	1904
Cycle length	EFPD	380	1110	413
Cycle reactivity swing	%dk	1.5	1.9	1.9
VCR (BOEC/EOEC)	pcm/% void	-24/-14	-4/-2	-4/-2
Shutdown margin	%dk	not avilable	3	1.9

Table 6 RBEWR-Th versus RBWR-AC discharge isotopics from the seed(s)

Mass fraction [%]	RBWR-AC	RBWR-Th YCISE/LPG	RBWR-Th H-CISE/RELAP

TRF / HM	34.0%	16.3%	17.7%
fissile / HM	16.8%	10.0%	10.9%
Pa / TRF	0.0%	60.0%	0.3%
nonfertile U / TRF	0.5%	1.5%	54.0%
Np / TRF	0.4%	33.8%	1.3%
Pu / TRF	92.2%	3.8%	40.4%
Am / TRF	4.8%	0.6%	2.9%
Cm / TRF	2.1%	0.0%	1.1%
Cf / TRF	0.0%	60.0%	0.0%
^{232}U / U nonfertile	0.0%	0.3%	0.4%
^{233}U / U nonfertile	0.0%	57.0%	57.6%
^{234}U / U nonfertile	18.8%	27.4%	27.0%
^{235}U / U nonfertile	62.5%	7.7%	7.6%
^{236}U / U nonfertile	18.8%	7.5%	7.4%
fissile U / total U	0.2%	19.5%	15.2%
^{238}Pu / Pu	3.6%	9.0%	6.5%
^{239}Pu / Pu	40.9%	48.1%	48.7%
^{240}Pu / Pu	42.9%	34.4%	34.1%
^{241}Pu / Pu	6.6%	4.4%	6.1%
^{242}Pu / Pu	6.0%	4.0%	4.6%
fissile Pu / total Pu	47.5%	52.5%	54.8%

It is found that using the conservative T-H correlations results in a very large performance penalty – reduced power level and significant increase in the HM loading and, therefore, a significantly lower specific power and power density. However, using the same correlations used for the RBWR-AC design, the performance of the RBWR-Th is comparable; the major difference is a significantly lower LHGR which is due to the significantly longer seed as illustrated in Figure 16. The optimal radial enrichment distribution found is shown in Figure 17.

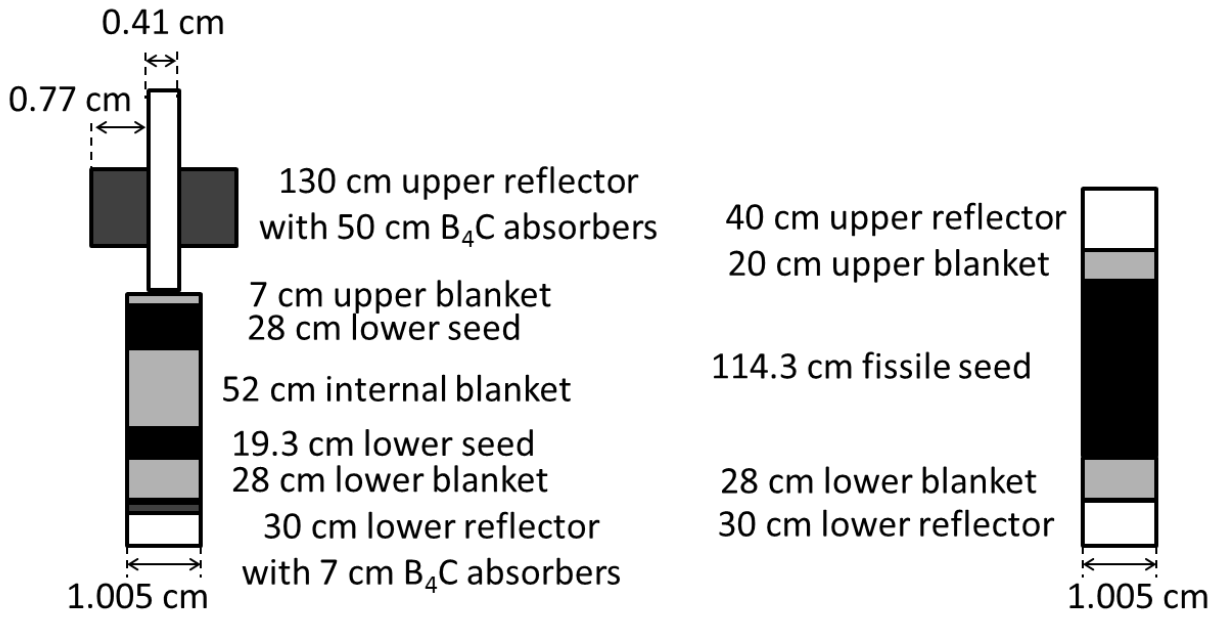

Figure 16 Layout of the RBWR-Th using Hitachi T/H correlations versus RBWR-AC fuel rod design

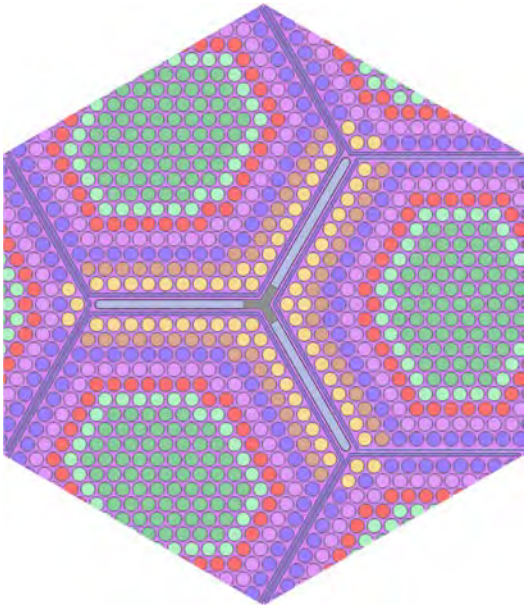

Figure 17 The 7 enrichment zones used to flatten the radial power in the RBWR-Th three-assembly unit cell using 271 pins per assembly.

Table 7 Key for Figure 4.2.

Group color	# of pins	BOEL TRF moles per pin / average moles per pin (%)
Tan	23	40%
Brown	19	60%
Blue	48	77.5%
Purple	44	100%
Red	38	115%
Light Green	32	120.00%
Dark Green	67	130.00%

Figure 18 compares the fission-rate spectrum of the RBWR-Th core with that of a fuel-self-sustaining SFR and a standard BWR. The fission-rate spectrum is defined here as the fraction of the fission rate induced by neutrons of a given energy. It is seen that the majority (>50%) of the fissions of the RBWR-Th are induced by neutrons in the energy range between 1eV and 100 KeV.

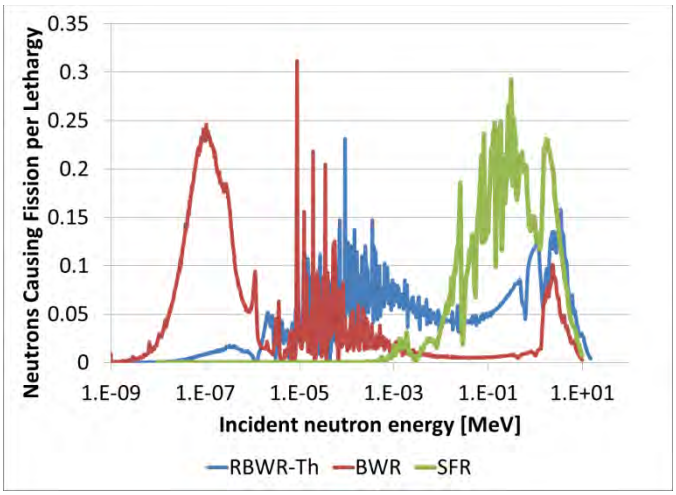

Figure 18 Normalized fission-rate spectrum of a typical RBWR-Th, compared against that of a BWR and a self-sustaining SFR.

Additional information and results are provided in Attachment 5.

4.3 RBWR-Th safety and stability

As the full 3-D core analysis of the RBWR-Th cores was not completed by the time needed for the safety analysis, the safety analysis was based on a number of simplifying assumptions as described in Attachment 7.

To assess the performance of the RBWR-Th reactors under loss of flow scenarios, a total pump trip accident was analyzed. Both of the RBWR-Th cores – that designed using the Hitachi correlations (ThH) and that designed using the more conservative MIT correlations (ThM), feature mass flow rates that are less than half of the ABWR. The peak cladding temperature (PCT) for the RBWR-ThH and RBWR-ThM designs was estimated to be 752 and 683 K, respectively. These are lower than of the conventional ABWR design PCT of 800 K. The results of this transient simulation imply that the lower LHGR of the RBWR-Th cores more than offsets their lower thermal capacity compared to the ABWR. The fluid volume of the RBWR-ThH and ThM cores are 1.3 and 2.3 times higher than of the RBWR-AC which has much higher LHGR, the RBWR-Th cores have much greater safety margin against loss of flow accidents.

The loss of coolant accident (LOCA) simulations of main steam line break were performed by Hitachi and MIT for the RBWR-AC and yielded satisfactory results. Therefore, having lower LHGR and larger core fluid volume relative to RBWR-AC, it is expected that both RBWR-Th designs have acceptable performance during LOCAs. Thus, it is expected that both RBWR-ThM and ThH designs will have satisfactory response to design basis accidents.

The higher core void fraction and much higher exit quality of RBWR-ThM and ThH compared to ABWR raise concerns about their stability. The global mode of perturbation was found to be the most limiting mode at hot full power (HFP) conditions for the ABWR and RBWR reactors. The preliminary analysis performed concluded that here is sufficient margin for stable operation at 100% power and flow for both RBWR-Th designs. The longer RBWR-ThM core design has much smaller margin to stability than the shorter RBWR-ThH design. The RBWR-ThH design can operate with void coefficients similar to the

conventional ABWR as the stabilizing effect of shorter length is countered by the higher void fraction. Additional information and results are provided in Attachment 7.

4.4 RBWR-Th fuel performance

The fuel performance analysis of the two RBWR-Th cores was carried out for the nominal and 130% pin power. Due to the lack of power history information at the time of this analysis, both cases make use of the conservative assumption that the pin power remains constant throughout irradiation.

Due to low LHGR of the RBWR-ThM fuel pin, the peak centerline fuel temperature is low, with the 130% peaked case remaining below 800K. As a result of the low fuel temperatures and the relative small diffusion rate of fission gases through ThO_2-based fuels, neither of the simulated RBWR-ThM pins experience Fission Gas Release (FGR) of more than 6.5%. The low FGR, in turn, ensures that the plenum pressures for the RBWR-ThM fuel remain well below the coolant pressure. The higher LHGR of the RBWR-ThH case results in much higher peak centerline fuel temperatures. The maximum temperature for the 130% peaked case is found to be 1840K. While this temperature is over 1000K hotter than of the RBWR-ThM case, the margin to melting (approximately 3400K) remains very generous. However, the high temperatures lead to high calculated FGR values; the EOL pin average FGR is 38.4%. This high FGR results in high plenum pressures which can potentially exceed the coolant pressure of 7.14 MPa and, therefore, the no cladding lift-off criterion. To mitigate this possibility, the cold plenum length of the RBWR-ThH pin need be extended to 40cm (assuming identical fuel pin and plenum diameters). In conclusion, both RBWR-Th cores can be designed to safely accommodate the FGR without exceeding the 1% cladding hoop strain limit.

Due to the harder spectrum of the RBWR-Th cores compared to typical BWRs, the peak fluence of fast (E>0.1 MeV) the cladding is exposed to far exceeds the bounds of Zircaloy-2 operational experience. In the RBWR-Th cores Zircaloy-2 cladding is expected to experience accelerated oxidation and hydrogen pickup much earlier in life – starting around 20 MWd/kgHM for both designs. The cladding hydrogen content is expected to exceed the practical limit of 600 ppm(wt) at 28 and 32 MWd/kgHM for the RBWR-ThM and RBWR-ThH cores, respectively.

An important fuel performance criterion during LOCAs is loss of cladding ductility that will result in cladding failure when quenching occurs during the core reflood stage. This ductility change is quantified using the Equivalent Cladding Reacted (ECR), which is a measure of the portion of the cladding that has been oxidized. As the hydrogen content increases, the ductile-to-brittle transition occurs at decreasing ECR values. It is estimated that Zircaloy-2 is not expected to have any ECR margin by the time the RBWR-Th cores reach their average discharge burnup. An advanced alloy will be required for the RBWR-Th fuel cladding. One such alloy, GNF-Ziron, has demonstrated the potential to experience a delay in the onset of hydrogen pickup acceleration, though not in oxidation acceleration. It is estimated that the advanced cladding material for the RBWR-Th will have to provide 150, 260, 100, 180% delay in the accelerated hydrogen pickup behavior for the average and 130% peaked pins of the RBWR-ThM and RBWR-ThH cases, respectively. Additional information and results are provided in Attachment 3.

5. Feasibility of TRU transmuting RBWR-TR core design

5.1 Study strategy

The approach used for the design of the optimal transmuting RBWR-TR cores was similar to that used for the design of the self-sustaining cores described in Section 4. However, as the lattice is significantly less tight than in the fuel self-sustaining core, the correlations used by Hitachi for the void fraction and critical power prediction are considered acceptable and were used for this study. The feed fuel is taken to be TRU from LWR used nuclear fuel and thorium. The addition of depleted uranium feed is not needed for the transmuting core because the TRU tends to make the void coefficient of reactivity positive and the desirable magnitude of void coefficient is achieved by adjusting the TRU concentration in the seed (as well as by adjusting the axial neutron leakage probability). A couple of fuel cycles were considered – one recycles all the trans-thorium elements along with the left over TRU into the seed, and the other removes the uranium and protactinium bred from the seed. The design objective is to maximize the fraction of power generated by the TRU – that is, to maximize the TRU fractional transmutation while attaining adequate burnup.

The design of the second TRU transmuting core variant (with removal of bred ^{233}U) was not complete by the time of this writing and will not be reported in this summary.

5.2 RBWR-TR core design

The design information of the RBWR-TR is compared to the RBWR-TB2 in Table 8. Performance metrics are compared in Table 9, and the average discharge isotopics are compared in Table 10.

Although the design presented in Table 9 has a slightly positive VCR, it has been determined that it is feasible to design the RBWR-TR so that the VCR is negative while still maintaining a higher TRU efficiency than the RBWR-TB2. There will be a slight penalty on burnup, however. More details are provided in Attachment 6.

Table 8. Design information for the RBWR-TR and the RBWR-TB2.

Parameter	Units	RBWR-TB2[7]	RBWR-TR
Coolant	-	light water	light water
Fuel form	-	oxide	oxide
Core thermal power	MWth	3926	3926
Thermal efficiency	MWe/MWth	34.5%	34.5%
Core electric power	MWe	1356	1354
# of assemblies	#	720	720
Core HM mass (BOEC)	t	73	88
Core TRF mass (BOEC)	t	23.9	20.5
TRF/HM core avg at BOEC	w/o	32.6%	23.3%
Specific power	MWe/t	18	15
Blanket configuration	-	parfait	parfait

[7] Hitachi is in the process of redesigning their RBWR-TB2; the performance of the revised design is likely to be somewhat degraded relative to that presented.

Parameter	Units	RBWR-TB2[7]	RBWR-TR
Assembly area	cm^2	338	338
Core flow rate	t/hr	2.4E+04	6.3E+04
Outlet quality	%	36%	13.2%
Core volume	m^3	25	32
Power density	Wth/cm^3	158	124
Upper blanket length	cm	2	15
Upper seed length	cm	22	100
Internal blanket length	cm	56	-
Lower seed length	cm	22.1	-
Lower blanket length	cm	7	15
Total fuel length	cm	110	130
Active fuel length	cm	44.5	100
Fuel pin OD	cm	0.724	0.705
Fuel pin pitch	cm	0.941	0.944
Fuel pin P/D	-	1.30	1.34
Hydraulic diameter	cm	0.60	0.66
Heated diameter	cm	0.65	0.70
Pins per assembly	-	397	397

Table 9. RBWR-TB2 and RBWR-TR performance metrics.

Metric	Units	RBWR-TB2	RBWR-TR
Pressure Drop	MPa	0.06	0.15
Maximum LHGR	Wth/cm	470	189
# of batches	#	4	4
Average discharge burnup	GWd/t	65	55
TRU fission efficiency	%	45	48
Fuel residence time	EFPD	1215	1250
Cycle length	EFPD	304	313
VCR (BOEC/EOEC)	pcm/% void	-42/-35	+2/+4
Shutdown margin	%dk	Not available	3.5

Table 10. Average discharge isotopics of the RBWR-TB2 and the RBWR-TR.

Mass fraction [%]	RBWR-TB2	RBWR-TR
TRF / HM		20.5%
fissile / HM		9.4%
Pa / TRF	0.0%	0.2%
nonfertile U / TRF	0.0%	37.8%
Np / TRF	1.4%	2.4%
Pu / TRF	87.8%	47.1%
Am / TRF	8.0%	6.9%

Cm / TRF	2.8%	5.6%
Cf / TRF	0.0%	0.0%
232U / U nonfertile		0.4%
233U / U nonfertile		52.4%
234U / U nonfertile		28.1%
235U / U nonfertile		10.3%
236U / U nonfertile		8.7%
fissile U / total U		62.7%
238Pu / Pu	7.6%	19.1%
239Pu / Pu	29.0%	17.6%
240Pu / Pu	45.7%	33.6%
241Pu / Pu	6.2%	10.8%
242Pu / Pu	11.5%	18.9%
fissile Pu / total Pu	35.2%	28.4%

Additional information and results are provided in Attachment 6.

5.3 RBWRE-TR safety and stability

The Hitachi RBWR-AC core radial power and burnup distribution and orificing scheme was used for the safety analysis of RBWR-Th burner core (RBWR-TR) design as the full core analysis of this core was not completed in time for the safety analysis. Likewise, the middle of life (MOL) axial power shape from RBWR-Th single assembly calculations were used for the core average axial power shape.

The RBWR-TR design does not differ significantly from the ABWR in terms of the coolant flow conditions – they have similar exit quality and similar P/D ratio. The RBWR-TR features a shorter core and smaller void coefficient of reactivity. The benefits of shorter core height and smaller void coefficient for safety response except for loss of flow transients were discussed in Section 4.3 and in Attachment 6. Simulating the all pump trip transient for the RBWR-TR it was found that the peak cladding temperature (PCT) does not exceed 681 K; this is lower than of a conventional ABWR as well as of the RBWR-ThH design, mainly due to the lower LHGR and higher MCPR margin of the RBWR-TR design. Similarly, the RBWR-TR performance during LOCA is expected to be satisfactory as the total mass of water in the vessel has not decreased significantly compared to a conventional ABWR.

The shorter core height, higher inlet orificing and lower void coefficient while operating at similar core average void fraction (in the fuel area) compared to ABWR, makes the RBWR-TR design to have better response to the stability modes. Overall, both safety and stability of RBWR-TR design are expected to be superior compared to the ABWR.

Additional information and results are provided in Attachment 7.

5.4 RBWR-TR fuel performance

This fuel performance analysis uses the methodology described in Section 3.4. With an average LHGR ~15% lower than that of the RBWR-ThH design (Section 4), the RBWR-TR fuel maintains a comfortable margin to the melting temperature of approximately 3400K, with a 130% peaked pin maximum centerline temperature of 1630K. The FGR of the 130% peaked pin is estimated to be 35%. A 40cm cold plenum length is sufficient to assure that plenum pressure remains below the 7.14 MPa coolant pressure without challenging the 1% cladding hoop strain limit.

Thanks to the softer spectrum of the RBWR-TR, the oxidation and hydrogen pickup transition to accelerated behavior start much later than in the RBWR-Th cores. However, the accelerated behavior does begin at 25 MWd/kgHM and the cladding hydrogen content exceeds the practical 600 ppm(wt) by 45 MWd/kgHM so Zircaloy-2 cladding will not enable the RBWR-TR to reach its EOL. However, the limited irradiation data available suggests that the new Ziron cladding material is close to enabling the RBWR-TR fuel to reach its neutronically attainable burnup. It is likely that smaller effort (time and resources) will be required for the development of an advanced alloy for the cladding material for the RBWR-TR than for the RBWR-Th cores. Additional information and results are provided in Attachment 3.

6. Comparison of RBWR-Th versus RBWR-AC and ARR

Selected design, performance and fuel cycle characteristics of the RBWR-Th are compared in Table 11 against those of the RBWR-AC and ARR. The RBWR-Th core considered in this comparison is designed using the same thermal hydraulic correlations and constraints as used by Hitachi for their RBWR-AC core design. Both RBWR-Th and RBWR-AC designs deliver the nominal power of ABWR. All three core designs feature a fissile inventory ratio of 1.

Relative to the RBWR-AC, the RBWR-Th design has significantly longer seed (or “driver”) fuel without central axial blanket and, therefore, much lower peak linear heat generation rate; more stable axial power distribution along with larger safety margins; slightly higher discharge burnup; lower power density and specific power; smaller HM reprocessing capacity per unit of electricity generated; higher short term radioactivity and ingestion radio-toxicity of the HLW, primarily, due to the about 3 times higher yield of ^{90}Sr from fissions of ^{233}U; lower short term inhalation radio-toxicity due to smaller fraction of Pu and MA in the waste; higher long term radioactivity and radio-toxicity due to the decay products of the long-lived ^{233}U; smaller throughput of Pu and MA, lower (fissile Pu)/Pu ratio, higher ^{238}Pu/Pu ratio, higher specific decay heat of the Pu, higher spontaneous fission rate of the Pu. The discharged plutonium from RBWR-Th is less attractive than that from RBWR-AC. Significant amount of ^{233}U is recycled for RBWR-Th core but the ^{233}U discharged is contaminated with significant concentration of ^{232}U whose decay daughters are strong gamma emitters.

However, relative to the ARR, the RBWR-Th core features a significantly lower average discharge burnup due to its softer neutron spectra. This, along with smaller thermal efficiency, lead to a significantly larger capacity required for fuel cycling that result in a higher fuel cycle cost and less favorable waste characteristics – higher radioactivity along with higher inhalation and ingestion toxicity. On the other hand, the plutonium discharged from the RBWR cores has a lower (fissile Pu)/Pu ratio, a larger ^{238}Pu/Pu

ratio and, therefore, higher specific decay heat along with higher spontaneous fission rate making this plutonium of lower attractiveness for weapon-use than the Pu recycled from ARR.

The overall fuel cycle evaluation concluded that the RBWR core can successfully accomplish the missions previously assigned to SFR and score similarly to ARR-based fuel cycle in terms of nuclear waste management, environmental impact, and resource utilization.

Table 11. Performance Metrics for the RBWR-AC, the AC-equivalent RBWR-Th, and the ARR

	Parameters	RBWR-Th	RBWR-AC	ARR
Design Parameters	Reactor power, MWt/MWe	3926/1356	3926/1356	1000/400
	Feed fuel	Thorium+DU	DU	DU
	Pressure drop, MPa	0.13	0.14	N/A
	Coolant flow rate, kg/sec	6358	7222	~5729
	Void fraction correlation	RELAP	RELAP	N/A
	Critical power ratio correlation	H-CISE	H-CISE	N/A
	Outlet void fraction	89%	81%	-
	Pin pitch-to-diameter ratio	1.13	1.13	1.10
	Fuel pin OD, cm	1.005	1.005	0.808
	Pins per assembly	271	271	271
	Fuel smeared density	89.9%	89.9%	75%
	Number of fuel assembly	720	720	151
Fuel Cycle Characteristics	Capacity Factor, %	90	90	85
	Average discharge burnup, GWD/t	48.8	45	73.0
	Power density, W/cc	61.1	73.8	122.4
	Peak LHGR, W/cm	261	472	389
	Fuel inventory in core, t	153.0	144.0	16.7
	Cycle length per batch, EFPD	412	389	370
	Burnup reactivity swing, %Δk/k	-1.9	-1.5	0.1
	TRU transmutation efficiency	-1%	0%	0%
	Reprocessing capacity, kg/GWeYr			
	Aqueous reprocessing	-	-	-
	Electro-chemical reprocessing	21664.2	23483.9	12500.0
	Charge mass fraction, %			
	- Th232	65.4	-	-
	- TransTh	6.8	-	-
	- U238	22.5	87.5	86.3
	- TRU	5.4	12.5	13.7
	Discharge mass fraction, %			
	- Th232	62.4	-	-
	- TransTh	6.9	-	-
	- U238	20.8	82.9	78.5
	- TRU	5.4	12.6	13.7
	- FPs	4.6	4.6	7.8
	Fuel mass at time of recycle, %			

	- Th232	62.4	-	-
	- TransTh	6.9	-	-
	- U238	20.8	82.9	78.5
	- TRU	5.4	12.5	13.7
	- FPs	4.6	4.6	7.8
Nuclear Waste	Radioactivity at 10 Yrs, Ci/GWe-Yr	9.50E+06	8.32E+06	7.10E+06
	Radioactivity at 100,000 Yrs, Ci/GWe-Yr	1.16E+03	5.62E+02	4.89E+02
	Inhalation Radiotoxicity at 10 Yrs, Sv/GWe-Yr	8.52E+10	1.46E+11	4.16E+10
	Inhalation Radiotoxicity at 100,000 Yrs., Sv/GWe-Yr	6.85E+08	2.50E+08	1.83E+08
	Ingestion Radiotoxicity at 10 Yrs , Sv/GWe-Yr	3.60E+09	2.79E+09	2.19E+09
	Ingestion Radiotoxicity at 100,000 Yrs , Sv/GWe-Yr	2.97E+06	8.01E+05	4.74E+05
Proliferation Resistance	Fissile plutonium fraction at reprocessing, %	55%	52%	69%
	^{238}Pu/Pu ratio at reprocessing, %	6.4%	3.2%	1.4%
	Specific decay heat of plutonium at reprocessing, W/kg	39.69	22.01	11.21
	Tot. plutonium reprocessed, tons/GWe-yr	1.04	2.72	1.64
	Spontaneous fission neutrons per kg Pu at reprocessing, n/sec-kg	5.6E+05	5.3E+05	3.3E+05
	Pu/^{238}U ratio at reprocessing	23%	14%	17%
	^{232}U/^{233}U ratio at reprocessing, ppm	5429	-	-
	Fissile U/U ratio at reprocessing, %	17%	-	-
	Fissile U/Th ratio at reprocessing	7%	-	-
	(Pu+fissile U)/(238U+Th) ratio at reprocessing	10%	14%	17%
Economics	Fuel cycle cost (cents/kWe-h)	1.386	1.501	0.847
	- Fuel Mining/ Conversion/ Fabrication	0.003	0.001	0.001
	- Electrochemical Separation + Remote Fuel	1.268	1.374	0.732
	- Geologic Repository	0.116	0.126	0.115
	- TRU Separation	0.000	0.000	0.000
Fuel Cycle Evaluation	Mass of SNF+HLW disposed	A	A	A
	Activity of SNF+HLW (@100 years)	C	B	A
	Activity of SNF+HLW (@100,000 years)	C	B	B
	Mass of DU+RU+RTh disposed	A	A	B
	Volume of LLW	D	D	A
	Land use per energy generated	A	A	C
	Water use per energy generated	B	B	A
	Radiological exposure	B	B	B
	Carbon emission - CO2 released per energy generated	B	B	B
	Natural Uranium required per energy generated	A	A	A

7. Comparison of RBWR-TR versus RBWR-TB2 and ABR

Selected design, performance and fuel cycle characteristics of the RBWR-TR were compared in Table 12 against those of the RBWR-TB2 and CR=0.5 ABR – their sodium-cooled counterpart. All three designs feature a conversion ratio of roughly 0.5.

It is found that relative to the RBWR-TB2, the RBWR-TR features a slightly lower discharge burnup along with lower peak discharge burnup; significantly lower peak linear heat generation rate and lower specific power; higher HM reprocessing rate; much lower TRU fraction in the charge fuel as very few TRU are bred from thorium-based fuel cycle; lower fuel residence times; a much lower fraction of fissile-to-total plutonium as well as significantly higher decay heat and spontaneous fission rate of the discharged Pu – less favorable for weapon-use. The two TRU transmuting RBWR cores have comparable TRU transmutation rates per unit of electricity generated, and both PWR support ratios are approximately 2.

Relative to the CR=0.5 ABR, the RBWR-TR has roughly a third the discharge burnup and lower power density, a slightly higher TRU fission efficiency and more TRU consumed per GWeY – mainly due to the lower thermal efficiency of RBWR core; higher HM reprocessing per unit electricity generated; longer cycles but smaller cycle reactivity swing over a cycle; a significantly smaller amount of TRU per HM mass discharged as a thorium reactor; has a smaller fissile-to-total mass of plutonium; and significantly higher decay heat and spontaneous fission rate so that the discharged plutonium has very high proliferation resistance.

Unlike the RBWR-TB2 and the ABR, the RBWR-TR discharges uranium with a significant amount of ^{233}U. Over 60% of this uranium is fissile, which could cause it to be a proliferation concern. However, the large amount of thorium (>70% of the discharge fuel) in the discharge fuel mitigates the attractiveness for weapons purposes somewhat. The ^{233}U discharge from RBWR-TR is also contaminated with high level of ^{232}U so a large radiation dose is expected.

The overall fuel cycle evaluation shows that RBWR-TR can fully deliver the functions proposed for ABR – reducing the waste from contemporary LWR fleet and improving the fuel utilization – with more mature LWR technology.

Table 12. Performance Metrics for the TB2-equivalent RBWR-TR, the RBWR-TB2, and the ABR

	Parameters	RBWR-TR	RBWR-TB2	ABR
Design Parameters	Reactor power, MWt/MWe	3926/1356	3926/1356	1000/400
	Feed fuel	Thorium+DU +LWR's TRU	DU+LWR's TRU	DU+LWR's TRU
	Pressure drop, MPa	0.15	0.06	N/A
	Coolant flow rate, kg/sec	17395	6667	~5599
	Void fraction correlation	RELAP	RELAP	N/A
	Critical power ratio correlation	M-CISE	H-CISE	N/A
	Core Outlet void fraction	69%	80%	-
	Pin pitch-to-diameter ratio	1.34	1.30	1.29
	Fuel pin OD, cm	0.705	0.724	0.623
	Pins per assembly	397	397	324
	Fuel smeared density	89.9%	89.9%	75.0%
	Number of fuel assembly	720	720	144
Fuel Cycle Characteristics	Capacity Factor, %	90	90	85
	Average discharge burnup, GWD/t	55.0	65.0	131.9
	Power density, W/cc	76.3	96.7	130.4
	Peak LHGR, W/cm	189	470	327
	Fuel inventory in core, t	89.7	73.0	9.5
	Cycle length per batch, EFPD	313	304	221
	Burnup reactivity swing, %Δk/k	-2.0	-2.5	-2.9
	TRU transmutation efficiency	48%	44%	45%
	TRU transmutation rate, kg/GWeYr	453.6	455.3	396.8
	Reprocessing capacity, kg/GWeYr			
	Aqueous reprocessing	14098.4	14117.0	13435.8
	Electro-chemical reprocessing	6844.7	5777.9	2673.8
	Charge mass fraction, %			
	- Th232	78.2	-	-
	- TransTh	7.4	-	-
	- U238	-	67.3	66.7
	- TRU	14.4	32.7	33.3
	Discharge mass fraction, %			
	- Th232	75.7	-	-
	- TransTh	7.4	-	-
	- U238	-	63.9	59.6
	- TRU	12.2	30.0	27.6
	- FPs	4.7	6.1	12.8
	Fuel mass at time of recycle, %			
	- Th232	75.7	-	-
	- TransTh	7.5	-	-
	- U238	-	64.0	59.7
	- TRU	12.1	29.9	27.5

	- FPs	4.7	6.1	12.8
Nuclear Waste	Radioactivity at 10 Yrs, Ci/GWe-Yr	9.49E+06	9.18E+06	8.66E+06
	Radioactivity at 100,000 Yrs, Ci/GWe-Yr	7.44E+02	5.61E+02	5.02E+02
	Inhalation Radiotoxicity at 10 Yrs, Sv/GWe-Yr	1.57E+11	1.56E+11	5.49E+10
	Inhalation Radiotoxicity at 100,000 Yrs , Sv/GWe-Yr	2.62E+08	1.42E+08	8.07E+07
	Ingestion Radiotoxicity at 10 Yrs , Sv/GWe-Yr	3.71E+09	3.44E+09	3.06E+09
	Ingestion Radiotoxicity at 100,000 Yrs , Sv/GWe-Yr	1.48E+06	7.60E+05	3.83E+05
Proliferation Resistance	Fissile plutonium fraction at reprocessing, %	27%	35%	46%
	^{238}Pu/Pu ratio at reprocessing, %	19.1%	7.6%	4.1%
	Specific decay heat of plutonium at reprocessing, W/kg	111.46	46.95	26.94
	Tot. plutonium reprocessed, tons/GWe-yr	1.76	4.23	1.67
	Spontaneous fission neutrons per kg Pu at reprocessing, n/sec-kg	1.1E+06	8.1E+05	6.5E+05
	Pu/^{238}U ratio at reprocessing	Infinite	41%	41%
	^{232}U/^{233}U ratio at reprocessing, ppm	8053	-	-
	Fissile U/U ratio at reprocessing, %	63%	-	-
	Fissile U/Th ratio at reprocessing	6%	-	-
	(Pu+fissile U)/(238U+Th) ratio at reprocessing	17%	41%	41%
Economics	Fuel cycle cost (cents/kWe-h)	0.996	0.937	0.727
	- Fuel Mining/ Conversion/ Fabrication	0.269	0.267	0.255
	- Electrochemical Separation + Remote Fuel	0.401	0.338	0.156
	- Geologic Repository	0.162	0.166	0.159
	- TRU Separation	0.165	0.165	0.157
Fuel Cycle Evaluation	Mass of SNF+HLW disposed	A	A	A
	Activity of SNF+HLW (@100 years)	C	B	C
	Activity of SNF+HLW (@100,000 years)	B	B	B
	Mass of DU+RU+RTh disposed	D	D	E
	Volume of LLW	D	D	C
	Land use per energy generated	B	B	B
	Water use per energy generated	B	B	B
	Radiological exposure	B	B	B
	Carbon emission - CO2 released per energy generated	B	B	B
	Natural Uranium required per energy generated	C	C	C

8. Technical Gap Analysis and Roadmap

The RBWR core designs described in the previous sections employ tight lattices cooled by light water to produce a hard enough neutron spectrum to enable the RBWR to perform functions traditionally assigned to fast spectrum reactors -- sustainability (conversion ratio ~1.0) and transmutation of TRU from LWR. The designs are of essentially a new fuel, fuel assembly and core rather than a new reactor and are intended to fit within the pressure vessel of an ABWR. The core designs are significantly different from a conventional ABWR (or any other light-water reactor) and the operating parameters and environment present new challenges.

Mechanical design/fabrication/performance: The fuel rods, hexagonal assembly lattice and y-shaped control rods are significantly different from those of an ABWR. While the specific rod diameter and pitch-to-diameter ratio depend on whether the system is intended to be self-sustaining or a burner, these parameters are closer to those of a sodium fast reactor than an ABWR. The active length of the fuel rods of one variant of the RBWR cores are significantly longer than that of an SFR but not longer than that of the ABWR. Whether grid spacers or wire-wrap are used will affect the mechanical "rigidity" of the assembly under operating, refueling and transportation conditions. On the other hand, the total coolant flow rates of the RBWR cores are lower than of the ABWR. This and the shorter fuel lead to different total forces of vibration and liftoff.

Thermal-Hydraulic Performance: The performance and the details of the designs described in this paper are extremely sensitive to the assumed void fraction and critical power correlations. There are unacceptable uncertainties in these correlations due to very limited relevant experimental data on void fraction and critical power for the tight lattices. Validation of these correlations for the conditions in RBWR cores will require additional experiments including appropriately scaled test sections. Experiments may be required also for determining the axially dependent void fraction along the bypass channels between fuel assemblies.

Fuel and Cladding Performance and Qualification: Validation/confirmation of the performance of the fuel and cladding under conditions that are atypical for a water-cooled reactor will require experiments. Issues include fuel pellet swelling, fission product transport/release, fuel pellet chemical/mechanical interaction, clad performance under high fluence of high-energy neutrons and, in particular, hydrogen pickup and corrosion in the high energy neutron and high void water environment. Extrapolation of current knowledge to the RBWR conditions implies that use of Zircaloy2 may not be feasible. Executing a roadmap for fuel qualification for either the transmuting or the self-sustaining RBWRs (both using ThO_2 as the primary fuel constituent, as well as a new cladding material) would be expected to take a decade or longer.

Reactor Physics: The tight-lattice, the use of thorium, the strongly axially varying water density, the radially heterogeneous fuel assembly design and intermediate neutron spectrum present challenges for analytic tools, although significant progress has been made in this project as described earlier. The nuclear data for intermediate spectrum tends to be sparse and have greater uncertainties, in particular for thorium and trans-thorium isotopes, than for conventional LWRs or SFRs. Differential and integral experiments (e.g., criticality) may be necessary to improve the quality of data evaluations, benchmark computational tools, confirm design predictions, and reduce uncertainties.

Out of Core Components: The harder neutron spectrum will increase the heating and radiation induced damage in the in-vessel components and the pressure vessel. Also, the performance of balance-of plant components such as the steam separator need to be confirmed as the design core outlet steam quality of the RBWR is about three times that of the ABWR. No major problem is envisioned as the total steam flow rate into the steam separators will be the same as for similar powered ABWR but with much less water. This will lead to a smaller recirculation ratio in the vessel. It also implies that fewer separators may be required.

Reprocessing: Commercial thorium fuel reprocessing and recycling capability will have to be developed. Reprocessing of axially heterogeneous fuel with uranium and thorium involves additional complexities to recycling of the RBWR fuels.

Licensing: Licensing of the RBWR variants described earlier (as for any reactor concept) will require validated tools for nuclear, thermal-hydraulic, and mechanical performance of the fuel and core components in steady state and transient/accident conditions. This will generally require both in-core and ex-core experiments to generate the needed data for the computational models, and demonstrate adequate safe performance.

Economics: Relative to the its sodium-cooled fast reactor counterpart (ARR), the RBWR-Th using the Hitachi T/H correlations features roughly one third the core power density and specific power; ~70% of the discharge burnup; roughly the same Trans-Fertile Fuel (TRF) loading; a ~55% higher rate of HM reprocessing; and double the TRF discharge per unit of electricity generated. Significantly lower power density and specific power are featured by the RBWR-Th when designed using the MIT-recommended T/H correlations. Relative to the reference ABR, the RBWR-TR has roughly a third the discharge burnup, power density, and specific power; requires more TRF loading, HM reprocessing, and TRF discharge per unit electricity generated. As a result, the fuel cycle cost of the RBWRs is estimated to be higher than that of a similarly performing SFR by close to 50%. However, the capital cost of the ABWRs is presently lower than that of SFRs and this may compensate for the higher fuel cycle cost of the RBWRs. In addition, the technology of the RBWR, excluding its fuel, is more mature and accepted by the nuclear industry than that of SFR. A detailed economic analysis is required before the economic viability of the RBWR could be determined.

9. Conclusions and summary

The major findings and conclusions of this project are listed in the Executive Summary. Tables 13 to 18 summarize important design and performance characteristics of the two out of the three thorium-based RBWR cores designed in this project – the fuel-self-sustaining RBWR-ThH and the TRU transmuting RBWR-TR – and compares them with those of the uranium-based Hitachi RBWR cores as well as of the reference SFR cores. The most important conclusions are that it is possible to design an effective LWR TRU transmuting thorium based RBWR but improved cladding material will have to be found for this reactor concept to realize its full potential. The feasibility of a viable fuel-self-sustaining RBWR design is not certain; it could be determines only after additional experimental data will be generated on the void fraction and critical power in tight, low mass flow rate boiling water fuel bundles and on the behavior of advanced structural materials under elevated fluences of high energy neutrons.

Table 13 Design characteristics of the RBWR-ThH and RBWR-TR cores in comparison with the Hitachi RBWR and SFR reference core

Parameter	RBWR-ThH	RBWR-AC	ARR	RBWR-TR	RBWR-TB2	ABR
Reactor power, MWt	3926	3926	1000	3926	3926	1000
MWe	1356	1356	400	1356	1356	400
Feed fuel	Thorium +DU	DU	DU	Th+DU+LWR TRU	DU+LWR TRU	DU+LWR TRU
Conversion ratio	1.0	1.0	1.0	0.5	0.5	0.5
Pressure drop, MPa	0.13	0.14	N/A	0.15	0.06	N/A
Coolant flow rate, kg/sec	6358	7222	~5729	17395	6667	~5599
Void fraction correlation	RELAP	RELAP	N/A	RELAP	RELAP	N/A
Critical power ratio correlation	H-CISE	H-CISE	N/A	M-CISE	H-CISE	N/A
Core Outlet void fraction	89%	81%	-	69%	80%	-
Pin P/D ratio	1.13	1.13	1.10	1.34	1.30	1.29
Fuel pin OD (D), cm	1.005	1.005	0.808	0.705	0.724	0.623
Pins per assembly	271	271	271	397	397	324
Fuel smeared density	89.9%	89.9%	75%	89.9%	89.9%	75.0%
Number of fuel assemblies	720	720	151	720	720	144

Table 14 Performance characteristics of the RBWR-ThH and RBWR-TR cores in comparison with the Hitachi RBWR and SFR reference core

Parameter	RBWR-ThH	RBWR-AC	ARR	RBWR-TR	RBWR-TB2	ABR
Capacity Factor, %	90	90	85	90	90	85
Average discharge burnup, GWD/t	48.8	45	73.0	55.0	65.0	131.9
Power density, W/cc	61.1	73.8	122.4	76.3	96.7	130.4
Peak LHGR, W/cm	261	472[8]	389	189	470	327
Fuel inventory in core, t	153.0	144.0	16.7	89.7	73.0	9.5
Cycle length per batch, EFPD	41	389	370	313	304	221
Burnup reactivity swing, %Δk/k	-1.9	-1.5	0.1	-2.0	-2.5	-2.9
TRU transmutation efficiency	-1%	0%	0%	48%	44%	45%
Reprocessing capacity, kg/GWeYr						

[8] Recent analysis by the University of Michigan collaborators came up with a peak LHGR of 75 kW/m and 55 kW/m for, respectively, the RBWR-AC and RBWRE-TB2

Aqueous				14098	14117	13436
Electro-chemical	21664	23484	12500	6845	5778	2674
Charge mass fraction, %						
Th232	65.4	-	-	78.2	-	-
TransTh	6.8	-	-	7.4	-	-
U238	22.5	87.5	86.3	-	67.3	66.7
TRU	5.4	12.5	13.7	14.4	32.7	33.3
Discharge mass fraction, %						
Th232	62.4	-	-	75.7	-	-
TransTh	6.9	-	-	7.4	-	-
U238	20.8	82.9	78.5	-	63.9	59.6
TRU	5.4	12.6	13.7	12.2	30.0	27.6
FPs	4.6	4.6	7.8	4.7	6.1	12.8
Fuel mass at time of recycle, %						
Th232	62.4	-	-	75.7	-	-
TransTh	6.9	-	-	7.5	-	-
U238	20.8	82.9	78.5	-	64.0	59.7
TRU	5.4	12.5	13.7	12.1	29.9	27.5
FPs	4.6	4.6	7.8	4.7	6.1	12.8

Table 15 Waste characteristics of the RBWR-ThH and RBWR-TR cores in comparison with the Hitachi RBWR and SFR reference cores

Parameter	RBWR-ThH	RBWR-AC	ARR	RBWR-TR	RBWR-TB2	ABR
Radioactivity at 10 Yrs (Ci/GWe-Yr)	9.50E+06	8.32E+06	7.10E+06	9.46E+06	9.18E+06	8.66E+06
Radioactivity at 100,000 Yrs (Ci/GWe-Yr)	1.16E+03	5.62E+02	4.89E+02	7.44E+02	5.61E+02	5.02E+02
Inhalation Radiotoxicity at 10 Yrs (Sv/GWe-Yr)	8.52E+10	1.46E+11	4.16E+10	1.57E+11	1.56E+11	5.49E+10
Inhalation Radiotoxicity at 100,000 Yrs (Sv/GWe-Yr)	6.85E+08	2.50E+08	1.83E+08	2.62E+08	1.42E+08	8.07E+07
Ingestion Radiotoxicity at 10 Yrs (Sv/GWe-Yr)	3.60E+09	2.79E+09	2.19E+09	3.71E+09	3.44E+09	3.06E+09
Ingestion Radiotoxicity at 100,000 Yrs (Sv/GWe-Yr)	2.97E+06	8.01E+05	4.74E+05	1.48E+06	7.60E+05	3.83E+05

Table 16 Proliferation resistant characteristics of the RBWR-ThH and RBWR-TR cores in comparison with the Hitachi RBWR and SFR reference cores

Parameter	RBWR-ThH	RBWR-AC	ARR	RBWR-TR	RBWR-TB2	ABR
Tot. plutonium reprocessed, tons/GWe-yr	1.04	2.72	1.64	1.79	4.23	1.67
Fissile plutonium fraction %	55%	52%	69%	27%	35%	46%
^{238}Pu/Pu ratio, %	6.4%	3.2%	1.4%	19.1%	7.6%	4.1%
Specific decay heat of Pu at reprocessing, W/kg	39.69	22.01	11.21	111.46	46.95	26.94
Pu/^{238}U ratio at reprocessing	23%	14%	17%	Infinite	41%	41%
Spontaneous fission neutrons per kg Pu at reprocessing, n/sec-kg	5.6E+05	5.3E+05	3.3E+05	1.1E+06	8.1E+05	6.5E+05
^{232}U/^{233}U ratio at reprocessing, ppm	5429	-	-	8053	-	-
Fissile U/U ratio at reprocessing, %	17%	-	-	63%	-	-
Fissile U/Th ratio at reprocessing	7%	-	-	6%	-	-
(Pu+fissile U)/(238U+Th) ratio at reprocessing	10%	14%	17%	17%	41%	41%

Table 17 Fuel cycle cost of the RBWR-ThH and RBWR-TR cores in comparison with the Hitachi RBWR and SFR reference cores

Parameter	RBWR-ThH	RBWR-AC	ARR	RBWR-TR	RBWR-TB2	ABR
Total fuel cycle cost (cents/kWe-h)	1.386	1.501	0.847	0.996	0.937	0.727
- Fuel Mining/ Conversion/ Fabrication	0.003	0.001	0.001	0.269	0.267	0.255
- Electrochemical Separation + Remote Fuel Fabrication	1.268	1.374	0.732	0.401	0.338	0.156
- Geologic Repository	0.116	0.126	0.115	0.162	0.166	0.159
- TRU Separation	0.0	0.0	0.0	0.165	0.165	0.157

Table 18 Applying USDOE Fuel Cycle Evaluation & Screening metrics to rank the RBWR-ThH and RBWR-TR cores in comparison with the Hitachi RBWR and SFR reference cores

Parameter	RBWR-ThH	RBWR-AC	ARR	RBWR-TR	RBWR-TB2	ABR
Mass of SNF+HLW disposed, t/GWe-yr	A	A	A	A	A	A
Activity of SNF+HLW (@100 years), MCi/GWe-yr	C	B	A	C	B	C
Activity of SNF+HLW (@100,000 years), 10-4 MCi/GWe-Yr	C	B	B	B	B	B
Mass of DU+RU+RTh disposed, t/GWe-yr	A	A	B	D	D	E
Volume of LLW, m3/GWe-yr	D	D	A	D	D	C
Land use per energy generated, km2/GWe-yr	A	A	C	B	B	B
Water use per energy generated, ML/GWe-yr	B	B	A	B	B	B
Radiological exposure, Sv/GWe-yr	B	B	B	B	B	B
Carbon emission - CO2 released per energy generated, kt CO2/GWe-yr	B	B	B	B	B	B
Natural Uranium required per energy generated, t/GWe-yr	A	A	A	C	C	C

REFERENCES

1. R. TAKEDA, J. MIWA and K. MORIYA, "BWRs for Long-term Energy Supply and for Fissioning Almost All Transuraniums," Proc. GLOBAL 2007, Boise, Idaho, September 9-13 (2007).
2. R. TAKEDA, J. MIWA and K. MORIYA, "RBWRs for Fissioning Almost All Uranium and Transuraniums," Transactions of the American Nuclear Society, vol. 107, p. 853 (2012).
3. T. Hino, M. Ohtsuka, R. Takeda, J. Miwa, Y. Ishii, "Core Designs of RBWR (Resource-renewable BWR) for Recycling and Transmutation of Transuranium Elements - an Overview," Proc. of ICAPP-2014, Charlotte, NC, April 6-9 2014.
4. T. DOWNAR, A. HALL, D. JABBAY, A. WARD, E. GREENSPAN, F. GANDA, F. BARTOLONI, R. BERGMANN, C. VARELA, C. DISANZO, M. KAZIMI, A. KARAHAN, E. SHWAGERAUS, B. FENG, B. HERMAN, "Technical Evaluation of the Hitachi Resource-Renewable BWR (RBWR) Design Concept," EPRI Technical Report 1025086 (2012).
5. "Comparison between the RBWR-Th, Hitachi RBWRs and SFRs," Attachment 8.
6. T.K. Kim, W.S. Yang, C. Grandy and R.N. Hill, "Core design studies for a 1000 MW_{th} Advanced Burner Reactor," Annals of Nuclear Energy 36 (2009) 331–336
7. Francesco Ganda, Jasmina Vujic, Ehud Greenspan, "Thorium self sustaining BWR core with tight lattice", ICAPP-11, Nice, May 2-6, 2011

8. Francesco Ganda, Francisco J. Arias, Jasmina Vujic and Ehud Greenspan, “Self-Sustaining Thorium Boiling Water Reactors,” Sustainability 2012, 4, 2472-2497
9. R. Atherton, Coordinator and LWBR Staff, “Light Water Reactor Breeder Program Summary Report,” WAPD-TM-1600, October 1987.
10. Y. Ronen, *High converting water reactors*, CRC press, 1990.
11. Galperin, A., Reichert, P., Radkowsky, A., 1997. A thorium fuel cycle for light water reactor reducing proliferation potential of nuclear power fuel cycle. Science & Global Security 6, 265–290.
12. A. Radkowsky, A. Galperin, “The Nonproliferative Light Water Thorium Reactor: A New Approach To Light Water Reactor Core Technology”, *Nuclear Technology* **Vol. 124** Dec. 1998
13. A. Galperin, M. Segev and M. Todosow, “A Pressurized Water Reactor Plutonium Incinerator Based On Thorium Fuel And Seed-Blanket Assembly Geometry”, Nuclear Technology **Vol. 132** Nov. 2000
14. H. Takahashi, J. J. Zhang, D. Cokinos, T. Downar and J. Cetnar, “Pu and Th Fueled Tight Lattice Light Water Reactor (LWR) with Hard Neutron Spectrum,” Proc. 12th Pacific Basin Nuclear Conf. (PBNC’00), Seoul, Korea, October 15–19, 2000.
15. T. K. Kim and T. J. Downar “Thorium Fuel Performance in a Tight-Pitch Light Water Reactor Lattice”, Nuclear Technology, Vol. 138, Apr. 2002.
16. Alexander Galperin, Eugene Shwageraus, Michael Todosow, “Assessment Of Homogeneous Thorium-Uranium Fuel For Pressurized Water Reactors,” Nuclear Technology Vol. 138 May 2002
17. M. Todosow, A. Galperin, S. Herring, M. Kazimi, T. Downar and A. Morozov, “Use Of Thorium In Light Water Reactors”, Nuclear Technology Vol. 151 Aug. 2005
18. N. Takaki, S. Permana, H. Sekimoto, “Feasibility of Water Cooled Thorium Breeder Reactor Based on LWR Technology”, Global 2007, Boise, Idaho, September 9-13, 2007
19. E. Shwageraus, D. Volaski and E. Fridman, “Investigation of Fuel Assembly Design Options for High Conversion Thorium Fuel Cycle in PWRs”, ANFM 2009, South Carolina (2009).
20. National Nuclear Data Center, ENDF/B-VII.1, BNL, December 2011.
21. X-5 Monte Carlo Team, “MCNP — A General Monte Carlo N-Particle Transport Code, Version 5, Volume II: User’s Guide” Technical Report LA-CP-03-0245, LANL, Los Alamos, NM, USA (2003).
22. A. Cross, “A User’s Manual for the ORIGEN2 Computer Code,” Technical Report TM-7175, ORNL, Oak Ridge, TN, USA (1980).
23. A. Wysocki, Y. Xu, B. Collins, A. Manera, T. Downar, “PATHS: PARCS Advanced Thermal Hydraulic Solver,” University of Michigan (2012).
24. B. Herman, “SerpentXS Documentation,” Massachusetts Institute of Technology (2011).
25. A. Ward, Y. Xu, T. Downar, “GenPMAXS – v6.1.2ucb, Code for Generating the PARCS Cross Section Interface File PMAXS”, University of Michigan (2013).
26. T. Downar, Y. Xu, V. Seker, “PARCS v3.0 U.S. NRC Core Neutronics Simulator User Manual”, University of Michigan (2010).
27. K. Shirvan, M.S Kazimi, “STABILITY ANALYSIS OF BWR-HD: AN OPTIMIZED BOILING WATER REACTOR WITH HIGH POWER DENSITY,” Nuclear Technology, 184, 2013
28. US NRC, “TRACE V5.0: Theory Manual,” Division of Safety Analysis, Washington DC, 2012.
29. K. Shirvan et al., “Stability and Safety analysis of Tight Lattice Breeding LWR,” Proceedings of ICAPP, 14276, 2014.
30. GE, “ABWR Design Control Document/Tier 2," Available from NRC.gov (2007).
31. K. Shirvan, N. Andrews, M. Kazimi, “Best Estimate Void Fraction and Critical Power Correlations for Tight Lattice BWR Bundles,” ICAPP, Korea, (2013).

32. W. Liu, M. Kureta, H. Yoshida, H. Tamai, A. Ohnuki and H. Akimoto, " Critical Power Characteristics in 37-rod Tight Lattice Bundles under Transient Conditions," Journal of Nuclear Science and technology, 44, no. 4, pp. 1172-1181 (2007).
33. T. Downar et al., "Transient Safety Analysis of Fast Spectrum TRU Burning LWRs with Internal Blankets," DOE NEUP Final Report, 89536, 2015.
T. Downar et al., "Transient Safety Analysis of Fast Spectrum TRU Burning LWRs with Internal Blankets," DOE NEUP Final Report, 89536, 2015.

Project Related Publications

1. C. R. Varela J. Seifried, J. Vujic, E. Greenspan, "Sensitivity of Thorium-Fueled Reduced Moderation BWR Performance to Void Fraction Correlation," Transactions 2013 ANS Annual Meeting, Atlanta, Georgia, June 16-20, 2013.
2. G. Zhang, J. Seifried, J. Vujic and E. Greenspan, "Variable Enrichment Thorium-Fueled Boiling Water Breeder Reactor", Transactions 2013 ANS Annual Meeting, Atlanta, Georgia, June 16-20, 2013.
3. G. Zhang, J. Seifried, J. Vujic and E. Greenspan, "Analysis of Local Void Reactivity Coefficients for the RBWR-Th," Transactions 2013 ANS Annual Meeting, Atlanta, Georgia, June 16-20, 2013.
4. A. Hall, Y. Xu, A Ward, T. Downar, K. Shirvan and M. Kazimi, "Advanced Neutronics Methods for Analysis of the RBWR-AC", Transactions 2013 ANS Annual Meeting, Atlanta, Georgia, June 16-20, 2013.
5. J.E. Seifried, P.M. Gorman, J.L. Vujic, and E. Greenspan, "Accelerated Equilibrium Core Composition Search Using a New MCNP-Based Simulator," Joint International Conference on Supercomputing in Nuclear Applications and Monte Carlo 2013 (SNA + MC 2013), La Cité des Sciences et de l'Industrie, Paris, France, October 27–31, 2013.
6. J.E. Seifried, G. Zhang, C.R. Varela, P.M. Gorman, E. Greenspan, and J.L. Vujic, "Self-Sustaining Thorium-Fueled BWR," The fourth International Symposium on Innovative Nuclear Energy Systems (INES-4), Tokyo, Japan, November 6-8, 2013. To be published in Energy Procedia, 2014.
7. P.M. Gorman, G. Zhang, J.E. Seifried, C.R. Varela, J.L. Vujic and E. Greenspan, "The fuel-self-sustaining RBWR-Thorium core concept and parametric study results," International Congress on the Advances in Nuclear Power Plants - ICAPP 2014, , Charlotte, North Carolina, April 6-9, 2014.
8. Andrew Hall, Thomas Downar, Andrew Ward, Michael Jarrett, Aaron Wysocki, Yunlin Xu and Koroush Shirvan, "Advanced Methods Development for Equilibrium Cycle Calculations of the RBWR," Accepted for ICAPP-2014, Charlotte, USA, April 6-9, 2014
9. K. Shirvan (MIT), M.S. Kazimi (MIT), L. Cheng (BNL), M. Todosow (BNL), A. Hall (UM), M. Jarrett (UM), A. M. Ward(UM), T. J. Downar (UM), "Stability and Safety analysis of Tight Lattice Breeding LWR," Accepted for ICAPP-2014, Charlotte, USA, April 6-9, 2014
10. J.E. Seifried, P.M. Gorman, E. Greenspan, C.R. Varela, J.L. Vujic, and G. Zhang, "Comparison of RBWR and SFR design and performance characteristic," International Congress on the Advances in Nuclear Power Plants - ICAPP 2014, Charlotte, North Carolina.

11. Alexander J. Mieloszyk and Mujid S. Kazimi, “Analysis of Fuel Performance in Reduced Moderation Boiling Water Reactors,” ICAPP-2014, Charlotte, North Carolina, April 6-9, 2014.

12. Phillip M. Gorman, Jasmina L. Vujic and Ehud Greenspan, “Tradeoff studies for the fuel-self-sustaining RBWR-Th core,” Submitted to Nuclear Technology, 2014.

13. Phillip Gorman, Sandra Bogetic, Jia Hou, Jeffrey E. Seifried, Guanheng Zhang, Jasmina Vujic and Ehud Greenspan, “Thorium Fuelled Resource-Renewable BWR (RBWR) Design Update”, Transactions ANS Winter Meeting, Anaheim, CA, November 2014

14. J. Seifried and E. Greenspan, “Analysis of void coefficient of reactivity in reduced moderation BWR,” submitted to Nuclear Science and Engineering, 2014.

15. Phillip Gorman, Sandra Bogetic, Guanheng Zhang, Massimiliano Fratoni, Jasmina Vujic, and Ehud Greenspan, “The TRU-incinerating thorium RBWR core preliminary design,” Advances in Nuclear Fuel Management V – ANFM 2015, Hilton Head, South Carolina, March 29 – April 1 2015.

16. Phillip Gorman, Sandra Bogetic, Guanheng Zhang, Massimiliano Fratoni, Jasmina Vujic, and Ehud Greenspan, “The fuel self-sufficient RBWR-Th core designs,” GLOBAL 2015, Paris, France, September 20-24, 2015.

17. G. Zhang, P. M. Gorman, M. Fratoni, E. Greenspan. “Comparison of Reduced-moderation Boiling Water Reactor and Sodium-cooled Fast Reactor Technologies” (submit soon to a journal)

18. N. R. Brown, J. J. Powers, B. Feng, F. Heidet, N. E. Stauff, G. Zhang, M. Todosow, A. Worrall, J. C. Gehin, T. K. Kim, T. A. Taiwo. “Sustainable Thorium Fuel Cycles: A Comparison of Intermediate and Fast Neutron Spectrum Systems” (submitted to Energy Conversion and Management)

19. B. Feng, G. Zhang, T. K. Kim, and T. A. Taiwo (2014). Continuous Recycling of U-233/Th in Intermediate Spectrum Reactors. ANL-FCT-346, US-DOE

20. F. Ganda, G. Zhang, T. K. Kim, and T. A. Taiwo (2014). U/TRU and U/Pu with New Natural-UTh Fuel in Intermediate Spectrum Critical Reactors Using Water Coolant. ANL-FCT-347, US-DOE.

21. G. Zhang, P. Gorman, S. Bogetic, M. Fratoni, E. Greenspan (2015). Fuel Cycle Analysis of the Thorium Fueled Reduced-Moderation BWRs (RBWR). GLOBAL 2015 (submit soon)

22. F. Ganda, N. Brown, H. Hiruta, T.K. Kim, G. Raitses, T. Taiwo, M. Todosow, R. Wigeland, G. Youinou, G. Zhang (2015). Systems Using Water-cooled Reactor Technology to Achieve Fast Reactor Performance. ICAPP 2015 (submit for review)

Attachment 1

For NEUP Project # 11-3023: Self-sustaining thorium boiling water reactors

SERPENT/PARCS/PATHS Core Simulator

The objective of this task was to develop a 3D core simulator capable of accurately modeling the strong axially non-uniform RBWR cores. Section 1 discusses the core simulator methods for cross section generation, processing and full core modeling. Section 2 provides an overview of the PARCS and PATHS codes along with the equilibrium cycle search methodology. Section 3 outlines the validation of the core simulator cross sections using single assembly analysis.

1. Methods

The neutronics modeling of the RBWR consists of a multi-step calculation process similar to existing LWR analysis methods. For the first step, 3D cross sections are generated for a single assembly. These cross sections are generated at all anticipated temperature and fluid conditions in the reactor and are then processed and converted into a PMAXS format which can be read by the PARCS code. The final step involves a coupled-code simulation using the tabulated group constants to model the full core behavior. An overview of the codes used for this analysis can be seen in Fig. 1.

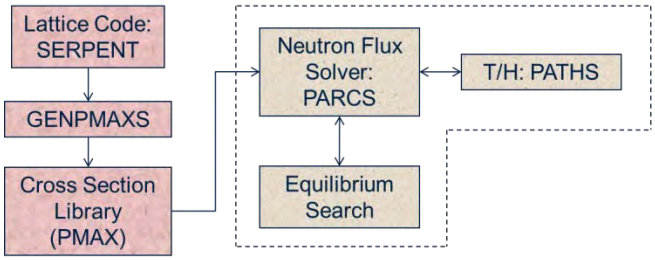

Figure 1. Core simulator diagram.

1.1 Cross Section Generation

Cross sections for the RBWR were created using the Monte Carlo code Serpent. The code utilizes delta tracking to accelerate the calculation while generating group-wise homogenized parameters.[1] These group constants were collapsed based on ENDF/B-VII continuous energy data. Reflective boundary conditions were applied in the radial direction, while zero incoming current conditions were applied for the top and bottom of the assemblies. The cross sections were calculated with the P1 infinite spectrum. When developing 3D Monte Carlo cross sections, the total number of particle histories is crucial in reducing the error associated with the generated group constants. Each cross section is calculated with tallies from the simulation. If the number of simulated particles is too small, the uncertainty of these tallies will be large. Increased uncertainties may lead to greater errors in the cross sections, which affect the accuracy of the nodal solution.

The use of 3D cross sections has required changes in the typical scheme for generating branch conditions. When performing 2D lattice calculations, individual conditions are perturbed including fuel

temperature, coolant void, control rod insertion, etc. For 3D assembly calculations, the conditions at multiple positions in the core must be changed simultaneously. A small study was performed at Brookhaven National Lab (BNL) that illustrated the effect of the spectrum when perturbing individual regions as opposed to all regions simultaneously (integral method).[2] A comparison of the spectrum for an upper fissile region for the RBWR-AC is shown in Fig. 2. From this analysis, significant changes in the spectrum were observed when perturbing the coolant void for individual nodes. The same study was performed for the spectrum when perturbing the fuel temperature and showed minimal changes. Therefore a system was devised to perturb the entire axial void distribution for branching calculations to maintain a physical distribution within the assembly. This technique provides a coolant void distribution that is closer to that of the physical system compared to a uniform distribution.

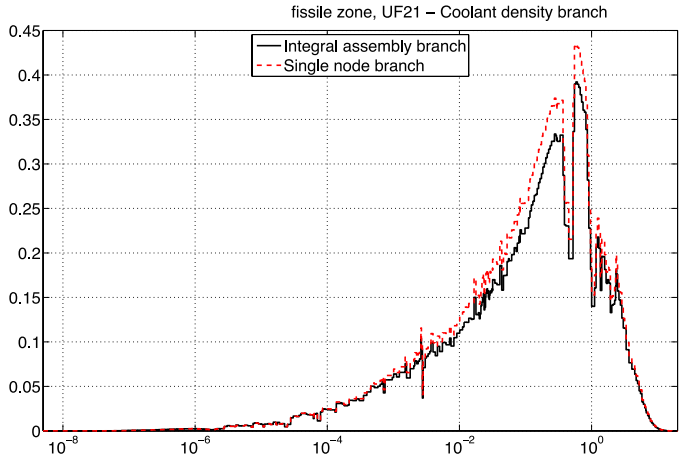

Figure 2. Flux spectrum for upper fissile zone.[5]

The SerpentXS script developed at MIT was used to execute the Serpent code for all of the branching and history calculations.[3] Each state condition is specified within the SerpentXS input and the code generates Serpent input files for all of the history and branch cases. Once the inputs are generated, SerpentXS submits each calculation for simulation. This process can involve hundreds or even thousands of Monte Carlo simulations to model each of the specified branches for each burnup step of interest.

Generating cross sections for the radial reflector required an unusual approach in Serpent. Typical methods for generating radial reflector cross sections involve generating a 2D fuel-reflector interface with reflective boundary conditions on all sides except for the reflector-boundary interface which is set as a vacuum boundary. The fuel and reflector lengths are set such that they cover several mean free paths. However, Serpent requires that the same boundary condition must be applied for all surfaces in a set Cartesian direction (for example, the left and right boundaries of a problem must have the same boundary condition).[1] Three separate boundary conditions can be applied in the x, y, and z direction. To avoid any issues with the boundary conditions, 2D core-reflector interface problems were created such that the typical reflective boundary condition applied on the fuel-boundary interface was modified. Instead of using a reflective boundary condition, a mirror image of the model was placed next to the existing model such that there is a single large lattice of fuel elements in the center surrounded by a reflector model on either side. This leads to a geometry that is twice the size of a typical radial reflector

cross section calculation, but avoids the issue of not being able to apply separate boundary conditions in the same direction. An example model can be seen in Fig. 3.

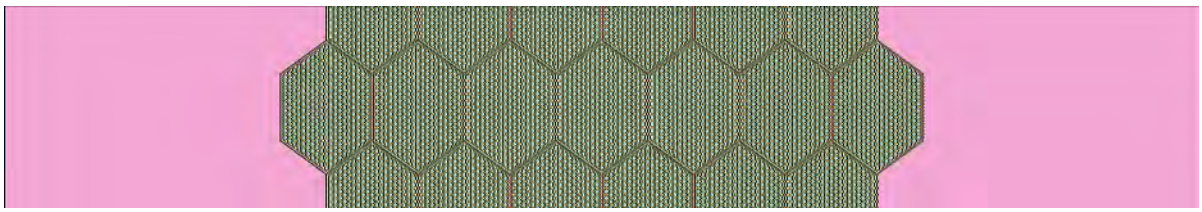

Figure 3. Supercell for modeling radial reflector cross sections.

A separate 2D core-reflector interface problem was created for each of the axial core regions to capture the spectral effects in the different regions. An average of the coolant density within each region was used for the coolant density inside the axial core elements. Inside the reflector, the saturation density of the coolant was used. All of the Monte Carlo calculations were done with the control rods removed from the fuel elements.

1.2 Cross Section Processing

Serpent simulations with user specified tallies produce a significant amount of data for the generation of the group constants. However, this data must be tabulated and organized for use with a nodal diffusion code such as PARCS. The GenPMAXS code[4] was developed to convert lattice level output into a usable format (PMAXS) for the core simulator PARCS. Prior to the creation of Serpent, the code supported multiple lattice codes including HELIOS, CASMO, WIMS, CONDOR and TRITON. Additional coding was introduced into the GenPMAXS code which now supports both Serpent and Serpent2. The GenPMAXS code is also capable of performing several other group constant calculations that are not supported within Serpent, including the calculation of axial discontinuity factors.

The use of 3D cross sections for the RBWR was first investigated at MIT in 2011.[3] During that study, it was found that 3D cross sections alone were not sufficient in reproducing a similar 3D Monte Carlo solution. This led to the creation of axial discontinuity factors (ZDF) which are similar to the conventional assembly discontinuity factors (ADF)[5] except for the axial direction. For a given axial interface, a ZDF is defined as the ratio of the heterogeneous surface flux to the homogeneous surface flux:

$$f = \frac{\phi_{s,i,g}^{het}}{\phi_{s,i,g}^{\text{hom}}} \qquad (1)$$

Where the heterogeneous surface flux is approximated using the partial currents from Serpent:

$$\phi_{s,i,g}^{het} = 2\left(J_{i,g}^{+} + J_{i,g}^{-}\right) \qquad (2)$$

And the homogeneous surface flux is found by solving the one-dimensional axial diffusion equation using the nodal expansion method (NEM) for a single node with the calculated group constants. The homogeneous surface flux is solved using the same method as PARCS (NEM for this case) in order to reproduce the Monte Carlo solution. The NEM approximates the flux solution within each mesh region using a fourth order Legendre polynomial:

$$\vec{\phi}(\xi) = \sum_{i=0}^{4} \vec{a}_i P_i(\xi) \tag{3}$$

The five coefficients associated with the flux expansion derive from the heterogeneous cell average flux, the net currents on the top and bottom surfaces and two weighted residual equations. The homogeneous surface fluxes for the top and bottom surfaces are found using the evaluated coefficients:

$$\vec{a}_0 = \bar{\phi} \tag{4}$$

$$\left(\bar{\bar{A}} + \frac{5\bar{\bar{D}}}{2h^2}\right)\vec{a}_1 = -\frac{5}{4h}\left(\vec{J}^B + \vec{J}^T\right) \tag{5}$$

$$\left(\bar{\bar{A}} + \frac{21\bar{\bar{D}}}{2h^2}\right)\vec{a}_2 = -\frac{7}{4h}\left(\vec{J}^B - \vec{J}^T\right) \tag{6}$$

$$\vec{a}_3 = -\frac{h}{12\bar{\bar{D}}}\left(\vec{J}^B + \vec{J}^T\right) - \frac{1}{6}\vec{a}_1 \tag{7}$$

$$\vec{a}_4 = \frac{h}{20\bar{\bar{D}}}\left(\vec{J}^B - \vec{J}^T\right) - \frac{3}{10}\vec{a}_2 \tag{8}$$

$$\vec{\phi}_{i,g}^{B,Hom} = \vec{a}_0 - \vec{a}_1 + \vec{a}_2 - \vec{a}_3 + \vec{a}_4 \tag{9}$$

$$\vec{\phi}_{i,g}^{T,Hom} = \vec{a}_0 + \vec{a}_1 + \vec{a}_2 + \vec{a}_3 + \vec{a}_4 \tag{10}$$

The axial discontinuity factors are included in the PMAXS cross section file for the top and bottom surfaces of a given material node. A separate cross section file was created for each nodal region to accommodate the axial discontinuity factors and the 3D cross sections.

For interfaces with large gradients, such as the region between seed and blanket zones, the homogeneous flux can become negative which leads to a negative discontinuity factor. This can result in negative fluxes within PARCS and numerical problems during the flux solution. A scheme was developed to avoid this based on modifying the diffusion coefficient such that the axial discontinuity factor would

be bounded within an acceptable range, while still preserving the net current on the node interface. However, the modification of the diffusion coefficient also affected the radial 2D calculation within TPEN causing instabilities within the core calculation. Instead, limits were placed on the axial discontinuity factors. If the calculated value exceeded the specified range, then the quantity was changed to the closest bound.

1.3 Full Core Modeling

The final stage of the core simulator consists of executing the coupled codes PARCS[6] and PATHS[8]. For the tight pitch lattice in the RBWR, the hexagonal nodal diffusion kernel is used in PARCS which is based on the triangular polynomial expansion method (TPEN) to solve for the few group fluxes in the radial direction. As noted earlier, the axial flux is solved using the 1D NEM method and coupled to the radial solution using the traditional transverse leakage approximation. The codes are coupled with PARCS providing the node-wise powers to PATHS, while PATHS provides PARCS with the fuel temperature, coolant density and coolant temperature. The two codes iterate until a converged solution is achieved.

The principle application of this coupled code simulator in the work here is to search for the equilibrium cycle of the RBWR. This is an iterative process that consists of depleting the full core and then shuffling the fuel bundles. The process is repeated until a desired maximum burnup difference between fuel recycles is met.

2. Equilibrium Cycle Codes/Methods

2.1 PARCS Modeling

PARCS[6] (Parallel Advanced Reactor Core Simulator) is a three dimensional reactor core simulator which solves steady-state and time-dependent, multi-group neutron diffusion and SP3 transport equations in cartesian, cylindrical, and hexagonal geometries. PARCS is coupled directly to the thermal-hydraulics code PATHS (for equilibrium cycle simulation) and TRACE (for transient simulation), which provide the temperature and flow field information to PARCS. The major calculation features in PARCS include the ability to perform eigenvalue calculations, transient (kinetics) calculations, Xenon transient calculations, decay heat calculations, pin-power calculations, and adjoint calculations for commercial Light Water Reactors. The hexagonal nodal method was used to model the RBWR core and has been previously tested for fast reactor applications using multigroup hexagonal nodal solutions.[7]

2.2 PATHS Modeling

PATHS[8] (PARCS Advanced Thermal Hydraulic Solver) has been developed to calculate a steady-state thermal-hydraulics solution for LWRs. PATHS is simpler than six-equation, two-fluid codes such as TRACE or RELAP5, which have a higher fidelity than is necessary to perform steady-state coupled neutronics/thermal-hydraulics calculations for depletion analysis. Because of this, PATHS runs more quickly and allows for improved turnaround time during core analysis. The efficiency of PATHS makes one-to-one neutronics/thermal-hydraulics coupled calculations practical, even for very quick and simple calculations.

PATHS utilizes a four-equation drift flux model with simplified equations and solution algorithms which considerably reduce the runtime. User-specified boundary conditions include outlet pressure, total core mass flow rate, and inlet enthalpy. The following description is from the PATHS manual.[8]

"The PATHS methodology is based on the two fluid model developed by Ishii,[9] averaged to consider the mixture instead of two separate fluids. The finite volume method is applied and the equations are cast into a face-based scheme. Since the control volume is set to include the entire cross-sectional area in a channel, the equations are reduced to a one-dimensional flow with heat fluxes and stress terms coming from the boundary. The void fraction and drift velocity are introduced through constitutive relationships instead of a fourth field equation that would normally show up in the drift flux model."

The discretized conservation equations for mass, momentum, and energy, are given by

$$(\rho_m^* v_m A\,)_n - (\rho_m^* v_m A)_s = 0 \tag{12}$$

$$\left(\rho_m^* |v_m^*| v_m \left(A + \tfrac{1}{2} F_z^* \Delta V\right)\right)_n - \left(\rho_m^* |v_m^*| v_m \left(A - \tfrac{1}{2} F_z^* \Delta V\right)\right)_s + (PA)_n - (PA)_s$$
$$= \left(\frac{\alpha^*}{1-\alpha^*} \frac{\rho_f^* \rho_g^*}{\rho_m^*} v_{gj}^{2*} A\right)_s - \left(\frac{\alpha^*}{1-\alpha^*} \frac{\rho_f^* \rho_g^*}{\rho_m^*} v_{gj}^{2*} A\right)_n - \frac{(\rho_m^*)_n + (\rho_m^*)_n}{2} g \Delta V \tag{13}$$

$$F_z^* = \frac{1}{2}\left(\frac{\Phi_{2\Phi} f}{D_h} + \frac{K_{loss}}{\Delta z}\right) \tag{14}$$

$$((\rho_m^* v_m^* h A)_n) - ((\rho_m^* v_m^* h A)_s) = q_{wall}^{"} \xi_h \Delta z + \left(\alpha^* \frac{\rho_f^* \rho_g^*}{\rho_m^*} \Delta h_{fg}^* v_{gj}^* A\right)_s - \left(\alpha^* \frac{\rho_f^* \rho_g^*}{\rho_m^*} \Delta h_{fg}^* v_{gj}^* A\right)_n$$
$$+ \left(v_m^* + \frac{\alpha^* \left(\rho_f^* - \rho_g^*\right)}{\rho_m^*} \bar{v}_{gj}\right) ((P^* A)_n - (P^* A)_s) \tag{15}$$

where standard greek letters are used to refer fluid quantities (e.g. ρ for density) and the subscripts *f,g,* and *m* denote fluid (liquid), gas, and mixture, respectively.

2.3 Equilibrium Cycle Search Methodology

An iterative algorithm has been developed to provide nested iterations to determine the equilibrium core configuration using the SERPENT/PARCS/PATHS code system. It takes into consideration explicit treatment of fuel bundles shuffling and control rod scheduling as defined by the user and the core was depleted with PARCS by steps defined by the user specified control rod sequence.

An equilibrium cycle search algorithm was implemented for the coupled codes. The convergence criterion was set to 0.1 GWD/T for the infinite norm of node-wise burnup at the End of Cycle (EOC). The overall flowchart is shown in Fig. 4.

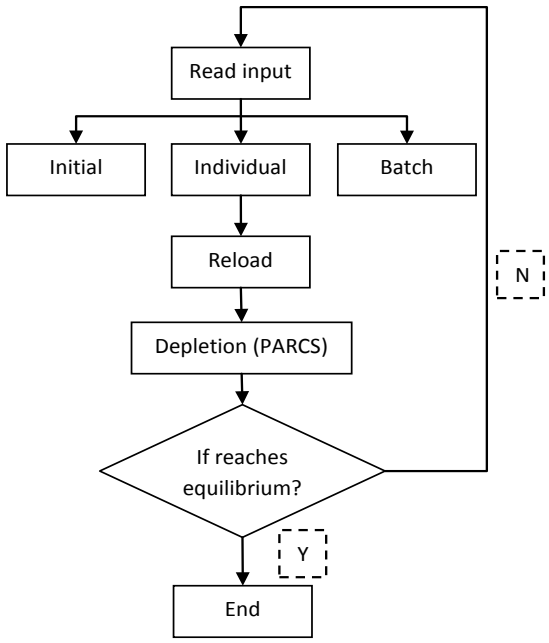

Figure 4. Equilibrium Cycle Search Flowchart

3. Validation of Core Simulator Cross Sections

The RBWR core simulator was validated using a single assembly benchmark problem similar to the RBWR-AC. The ability to reproduce the Monte Carlo solution using 3D Serpent cross sections in PARCS is demonstrated for the single assembly.

3.1 Single Assembly Analysis

In order to demonstrate that 3D cross sections with axial discontinuity factors can reproduce the reference Monte Carlo solution, a single assembly benchmark problem was simulated. An image of the assembly model is shown in Fig. 5. The Serpent calculation was performed using 150,000 source particles per cycle with 300 active cycles and 100 inactive cycles using ENDF/B-VII neutron cross section library. Reflective boundary conditions were applied to all sides of the assembly and group constants were found for each axial level. Based on previous experience, axial discontinuity factors were bounded over the range of 0.85 to 1.15 to mitigate potential numerical issues in PARCS. Cross sections were collapsed to 12 energy groups based on previous Hitachi studies.[10] The same model was generated in PARCS and the cross sections from Serpent were used in the PARCS simulation. Table 1 shows the comparison of the single assembly results.

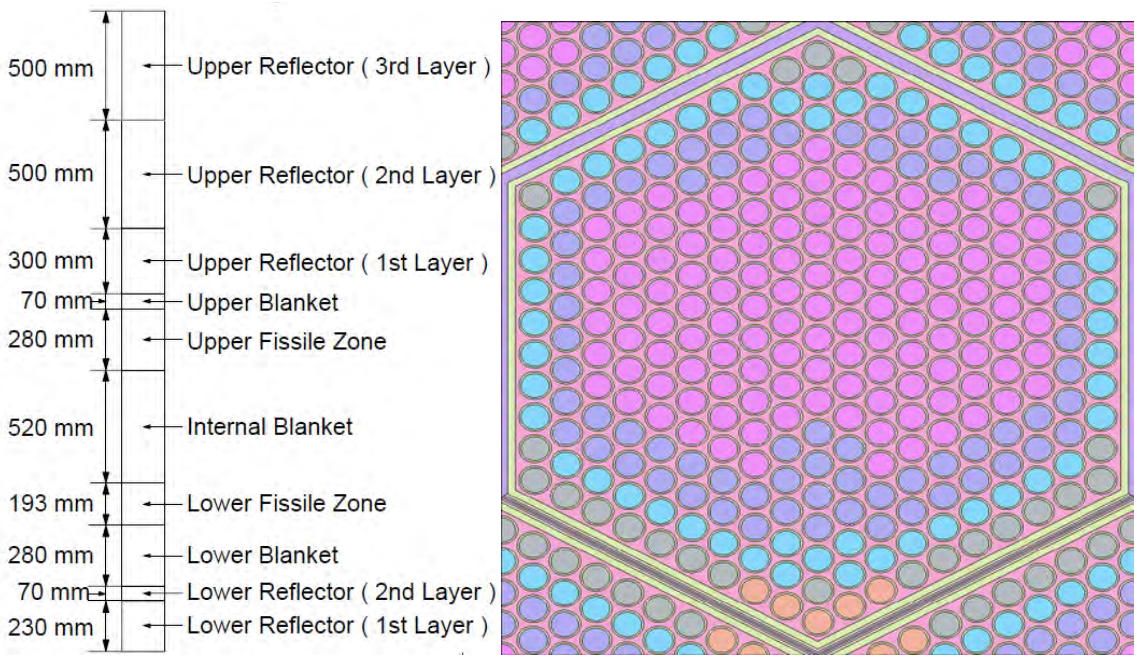

Figure 5. Benchmark axial (left) and radial (right) assembly model.

Table 1

Eigenvalue Comparison for Single Assembly Case

Method	k-eff	Difference from Serpent (pcm)
3D Serpent	1.09601	-
3D PARCS, 2D Serpent XS	1.05422	-4179
3D PARCS, 3D Serpent XS without ZDFs	1.08772	-829
3D PARCS, 3D Serpent XS with ZDFs	1.09601	0

When using only 3D cross sections, with a relative error of 9.6 pcm on k-eff for the Monte Carlo solution, the PARCS solution is over 800 pcm different from the Monte Carlo solution. This is a large improvement compared to the 2D cross section methodology which is over 4000 pcm off from the reference calculation. The large difference in the 2D cross section simulation is due to the inability to capture the correct spectrum from axial streaming in both the fuel and axial reflector regions. Finally, if 3D cross sections with axial discontinuity factors are used, PARCS is able to reproduce the exact Monte Carlo solution.

A comparison of the normalized fluxes between Serpent and PARCS with and without axial discontinuity factors for the fast (group 1) and thermal (group 9) are shown in Fig. 6. These plots represent the flux over the active core region. From 0-30 cm represents the lower blanket, 30-50 cm the lower fissile, 50-

100 cm the internal blanket, 100-130 cm the upper fissile and 130-140 cm the upper blanket. Each of these regions is divided by a solid line in the Figure. For the fast group, the PARCS solution without axial discontinuity factors underestimates the flux in the lower fissile zone and over predicts the flux in the blanket regions near the upper fissile zone. With axial discontinuity factors, the solution is consistent with the Serpent flux profile. For the thermal group, the PARCS solution without axial discontinuity factors underestimates the flux in the lower fissile region. It also has difficulty reproducing the solution in the upper blanket, where it over predicts the flux. The flux shape in the thermal group is not as smooth as the fast group flux shape and it is much more difficult for the diffusion solution to reproduce the Monte Carlo solution without the use of axial discontinuity factors.

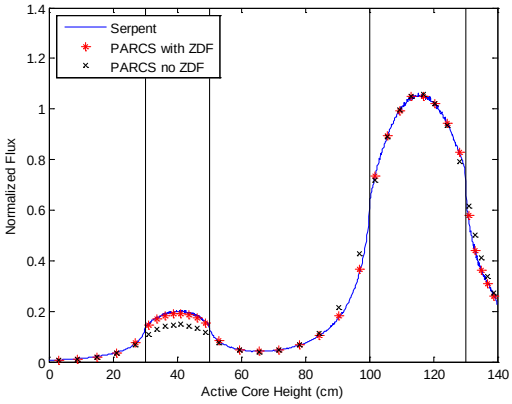

Fig. 6a. Fast (group 1) flux comparison.

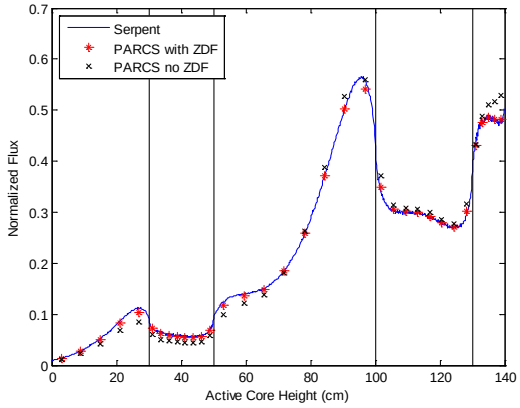

Fig. 6b. Thermal (group 9) flux comparison.

For the equilibrium cycle analysis, the method was modified in order to achieve stability and accuracy of the solution. While modifying the diffusion coefficient allows the deterministic solution to match the Monte Carlo solution exactly for a single assembly (Table 1), the modified diffusion coefficients were adversely affecting the radial streaming in the core simulation. Thus, modifying the diffusion coefficient to keep the ZDFs within a reasonable range was unfeasible. Instead, the ZDFs were simply bounded (between 0.85 and 1.15) without significant detriment to the accuracy of the solution. Any ZDF outside of this range was simply set to the nearest bound.

4. Conclusions

This work solved some of the challenges associated with modeling an axially heterogeneous, mixed-spectrum reactor with an innovative approach to the conventional two-step method for LWR analysis. The work showed that 2D lattice methods were not sufficient to generate cross sections for this problem because the underlying assumption of no net current in the vertical direction breaks down at the interfaces between enriched seed and blanket regions of the core, and also due to strong variation of the moderator density in the axial direction. Cross sections were generated with a 3D single assembly model, instead of a 2D lattice, in order to capture the important effects of axial streaming in this core. Axial discontinuity factors were also generated to help the 3D nodal diffusion solution better match the 3D Monte Carlo results. Modifications to the PARCS core simulator allowed the use of 3D cross sections

for the generation of an equilibrium cycle. This was one of the significant original advances resulting from the research.

REFERENCES FOR ATTACHMENT 1

1. J. LEPPÄNEN, "PSG2 / Serpent – A Continuous-energy Monte Carlo Reactor Physics Burnup Calculation Code," http://montecarlo.vtt.fi (2009).
2. Brown, Nicholas. *3D Branching*. Personal Correspondence. BNL (2012).
3. B. HERMAN, E. Shwageraus, B. Forget and M.S. Kazimi, "Cross Section Generation Strategy for High Conversion Light Water Reactors," MIT-NFC-TR-126, CANES, MIT (2011).
4. Y. Xu and T. Downar, "GenPMAXS-V5, Code for Generating the PARCS Cross Section Interface File PMAXS," University of Michigan (2009).
5. K. SMITH, "Assembly Homogenization Techniques for Light Water Reactor Analysis," *Progress in Nuclear Energy*, Vol. 17, No. 3, pp. 303-335 (1986).
6. T. Downar, Y. Xu, V. Seker, "PARCS, U.S. NRC Core Neutronics Simulator," University of Michigan (2009).
7. "FAST: An advanced code system for fast reactor transient analysis", *Annals of Nuclear Energy 32, 1613-1631*, (2005).
8. A. Wysocki, Y. Xu, B. Collins, A. Manera, T. Downar, "PATHS: PARCS Advanced Thermal Hydraulic Solver," University of Michigan (2012).
9. M. Ishii, T. Hibiki, "Thermo-Fluid Dynamics of Two-Phase Flow," Springer, New-York (2006).
10. Technical Evaluation of the HITACHI Resource-Renewable BWR (RBWR) Design Concept. EPRI, Palo Alto, CA: 2012. 1025086.

Attachment 2

For NEUP Project # 11-3023: Self-sustaining thorium boiling water reactors

The MocDown/PATHS Assembly Unit Cell Design Tool

The objective of this task is to design a tool, MocDown, which can accurately and efficiently account for the strong coupling between the neutronics and thermal-hydraulics in reduced-moderation boiling water reactor cores and to search for the equilibrium composition of such cores that operate in a multi-recycling mode. Section 1 discusses the general design and programming approaches that were taken while developing MocDown. Section 2 demonstrates and describes the accelerated recycling scheme that MocDown takes in seeking equilibrium core compositions for multi-recycling fuel cycles. Section 3 shows an example of the online thermo-fluids coupling. In section 4, MocDown's simple approach for source rate scaling, which accounts for isotopic composition-dependent decay heat, is described. Section 5 summarizes this document.

1. Introduction and Motivation

Existing core simulation codes are either insufficiently accurate or computationally inefficient in the search for the equilibrium composition of recently proposed reduced-moderation boiling water reactor designs. The cores of such reactors feature a strongly varying axial coolant density distribution, hard and axially varying neutron spectra, and large axially varying flux gradients, which together mandate the use of continuous-energy three-dimensional Monte Carlo neutron transport. Tight physical coupling between the spatial variation of the fission power density and coolant density require tight numerical coupling between neutron transport and thermo-fluids models. Interest in, primarily, the equilibrium cycle necessitates an efficient means of finding the equilibrium core composition. MocDown was created to suite these needs.

The SerpentXS/PARCS code suite has been developed for equilibrium core analysis,[12] but it is not suitable for an equilibrium assembly analysis. The SerpentXS simulations rely on using multiple flow histories to bound the performance with burnup, instead of having TH coupling to update the water densities. Additionally, PARCS does not track individual isotopes; instead, it uses few-group homogenized macroscopic cross sections that are determined by the power history and from the SerpentXS history and branch scheme. Therefore, a fuel recycling model is not feasible to implement within the PARCS/SerpentXS suite; it depends on already knowing (either a priori or from another model) the composition of the freed assemblies. MocDown was designed to arrive at the equilibrium cycle using average flow and power conditions by tracking all of the neutronically important isotopes and using online thermo-fluid coupling to predict the discharge composition, which can then be used with a recycling scheme. Section 2 provides an overview of MocDown; Section 3 describes in detail the accelerated equilibrium cycle search; Section 4 details the online thermos-fluids coupling; Section 5 describes the neutron source rate scaling; and Section 6 concludes this paper.

2. General Design and Programming Approach

MocDown is an advanced Monte Carlo depletion simulator. Just as MOCUP,[1] MONTEBURNS,[2] IMOCUP,[3] Mocup.py,[4] VESTA,[5] and countless other codes do, MocDown simulates the depletion of nuclear reactor cores by coupling neutron transport with MCNP[6] and transmutation with ORIGEN2.2.[7] In addition, it facilitates the search for the equilibrium composition of multi-recycling fuel cycles in an efficient manner, enables online coupling of thermo-fluids models, and employs a simple approach towards neutron source rate scaling. MocDown also incorporates many other programming best practices which provide for a robust, reliable experience for users.

MocDown is written in object-oriented Python 3. Auxiliary operations, like thermo-fluids models and fuel processing, are completely customizable in external modules. These modules take advantage of interface methods (e.g., GetBurnCells or GetIsDecayStep), which pass all data in memory and eliminate error prone I/O and file parsing. For example, a Python 3 library, which offers IAPWS-IF97 steam table property lookups within Python,[8] was readily found and integrated into the existing thermo-fluids model, while the PATHS code (maintained by the University of Michigan) is used for the majority of the thermos-fluids calculations.[9] This modular approach also allows MocDown to remain separate and intact for a number of projects, greatly simplifying version control and software verification.

Execution of ORIGEN2.2 is concurrently threaded using standard Python 3 libraries, enabling the depletion of twenty regions in parallel (although this number depends upon the hardware, it is thought to be a typical number). When depleting large systems in parallel, runtime speedups of 6-7x have been observed over serial execution. Transmutation constants (region-wise total flux magnitudes and region-, isotope-, and reaction-wise one-group cross sections) are extracted with a single MCNP tally which is dynamically generated. This removes restraints upon the number of regions or isotopes that can be depleted. In contrast, MONTEBURNS and MOCUP use one tally per depletion region and can tolerate only a certain number of regions, based upon their configuration and the version of MCNP. The isotopes whose transmutation constants are calculated with MCNP are determined according to the isotope's contribution to regional molar and mass densities and absorption and fission rates. This removes the need for a priori specification of which isotopes are tracked and automatically allows different sets of isotopes to be tracked in different depletion regions. MONTEBURNS incorporates this strategy, but requires a master list of isotopes to be provided.

Regular expressions parsing is used for robust extraction of transmutation constants from MCNP and isotopic inventories from ORIGEN2.2 output files. This allows for the flexibility to use MCNP5, MCNPX, or MCNP6 for neutron transport calculations and removes restrictions on the formatting of neutron transport code input files. Other codes are confined to certain versions of MCNP due to periodic changes in the formatting of output files. For simulations which deplete many regions and track many isotopes, regular expressions can also parse text faster than finite state-based parsing approaches. Depletion control parameters (e.g., depletion power, cycle length, the list of cells to deplete, etc.) are defined in a verbose, free-format input file. This centralization of inputs to a single location eliminates duplication and removes any requirements for special flags or comments within the neutron transport input file.

MocDown periodically serializes, compresses, and writes objects which are in memory to hierarchical data files. This archival memory dump facilitates simple post-processing and debugging of simulation

results through MocDown's object-oriented interfaces. Additionally, these serializations offer a convenient means to reload depletion control and state parameters into memory in order to restart a simulation which may have ended prematurely.

3. Accelerated Recycling Scheme for the Search of Equilibrium Core Compositions

MocDown is most powerful when searching for the equilibrium core composition as a result of multi-recycling its own discharged fuel supplemented by makeup fuel of specified composition. . When is it used for this purpose, it is beneficial to consider its operation as the self-consistent convergence of three inter-dependent models: neutron transport, transmutation and recycling, and thermo-fluids. Transport derives power distributions (Pth) and transmutation constants (σ,ϕ) from thermo-fluids conditions and isotopic inventories, transmutation and recycling derives isotopic inventories (N) from transmutation constants, and thermo-fluids derive thermofluids conditions (ρ,T) from power distributions. For the RBWR models, MCNP5.1.60 is used for the neutron transport model,[6] PATHS is used for the thermo-fluids model,[9] and ORIGEN2.2 is used for transmutation.[7] These dependencies are illustrated in Figure 1.

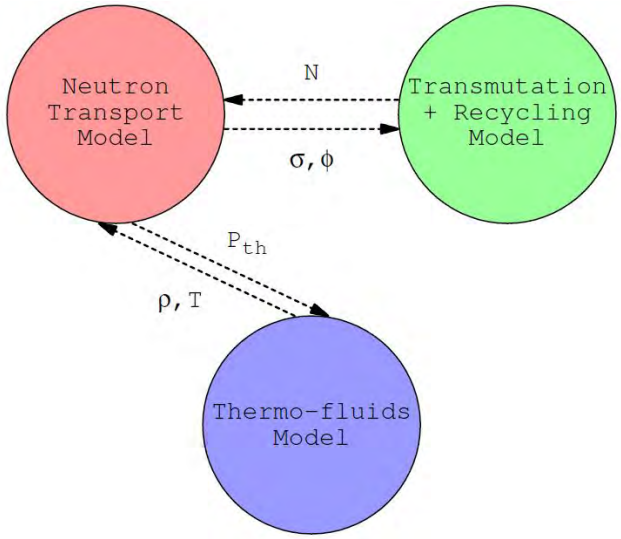

Figure 1. MocDown coupling scheme. Thermo-fluids-coupled depletion simulations can be broken into three independent models which must be selfconsistent: neutron transport, transmutation and recycling, and thermo-fluids.

Traditionally, depletion (without thermo-fluids feedback) is performed by alternating between neutron transport and transmutation in lockstep, holding N constant during the former and holding σ and ϕ constant during the latter. This ensures a good degree of consistency between the two models. A typical cycle requires 20 time-steps. When thermo-fluids is coupled, each single neutron transport execution is replaced by a fixed point iteration between neutron transport and thermo-fluids models, a process which continues until agreement is reached. This doubles the number of neutron transport executions per cycle on the average. If the cycle equilibrium is sought, dozens of cycles will need to be simulated. The result is an approach with requires on the order of one thousand executions of the neutron transport and thermo-fluids models and one half as many executions of the transmutation model.

The alternative approach taken by MocDown recognizes the >20x imbalance of computational expense between the neutron transport/thermo-fluids couplet and the transmutation model, which is only exaggerated by concurrently threaded transmutation. By loosening the numerical coupling of the three models somewhat, the number of neutron transport/thermo-fluids couplets can be drastically reduced. While this approach slightly increases the number of cycles required for convergence, the overall runtime plummets.

This accelerated approach to recycling is depicted in Figure 2 and proceeds as follows. The outer loop performs full-fidelity cycles (with neutron transport-updated transmutation constants and thermo-fluids feedback) until some norm of successive cycle multiplication factors falls below a tolerance. Following each failed (i.e., unconverged) iteration of the outer loop, the scheme enters the inner loop. The inner loop performs accelerated cycles (transmutation constants are held constant, avoiding the neutron transport/thermo-fluids couplet), pushing the fuel through depletion and recycling until some norm of successive cycle isotopic abundances falls below a tolerance. Upon success (i.e., convergence) of the outer loop, the cycle equilibrium is declared to be found and the search is complete.

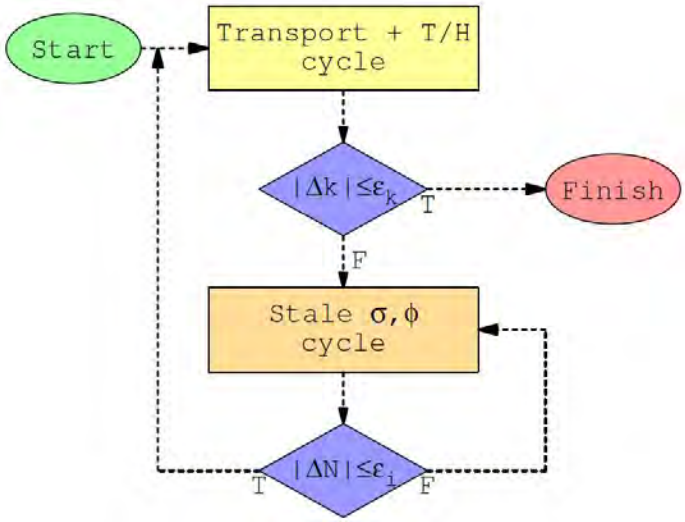

Figure 2. The accelerated recycling scheme used in MocDown eliminates many executions of neutron transport and thermos-fluids calculations by holding transmutation constants fixed in the search for equilibrium fuel cycles. ε is used designate a convergence criteria, and bars around a value indicate that the maximum difference in values within that value is used.

In order to demonstrate the effectiveness and efficiency of MocDown's accelerated recycling scheme, the analysis is performed and discussed for an early RBWR-Th pin cell.[10] A deprecated version of MocDown's thermo-fluids model was used in this benchmark, but as this benchmark focuses on the accelerated recycling scheme, the impact of this is minimal. As a single full-fidelity cycle for this design completes in 4.5 hours, 40 cycles (which would be required for convergence towards cycle equilibrium) would take over a week to finish. However, when MocDown is used for the equilibrium search, most of the full-fidelity cycles are replaced with accelerated cycles which complete in 12 minutes. In total, 4 full-fidelity and 85 accelerated cycles are simulated and the cycle equilibrium is found in only 35 hours. This is almost ten times faster than the traditional approach.

Convergence after this number of accelerated cycles is demonstrated qualitatively with Figure 3, which shows that the core composition ceases to change with additional cycles. Full-fidelity cycles are performed at the dashed line and accelerated cycles are performed in between. Following each full-fidelity cycle, transmutation constants are fixed and the isotopic abundances asymptotically approach a new core composition; each new core composition differs less and less from the previous one until an equilibrium core composition is reached. Figure 4 qualitatively shows that the multiplication factor for successive full-fidelity cycles has converged. A quantitative measure of convergence is demonstrated in Figure 5, which shows the ∞-norm of isotopic abundance differences versus cycle.

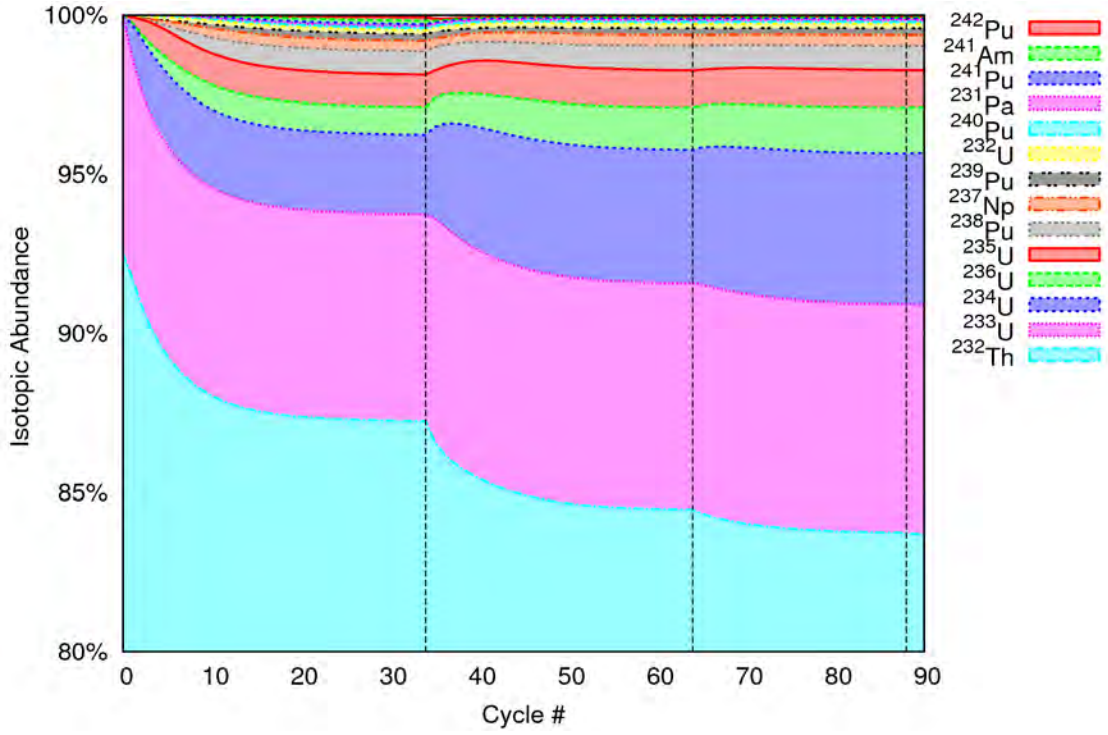

Figure 3. The MocDown accelerated recycling scheme efficiently finds the equilibrium cycle, whose isotopic composition matches that of its successor. Dashed lines denote full-fidelity cycles.

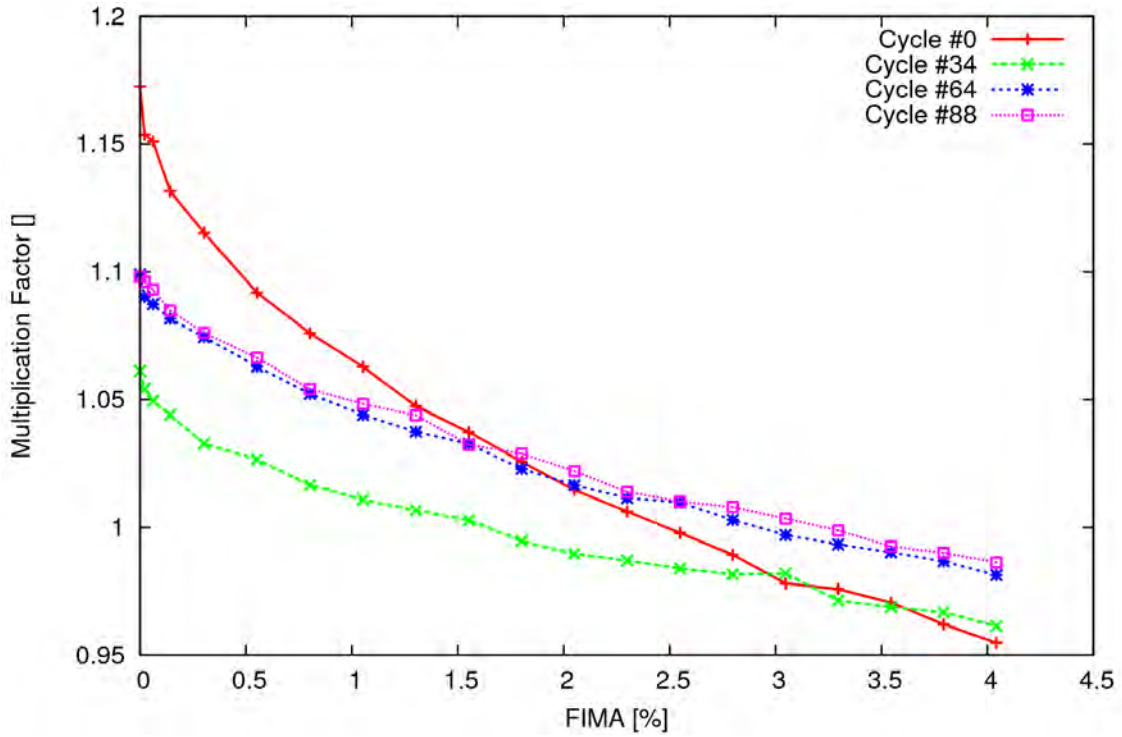

Figure 4. The MocDown accelerated recycling scheme efficiently finds the equilibrium cycle, whose cycle multiplication factor matches that of its successor.

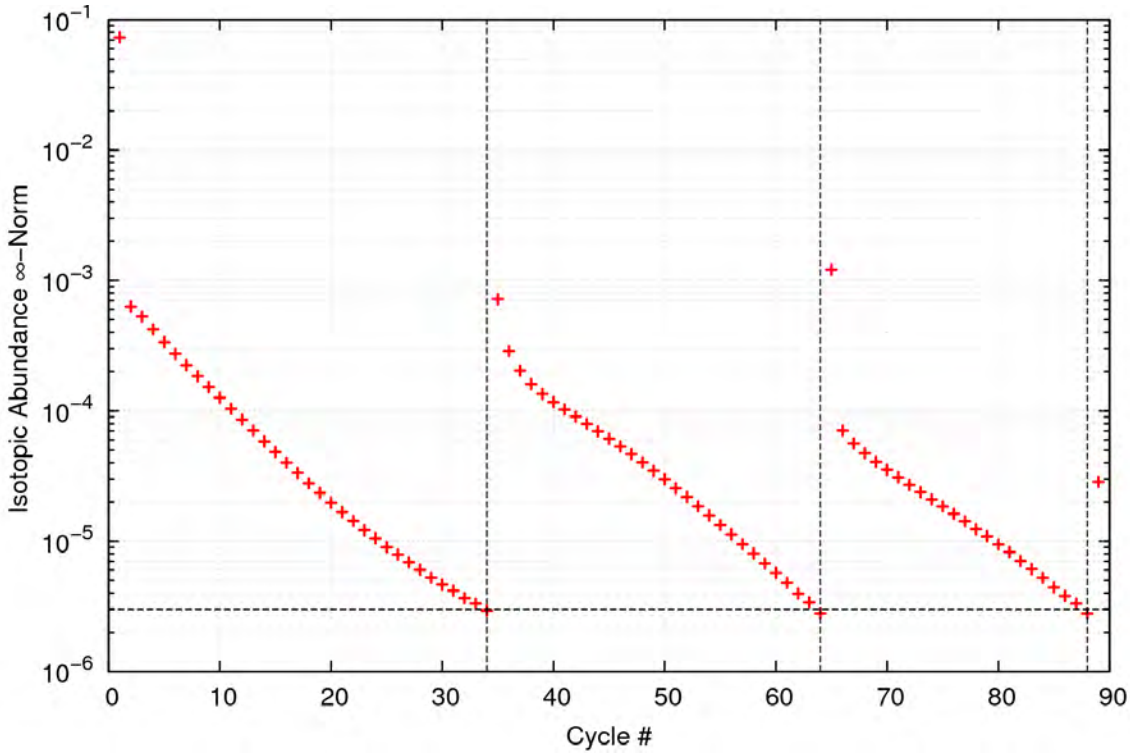

Figure 5. The difference in isotopic composition abundances becomes progressively smaller upon each accelerated cycle.

4. Online Thermo-Fluids Coupling

As described earlier, online neutronics – thermo-fluids coupling is achieved by performing a fixed-point iteration between neutron transport and thermo-fluids models until self-consistency is reached between the axial power and axial water density distributions. Figure 6 shows the thermo-fluids coupling scheme. The ρ_{guess} vector is taken to be the converged values from the previous T/H-neutronics coupled cycle at the same time step; for the first cycle, the ρ_{guess} vector is taken from the previous depletion step.

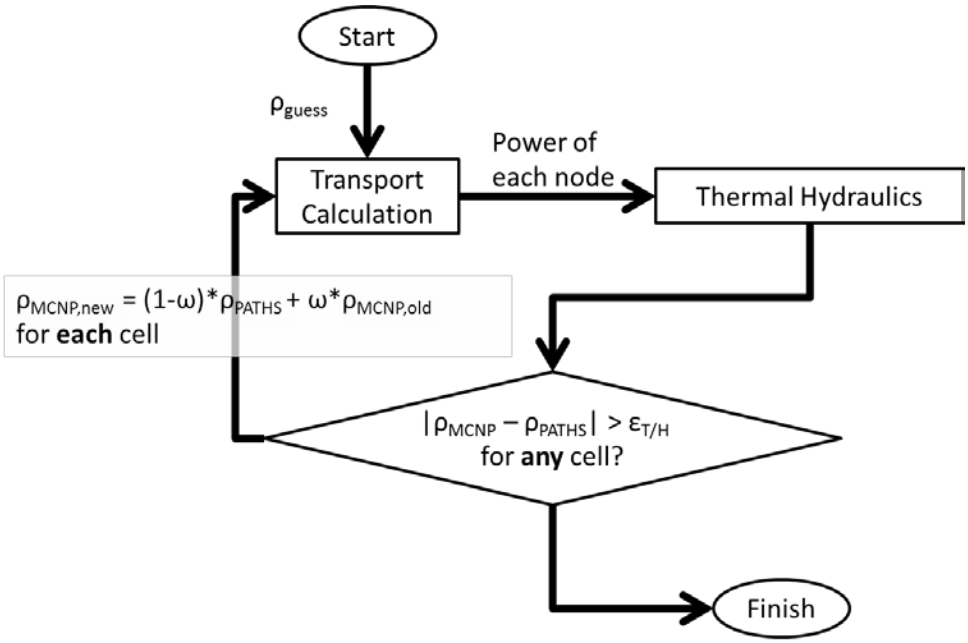

Figure 6. Thermo-fluid coupling scheme with relaxation. In this figure, ω is the relaxation coefficient, and $\varepsilon_{T/H}$ is the convergence criterion.

During parametric studies of the RBWR-Th core, several design variants were found whose neutron transport/thermo-fluids couplets oscillated between multiple solutions and then converged slowly to self-consistency in an underdamped fashion. For these cases, MocDown allows a relaxation factor to be applied to the thermo-fluids results. When under-relaxation is used, the most recent results are effectively averaged with the previous results and convergence occurs in three or four instead of tens of iterations.

The reference assembly model for the RBWR-Th using the Y-CISE CPR correlation and the LPG void fraction correlation[13] is used to demonstrate the necessity and effectiveness of thermo-fluids coupling in MocDown. For this design, the thermo-fluids model interfaces with PATHS[9] using the following procedure: (1) MocDown extracts the thermal power axial traverse from MCNP and enters it in simple stand-alone PATHS model; (2) PATHS calculates the coolant void fraction and pressure traverse based on the steam properties and coolant flow parameters; (3) convergence is determined by comparing successive coolant density traverses; and (4) a number of secondary operations are performed, including the minimum critical power ratio calculation. Figure 6 shows how the linear heat generation rate traverse shifts upwards over a cycle, as fissile material is consumed at a higher rate at the bottom (softer spectrum). As a consequence, the coolant density traverse also drifts upwards as shown in Figure 7.

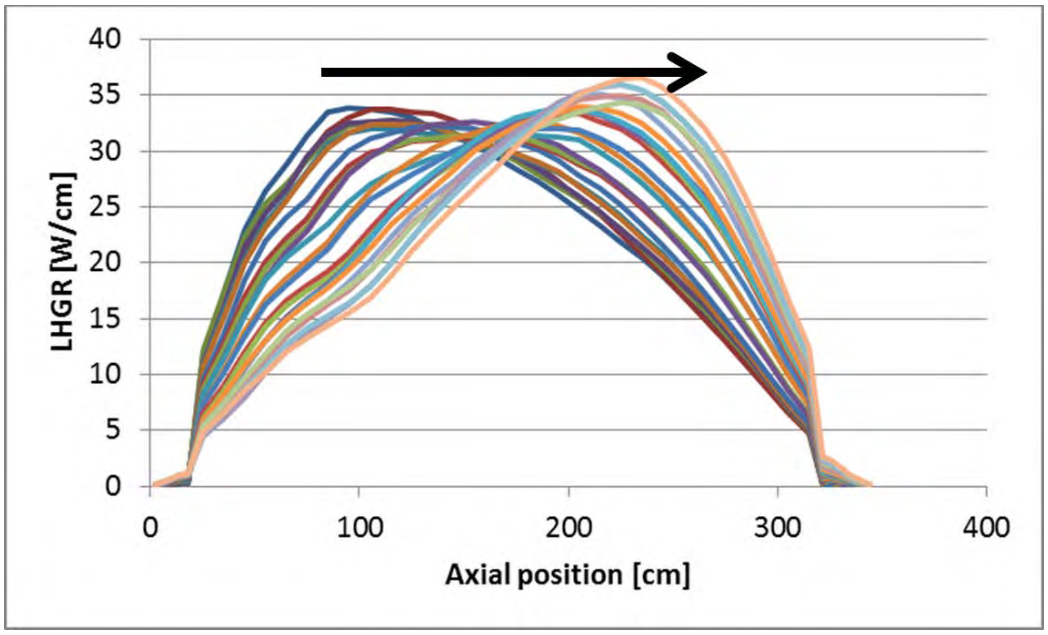

Figure 7. As the system accrues burnup, the linear heat generation rate (LHGR) shifts upwards.

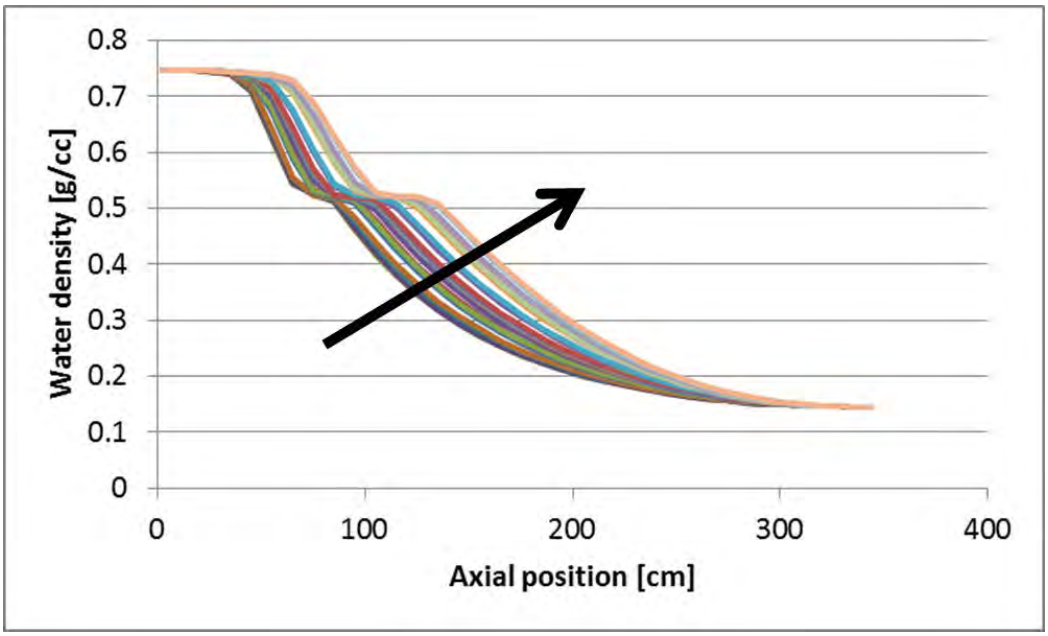

Figure 8. The corresponding coolant density traverse drifts upwards with the LHGR.

5. Neutron Source Rate Scaling and Decay Heat

Depletion analysis requires accurate knowledge of the burnup-dependent neutron flux magnitude. In Monte Carlo neutron transport codes, quantities like the flux magnitude are reported on a per source (fission) neutron basis. Consequently, in order to obtain the flux magnitude on a per second basis, the number of source neutrons generated per second (S) must be known. Only three quantities are required to deduce S: the total energy deposited in the core per source neutron (E), the thermal power at which the core operates (P_{th}), and the decay heat (P_d). E is made up of neutron and photon heating which

includes fission, radiative capture, Compton scattering, and other endothermic and exothermic reactions. P_{th} is the sum of particle heating (the product of E and S) and P_d. Putting all of this together, an expression can be written for S:

$$S = \frac{P_{th} - P_d}{E}$$

In this formulation, each term is known or can be derived quite easily: P_{th} is specified for each simulation; E can be estimated directly with MCNP using a single F6:np neutron/photon track-length estimated energy deposition tally [11, 2-88]; and P_d can be calculated with isotopic inventories, half-lives, and recoverable energy Q-values.

With this neutron source rate, heating rates can be derived which are self-consistent and which appropriately account for decay heat. Figure 9 shows how the decay heat starts at 0% and saturates to around 5.5% of the total thermal power after the first time step; consequently, the neutron source rate simultaneously drops to 94.5% of its initial value. It is important to note that if decay heat is neglected, flux magnitudes and nuclear reaction rates will be in error by +5-7%.

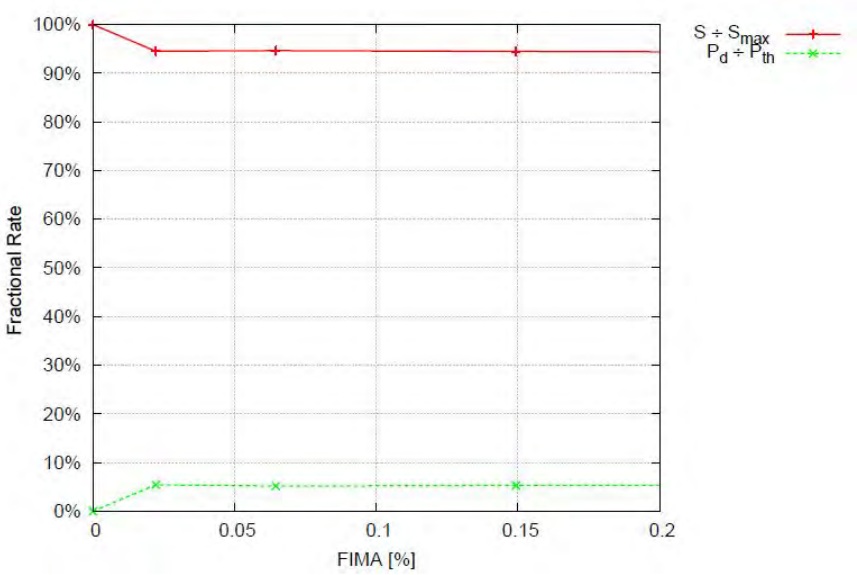

Figure 9. Because the thermal power is held constant, the neutron source rate, which is used to scale all nuclear reaction rates, depends upon the decay heat from radioisotope inventories.

Another point which deserves mentioning is the matching of flux magnitudes between MCNP and ORIGEN2.2. When ORIGEN2.2 is instructed to transmute at a constant power, it internally calculates a flux magnitude based upon that provided power, isotopic fission rates, and isotopic recoverable fission energies ($Q_{Z,A}$). ORIGEN2.2 calculates $Q_{Z,A}$ using the correlation:

$$Q_{Z,A}\ [\mathrm{MeV}] = 1.29927 \times 10^{-3} Z^2 \sqrt{A} + 33.12$$

where Z and A are the atomic and mass numbers respectively of a fissile isotope. In order to ensure that this flux magnitude which ORIGEN2.2 calculates is consistent with MCNP, MocDown provides

ORIGEN2.2 with a special "ORIGEN power" calculated from $Q_{Z,A}$ in the above equation. This ORIGEN power differs from all other physical powers and exists only to ensure consistency in neutron transport and transmutation fluxes and is otherwise not used.

6. Conclusions

MocDown is a modern Monte Carlo depletion and recycling simulator which incorporates many programming best practices and offers a robust user experience. Compared to MOCUP, our previous depletion and recycling workhorse, MocDown enables coupling between neutronics and thermal hydraulics calculations, automates tasks like isotope tracking and tally generation, allows usage of current versions of MCNP, centralizes inputs to a single location, simplifies post-processing, and greatly accelerates transmutation. The modular approach towards online coupling of thermo-fluids presents an easy and flexible way of simulating a nuclear system with self-consistency. The accelerated recycling scheme (with concurrent threading of transmutation) efficiently finds the equilibrium core composition of multirecycling fuel cycles. The simple approach for source rate scaling accurately accounts for decay heat and requires very little computational overhead beyond standard transmutation constant estimation. It was found highly valuable for performing assembly level tradeoff studies and searching for optimal designs of RBWR cores.

7. References

1. R. Moore, B. Schnitzler, C. Wemple, R. Babcock, and D. Wessol, "MOCUP: MCNP-ORIGEN2 Coupled Utility Program," INEL-95/0523, INL (1995).
2. H. Trellue and D. Poston, "MONTEBURNS 2.0 | An Automated Multi-Step Monte Carlo Burnup Code System," PSR-455, ORNL (2003).
3. F. Heidet, "IMOCUP Description," internal memo, UCBNE (2010).
4. A. Cisneros, "mocup.py," internal memo, UCBNE (2012).
5. W. Haeck, "VESTA User's Manual - Version 2.1.0," DSU/SEC/T/2011-81, IRSN (2012).
6. X-5 Monte Carlo Team, "MCNP – A General Monte Carlo N-Particle Transport Code, Version 5 | Volume I: Overview and Transport," LA-UR-03-1987, LANL (2008).
7. A. Croff, "A User's Manual for the ORIGEN2 Computer Code," TM-7175, ORNL (1980).
8. jjgomera, "iapws 1.0.0," 2012, http://pypi.python.org/pypi/iapws/.
9. A. Wysocki, Y. Xu, B. Collins, A. Manera, T. Downar, "PATHS: PARCS Advanced Thermal Hydraulic Solver," University of Michigan (2012).
10. F. Ganda, J. Vujic, and E. Greenspan, "Thorium self sustaining BWR cores," Proc. Proceedings of the 2011 International Congress on Advances in Nuclear Power Plants (ICAPP) Embedded Topical Conference, May, 2011.
11. R. Takeda, J. Miwa, and K. Moriya, "BWRs for Long-Term Energy Supply and for Fissioning Almost All Transuranics," Proc. Proceedings of the 2007 Advanced Nuclear Fuel Cycles and Systems (Global) Conference, September, 2007.
12. The SERPENT/PARCS/PATH core simulator, Attachment 1
13. "Void fraction and critical power correlations for the RBWRs," Attachment 5

Attachment 3

For NEUP Project # 11-3023: Self-sustaining thorium boiling water reactors

The FRAPCON-Th code for fuel performance analysis

Objective

The objective of this task is to develop the necessary methodologies to analyze the steady-state fuel performance of the RBWR-Th designs and evaluate the viability of various fuel designs. This was accomplished by modifying the existing FRAPCON-MIT code to accommodate Th-based fuels in the faster neutron spectrum of the RBWR. These modifications include the development of a new thermal conductivity correlation, adoption of new isotope cross sections for finding the radial power profile, the application of an improved Zircaloy-2 hydrogen pickup model, and well as the introduction of previously developed Th-based fuel modifications. This new code was then applied to the RBWR-Th variants using operating conditions provided by UCB. In particular, the high fast neutron fluence to the cladding resulted in large cladding hydrogen concentrations. Application of NRC hydrogen-based accident tolerances revealed that such high hydrogen concentrations would not be allowable. To address this, sensitivity studies were performed to determine the fast fluence tolerance required of the cladding. These analyses revealed that substantial, though potentially achievable, developments in cladding alloy design would be required for the RBWR-Th, or any other RBWR variant, to maintain acceptable hydrogen pickup behavior.

Abstract

To provide steady state fuel performance evaluations for the $(ThU)O_2$ fueled Reduced moderation Boiling Water Reactor (RBWR-Th), modifications have been made to FRAPCON-MIT code. In addition to the use of existing $(ThU)O_2$ capabilities in FRAPCON-MIT, a radial power profile specific to the RBWR-Th was implemented. To more accurately model the corrosion acceleration due to high fast neutron fluence, the oxidation model was modified and a new hydrogen uptake model was introduced. A preliminary assessment of an average and 130% peaked RBWR-Th fuel rod indicates that fuel temperatures remain well below the melting temperature and the plenum gas pressure does not exceed that of the coolant. Of concern is the high cladding hydrogen content that results from the acceleration of hydrogen pickup at relatively low burnups, which is caused by the high fast neutron fluence on the cladding in the RBWR-Th. This high hydrogen content leads to significant restrictions and, ultimately, elimination of the margin to acceptable accident limits, presenting a distinct challenge to the RBWR-Th design. A new cladding material, GNF-Ziron, from Global Nuclear Fuels (GNF) offers a potential solution to this challenge by delaying the acceleration of the hydrogen pickup. The potential benefits of using

GNF-Ziron cladding are explored in a sensitivity study. This study illustrates that the selection of an appropriate cladding material for the RBWR-Th is crucial for its success.

1. Introduction

Unlike conventional Boiling Water Reactors (BWRs), the Reduced moderation Boiling Water Reactor (RBWR) uses a combination of a tight hexagonal fuel lattice and high coolant void fractions to operate with an epithermal neutron spectrum. This hardened spectrum allows for separate core designs to achieve breeding ratios greater than 1.0 or to fission transuranic elements efficiently.[1] These separate core configurations allow the RBWR fuel cycle to be self-sufficient and compete with breakeven Sodium Fast Reactor (SFR) based fuel cycles. However, outside its tight pitched, hexagonal assemblies, the RBWR's nuclear steam supply system and balance of plant are able to utilize established BWR technologies. This fact is expected to greatly lower barriers to commercial deployment of the RBWR-Th.

While the original RBWR fuel designs employed $(UPu)O_2$ Mixed OXide (MOX) fuel,[2] a new design has been proposed using $(ThU)O_2$ MOX to breed and recycle fissile uranium. This new reactor, the RBWR-Th, is currently being designed as an alternative to the original RBWR-AC. Unlike the original RBWR designs, the RBWR-Th takes advantage of thorium's preferable neutronic properties and employs a single axial seed region and upper and lower blankets. The use of thorium also allows the core to operate with a negative void coefficient, while the uranium-based RBWR design void coefficient has been shown to vary between positive and negative, depending on analysis assumptions.

Because the ability of a commercial reactor to operate efficiently is heavily dependent on fuel reliability, fuel performance investigations for the RBWR-Th were initiated at an early stage in the design process. The steady state fuel performance code, FRAPCON-MIT, which is intended to analyze innovative fuel designs,[3] was augmented, as detailed in Section 2, to accommodate the unique fuel material and neutron spectrum of the RBWR-Th. Section 3 describes the limits applied to the fuel performance assessments. The code was then applied to cases with constant power histories in Section 4, revealing potential cladding hydrogen pickup concerns. Those concerns are then addressed in Section 5 with sensitivity analyses based on potential advanced cladding options. Lastly, a qualitative comparison of the RBWR-Th and RBWR-AC are detailed in Section 6.

2. RBWR-Th Fuel Rod Modeling

The steady state fuel performance analyses of the RBWR-Th were obtained using the FRAPCON-MIT code, which is a modified version of the NRC's steady state fuel performance code, FRAPCON-3.4.[4] The modifications encompassed within FRAPCON-MIT are an agglomeration of modifications that have been made to simulate innovative nuclear fuel designs (e.g. SiC cladding, LBE gap, etc.) within the existing FRAPCON framework. For the RBWR-Th's fuel, further changes were necessary to model the $(ThU)O_2$ fuel and Zircaloy-2 cladding under RBWR-Th conditions.

2.1. $(ThU)O_2$ Fuel Modeling

2.1.1 Thermal Conductivity

Unlike some other material property modifications, the thermal conductivity of the (ThUPu)O_2 fuel does not follow a simple mixing rule. At low temperatures (<1300K), the heat conduction of the ceramic is dominated by phonon diffusion, which is inversely related to temperature. As molecules are substituted (i.e. mixed) in the bulk lattice, they introduce lattice strain, increasing the phonon scattering, which lowers the thermal conductivity. Because of this increased phonon scattering, it is possible for a mixture of (ThUPu)O_2 to have a lower thermal conductivity than that of pure ThO_2, UO_2, or PuO_2. Alternatively, at high temperatures (>1300K), the thermal conductivity of UO_2 begins to increase with increasing temperatures. This increase is due to heat being transferred via freed valence electrons. This behavior is due to a conduction band in UO_2 that is not present in either ThO_2 or PuO_2. Previous adaptations of FRAPCON to include ThO_2-based fuels used a relatively simple empirical correlation, which did not consider the presence of PuO2.[5]

This work focused on introducing a more generalized method for finding the low temperature thermal conductivity of ThO2-based mixed oxide fuel. This methodology is intended to be capable of accounting for diverse (ThUPu)O_2 mixture possibilities. A derivation of the Klemens-Callaway model for phonon transport has been adopted,[6] shown in Equations 1 and 2,

$$\frac{W}{W_0} = \left(1+\frac{5}{9}\alpha\right)\left[\frac{\tan^{-1}U}{U} + \frac{\left(1-\frac{\tan^{-1}U}{U}\right)^2}{\left(\frac{1+\alpha}{5\alpha}\right)U^4 - \frac{1}{3}U^2 + 1 - \frac{\tan^{-1}U}{U}}\right]^{-1} \tag{1}$$

$$U^2 = \left(1+\frac{5}{9}\alpha\right)^{-1}\left(\frac{9}{2}\pi\right)^{\frac{1}{3}}\left(\frac{\pi}{2}h\right)k_B^{-2}\delta\Gamma\theta^{-1}W_0^{-1} \tag{2}$$

where W is the thermal resistance accounting for phonon scattering in m−K/W, W_0 is the lattice thermal resistivity in m−K/W, α is (9/5), h is the Planck constant, k_B is the Boltzmann constant, δ is the bulk average lattice parameter in m, θ is the Debye temperature in K, and Γ is a disorder parameter that characterizes the phonon scattering cross section and is defined by Equation 3. The lattice thermal resistivity, W_0, is found by applying a simple mixing rule to the inverse of the thermal conductivity of each of the mixture components.

$$\Gamma = \sum x_i\left[\left(\frac{\Delta M_i}{M}\right)^2 + \varepsilon\left(\frac{\Delta\delta_i}{\delta}\right)^2\right] \tag{3}$$

where x_i represents the molar fraction of each mixture component, M is the bulk average molecular mass of the material in g/mol, ΔM_i is the difference between the molecular mass of each mixture

component and the bulk, ε is an adjustable parameter, δ is the bulk average lattice parameter in m, and $\Delta\delta_i$ is the difference between the lattice parameter of each mixture component and the bulk average.

In order to determine the appropriate ε parameter, this methodology was applied to (ThU)O_2 thermal conductivity data. [7,8,9,10,11] A value of ε = 28 provides the minimal error over the range of available data and is therefore employed for all mixtures.

To model the electronic component of the thermal conductivity, the same form as that of pure UO_2 is applied,[12] as shown in Equation 4,

$$k_{elect} = \frac{C}{T^2}\exp\left(-D/T\right) \tag{4}$$

where C and D are fit constants and T is the temperature in K. The constant C is identical to that used by the modified Nuclear Fuels Industries (NFI) correlation.[12] The constant D represents the effect of the temperature acting to free valence electrons and can be translated to the activation energy of valence electrons by Equation 5,

$$D = \frac{\Delta E}{8.617\times10^{-5}\left[\frac{eV}{K}\right]} \tag{5}$$

where ΔE is the activation energy of the material. This activation energy was determined using (ThU)O_2 electrical conductivity experiments[13] and is described by Equations 6 and 7,

$$\Delta E = \Delta E_{UO_2} + f(y)\left(\Delta E_{ThO_2} - \Delta E_{UO_2}\right) \tag{6}$$

$$f(y) = \begin{cases} -2.7309y^2 - 0.8353y + 1 & 0.0 \le y \le 0.25 \\ 12.782\exp(-12.1y) & 0.25 < y \le 1.0 \end{cases} \tag{7}$$

where y is the fraction of UO_2 in the mixture, ΔE_{UO2} is 1.41 eV , and ΔE_{ThO2} is 3.2 eV .[12,14] The total thermal conductivity of the fuel material is found by simply summing the phonon- and electron-dependent components. The application of the molar fraction of each of the material components is based on the isotopic tracking performed by FRAPCON's radial power profile calculations, allowing for dynamic changes to the thermal conductivity. The correlations used for the treatment of fuel porosity and burnup are the same as those applied in FRAPCON-3.3 for UO_2 fuel.[5]

In practice, the typical fuel mixtures used in the RBWR-Th (approximately 60-70% ThO_2, 1-5% PuO2, and a balance of UO_2) have a thermal conductivity much nearer that of pure UO_2, if not slightly lower.

Figure 1 compares the thermal conductivity of a binary mixture of 70% ThO_2 and 30% UO_2, illustrating the degradation associated with mixing effects.

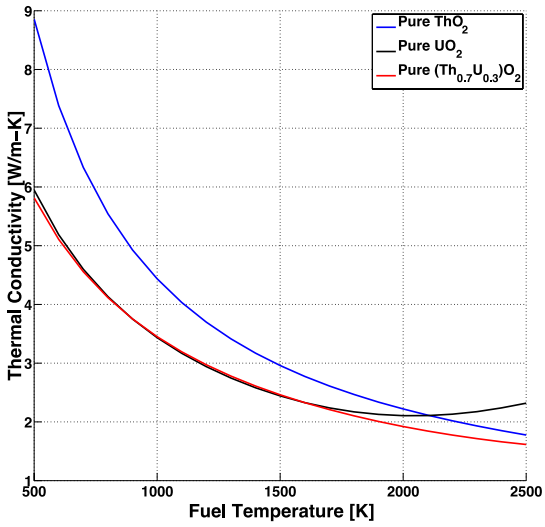

Figure 1. Comparison of pure ThO_2 and UO_2 thermal conductivities with that of a binary 0.7/0.3 ThO_2/UO_2 mixture.

2.1.2. Melting Temperature

The phase diagrams of ThO_2-UO_2, ThO_2-PuO_2, and UO_2-PuO_2 show each system to follow an approximately linear relationship between the melting temperature and molar fraction of components.[15] While this system does deviate from linearity, the operating temperatures of the RBWR-Th fuel remain much cooler than the melting point of any individual constituent. Therefore, the melting temperature is calculated using a simple mixing rule with the melting temperatures listed in Table 1 and the individual component mass fractions.

Table 1. Melting temperatures of pure ThO_2, UO_2, and PuO_2.

Material	Melting Temperature [K]
ThO_2	3651
UO_2	3113
PuO_2	2663

2.1.3. Thermal Expansion

Unfortunately, no data are openly available to describe the thermal expansion of $(ThUPu)O_2$ systems. However, the ThO_2-UO_2, ThO_2-PuO_2, and UO_2-PuO_2 systems all form solid solutions that follow

Vegard's law, exhibiting linear variation of their lattice parameter over the entire composition range.[11] Therefore, the thermal expansion of the mixed $(ThUPu)O_2$ fuel used in the RBWR-Th is assumed to follow a simple mixing rule based on mass fraction and the pure component linear thermal expansion coefficients, as shown in Equations 8 and 9,[12,15]

$$\alpha_{ThO_2} = -0.179 + 5.097 \times 10^{-4}T + 3.732 \times 10^{-7}T^2 - 7.594 \times 10^{-11}T^3 \quad (8)$$

$$\alpha_{UO_2,PuO2} = K_1T - K_2 + K_3\exp\left(\frac{E_d}{k_BT}\right) \quad (9)$$

where K_1, K_2, K_3, and E_d are coefficients listed in Table 2,[12] and k_B is the Boltzmann constant.

Table 2. Coefficients for Equation 9.

Component	K_1 [1/K]	K_2	K_3	E_d [J]
UO_2	9.8x10-6	2.61 x10-3	3.16 x10-1	1.32 x10-19
PuO_2	9.0x10-6	2.7x10-3	7.0 x10-2	7.0 x10-20

2.1.4. Density

Due to the previously mentioned applicability of Vegard's law with regard to the binary fuel systems, the fuel density is found using a simple mixing rule and the component densities listed in Table 3.

Table 3. Theoretical densities of pure ThO_2, UO_2, & PuO_2.

Component	Density [g/cm^3]
ThO_2	10.0
UO_2	10.97
PuO_2	11.5

2.1.5. Fission Gas Release (FGR) Behavior

Examination of irradiated ThO_2–based fuels have shown them to experience significantly lower FGR than UO_2-based fuel irradiated under similar conditions.[16] This tendency towards lower FGR is generally attributed to a decreased mobility of fission gas atoms in the fuel grains. To account for this effect in the FGR model of FRAPCON (a modified version of the Forsberg-Massih model[4]), the diffusion coefficients of the fission gas in the fuel were fractionally reduced. Previously, modifications were made to the base FRAPCON fission gas diffusion coefficients to fit the available ThO_2-based FGR data. The base FRAPCON-3.4 high temperature value was reduced to 50% of its original value, while the low temperature relation was reduced to 10% of its original value.[5] These modifications reflect the expected lower mobility of fission gas in the more stable ThO_2 lattice, which has been observed to lower FGR in integral experiments.

2.2. Modifications to Radial Power Calculations

Previous work has implemented a model to account for the different evolution of the radial power profile through the pellet in (ThU)O_2 fuel, titled the THoria-Urania Power Shape (THUPS) model, but focused on a Pressurized Water Reactor (PWR) environment.[5] Compared to a PWR, the harder neutron spectrum of the RBWR-Th leads to a much flatter radial power profile in the RBWR-Th environment than in a PWR, as shown in Figure 2. Unlike typical LWR fuels, the radial power profile of RBWR-Th fuel does not experience significant rim peaking. This is largely attributable to the longer mean free path of higher energy neutrons reducing the localization of fertile to fissile capture. For fuel rods with the same irradiation history, lower fuel peaking at the rim of the pellet results in higher centerline temperature and burnup. Because both of these factors tend to lead to more challenging fuel conditions, it is important to treat the radial power profile with care.

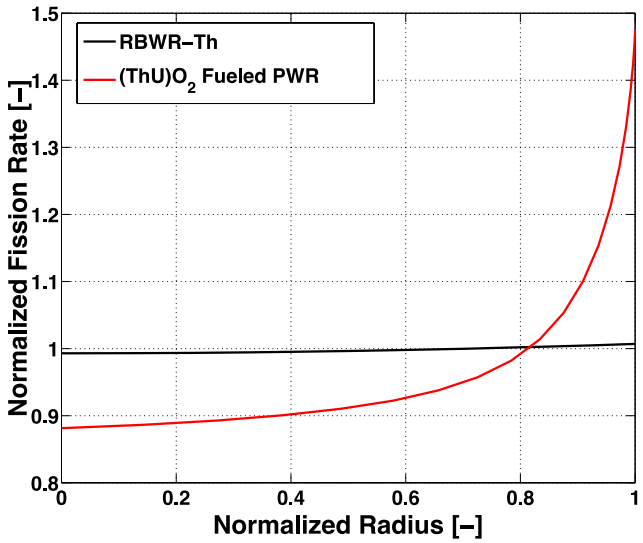

Figure 2. At EOL, the very shallow radial power distribution of the RBWR-Th exhibits notably higher centerline burnups and temperatures than the analogous (ThU)O_2-fueled PWR.

In order to model the different radial profile of the fission rate within the RBWR-Th fuel pellet, the THUPS model (which itself is an extension of TRANSURANUS Burnup (TUBRNP) model[17] to include ^{232}Th, ^{233}Pa, ^{233}U, and ^{234}U) was modified based on reaction rates extracted from the MCNP model used to design the fuel.[18] These reaction rates were used to adjust the average capture and fission cross sections, as well as the radial shape of the ^{232}Th and ^{238}U capture cross sections, shown in Equations 10 and 11, respectively. The cross sections and radial shape functions applied to the entire rod are those associated with an exit void fraction of 88%. While this does not capture the expected higher rim peaking in the lower void regions, it will provide the most conservative radial power for the broader general fuel performance.

$$f_{capt,Th232}(r) = 0.9196 + 0.3497\exp\left(-3.4548\left(1.0 - {}^{r}/_{rfo}\right)^{0.5409}\right), \quad (10)$$

$$f_{capt,U238}(r) = 0.8961 + 0.6469\exp\left(-4.4425\left(1.0 - {}^{r}/_{rfo}\right)^{0.5293}\right), \quad (11)$$

where $f_{capt,iso}$ is the unitless peaking value applied to the isotope's average capture cross section, r is the radial position, and r_{fo} is the fuel pellet outer radius.

2.3. Modified Corrosion & Hydrogen Pickup Behavior

2.3.1 Background

During operation, Zircaloy cladding experiences waterside corrosion, which results in the buildup of an oxide layer on its surface. This oxidation process also results in freed hydrogen, a fraction of which is absorbed by the cladding. If the hydrogen content in the cladding exceeds the local solubility limit, it will precipitate into zirconium hydrides ($ZrH_{1.5}$). These hydrides, in turn, lead to cladding embrittlement. Within current LWRs, oxidation and hydrogen pickup both act to limit the fuel residence time. Historically in BWRs, nodular oxidation has led to fuel failures, though improved alloys have largely resolved this issue. Alternatively, hydrogen embrittlement of the cladding is largely to blame for the reduced margin to failure in high burnup PWR and BWR fuels.

The oxide growth of Zircaloy is typically represented as having two stages.[19] During the first stage, the oxidation growth follows a cubic growth rate. After reaching a thickness of approximately five microns, the oxide growth rate transitions to be linear with time. This behavior is generally credited to the development of a two-layer oxide structure. During the initial, pre-transition growth, the oxide is composed of a single dense layer, termed the barrier layer, which increasingly limits oxygen diffusion as it increases in thickness. After the oxide layer reaches the transition thickness, its growth rate becomes linear as the barrier layer ceases to grow. External to the barrier layer, a second characteristic oxide layer forms, termed the breakaway layer, which is relatively porous, allowing for water penetration. The rate of both the oxidation and hydrogen pickup are each controlled by the diffusion of species across the barrier layer, making it a critical component to limiting the impact of corrosion on cladding performance.

For every oxidation reaction, four free hydrogen atoms are produced. Early in life, the fraction of free hydrogen atoms absorbed by the cladding generally decreases with increases in oxide weight gain,[20] as the barrier layer becomes a thicker diffusion barrier. However, this fraction is heavily dependent on the water chemistry of the reactor coolant,[21] as well as cladding specific alloy components and heat treatment.[22] Due to the complexity of determining the hydrogen pickup, this value is typically determined empirically based on Post Irradiation Examination (PIE) data from operating reactors.[23]

Given its nearly exclusive use in BWRs and the desire to leverage BWR technology, it is assumed that the RBWR-Th will initially make use of modern Zircaloy-2 as the fuel cladding. While the alloying components and contents of Zircaloy-2 have remained within dictated ranges[24,25] for decades, the heat

treatment processes have been refined and optimized, resulting in several proprietary versions of the alloy. This heat treatment is largely aimed at optimizing the microstructure of the cladding material. In addition to the grain size and orientation, the heat treatment process affects the size distribution of Secondary Phase Particles (SPPs).

Owing to the low solubility of the Fe, Cr, and Ni alloying elements in the bulk alpha phase of Zr, these metals precipitate to form SPPs. The SPPs are comprised of two distinct types: Laves phase $Zr(FeCr)_2$ and Zintl phase $Zr_2(NiFe)$.[26] Although the specific role of SPPs in the corrosion process is still not established, experiments on similar alloys with varying SPP sizes have shown them to have a tangible effect on oxidation and hydrogen pickup performance.[27,28] Further, by altering the fraction of different sized SPPs in the cladding, manufacturers have been able to slow corrosion and hydrogen pickup by supporting the barrier layer and slowing diffusion.[26,29] This optimization has also largely eliminated the occurrence of nodular corrosion, which is believed to be attributable to coupled hydrogen diffusion, hydride precipitation, and barrier layer disruption caused by large diameter Ni-containing SPPs.[30]

Examination of high burnup Zircaloy-2 data shows a second, much later, transition in the rate of cladding oxidation and hydrogen pickup.[21,22] It is characterized by an increase in the oxidation rate constant, though the general behavior appears to remain linear, and an exponential increase in cladding hydrogen content with increasing burnup. Current optimized Zircaloy-2 cladding experiences this transition to accelerated oxidation and hydrogen pickup near 10^{26} n/m^2 (>1MeV). This acceleration is attributed to the loss of the protective diffusion properties of the barrier layer due to the dissolution of SPPs by fast neutron irradiation. As they dissolve, the alloying elements from the SPPs are redistributed into the bulk alpha phase Zr[26,29,31,32,33] and remain in solution well above their known solubility limits.[26] In particular, Ni and Fe are known to uniformly redistribute due to relatively high diffusion coefficients in Zr,[34] while Cr is much less mobile and remains within a few microns of the original SPP site. [35,29]

Recent studies have shown that as the SPPs in unirradiated Zircaloy-2 are consumed by the encroaching oxide layer, the various alloying metals behave differently within the oxide layer.[36] Both Cr and Fe tend to oxidize, while Ni remains a distinct metal within the oxide. Additionally, Cr and Ni remain relatively proximal to the original SPP sites, while Fe is more widely distributed. Based on the knowledge of how SPPs dissolve, we can infer that the most significant difference between the behavior of irradiated and unirradiated cladding is the redistribution of Ni, resulting in the loss of localized Ni metallic regions in the barrier layer. Furthermore, the presence of Ni in Zircaloy-2 is intended primarily to prevent nodular corrosion in the more oxidative BWR environment.[22,37] Therefore, it can be reasoned that the redistribution of Ni via fast neutron dissolution of the SPPs results in the accelerated oxidation behavior.

Historically, the Ni in Zircaloy-2 was associated with higher hydrogen pickup in PWR environments and its subsequent replacement with increased Fe resulted in the development of Zircaloy-4.[25] A more recent study[38] has supported this historical perspective, showing that Ni encourages proton transport

and inhibits electron transport, both allowing hydrogen diffusion and preventing deionization at the oxide-coolant interface. As such, it can be assumed that increases in the concentration of soluble Ni uniformly within the oxide are detrimental with regards to hydrogen pickup.

Since there is no RBWR-Th operational data for comparison, this study extrapolates current BWR Zircaloy-2 relations, with some modifications, to RBWR-Th conditions. From the perspective of the cladding, the largest differences between the RBWR-Th and the BWR are the harder neutron spectrum and the higher axial peaking factors, which in combination result in higher peak fast neutron fluxes. Because of the higher flux, the fluence at which the oxidation and hydrogen pickup accelerate will be reached much earlier in the residence time of RBWR-Th fuel. In extrapolating the behavior of Zircaloy-2 from BWRs to the RBWR-Th, it is therefore critical to account for this difference.

2.3.2. Modeling Fast Neutron Dose Induced Oxidation and Hydrogen Pickup Acceleration

Within FRAPCON-3.4, the hydrogen pickup of Zircaloy-2 in a BWR is calculated using an exponential function, shown in Equation 12, which is only dependent on the local fuel burnup.[39] This formulation is tuned to data from several proprietary Zircaloy-2 claddings, which have been irradiated in various commercial BWRs. The acceleration of the hydrogen uptake in the vicinity of 45 MWd/kgHM corresponds to a fast fluence of approximately 9×10^{25} n/m^2 (>1MeV), which is in line with the expected SPP dissolution fluence.

$$\mathrm{H_{tot}} = 22.8 + \exp[0.117\ (\mathrm{BU} - 20)] \tag{12}$$

where Htot is the bulk cladding hydrogen content in ppm by weight (ppm(wt)), and BU is the axially local, radially averaged fuel burnup in MWd/kgHM.

The use of the FRAPCON-3.4 relation to model the RBWR-Th would wholly ignore the differences in fast neutron flux between the reactors because it relies solely on the fuel burnup. Additionally, at burnups beyond its developed range of 62 MWd/kgHM, the exponential term in this model returns non-physical, high hydrogen contents.

Rather than applying the default FRAPCON model, a more physical relation, developed for Zircaloy-2 in BWRs by Zhou, et al.,[19] was implemented in FRAPCON-MIT for use with the RBWR-Th. Using this relation, the hydrogen content of the cladding is found by applying two separate methods and using the maximum value, so long as it exceeds the as-fabricated hydrogen content. The first method, described by Equation 13, uses a hydrogen pickup fraction to find the amount of hydrogen absorbed as a function of cladding thickness. The second method, described by Equation 16, uses an exponential function of the fast neutron fluence to describe the accelerated pickup after the barrier layer's destabilization.

$$\mathrm{H_{PU}} = 28.94\ \mathrm{F(S)} \frac{\mathrm{S}}{\mathrm{wc}} \tag{13}$$

where HPU is the hydrogen picked up from oxidation in ppm(wt), S is the oxide thickness, in μm, w is the cladding wall thickness in mm, c is a correction factor, described by Equation 14, and F(S) is the

hydrogen pickup fraction and is described by Equation 15. It should be noted that F(S) represents a cumulative hydrogen pickup fraction and is not a measure of the hydrogen pickup fraction at any particular moment, though this can be found through manipulation.

$$c = \frac{d_o - d_i}{2d_o} \quad (14)$$

where d_o is the cladding outer diameter and d_i is the cladding inner diameter.

$$F(S) = K_1 + \frac{K_2}{K_3 S}[1 - \exp(K_3 S)] \quad (15)$$

$$H_{Acc} = 24.219\, K_0 \exp(K_4 4.638 \times 10^{-25} \Phi) \quad (16)$$

where Φ is the fast fluence in n/m^2 (>1 MeV) on the cladding. The coefficients K_1, K_2, and K_3 were tuned to conservatively fit the default FRAPCON Zircaloy-2 hydrogen pickup relation. The coefficients used in the accelerated pickup model, K_0 and K_4, were determined by fitting Equation 16 to match Equation 12 at fluences greater than 10^{26} n/m^2 (>1MeV). This was accomplished by using the specific fast neutron flux (normalized by specific power) of a typical BWR to convert burnup, used in Equation 12, to fluence, used in Equation 16. To accommodate the possibility that the transition to accelerated oxidation and hydrogen pickup may occur at a fluence other than 1026 n/m2(>1MeV), Equation 16 was modified to allow for the acceleration to start at any specified fluence. Table 4 lists the coefficient values used in Equations 15 and 16. The maximum and mean values found by the Zhou and FRAPCON-3.4 models are compared for a typical BWR fuel rod in Figure 3, and show good agreement.

Table 4. Coefficients associated with Equations 15 and 16.

Coefficient	Value
K_0	0.03868
K_1	0.00760
K_2	0.16075
K_3	0.23113
K_4	0.08075

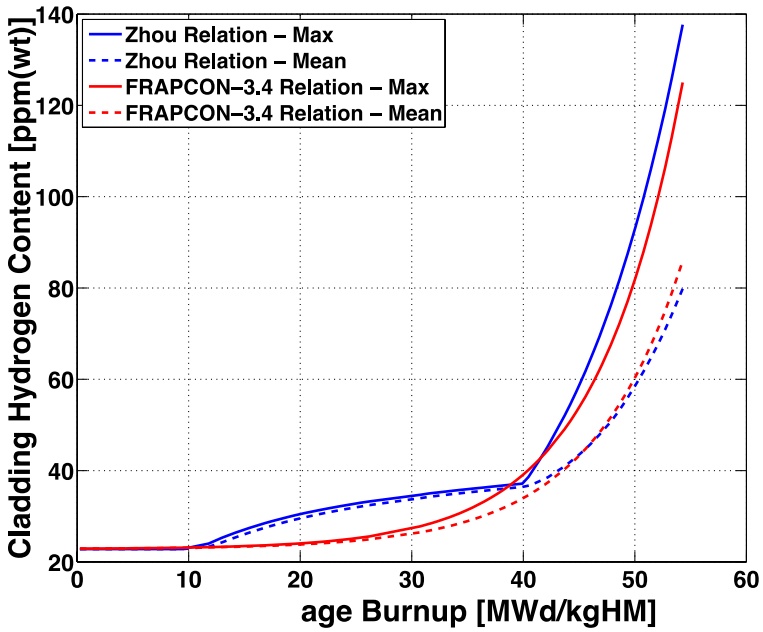

Figure 3. For a typical BWR rod, the Zhou relation is conservatively well fit to the FRAPCON-3.4 relation it has been tuned to match.

The unbounded exponential term in Equation 12 leads to non-physically high hydrogen content predictions at high fluences. To avoid such issues, a third relation was added to the model to cap the hydrogen pickup fraction to 100% of the hydrogen created by oxidation events. The final relation takes a similar form to Equation 16, but with the use of F(S) = 1.0 and ΔS rather than S. This relation accounts for the fact that, like a BWR, the RBWR is expected to operate with a coolant oxygen overpressure, resulting in very little free hydrogen outside of that created by the oxidation process. A hydrogen pickup fraction greater than 100% implies that hydrogen that has not been freed by an oxidation event would be absorbed. While radiolysis can provide additional free hydrogen, it is unlikely to support such a high pickup fraction. Though the maximum value of 100% hydrogen pickup is very high, it is assumed in order to provide a conservative assessment in the face of limited experimental data.

While FRAPCON-3.4's hydrogen uptake model captured the accelerated hydrogen absorption at high burnups, its oxidation model neglects the accelerated growth of the oxide layer after the loss of the barrier layer's protection. Zhou, et al.[19] did provide an oxidation model that experiences acceleration. However, not enough detailed data are available to determine adequate fitting coefficients for its use.

To accommodate the accelerated oxidation, a simple multiplier of 2.2 was applied after the transition fluence to the oxidation rate constant. This value was chosen based on a previously performed fit to available data.[40]

3. Fuel Rod Limits

Recently, the NRC has reevaluated the acceptance criteria for rod survival during both Loss of Coolant Accidents (LOCAs) and Reactivity Insertion Accidents (RIAs). These new criteria are intended to account for the degradation of the cladding's mechanical properties during irradiation.[41,42] In particular, they focus on the role of embrittlement due to hydrogen in the cladding lowering the threshold to fuel failure under accident conditions.

The application of the different failure criteria accounts for separate failure mechanisms between LOCA and RIA scenarios. For LOCAs, this criterion is based on a loss of ductility that will result in cladding failure when quenching occurs during the core reflood stage. This ductility change is quantified using the Equivalent Cladding Reacted (ECR), which is a measure of what portion of the cladding has become oxidized. As the hydrogen content increases, it is has been shown that the ductile-to-brittle transition occurs at decreasing ECR values.[43] During RIAs, on the other hand, the cladding experiences large stresses due to rapid fuel expansion. The degree of severity for this scenario is measured by the radially averaged specific enthalpy gain of the fuel (Δh). Hydrogen induced cladding embrittlement hinders the cladding's ability to withstand this rapid expansion, thereby resulting in limitations to the allowable Δh as a function of cladding hydrogen content.

Because the RBWR-Th is an extension of current BWR technology, this study will assume that it will be bound to current BWR safety guidelines in order to be considered a viable design. Therefore, the NRC's hydrogen based accident failure criteria will be applied to RBWR fuel designs. These limitations are detailed in Equations 17 and 18 and illustrated in Figures 4 and 5.

$$\mathrm{ECR_{Allowed}} = \begin{cases} 18 - 0.03\mathrm{H}; & \mathrm{H} < 400 \\ 18 - 0.01\mathrm{H}; & 400 \leq \mathrm{H} < 600 \\ 0; & 600 \leq \mathrm{H} \end{cases} \quad (17)$$

Where $\mathrm{ECR_{Allowed}}$ is the maximum allowed ECR in %, and H is the local hydrogen content of the cladding in ppm(wt).

$$\Delta\mathrm{h_{Allowed}} = \begin{cases} 150; & \mathrm{H} < 75 \\ 240 - 1.2\mathrm{H}; & 75 \leq \mathrm{H} < 150 \\ 70 - 0.0667\mathrm{H}; & 150 \leq \mathrm{H} \end{cases} \quad (18)$$

Where $\Delta\mathrm{h_{Allowed}}$ is the maximum allowed change in specific enthalpy due to the RIA in units of cal/g.

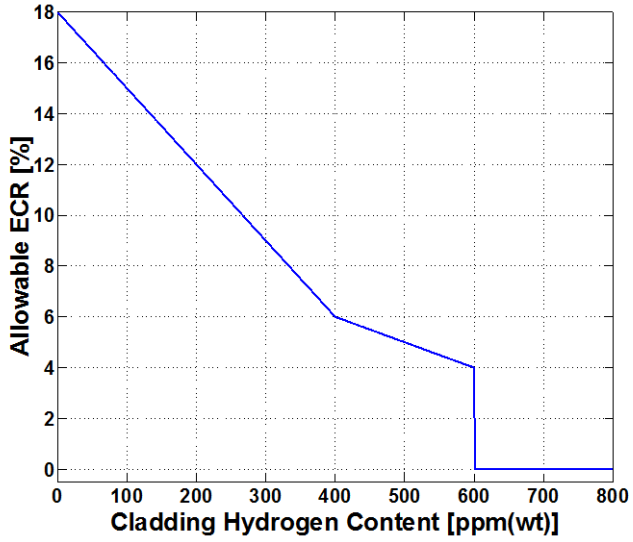

Figure 4. The allowable ECR for a BWR experiencing an accident suffers with increasing cladding hydrogen content, with zero available margin when cladding hydrogen contents exceed 600 ppm(wt).

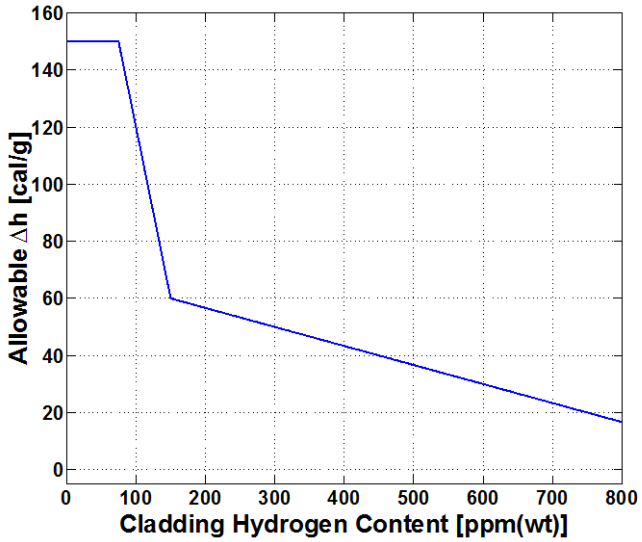

Figure 5. The allowable Δh for a BWR experiencing an RIA suffers with increasing cladding hydrogen content.

Unlike the accident limits, the steady state limitations imposed on the RBWR-Th are much simpler: the fuel must not melt, the plenum pressure must remain below the coolant pressure, and the hoop strain must remain under 1%. In general, these limitations do not provide many challenges, though the limited free gas volume of the rod designs can result in plenum pressures with rising FGR at high burnups.

4. Assessment of Average RBWR-Th Fuel Rods

Currently, the RBWR-Th lacks a full-scale core simulator. Therefore, current reactor physics calculations have been limited to single rod and assembly level Monte Carlo depletion assessments. This methodology provides useful axial power shapes and fast neutron fluxes for fuel performance studies, but lacks a realistic power history. While this lack of fuel power histories does limit the ability to simulate RBWR-Th fuel, a preliminary fuel performance assessment of an average fuel rod will provide useful insights into general fuel behaviors. For this analysis, the average rod power in the core is applied for the entirety of the anticipated residence time. In addition to a fuel rod operated at a constant average core power, a second rod was simulated to have been irradiated at 130% of the average core power for an equal amount of time. The use of 130% average power over the entire irradiation time is intended to conservatively account for inter- and intra-assembly radial peaking throughout the core, although such sustained peaking in a single fuel rod is unlikely.

Over the course of this study, the fuel design has undergone significant evolution, and it is expected to experience further minor iterations as a full core simulator is developed. The most recent of these designs are presented here, detailed in Table 5. The RBWR-Th makes use of a single axial seed (fissile) region with upper and lower blankets. The seed region contains fissile and other isotopes of UO_2 and PuO_2, the balance being ThO_2. The blanket region is pure ThO_2. Though this design makes use of heterogeneous axial fuel materials in a single rod, FRAPCON-MIT lacks the ability to simulate more than one fuel material. As the blanket regions do not significantly impact fuel performance, the seed region composition is assumed throughout the fuel rod without significant effects. Additionally, current assembly-level designs make use of radial seed and blanket regions. This analysis only evaluates the seed rods, due to their higher Linear Heat Generation Rates (LHGRs). For this analysis, an average LHGR of 12.65 kW/m is assumed throughout a full five cycles, totaling 1915 days, resulting in an average burnup of 48.8 MWd/kgHM.

Table 5. RBWR-Th Fuel Rod Parameters

Parameter	Value	Units
Pitch	1.135	cm
Cladding Outer Radius	5.025	mm
Cladding Thickness	0.6	mm
Fuel Outer Radius	4.35	mm
Upper Fuel Blanket Length	20	cm
Seed Fuel Length	114.3	cm
Lower Fuel Blanket Length	28	cm
Effective Cold Plenum Length	40	cm
Avg. Seed UO2 Content	29.43	% (wt)
Avg. Seed PuO2 Content	4.47	% (wt)
Seed 233U Enrichment	13.75	% (Utot)

Seed 234U Enrichment	5.95	% (Utot)
Seed 235U Enrichment	1.68	% (Utot)
Seed 236U Enrichment	1.62	% (Utot)
Seed 239Pu Enrichment	53.08	% (Putot)
Seed 240Pu Enrichment	33.48	% (Putot)
Seed 241Pu Enrichment	4.56	% (Putot)
Seed 242Pu Enrichment	4.88	% (Putot)
Fuel Density	91	% TD
Fill Gas	He	-
Fill Gas Initial Cold Pressure	1.0	MPa
System Pressure	7.14	MPa
Inlet Temperature	551.6	K
Average LHGR	12.40	kW/m
Residence Time	1915	EFPD

During their residence in the reactor, both designs experience significant bottom peaking, due to increased moderation, at Beginning Of Life (BOL), and top peaking, due to depletion in the bottom and fissile breeding in the harder spectrum of the top's higher void, at End Of Life (EOL). This evolution results in a center peaked EOL burnup profile, shown in Figure 6. While not explicitly shown here, six distinct axial power shapes are used throughout the irradiation history. These axial power shapes were dictated by the neutronic analysis of the current design.

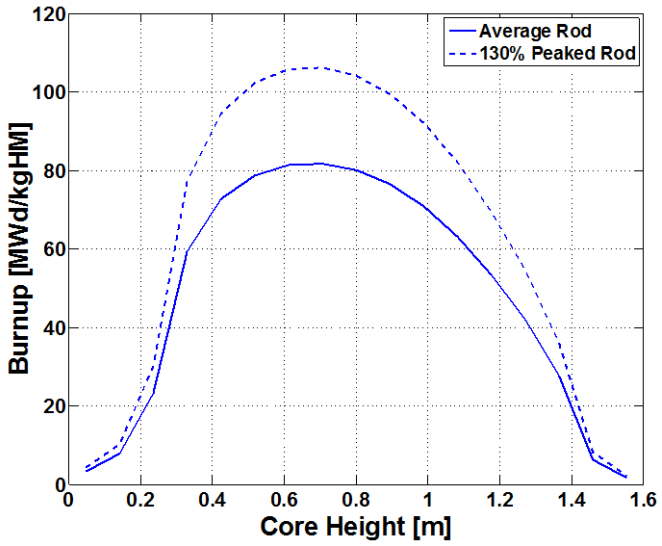

Figure 6. Despite high BOL bottom peaking and EOL top peaking, the EOL burnup profile (shown) is peaked near the center. The blanket regions at the axial periphery accumulate very little burnup due to their low power production.

The applied specific fast neutron flux (E >1 MeV) for the RBWR-Th is shown in Figure 7. Because of the low power production in the blankets, the specific fast flux in those regions is very high, though with little consequence. Figure 7 also includes a comparison to the typical specific fast flux profiles PWRs and BWRs. Due to the tight pitch and high void, the specific fast flux can be seen to be significantly higher than either a typical PWR or BWR. As will be discussed, this along with the relatively high burnups shown in Figure 6, result in much higher cladding fast fluences than are observed in current LWRs.

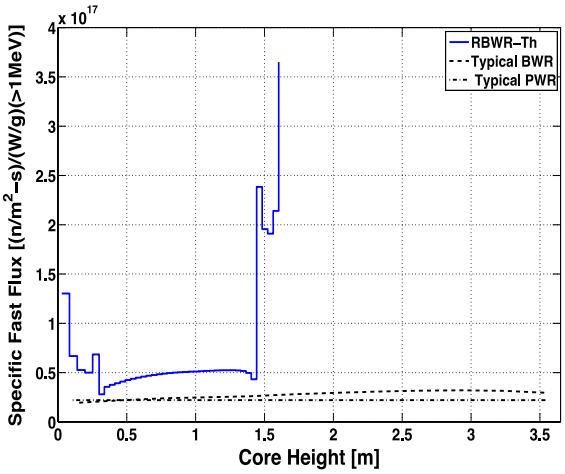

Figure 7. Once normalized to the specific power of the fuel, the RBWR-Th experience fast neutron fluxes that greatly exceed those of a typical BWR or PWR. The high values at the axial extremes are artifacts of the very low LHGRs in the blanket regions.

Despite high axial peaking in the seed region, the maximum fuel temperatures do not exceed 1450K and 1900K, for the average and 130% peaked rod, respectively. These temperatures provide a generous margin to melting for UO_2 fuel, and even more margin for $(ThUPu)O_2$. The assumed constant power history results in operating fuel temperatures, shown in Figure 8, which remain within 100K of the lifetime average value. In addition to the well-behaved fuel temperatures, neither case challenges the maximum cladding hoop strain limit of 1%.

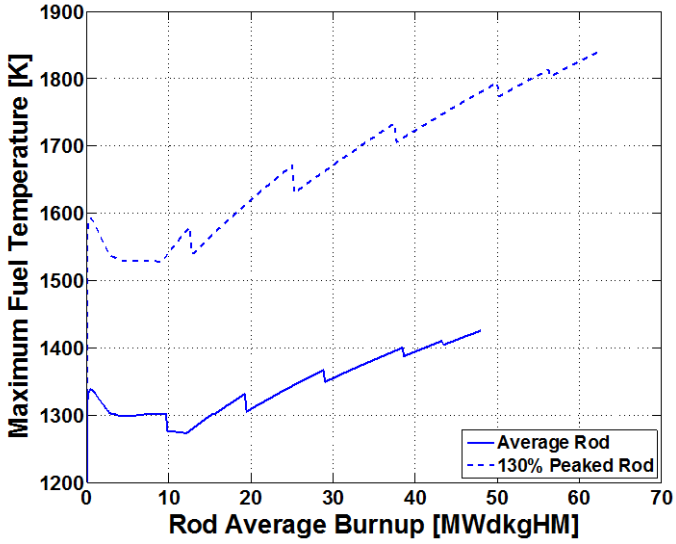

Figure 8. The maximum fuel temperatures throughout the irradiation history provide a wide margin to melting.

The general stability of ThO_2-based fuel results in low FGR fractions for the average rod, shown in Figure 9. Despite the improved performance of ThO_2-based fuel, the higher fuel temperatures of the 130% peaked case experiences significant FGR. Figure 10 shows this to result in high, though not unacceptable, plenum pressures. To prevent plenum pressures higher that the coolant pressure, the rod has been designed with a 40cm plenum. While this plenum is significantly longer than that of a typical BWR, it does not result in a restrictive core pressure drop.

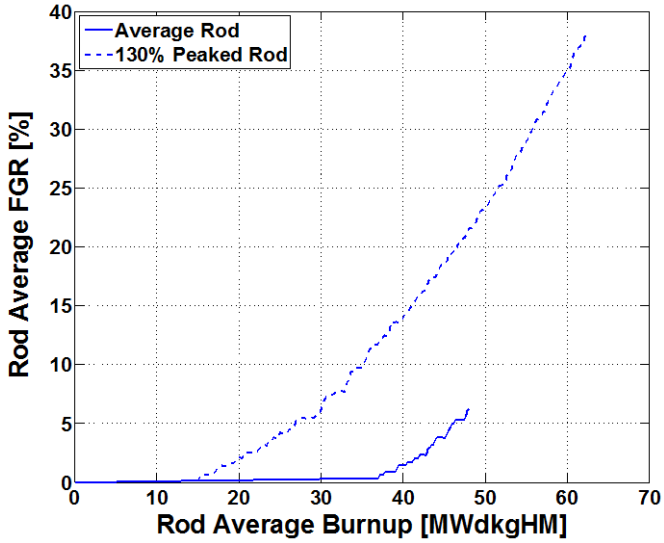

Figure 9. The global FGR fraction of the average rod remains low, while the 130% rod experiences large gas releases due to high fuel temperatures.

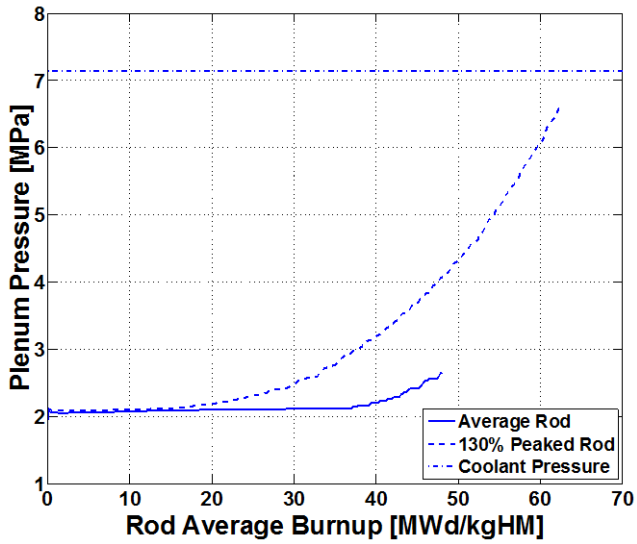

Figure 10. The plenum pressure of each case remains below the coolant pressure.

Though the scarcity of FGR data for ThO_2-based fuels leaves appreciable uncertainty in calculations, this assessment shows that it is unlikely to present a limiting issue. At an average LHGR, the fuel experiences very little FGR. However, the 130% peaked case is observed to experience high FGR values, well exceeding typical LWR rods. Despite this, the plenum pressure is not expected to exceed the coolant pressure. Thus, even at high FGR, the RBWR-Th is not expected to risk cladding lift-off. Further, the assumption that the peaked rod will experience 130% of average LHGR throughout a full 5-cycle irradiation history is very conservative. At EOL, when the observed plenum pressures and FGR are highest, it is reasonable to assume that a more realistic peak rod would have less power, and thus be further removed from limiting conditions associated with FGR. This conservatism provides confidence that, despite the uncertainty surrounding ThO_2 FGR, the RBWR-Th will not be challenged by a cladding lift-off condition.

Unlike the fuel temperature FGR, the cladding oxidation and hydrogen content calculations are largely insensitive to power history variation throughout irradiation. Therefore, values of these parameters found using a static power history will be highly representative of any rod irradiated to a similar burnup value. The calculated maximum cladding hydrogen content for each case is illustrated in Figure 11. The high fast fluence leads to a transition to accelerated corrosion and hydrogen pickup near 18 MWd/kgHM. This early transition, compared to approximately 40 MWd/kgHM for a BWR, leads to a very high cladding hydrogen content at EOL. Similar to the hydrogen content, Figure 12 shows that the oxidation experiences a similar transition. However, unlike the hydrogen content, the accelerated oxide growth alone has little consequence on the rods' performance.

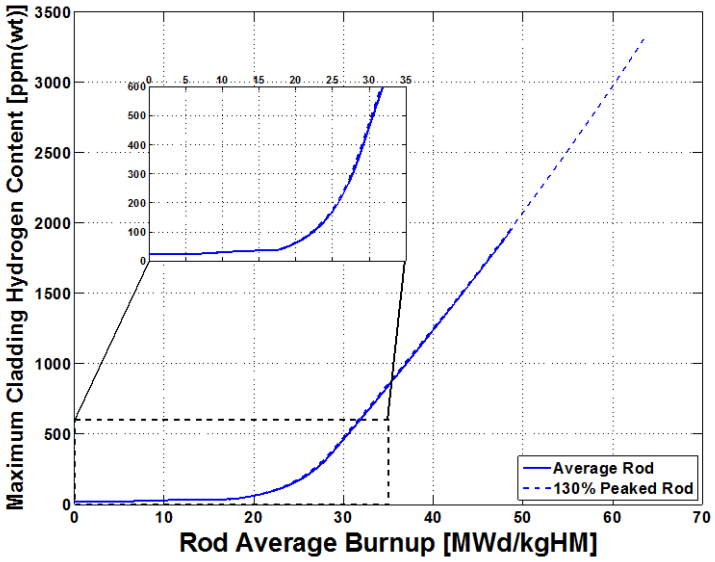

Figure 11. The hydrogen content of the cladding for each case is shown to exceed 1500 ppm(wt). Closer inspection reveals the hydrogen pickup behavior to accelerate near 18 MWd/kgHM, eclipsing the practical limit of 600 ppm(wt) by 32 MWd/kgHM.

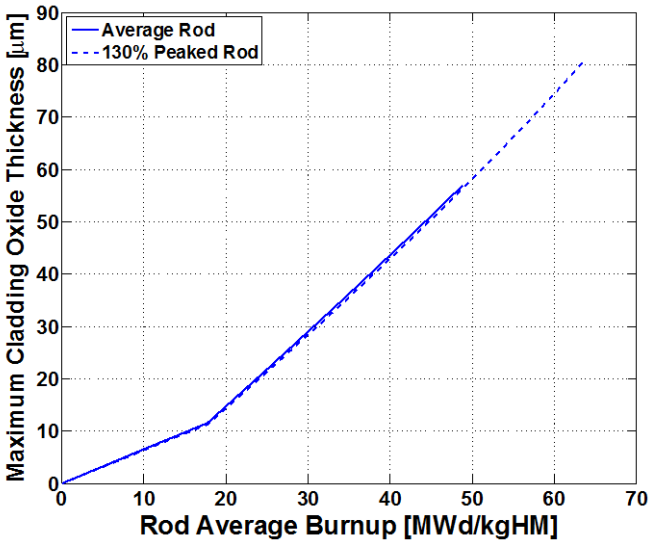

Figure 12. Zr-2 maximum cladding oxidation for both cases as a function of burnup. Oxide thickness alone does not challenge the limits in either case.

Without context, the hydrogen content of the cladding gives little information about the acceptability of an RBWR-Th fuel rod for commercial operation. However, by applying Equations 8 and 9,

we can determine the most limiting allowable fuel failure criteria for accident conditions, shown in Figures 13 and 14. The early acceleration of hydrogen uptake, starting at 18 MWd/kgHM (rod average) for both cases, can be seen to severely restrict the RBWR-Th's allowable accident additional oxidation and energy deposition very quickly. This rapid decrease is wholly attributable to the large fast fluences accumulated by the RBWR-Th's cladding. Ultimately, neither case reaches EOL with any remaining margins for accident conditions. Of the two criteria, the allowable ECR is most limiting, with neither case having non-zero value beyond 32 MWd/kgHM.

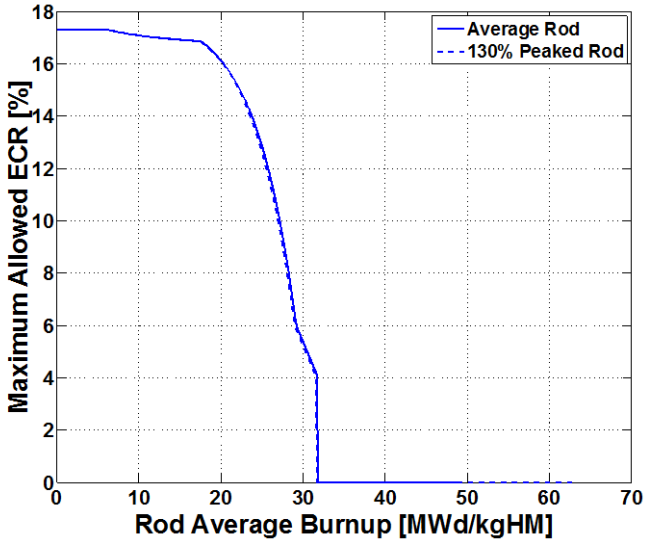

Figure 13. Application of the hydrogen-based ECR limit results in rapid reduction and elimination of any allowable ECR during an accident well before the EOL for both cases.

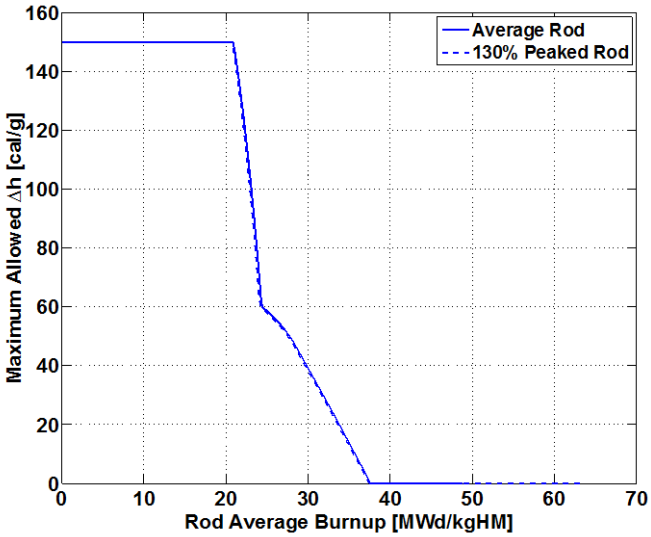

Figure 14. Application of the hydrogen-based Δh limit results in rapid reduction and elimination of the margin of additional Δh during an RIA well before the EOL for both cases.

Given the results of this analysis, the cladding hydrogen content is expected to present a major challenge to the successful design and operation of the RBWR-Th. Owing to the expected acceleration of the cladding oxidation and hydrogen pickup at fluences greater than 10^{26} n/m^2(>1MeV), the average case is expected to be able to retain non-zero accident margins for only 66% of its respective design lifetimes.

5. Irradiation Tolerant Cladding for Improved Accident Margins

The eliminated accident margins in the RBWR-Th are largely due to the fact that current Zircaloy-2 alloys are designed with the express intention of operating in current BWR cores without exceeding the mandated rod averaged burnup of 62 MWd/kgHM. Within this design envelope, current Zircaloy-2 cladding is optimized to provide minimum corrosion and hydrogen pickup. The onset of acceleration due to irradiation currently only occurs near the end of life for the highest burnt BWR rods. With this current burnup limit, little incentive exists for vendors to develop cladding that will better tolerate high fast neutron fluences.

Because of the RBWR-Th's much harder spectrum and high axial peaking, the cladding accumulates fast neutron fluence much more quickly than conventional BWRs. This is illustrated by Figure 15, which compares the EOL fast neutron fluence of both cases against two samples irradiated in commercial LWRs to very high fluences of 1.79x10^{26} and 3.0x10^{26} n/m^2.[31,35] The fluences accumulated in these samples lie at or near the boundary of current operational experience. The comparison with these samples demonstrates that the RBWR-Th design is expected to challenge the available experience of Zircaloy-2.

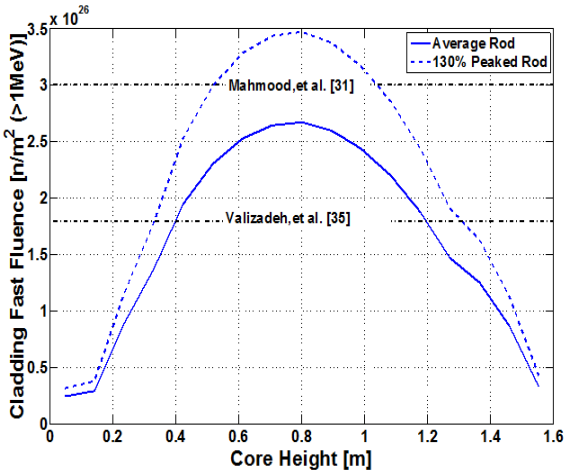

Figure 15. The fast neutron fluence of both cases at EOL can be seen to challenge available experiments[31,35] that mark the boundary of Zircaloy-2 operational experience.

Although the easiest way to improve the accident margins of the RBWR-Th is to reduce the fast neutron fluence imposed on the cladding, the end result of such reductions would hinder the ability of the reactor to sustainably breed fissile isotopes and maintain a reasonable fuel cycle. As such, the viability of the RBWR-Th may require the employment of a cladding material that better resists the acceleration of oxidation and hydrogen uptake. Because the RBWR-Th cannot afford to lose neutrons to increased cladding absorption, steel claddings, like HT-9, do not present an acceptable option. While HT-9 is generally deemed to be an acceptable high fluence fast reactor cladding, the parasitic nature of steel claddings, along with a lack of operation experience, has led to its dismissal as an option for the RBWR-Th. Likewise, the lack of any operational experience with ceramic cladding in LWRs excludes new SiC composites from consideration. Therefore, it is assumed that any new cladding used in the RBWR-Th will be adapted from current zirconium based alloys.

As discussed in Section 2.3.1, the dissolution of Ni from SPPs is suspected to be the root cause of the accelerated oxidation and hydrogen pickup at high fast neutron fluences. To address this, GNF is currently developing a new cladding material, referred to as GNF-Ziron.[34,44,45] Compared to Zircaloy-2, GNF-Ziron has a higher than permitted Fe content (0.26wt%). Additionally, the Ni content lies in the lower half of the Zircaloy-2 specification (0.05wt%) and the Sn and Cr contents remain relatively unchanged.[24]

The oxidation and hydrogen pickup behavior of GNF-Ziron are compared to Zircaloy-2 in Figures 16 and 17. While the oxidation behavior is similar to Zircaloy-2, accelerating after 10^{26} n/m^2 (>1MeV), the hydrogen pickup fraction remains comparatively low, without signs of major acceleration to 1.6×10^{26} n/m^2 (>1MeV). The reported operational experience with GNF-Ziron is extremely limited, but what is known is promising for high neutron fluence applications. Currently, four Lead Test Assemblies (LTAs) are being irradiated at the Edwin I. Hatch nuclear plant.[46]

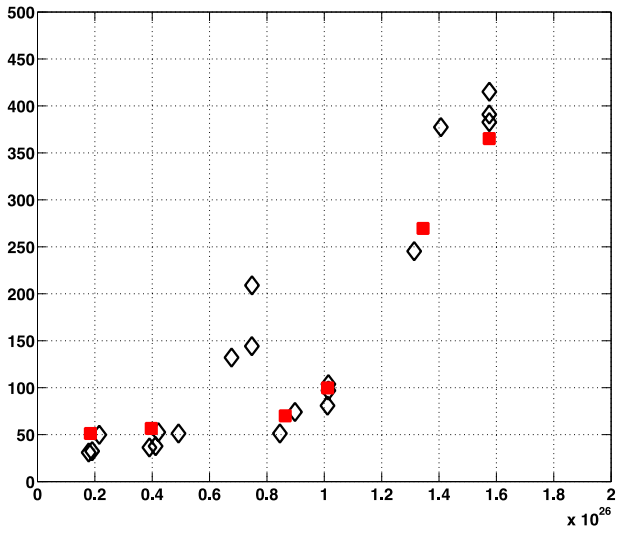

Figure 16. Corrosion weight gain data[45] suggest that GNF-Ziron will experience accelerated oxidation at high fast neutron fluences similar to Zircaloy-2.

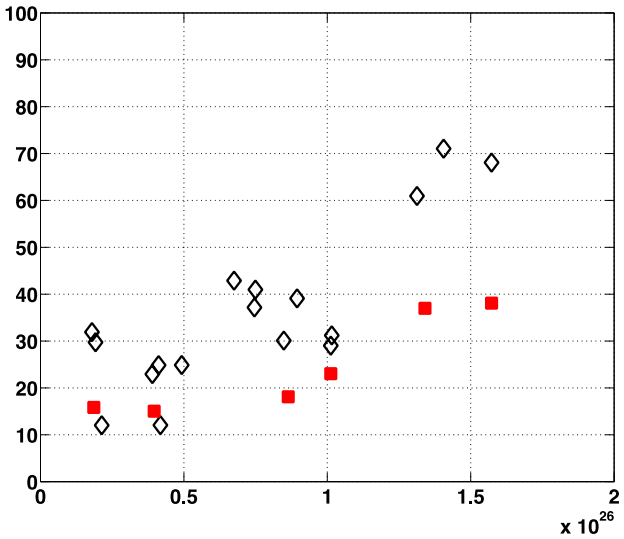

Figure 17. Hydrogen pickup data[45] suggest that GNF-Ziron will see lower accelerated hydrogen pickup than seen in Zircaloy-2 at high fast neutron fluences.

To understand how the use of GNF-Ziron cladding can benefit the RBWR-Th, a sensitivity study was performed on the effect of delaying the transition fluence to accelerated behavior on the accident tolerance of the fuel. While previous assessments had assumed the acceleration of the oxidation and hydrogen pickup to occur simultaneously, the available GNF-Ziron data suggests that it will experience oxidation acceleration at the same fluence as Zircaloy-2, though data on the hydrogen pickup is less clear. The expected accident tolerance of the RBWR-Th fuel designs was compared over a range of burnups and transition fluence of up to $5x10^{26}$ n/m^2(>1MeV).

Inspection of the maximum allowed ECR over the range of transition fluence and EOL burnup for each case, seen in Figure 18, shows that substantial gains in accident tolerance can be achieved by delaying the onset of accelerated hydrogen pickup. Once the transition to accelerated behavior has been delayed enough to allow for non-zero margins, near 1.9x1026 n/m2(>1MeV) the allowable ECR increases rapidly. In general, once a non-zero ECR value has been achieved for the desired burnup, a further delay of ~$0.6x10^{26}$ n/m^2(>1MeV) results in the allowed ECR reaching a plateau. Comparison with Figure 15 shows that this is the result of delaying the accelerated behavior beyond the maximum fluence observed in the cladding.

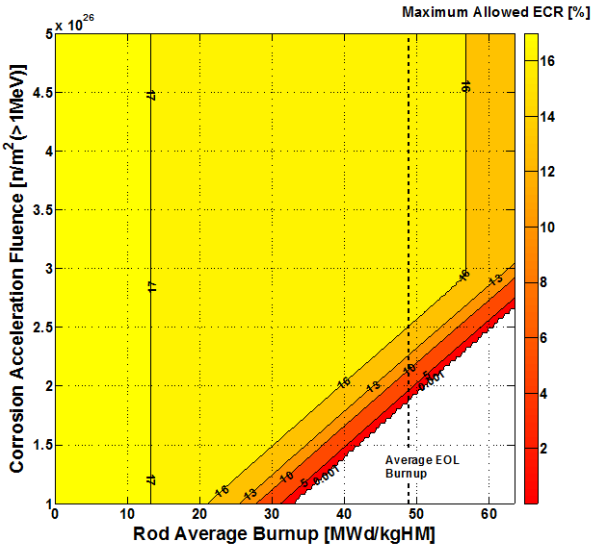

Figure 18. A comparison of allowable ECR values up to 130% of the average EOL burnup, given a delay to the accelerated hydrogen pickup behavior shows that a substantial delay is required to achieve non-zero margins for an average EOL burnup. Margins in ECR are rapidly recovered after non-zero values are achieved.

It can also be observed that lowering the rod average burnup could provide increased accident margins. However, such a strategy would be detrimental to the RBWR-Th's goal of achieving a breakeven breeding cycle. Therefore, decreasing the rod average burnup is not viewed as a viable strategy to regain accident margins.

While the effect of the delayed transition fluence on the allowable Δh, shown in Figure 19, is similar to the effect on ECR, non-zero values are realized at much lower transition fluences. Despite the relative ease of regaining a positive Δh margin, the rate at which the allowable Δh increases can be seen to be much lower with the ECR. This is due to the substantial drop in allowable Δh over the range of 75 to 200 ppm(wt).

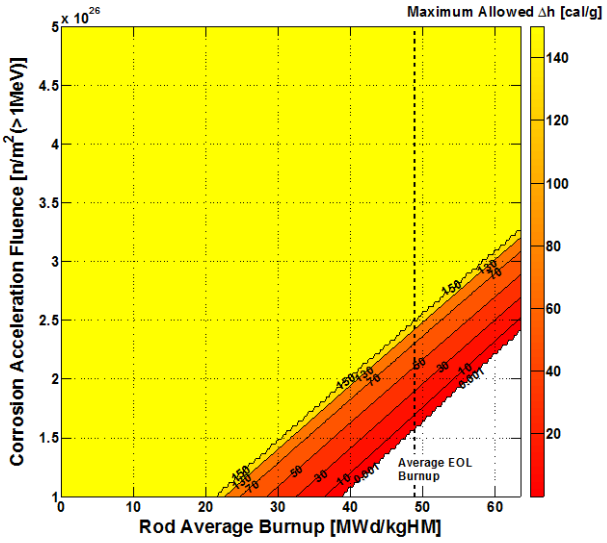

Figure 19. A comparison of allowable Δh values up to 130% of the average EOL burnup given, a delay to the accelerated hydrogen pickup behavior shows that a substantial delay is required to achieve non-zero margins for an average EOL burnup. After achieving a non-zero value, margins in Δh are recovered less quickly than those for ECR.

Though they provide an understanding of how accident margins can be regained, Figures 18 and 19 are of little use in the absence of reactor accident responses. Rather, these sensitivity studies are intended to supply reactor designers with an understanding of the limitations imposed on fuel designs by the choice of cladding materials and the fast fluence imposed upon them. As future studies provide improved understanding of the core's response to accident situations, these sensitivity studies will provide a basis for cladding performance requirements.

Especially with the limited available experimental data, there is no firm assurance that GNF-Ziron cladding will provide a viable solution for the RBWR-Th. However, it does demonstrate that the high burnup behavior of current Zircaloy claddings can be improved while maintaining acceptable corrosion behavior at BOL The most promising approaches to creating the optimal cladding material from a zirconium-based alloy are: developing a heat treatment procedure that results in a SPP size distribution that minimizes dissolution and altering the alloying components to optimize the protective properties of the barrier layer.

While some studies have modeled the dissolution dynamics of SPP dissolution due to fast neutron flux,[47,31] their applicability to understanding the amount solute alloying components in the bulk material is limited. Improved dissolution models coupled with detailed experiments could provide a more complete understanding of how SPP dissolution affects the cladding corrosion. This, in turn, could allow core designers to determine the optimal SPP size distribution for their required alloy, which could hopefully be achieved with proper heat treatments. The experiments required to establish such a model

would be extensive, including detailed characterization of the SPP distribution and oxidation and hydrogen uptake behavior of both fresh and irradiated cladding.

The second approach of altering the alloying components has already experienced major success in the nuclear industry prior to the development of GNF-Ziron. Due to the high hydrogen pickup rate of Zircaloy-2 in PWR environments, Zircaloy-4 was developed from Zircaloy-2. Further, the addition of niobium in M5 and ZIRLO claddings, has been demonstrated to further improve corrosion performance. Currently, these alloys have not seen much adoption in BWRs, but they may be able to provide the RBWR with a viable cladding.

6. Preliminary Comparison to an Average RBWR-AC Fuel Rod

Unlike the RBWR-Th, which has one axial seed region and $(ThUPu)O_2$ fuel, the RBWR-AC makes use of two axial seed regions and $(UPu)O_2$ fuel. However, the RBWR-AC does utilize a similar tight-pitched triangular lattice and high void fraction to achieve an epithermal neutron spectrum. Previously, a steady-state fuel assessment of the RBWR-AC was performed using a different version of FRAPCON, which had been modified to accommodate RBWR.[1] Particularly, this version of FRAPCON pre-dated the improved hydrogen pickup model and hydrogen-based accident limits that were applied as part of this study. Despite this, the RBWR-AC evaluation concluded that further development of an advanced Zircaloy would be required for steady-state fuel operations.

In general, the epithermal neutron spectra associated with all the RBWR reactor designs are expected to result in cladding fast fluences that challenge current Zircaloy-2 operational experience. The RBWR-AC, for example, experiences higher peak fast neutron fluences in the seed region than the RBWR-Th. While RBWR transuranic burner designs utilize softer neutron spectra, they still handily exceed the fluences of typical BWR cladding. Ultimately, these high fast fluences to Zircaloy-2 will result in severely restricted (or eliminated) cladding accident tolerances. This commonality between the designs further emphasizes the need for advanced RBWR cladding materials.

Additionally, the use of Th-based fuels and comparatively lower local LHGRs and burnups in the RBWR-Th design results in generally favorable fuel performance over the RBWR-AC. The decreased fission gas diffusion afforded by the addition of ThO_2 leads to lower FGR fractions, resulting in more manageable plenum gas pressures. Similarly, the lower centerline fuel temperatures and increased melting temperatures provide higher margins to fuel melting. However, these observations are based on the assumption of constant average power histories in the fuel rods, which are not indicative of realistic irradiation conditions. As such, the comparison of the RBWR-Th and RBWR-AC fuel parameters should not be viewed as a definitive ranking of the reactors' overall fuel performance.

7. Conclusions

To adequately model the fuel performance of the RBWR-Th, new radial ^{232}Th and ^{238}U capture cross-section distributions with lower peaking factors, along with models for accelerated oxidation and

hydrogen absorption at high fast neutron fluence were added to FRAPCON-MIT. These models were applied to an average and 130% peaked RBWR-Th rod. Each was simulated as irradiated at a constant power level for a full five cycles, totaling 1915 days. Over the course of irradiation, the RBWR-Th maintained large margins to melting and acceptable cladding strain values. The FGR of the 130% peaked case was found to be relatively high due to high fuel temperatures. However, by designing a plenum to provide adequate gas volume, the plenum pressure remains below the coolant pressure. The cladding hydrogen content, however, was found to significantly exceed that of a conventional BWR. The large hydrogen content values are attributable to an early acceleration of hydrogen uptake due to the RBWR-Th's higher fast neutron flux and high axial peaking.

When the cladding hydrogen contents were applied to the NRC's hydrogen based accident limits, the RBWR-Th was found to suffer substantial degradation in margins to the limits and total elimination of permissible LOCA and RIA occurrence. This illustrates the fact that current Zircaloy-2 cladding options will not be viable for the RBWR-Th. A new cladding material, GNF-Ziron, has shown promise for high fluence applications and was proposed for use in the RBWR-Th. Because of limited available GNF-Ziron data, a sensitivity study was performed to show the effect of delaying the acceleration of the hydrogen pickup. This study showed that delaying the acceleration to 1.9×10^{26} n/m^2 (>1MeV), would allow for non-zero accident margins. Further delay of the transition was shown to rapidly improve the LOCA and RIA limits.

While this study has provided valuable insights to the expected fuel challenges for the RBWR-Th, further investigations are required as the reactor design matures. With the future development of a whole core simulator, fuel performance evaluations will need to be performed to determine the potential effects due to expected power histories and axial power shapes. Additionally, the hydrogen-based accident limitations need to be applied to actual LOCA and RIA simulations as these become available. The results of such simulations could then inform the degree of irradiation tolerance required of the cladding.

Acknowledgments:

This work has been supported by the NEUP project 11-3023. The authors thank the project's design team, particularly Mr. Phillip Gorman, for supplying parameters for the most current design iteration, as well as for commenting on the results of the modeling at project meetings. Additionally, the insights of Dr. Koroush Shirvan and Mr. Yanin Sukjai at MIT into the RBWR designs and modeling of its fuel were invaluable.

References

1. "Technical Evaluation of the HITACHI Resource-Renewable BWR (RBWR) Design Concept," 1025086, EPRI, Palo Alto, CA (2012).

2. T. HINO, et al., “Core Designs of the RBWR (Resource –renewable BWR) for Recycling and Transmutation of Transuranium Elements – an Overview,” Proc. of ICAPP, Charlotte, North Carolina, April, 2014.

3. A. MIELOSZYK et al., “FRAPCON-MIT: A Fuel Performance Tool for Innovative Fuel Designs,” Proc. of TopFuel 2013, Charlotte, North Carolina, September 2013.

4. K. J. GEELHOOD, W. G. LUSCHER, and C. BEYER, “FRAPCON-3.4: A Computer Code for the Calculation of Steady-State, Thermal-Mechanical Behavior of Oxide Fuel Rods for High Burnup,” Technical Report NUREG/CR-7022, Vol. 1, Pacific Northwest National Laboratory (2010).

5. Y. LONG, “Modeling the Performance of High Burnup Thoria and Urania in PWR Fuel,” Ph.D. thesis, Massachusetts Institute of Technology (2002).

6. B. ABELES, “Lattice Thermal Conductivity of Disordered Semiconductor Alloys at High Temperatures,” Physical Review, Vol. 131 (1963).

7. J. BELLE and R. M. BERMAN, “Thorium Dioxide: Properties and Nuclear Applications,” DOE/NE-060 (1984).

8. U. BASAK, A. K. SENGUPTA, and C. GANGULY, “Hot Hardness and Thermal Conductivity of ThO2-PuO2 and ThO2-UO2 Sintered Pellets,” Journal of Materials Science Letters, Vol. 8 (1989).

9. M. MURABAYASHI, “Thermal Conductivity of Ceramic Solid Solutions,” Journal of Nuclear Science and Technology, Vol. 7 (1970).

10. C. PILLAI and P. RAJ, “Thermal Conductivity of ThO2 and Th0.98U0.02O2,” Journal of Nuclear Materials, Vol. 277 (2000).

11. Y. E. Kim, J.-W. Park, and J. Cleveland, “Thermophysical Properties Database of Materials for Light Water Reactors and Heavy Water Reactors,” IAEA-TECDOC-1496 (2006).

12. W. G. LUSCHER and K. J. GEELHOOD, “Material Property Correlations: Comparisons Between FRAPCON-3.4, FRAPTRAN 1.4, and MATPRO,” NUREG/CR-7024 (2011).

13. H. M. LEE, “Electrical Conductivity of UO2-ThO2 Solid Solutions,” Journal of Nuclear Materials, Vol. 48 (1973).

14. J. L. BATES and R. R. SCHEMMEL, “Electrical Conductivity of Thorium Dioxide,” BNWL-1671 (1972).

15. BAKKER, et al., “Critical evaluation of the thermal properties of Th02 and Th1−yUy02 and a survey of the literature data on Th1−yPuy02,” Journal of Nuclear Materials, Vol. 250 (1997)

16. M. KARAM, F. C. DIMAYUGA, and J. MONTIN, "Fission Gas Release of (Th,Pu)O2 CANDU fuel," CW-124950 (2008).

17. K. LASSMANN et al., "The Radial Distribution of Plutonium in High Burnup UO2 Fuels," J. Nucl. Mater., 208, 223 (1994).

18. P. M. GORMAN et al., “The Fuel-Self-Sustaining RBWR-Th Core Concept and Parametric Studies,” Proc. of ICAPP, Charlotte, North Carolina, April, 2014.

19. G. ZHOU et al., “Corrosion and Hydrogen Uptake Behavior and Modeling for Modern BWR Cladding Materials,” Proc. of Top Fuel 2009, Paris, France, September 2009.

20. R. J. M. KONINGS, Comprehensive Nuclear Materials, Elsevier, Boston, MA (2012).

21. H. SELL, S. TRAPP-PRITSCHING, and F. GARZAROLLI, “Effect of Alloying Elements and Impurities on in-BWR Corrosion of Zirconium Alloys,” Zirconium in the Nuclear Industry: 14th International Symposium, ASTM STP 1467 (2006).

22. F. GARZAROLLI, F. et al., "Optimization of Zry-2 for High Burnups," J. ASTM Intl., Vol. 7, No. 7 (2011).

23. Y. HIRANO et al., “Irradiation Characteristics of BWR High Burnup 9x9 Lead Use Assemblies,” Proc. of Water Reactor Fuel Performance Meeting, Kyoto, Japan, October, 2005.

24. ASTM Standard B351/B351M-13, 2013, ”Standard Specification for Hot-Rolled and Cold-Finished Zirconium and Zirconium Alloy Bars, Rod, and Wire for Nuclear Application,” ASTM West Conshohocken, PA, 2013, DOI: 310.1520/B0351_B0351M, www.astm.org

25. S. KASS, "The Development of Zircaloys," Corrosion of Zirconium Alloys, ASTM STP 368, (1964).

26. Y. ETOH et al., “The Effect of Microstructure on the Corrosion Behavior of Zircaloy-2 in BWRs,” Zirconium in the Nuclear Industry: 12th International Symposium, ASTM STP 1354, (2000).

27. P. TÄGTSTROM, et al., "Effects of Hydrogen Pickup and Second-Phase Particle Dissolution on the In-Reactor Corrosion Performance of BWR Claddings," Zirconium in the Nuclear Industry: 13th International Symposium, ASTM STP 1423, (2002).

28. P. Y. HUANG, S. T. MAHMOOD, and R. B. ADAMSON, "Effects of Thermomechanical Processing on In-Reactor Corrosion and Post-Irradiation Mechanical Properties of Zircaloy-2," Zirconium in the Nuclear Industry: 11th International Symposium, ASTM STP 1295 (1996).

29. S. SHIMADA, Y. ETOH, and K. TOMIDA, "BWR Zircaloy Cladding Corrosion Behavior - Effect of Microstructure," J. Nucl. Mater., 248, 275 (1997).

30. P. RUDLING and G. WIKMARK, “A Unified Model of Zircaloy BWR Corrosion and Hydriding Mechanisms,” J. Nucl. Mater., 265, 44 (1999).

31. S. VALIZADEH et al., "Effects of Secondary Phase Particle Dissolution on the In-Reactor Performance of BWR Cladding," J. ASTM Intl., Vol. 8, No. 2 (2011).

32. S. T. MAHMOOD et al., "Effects of SPP Dissolution on Mechanical Properties of Zircaloy-2," Proc. Of the International Topical Meeting on Light Water Reactor Fuel Performance, Portland, Oregon, March, 1997.

33. A. MOTTA and C. LEMAIGNAN, "A Ballistic Mixing Model for the Amorphization of Precipitates in Zircaloy under Neutron Irradiation," J. Nucl. Mater., 195, 277 (1992).

34. G. HOOD, "Point Defect Diffusion in α-Zr," J. Nucl. Mater., 159, 149 (1988).

35. S. MAHMOOD et al, "Post-Irradiation Characterization of Ultra-High-Fluence Zircaloy-2 Plate," Zirconium in the Nuclear Industry: 12th International Symposium, ASTM STP 1354, (2000).

36. K. UNE et al., "Hydrogen Absorption Mechanism of Zirconium Alloys Based on Characterization of Oxide Layer." J. ASTM Intl., Vol. 8, No. 5 (2011).

37. R. A. GRAHAM and C. M. EUCKEN, "Controlled Composition Zircaloy-2 Uniform Corrosion Resistance," Zirconium in the Nuclear Industry: 9th International Symposium, ASTM STP 1132 (1991).

38. M. YOUSSEF, "Predicting the Equilibria of Point Defects in Zirconium Oxide: a Route to Understand the Corrosion and Hydrogen Pickup of Zirconium Alloys," Ph.D. Thesis, Massachusetts Institute of Technology (2014).

39. K. J. GEELHOOD and C. BEYER, "Hydrogen Pickup Models for Zircaloy-2, Zircaloy-4, M5, and ZIRLO," Water Reactor Fuel Performance Meeting, Chengdu, China, September, 2011.

40. A. KARAHAN, A. LERCH, and M. S. KAZIMI, "Development of FRAPCON-EP for High Burnup and High Temperature Fuel Modeling," Proceedings of 2010 LWR Fuel Performance/TopFuel/WRFPM, Orlando, Florida, September, 2010.

41. USNRC. Generic Letter, ADAMS Accession Number ML100960505. (2010).

42. USNRC. NUREG-0800, Ch. 4.2, Rev. 3, pp. 33-36. (2007).

43. M. BILLONE et al., "Cladding Embrittlement During Postulated Loss-of-Coolant Accidents," NUREG/CR-6967, Argonne National Laboratory (2008).

44. S. ISHIMOTO et al., "Improved Zr Alloys for High Burnup BWR Fuel." Transactions of the International Meeting on LWR Fuel Performance, Salamanca, Spain, October, 2006

45. "Application of GNF-Ziron to GNF Fuel Designs," NEDO-33353, Global Nuclear Fuels, Revision 0, (2010).

46. Southern Nuclear Operating Company, Inc; Edwin I. Hatch Nuclear Plant, Units 1 and 2; Exception, 79 Fed Reg. 8738-8740 (February 13, 2014). Print.

Attachment 4

For NEUP Project # 11-3023: Self-sustaining thorium boiling water reactors

Thermal Hydraulic Correlations for Tight Lattice BWR Bundles

The objective of this task is to review the applicability of the available models for both void fraction and critical power for the tight-lattice high void fraction RBWR cores. Suggested correlations were checked against a range of experimental data for tight lattice bundles. For the void fraction analysis, two separate experimental facilities with 30 measurement points for void fraction in tight lattice bundles are considered. For the critical power analysis, three experimental facilities with 7 different geometries and over 100 data points are considered. The experimental data is compared to 12 void fraction correlations and 5 critical power correlations. A new modified void fraction model and two new modified critical power model are then proposed based on the best agreement with experimental data.

I. INTRODUCTION

For the next generation breeder/burner reactors, LWR with tight-lattice fuel designs have been proposed by various organizations including Hitachi's RBWR[1], JAERI's FLWR[2] and Toshiba's BARS[3]. Since these reactors' goal is to obtain a conversion ratio of 1 or more, they are designed with heterogeneous axial geometry, e.g., a blanked-fissile-blanket-fissile-blanket axial zoning. The fuel length, axial power shape, power to flow ratio, boiling length, mass flux, void fraction and hydraulic diameters of these proposed designs are very different from traditional Boiling Water Reactors (BWRs). Since the 1960s, few experiments have been performed to analyze the thermal hydraulic performance of tight lattice designs and few void fraction and critical power correlation have been proposed.

In order to accurately simulate core behavior of such BWRs, an accurate estimate of the void fraction distribution within the bundles is necessary. The axial void distribution is used in the neutronic calculations to estimate the bundle power under steady state and transient operation. The axial void fraction can range from 0 to 1 and its prediction is not only important for local vapor flux calculation but also affects the overall void reactivity calculation. The axial void distribution is also used for stability analysis. In a typical BWR neutronics analysis, the bundle's radial average void fraction is sufficient to give the correct reactivity and flux distribution predictions. This is due to the relatively small size of the bundles (10 cm). However, if the assembly sizes are increased, the local average void could play a role in accurate prediction of reactivity and flux distributions per axial section.

One of the most limiting parameters in BWR design is the Minimum Critical Power Ratio (MCPR) or margin to dryout. The Hitachi-GE limit for MCPR has always been 1.3 and the reasoning is straight forward, it covers 0.1 for uncertainty in data and 0.2 for margin against transients. However, plants under normal operation typically operate at above the 1.3 MCPR limit.[4] The Browns Ferry Unit 1, cycle 9 core design in 2009, operated with an MCPR of around 1.6.[5] Typical, 1D correlations are chosen that are function of pressure, mass flux, boiling length and quality but independent of the void fraction. The 1D analysis approach neglects the inner bundle channel mixing and lumps the presence of water rods and partial length rods which results in an underestimation of CP. Though, in the tight lattice geometries, water rods and partial length rods do not exist as their primary purpose in conventional BWRs is to increase moderation, which is the opposite of what the breeder/burner BWRs are aiming for in their design.

Table I shows the conditions reported for the RBWR design[1] used in this analysis, which is similar to the designs mentioned above and is compared to an Advanced BWR (ABWR) design. ABWRs are the only current operating Gen III+ plant in the world, and the vessel and containment structures proposed for the RBWR designs are same as the currently operating ABWR designs. As seen, the core exit quality is higher and the fuel rod height is shorter, while the reported MCPR is similar to the ABWR and the void coefficient is reported to be negative. Part of this analysis aims at verification of the void fraction and CPR models used for the reported data in Table I.

TABLE I The ABWR vs. RBWR type geometry.[1]

Parameters	ABWR	RBWR
Reactor thermal power (MW)	3958	3958
Core flow rate (kg/s)	14502	7420
System pressure (MPa)	7.2	7.2
Core inlet temperature (^{o}C)	278.3	282.3
Core Exit Quality (%)	14	35
Core Outer Radius	2.69	2.88
Number of fuel assemblies	872	720
Bundle Type	Square	Hexagonal
Average linear power (kW/m)	13.3	14
Fuel rod OD (mm)	10.3	10.1-7
Fuel rod pitch (mm)	12.95	11.4-9
Active fuel rod height (m)	3.71	1.4-1
Number of fuel rods	92	271-397
Assembly inner dimension (mm)	133	194.4

II. VOID FRACTION

The void distribution in a BWR bundle can be divided into two parts: axial void distribution and radial void distribution.

II.A Axial Void Fraction

While there are many experiments in the literature for void fraction measurements under nominal BWR design conditions, there are only few available experimental data for tighter lattice applications. Experiments at Japan Atomic Energy Agency (JAEA) are almost the only ones in the literature that provide both axial and radial void fraction measurements in bundles of RMBWR type geometry and operating conditions.[6] The JAEA report recommends using a drift flux type model to best match their experimental results for a 37 rod bundle with hexagonal geometry. The recommended drift flux type model, includes part of the Liao, Parlos and Griffith (1985), which was included in a detailed study done by PSI on 15 drift flux models' ability to predict void fraction data from 9 experimental sets.[7] Using the 2 sets of available data from the JAEA report, the axial void profiles for the JAEA experimental conditions are plotted in Fig. 1 for 12 different void fraction models.

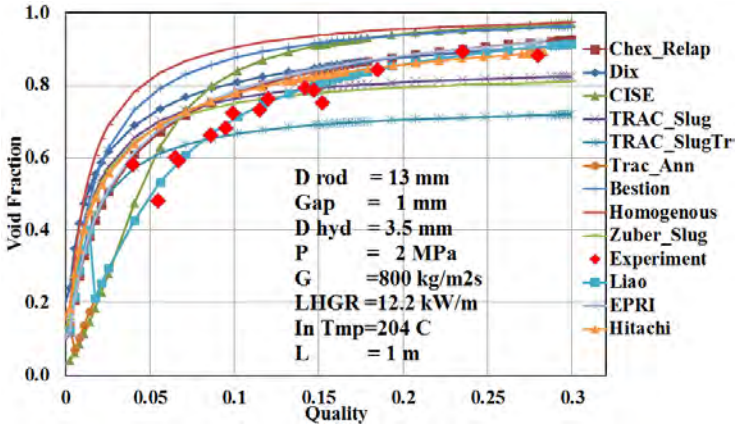

(a)

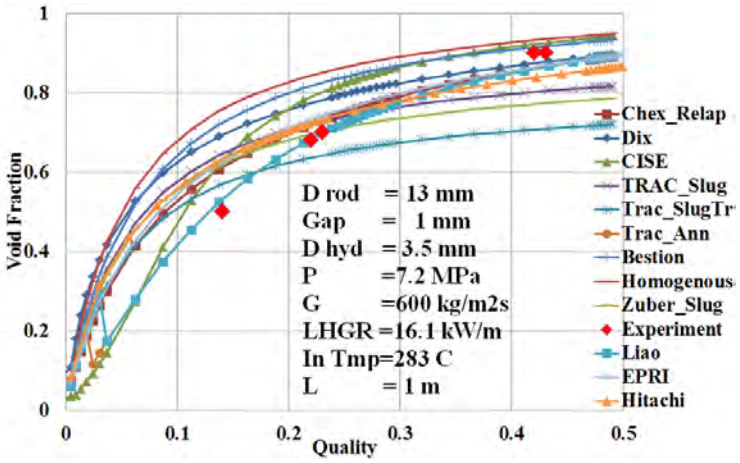

(b)

Fig. 1. The axial void for the 37-rod RMBWR bundle type from JAEA at 2 MPa (a) and 7 MPa(b).

The only other tight lattice bundle facility found in literature was the 37 rod bundle NEPTUN experimental facility operating at atmospheric conditions. The NEPTUN bundle has hydraulic diameter comparable to RBWR and length of 1.7 m and was used for validation of a high conversion PWR reactor. The same 12 void fraction models are compared against the NEPTUN data and shown in Fig. 2.

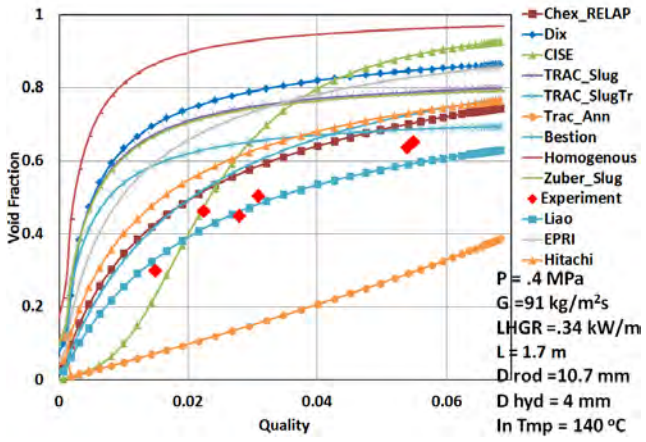

(a)

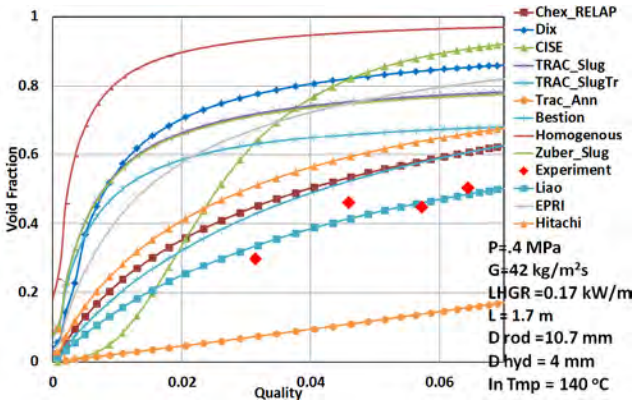

(b)

Fig. 2. The axial void for the 37-rod NEPTUN bundle type from high flux (a) and low flux (b).

As seen in Fig. 1, the well-established Chexal–Lellouche correlation[8] used in most safety analysis codes, such as the USA code RELAP5, overestimates the void fraction in the 10 and 25% quality region. Similarly, for NEPTUN data, it over estimates the void fraction by 5 to 10%. Another continuous drift flux model, the Dix correlation[9] developed for BWR type bundles over-predicts the void fraction below 90%. The CISE void correlation (non-drift flux type) that was shown to agree well for small diameter tubes under low void conditions agrees with the scarce low quality data points.[10] The correlation is also known to over-predict the void fraction at higher qualities as shown in Fig. 1 and 2.

The next three correlations in Fig. 1 are based on the JAEA recommended correlations.[6] The slug flow model for round tubes correlations show over-predictions in the low quality region, but the slug flow model for triangular ducts shows a closer behavior to the experimental data. In the annular flow regions the annular flow model does very well with both experimental data sets at both pressures. However, at lower flow and pressure conditions of the NEPTUN experiments; they perform poorly as shown in Fig. 2.

The Bestion model[7] used in the French safety analysis code CATHARE and TRACE, behaves similarly to the Dix model and over-predicts the void fraction up to 90%. The homogenous model[9] provides the upper bounding curve to all drift flux type models by consistently over predicting the void fraction. The Zuber-Findlay model[9] for slug flow displays over prediction and under prediction for the low and high quality regions, respectively. This model can be used with the commonly used, VIPRE code.[11] By default, VIPRE uses the EPRI void model, which shows good agreement with Chexal-Lellouche correlation at low pressures and high pressures as it is developed based on Chexal-Lellouche correlation data base. Similarly, the correlation used by Hitachi has similar performance as the EPRI and the Chexal-Lellouche correlations.

The void fraction model that agrees well with the NEPTUN experiments is the Liao, Parlos and Griffith (1985) model which also agrees well with the JAEA experimental data. However, its discontinuity at the start of the annular flow regime, given the unavailability of reliable experimental data at low void fraction, is under question. Generally, void fractions above the 50% level can be reasonably deduced from the available models. But, due to the lack of experimental data, there is much more uncertainty below 50% void fraction. While the CISE correlation is the only one that predicts continuous transition from a low void fraction to the annular flow region, it is preferred here to use the Liao et al. correlation for annular regime for the entire flow regime. However this approach can be non-conservative as there is a chance of under-predicting the void fraction at low qualities which is typically less conservative for most reactor design calculations.

The criterion used by Liao et al. is a modified version of the widely used criterion for onset of annular flow, a dimensionless superficial velocity (j_{gst} = 1) given in Eq. (1).

$$j_{gst} = j_v \sqrt{\frac{\rho_g}{g\, D_h\, (\rho_l - \rho_g)}} \qquad (1)$$

It has been shown by different experiments for small diameter tubes (<1.5 cm) that as the j_{gst} approaches unity, the slug/churn flow transitions to annular flow.[12] Liao et al. underestimate this transition point for the RBWR conditions by a void fraction of 5%. Therefore, for best estimate of the void fraction before and at the point of transition; it is recommended to use the slug flow correlation by Liao et al. For void fraction predictions after transition in the RBWR type geometry, the annular flow Liao et al. correlation is recommended. Furthermore, eventually; it is desired to utilize safety analysis codes such as RELAP5 or TRACE to be used to perform steady state and transient analysis. If the final optimized design will be close to the RBWR type geometry and conditions, the void correlations in both codes need to be modified to Liao et al.; however, the discontinuity could cause a numerical instability. It is therefore recommended to keep the void fraction predicted by the Liao slug flow correlation constant at j_{gst} = 1, until the annular void model catches up to the value of the slug flow void fraction.

The new best estimate model is therefore takes the following traditional drift flux form as shown in Eq. (2):

$$\alpha = \frac{1}{C_0\left(1 + \frac{(1-x)}{x}\frac{\rho_v}{\rho_l}\right) + \frac{V_{vj}\,\rho_v}{xG}} \qquad (2)$$

Where for bubbly flow with

$$j_l > 2.34 - 1.07\left(\frac{g\,\sigma(\rho_l - \rho_v)}{\rho_l^{\,2}}\right)^{1/4}:$$

$$C_0 = 1 \;\; and \;\; V_{vj} = 1.53(1-\alpha)^2\left(\frac{g\,\sigma(\rho_l - \rho_v)}{\rho_l^{\,2}}\right)^{1/4}$$

For churn/slug turbulent flow:

$$C_0 = 1.2 - 0.2\sqrt{\frac{\rho_v}{\rho_l}}\,(1 - e^{-18\alpha}) \;\; and \;\; V_{vj} = 0.33\left(\frac{g\,\sigma(\rho_l - \rho_v)}{\rho_v^{\,2}}\right)^{1/4}$$

For annular flow (j_{gst}>1):

$$C_0 = 1 + \frac{1-\alpha}{\alpha + 4\sqrt{\frac{\rho_v}{\rho_l}}} \;\; and \;\; V_{vj} = (C_0 - 1)\sqrt{\frac{g\, D_h\,(\rho_l - \rho_v)(1-\alpha)}{0.015\rho_l}}$$

For which if $\alpha_{annular} < \alpha_{j_{gst}=1}$ then $\alpha = \alpha_{j_{gst}=1}$ else $\alpha = \alpha_{annular}$.

The new best estimate model performance against the most commonly used correlations of Bestion and RELAP5 along with the original Lia et al. model is compared in Fig. 3b for a simulated RBWR type geometry with the given LHGR in Fig. 3a. Similar to the high pressure bundle experiments in Fig. 1b, the new best estimate model under-predicts the void fraction along most of the axial height of the bundle. The modification to Liao et al. at the point of transition also disallows the correlation to decrease void fraction along the axial height of the bundle.

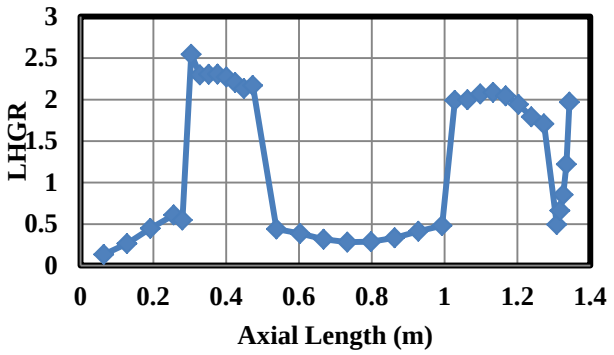

(a)

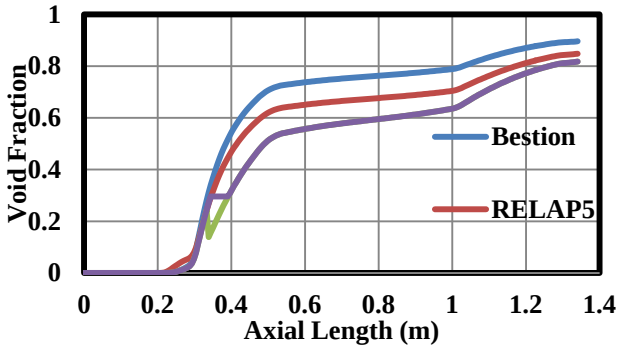

(b)

Fig. 3. The (a) normalized linear heat generation rate and (b) the void fraction comparison of a RBWR bundle design.

Due to the difference between the proposed model and previously used models for RBWR analysis, it is possible that the current geometry of the RBWR is not optimized. In fact, the newer JAEA FLWR design has slightly different dimensions from the ones listed in Table I. Therefore, if a design optimization is desired, the sensitivity of the new best estimate model to operating and geometric parameters needs to be shown. For this purpose, the void fraction of a conventional ABWR geometry is calculated using the Bestion, RELAP5, EPRI and best estimate models. For a reference ABWR, the outlet quality of 15% with void fraction of 70% is observed and is consistent with published results.[4] As seen in Fig. 4, the Bestion model tends to overestimate the void while the best estimate model recommended for the RBWR design tends to significantly underestimate the void fraction. The RELAP5 and EPRI correlations do well in predicting the void fraction compared to literature reported values and give essentially the same values.

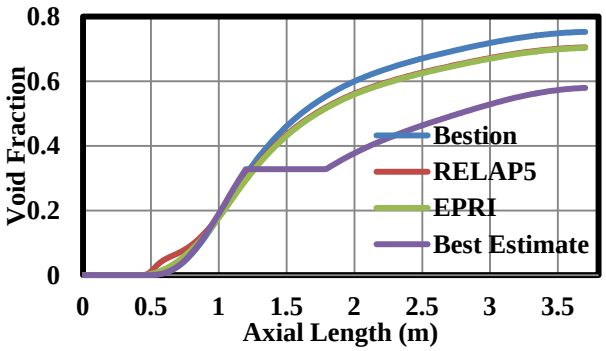

Fig. 4. The void fraction for a typical ABWR condition

Therefore, considering the results shown in Fig. 4, it is recommend to use the new best estimate model for RBWR type bundles, and the RELAP5 Chexal-Lellouche and ERPI void models for the purpose of scoping BWR type geometries due to their least outlier behavior. Another conclusion from the above analysis is that the void fraction prediction accuracy proves to be different depending on the hydraulic diameter and flow conditions. Therefore, in the absence of appropriate experimental data, for any final design a sensitivity study needs to be performed with the four correlations listed in Fig. 4.

II.B Radial Void Fraction

If the power distribution, predicted through the neutronics calculation, is based on an average void fraction or a local void fraction for a single channel (no cross flow) model; it could introduce errors in reactivity calculations. However, it is recommended that when no cross flow is modeled then the average radial void be used as the best estimate for the neutronics calculation, due to the fact that not modeling cross flow results in more heterogeneity in the void fraction distribution, which results in unphysical neutronic behavior.

Due to the inadequacy in accuracy of simulation of two phase flows using CFD, only subchannel analysis can be resorted to model the radial void profile in a RMBWR type bundle. On the subchannel level, calculation of turbulent mixing is typically done by lumping all of the physical parameters affecting the process into one mixing coefficient that is obtained empirically. There are experiments by Cheng et. al. on quantifying the turbulent mixing in a tight lattice 7 rod bundle. It has been shown that in the RMBWR type geometry, the mixing coefficient is still of the same order of magnitude compared to typical BWR bundles.[13] Therefore, the subchannel codes can use similar tuning parameters for the calculation of radial void distribution in an RBWR. It is expected that due to the longer neutron mean free path in RBWR type cores, the effect of radial bundle void distribution modeling on the prediction of reactivity and local flux is likely to be small.

III. CRITICAL POWER

One of the most limiting parameters in BWR design is the MCPR. The 1D analysis approach neglects the inner bundle channel mixing which results in an underestimation of CP. However, neglecting the local rod peaking within the bundle compensates for the underestimation of CP with the mentioned approximation. The CP is typically not as sensitive to axial power profile compared to CHF as it dependent on the integrated power. However, in case of RBWR there is significant power change where the axial profile crosses from the fissile to blanket regions and back to the blanket region. Also, the space between the bundle walls to rods and the hot rod location within the bundle become more

important as the gap between the rods becomes smaller. Hence, more recent experiments and developed correlations for tight lattice bundles have attempted to capture such unique conditions in tight lattice bundles such as the Modified Arai[15] and the Liu[16] correlations.

General intuition tells us that the smaller rod diameter or gaps and thus tighter lattices have more potential to increase the power density without CPR penalties. This can be seen in the evolution of the BWR assembly from 6x6 to 10x10 arrays in the last 40 years for relatively the same core volume. This is mainly due to the fact that the smaller diameter rod increases the surface area to volume ratio of the heat generating media. For a given flow rate, a lattice geometry with larger total flow area results in a reduction in the coolant mass flux, which in the case of appreciable saturated boiling increases the exit critical quality. However, different correlations were derived from different experimental data; and typically they are not able to cover the entire design space, which contributes significantly to the uncertainty of the design scoping analysis.

III.A Comparison to Experimental Data

A literature review of the most commonly used correlations has been undertaken. The same geometry and operating parameters of the bundle used in the void fraction analysis in Section II are used in this section. In the most recent literature study, the Liu correlation[16] was recommended for tight lattice fuel bundles. In case of square lattices the Hench-Gillis[9] correlation has been commonly used for typical BWR bundle designs. Both correlations have complex formulations and require pin power distribution and subchannel analysis for simulation of CP. This motivated the development of simpler CP formulations that only depend on bundle average thermal hydraulic conditions.

TABLE II CPR experiment test parameters (For heating U-Uniform, D-Double humped, C-Cosine shaped power distribution)

Test	Rod Diameter	D-hyd	Pressure	# Heated Rods
-	mm	mm	MPa	-
BAPL[17]	6.4, 7.1	6.46	8.27	20 U
JAEA-A[18]	12.3	2.35	1.0 - 8.0	7 U
JAEA-B[18]	13	2.86	2.0 - 8.5	7 D
JAEA-C[16]	13	4.42	2.0 - 8.5	37 D
JAEA-D[16]	13	3.71	2.0 - 8.6	37 D
Toshiba-1[15]	10.8	4.85	7	7 C
Toshiba-2[15]	10.8	5.91	7	7 C
Toshiba-3[15]	10.8	7.03	7	7 C
Toshiba-4[15]	10.8	5.74	1.0 - 8.0	14 C

Three separate CP correlations were examined to determine their effectiveness for predicting dryout in tight lattice bundles. The Hench-Gillis, Modified Arai and CISE-4[9] correlations were all examined against a series of three different experiments with varying rod diameters and rod gaps. The parameters of the experiments can be seen in Table II. For the purpose of comparison, it was assumed that the experiment's operating power was the same as the reported critical power (e.g. dryout occurred at the outlet). For the calculation of CP, the minimum CPR was calculated based on the axial power profile reported by each experiment. The radial pin peaking factor for all the experiments was also assumed to be 1; i.e. uniform pin power distribution was assumed.

Rod diameters ranged from 6.35 to 13 mm with hydraulic diameters ranging from 2.86 to 7.03. For a typical LWR, the hydraulic diameter is near 11 mm. Accordingly, these three correlations returned the results summarized in Table III.

TABLE III CPR mean and standard deviation of experimental/predicted critical power ratio for tight lattice BWR experiments

Correlation	Mean	σ	Mean-2STD
Hench-Gillis	0.659	2.197	-
Modified Arai	0.917	0.199	0.519
CISE-4	0.926	0.224	0.478
Modified CISE-4	1.001	0.220	0.561

It is seen that all three of the correlations under-predict the point of dryout when these assumptions are made. Fig. 5 show the results of these three correlations as function of the tests of hydraulic diameter. It can be seen that there is more spread in the predictions at hydraulic diameters less than 3 mm. It should also be noted that the Hench-Gillis correlation, shown in Fig. 5c, shows itself invalid for small rod diameters. It is the only correlation that has rod diameter as a parameter, and this causes it to explode since there is an inverse dependence upon it.

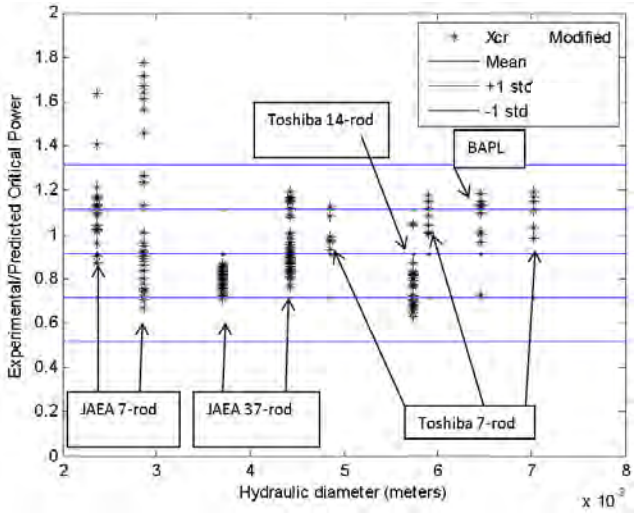

(a)

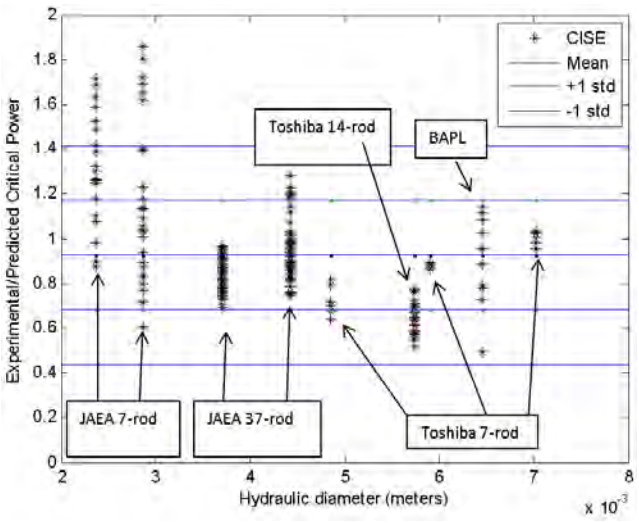
CISE
Mean
+1 std
-1 std
Toshiba 14-rod
BAPL
JAEA 7-rod
JAEA 37-rod
Toshiba 7-rod
Experimental/Predicted Critical Power
Hydraulic diameter (meters)
x 10^-3

(b)

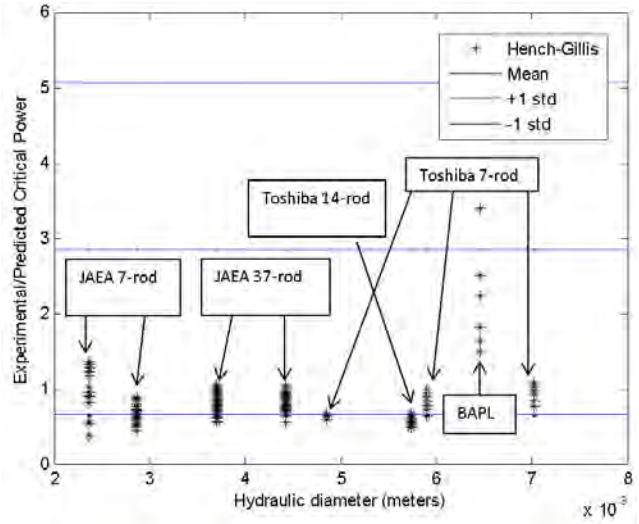
Hench-Gillis
Mean
+1 std
-1 std
Toshiba 7-rod
Toshiba 14-rod
JAEA 7-rod
JAEA 37-rod
BAPL
Experimental/Predicted Critical Power
Hydraulic diameter (meters)
x 10^-3

(c)

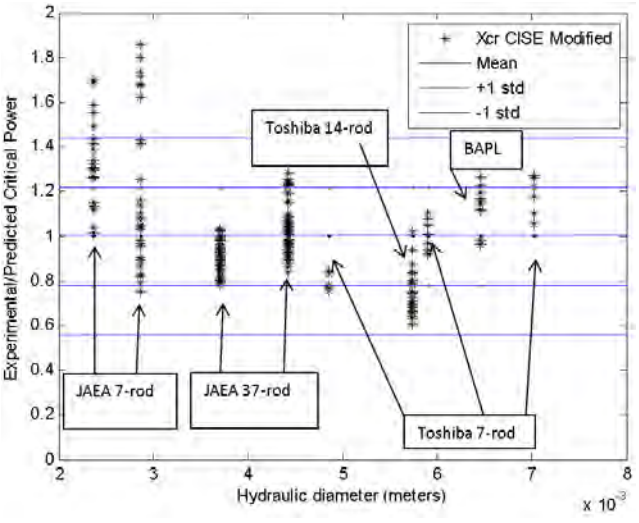
Xcr CISE Modified
Mean
+1 std
-1 std
Toshiba 14-rod
BAPL
JAEA 7-rod
JAEA 37-rod
Toshiba 7-rod
Experimental/Predicted Critical Power
Hydraulic diameter (meters)
x 10^-3

(d)

Fig. 5. Dependence of (a) Modified Arai (b) CISE (c) Hench-Gillis and (d) Modified CISE-4 correlation on hydraulic diameter.

In order to better model the data, the CISE-4 correlation is modified to account for changes in behavior at lower mass flux and hydraulic diameter since its performance is also listed in Table III and shown in Fig. 5d. Additionally, the CISE-4 correlation is the only one that does not need rod peaking in its formulation. Both Hench-Gillis and Arai require rod peaking data to be known; since that is not known at this point, the CISE-4 correlation is a better starting point. The Arai correlation also includes a factor that is dependent upon subchannel analysis. The modified correlation can be seen here in Eq. (3). The range of validity of the modified CISE-4 correlation is listed in Table IV.

$$X_{cr} = \frac{D_e}{D_h}\left(\frac{a\,L_b}{L_b + b}\right) \qquad (2)$$

Where:

$$b = 0.199\left(\frac{P_c}{P} - 1\right)^{0.4} G\,D_e^{1.2}$$

If $G \le G^*$ then,

$$a = \left(1 + 1.481e-4\left(1 - \frac{P}{P_c}\right)^{-3} 0.7\,G\right)^{-1}$$

Otherwise:

$$a = \frac{1 - \frac{P}{P_c}}{\left(\frac{0.7\,G}{1000}\right)^{0.33}}$$

With:

$$G^* = 3375\left(1 - \frac{P}{P_c}\right)^3$$

It is also noted that the new modified CISE correlation also produces CP close to the Hench-Gillis correlation for a typical ABWRs assuming a radial peaking factor of 1, which encourages its use for design scoping analysis.

Table IV Parameters ranges for the Modified CISE-4 correlation

Parameter	**Low**	**High**
Mass Flux (kg/m2s)	100	2035
Pressure (MPa)	1.0	8.6
Hydraulic Diameter (mm)	2.35	7.03
Heated Diameter (mm)	3.56	10.95
Rod Diameter (mm)	6.35	13

III.B Implication to MCPR Limit

For every fuel type that GE-Hitachi manufactures (e.g. GE12 or GE14), extensive CPR tests are performed and fuel assembly specific correlations are used to determine the CPR value. While GE-Hitachi performs CPR tests for the exact geometry of the fuel, new fuel designs have to rely on similar designs experimental data that are available. The performed analysis in Section III.A collected all of the available data on tight lattice tests and derived a new correlation that will give an MCPR of 1.0, the modified CISE-4 correlation. Though, it is clear from Fig. 5d that even with 1 sigma of uncertainty, the ΔMCPR is 0.2. Therefore, the uncertainty in calculation of CPR for tight lattice fuel will be larger than a current BWR fuel uncertainty margin.

The GE-Hitachi approach leaves 0.2 ΔMCPR of margin for transients. Qualitatively, the tight lattice fuel designs such as the RBWR have shorter cores and less negative void coefficients which lead to a different overall transient response. In fact, the transient response of the RBWR was compared to ABWR and the largest ΔMCPR out of the 6 analyzed transients between the ABWR and the RBWR was reported to be similar.[1] Therefore, one can imply that the 0.2 ΔMCPR of margin for transients can be also used for a new tight lattice fuel design.

As it was stated, due to the larger uncertainty in the data, MCPR of 1.5 is recommended for tight lattice fuel designs of the RBWR type cores instead of the traditional 1.3 value. Similar to GE-Hitachi approach, the extra 0.5 ΔMCPR is broken up in to two parts. The ΔMCPR of 0.3 (1.5 standard deviation in Fig. 5d) is used in place of ΔMCPR of 0.1 for traditional GE assemblies, due to the larger spread in the available data and lack of CPR data for the exact geometry considered for RBWR type designs. For transients in RBWR type designs, ΔMCPR margin of 0.2 is kept the same as the used GE-Hitachi value.

The Robustness of these correlations are tested against a RBWR bundle model with Table I specification at 125% of an average assembly power with 95% rated nominal flow rate. The trends of the correlation are consistent; except that the Liu correlation predicts dryout will occur within the first 0.5 meter of the bundle height as shown in Fig. 6. The new correlation shows an MCPR of greater than 1, lower than the recommended value of 1.5. Also, it is shown in Fig. 6 that the RBWR MCPR for all the correlation except for Liu occurs close to the outlet of the rod. Table III is consistent with recommendations made by Liu et al.[16] on the inadequate CPR margin of the original RBWR design since either the flow or power needs to be adjusted and the neutronic consequences of such adjustments need to be properly quantified. The Hitachi-CISE (H-CISE) correlation[19] in Table III is the correlation based on the BAPL data that was also used in development of the modified CISE-4 correlation and used of Hitachi-GE to estimate the MCPR. Fig. 5d clearly shows that the BAPL data show higher CPs than the average of the all other tests.

TABLE V The CPR sensitivity analysis for the RBWR-AC.

RMBWR	Outlet CPR at 1.25 Peak	MCPR at 1.25 Peak
Arai	1.45	1.38
M-Arai	1.43	1.35
CISE	1.32	1.25
Hench-Gillis	0.97	0.93
Liu	1.07	0.79
M-CISE	1.24	1.17
H-CISE	1.48	1.37

The BAPL data are based on 20 rod bundle with axially uniform heating in a triangular lattice channel box with high radial peaking factors reported in 1975. The H-CISE was then developed solely based on this specific data set from also modifying the CISE-4 correlation. The H-CISE correlation showed 8% agreement in prediction of CP with the experimental data of the BAPL tests.[1] However, the BAPL CP trends are different compared to recent tests based on geometry and conditions more representative of the RBWR type bundles.

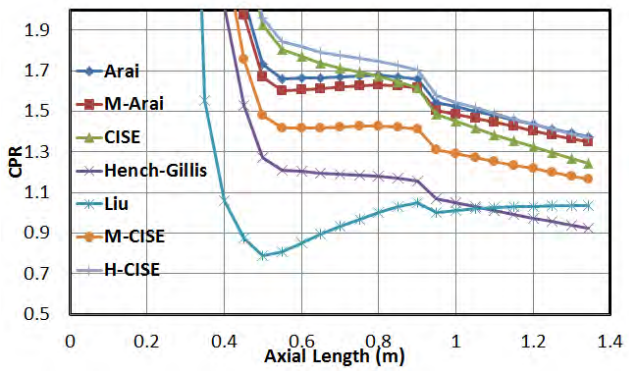

Fig. 6. The axial CPR of the RBWR type bundle.

As shown in Fig. 6, the sensitivity among the CP correlations, while large, gives confidence that a more conservative MCPR limit of 1.5 is required.

III.C Implications for Design

The sensitivity of the new correlation to power and flow is shown in Table VI. Other parameters that affect CP such as boiling length, rod diameter or P/D could be changed; however, the CP is much more sensitive to power and flow than those parameters. As listed in Table VII, it is recommended for the RBWR type designs similar to Table I parameters to go through about a 13% power downgrade and 20% higher flow rate. The 20% higher flow rate is easily achievable as it is less than the ABWR core flow rate and the RBWR design adopts all the ABWR internal pumps in its vessel. However, the 20% increase in flow rate combined with 13% decrease in power results in overall 7% reduction in the core axial void fraction and imposes a neutronic penalty. Alternatively, to reduce the economic penalty of lower electricity output, one could increase the number of assemblies in the reactor and effectively lower the

power density of the core. The increase in number of assembly will be limited by the maximum size of the reactor pressure vessel diameter that can be manufactured.

TABLE VI
Sensitivity of new CPR correlation to power and flow

Parameter	Power	Flow Rate	MCPR
Initial Parameters	3924 MW	7420 kg/s	1.17
Flow Rate Change	100%	120%	110%
Power Change	87%	100%	116%
Power/Flow Change	87%	120%	128%
Final Parameters	3414 MW	8904 kg/s	1.513

III.D Implication of narrowing data range

Due to such a high standard deviation of M-CISE correlation in predicting the experimental data (0.22), the recommended value of the Minimum CPR in the design was 1.5. While, this will give confidence that the design has a good thermal margin, the design of RBWR will likely to use only a subset of the range in the parameters given in Table IV. Therefore, a new modified correlation based on the following narrower range was developed:

- ✓ Pressures: 7$\pm$0.5MPa
- ✓ Mass flux: 500-1500kg/m^{2}s
- ✓ Equivalent hydraulic diameter:2.8-7.5mm

Table VII shows that the M-CISE correlation with the narrower range predicts the experimental conditions with a mean CPR ratio of 0.95 but with a much smaller standard deviation. Thus, the M-CISE correlation can be then modified (and here referred to as the Y-CISE) such that it would predict the experiments with a mean CPR ratio of ~1.0, as shown in Table 3.

Table VII
CPR correlations mean and standard deviation of the ratio experimental/predicted critical power for tight lattice BWR experiments

Correlation	Mean	Standard Deviation	Mean-2STD
M-CISE-4	0.9526	0.0925	0.7676
Y-CISE-4	1.0020	0.0975	0.8070

The Y-CISE is given by the following equations:

$$X_{cr} = \frac{D_e}{D_{ht}}\left(\frac{aL_b}{L_b+b}\right) \quad (3)$$

Where:

$$b = 0.199\left(\frac{P_c}{P}-1\right)^{0.4} G D_e^{1.1}$$

If $G \le G^*$ then,

$$a = \left(1 + 1.481\times 10^{-4}\left(\frac{P}{P_c}\right)^{-3} G_2\right)^{-1}$$

Otherwise:

$$a = \frac{1-\frac{P}{P_c}}{\left(\frac{G_2}{1000}\right)^{.33}}$$

With:

$$G^* = 3375\left(1 - \frac{P}{P_c}\right)^3$$
$$G_2 = G \times 0.4$$

Fig. 7summarizes the considered experimental data relative to the range of hydraulic diameters. Therefore, alternatively, for the RBWR analysis, the new Y-CISE correlation can be used along with a MCPR limit of 1.3, since the standard deviation has been reduced to ~0.1 ΔCPR.

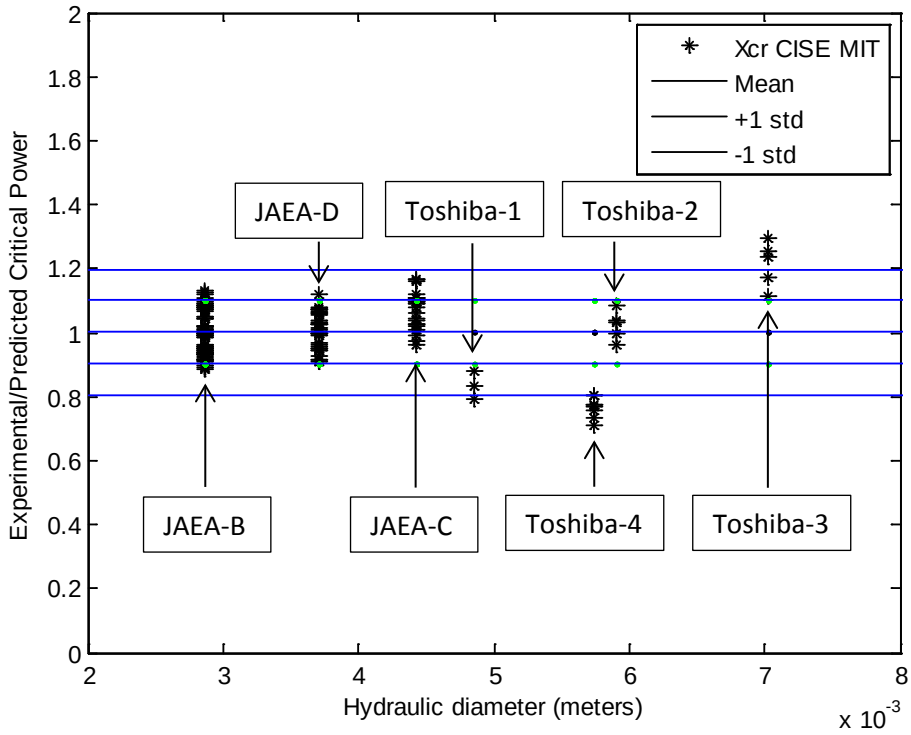

Fig. 7. Dependence of Y-CISE-4 correlation on hydraulic diameter

IV. CONCLUSIONS

An extensive literature review of void fraction and CP data in open literature was performed and two new modified correlations for estimation of void fraction and CPR for tight-lattice BWR bundles were derived. For void fraction, the best estimate model based on Liao et al. void fraction model is recommended as it shows smaller void fractions at high qualities; however, its applicability for outside RBWR type geometry analyzed in this study is questionable. The RBWR geometry shows sensitivity to the choice of void fraction in terms of both reactivity and void coefficient estimation due to its harder spectrum compared to conventional BWRs. The new modified CISE-4 CP correlation along with the more conservative MCPR limit of 1.5 was found to be the best design choice due to existence of high uncertainties in the available CP data. Alternatively, the narrowing the range of data to those of expected operating conditions, resulted in a correlation with similar mean but with smaller uncertainty where the MCPR limit of 1.3 can be justified As listed in Table VII, most of the published RBWR type cores need to either decrease their power output/power density or increase the flow rate in order to meet adequate CP margins, even with the 1.3 MCPR limit. While it is believed the recommended void fraction and CPR models are an improvement over existing models, more detailed neutronic implications of using the

newly recommended void fraction model as a function of burnup and its impact on stability of the design of such reactors are left as future works.

ACKNOWLEDGMENTS

This work was partially funded by DOE NEUP grants.

NOMENCLATURE

α Void fraction
C_0 Concentration parameter
V_{vj} Effective Drift velocity [m/s]
j Superficial Velocity [m/s]
Re Reynolds number (G D_h/μ)
G Mass Flux [kg/m^2-s]
g Gravitational acceleration [m/s^2]
P pressure [Pa]
P_c Critical Pressure (22.03e6 Pa for water) [Pa]
L_b Boiling Length [m]
x Flow Quality
D_e Equivalent Hydraulic Diameter [m]
D_h Heated Hydraulic Diameter [m]
ρ Density [kg/m^3]
σ Surface Tension [N m−1]
μ Viscosity [Pa-s]
v Vapor Phase
l Liquid phase

REFERENCES

1. R. Takeda, M. Aoyama, M. Moriwaki, S. Uchikawa, O. Yokomizo, K. Ochiai, "General Features of Resource-Renewable BWR (RBWR) and Scenario of Long-term Energy Supply," *Proc. of International Conference on Evaluation of Emerging Nuclear Fuel Cycle Systems*, p. 938 (1995).

2. T. Iwamura, S. Uchikawa, T. Okubo, T. Kugo, H. Akie, Y. Nakano, T. Nakatsuka, "Concept of innovative water reactor for flexible fuel cycle (FLWR)," *Nuclear Engineering and Design*, **236**, 1599-1605 (2006).

3. Y. Yamamoto, K. Hiraiwa, S. Morooka, N. Abe, “Critical Power Performance of Tight lattice Bundle,” *JSME International Journal*, **47**, *2*, (2004).

4. L. Fennern, “ABWR Seminar-Reactor, Core and Neutronics,” GE-HITACHI (2007).

5. AREVA, “Browns Ferry Unit 1 Cycle 9 Fuel Design Report,” ANP-2859 (2009).

6. M. Kureta, H. Tamai, H. Yoshida, A. Ohnuki, H. Akimoto, “Development of design technology on thermal hydraulic performance in tight lattice rod bundles: V- Estimation of void fraction,” *Journal of Power and Energy system*, **2**, *issue 1* (2008).

7. P. Coddington and R. Macian, “A study of the performance of void fraction correlations used in the context of drift-flux two-phase flow models,” *Nuclear Engineering and Design*, **215** (2002).

8. Idaho National Labratory, *RELAP5/MOD3.3 Beta Code Manual*, NUREG/CR-5535/Rev 1, INROMATION Systems Laboratoris, Inc. (2001).

9. N. Todreas and M. S. Kazimi, *Nuclear Systems I, Thermal Hydraulic Fundamentals*, Chapter 8, Taylor & Francis, 2nd Edition (2011).

10. K. Triplett, S. Ghiaasiaan, S. Abdel-Khalik, A. LeMouel, B. McCord, “Gas-liquid two-phase flow in microchannels Part II: void fraction and pressure drop,” *Int. Journal of Multiphase Flow,* **25**, 395-410 (1999).

11. C. Stewart, *VIPRE-01: A Thermal Hydraulic Code for Reactor Cores. Vol.2: User’s Manual*, PNL, (1989).

12. L. Cheng, G. Ribatski, J. Thome, “Two Phase Flow Patterns and Flow-Pattern Maps: Fundamentals and Applications,” *Applied Mechanics Reviews*, ASME (2008).

13. X. Cheng and Y. Yu, “Local thermal-hydraulic behavior in tight 7-rod bundles,” *Nuclear Engineering and Design*, **239**, Issue 10 (2009).

14. J. Leppanen, P. Maria, “*Burnup Calculation Capability in the PSG2/SERPENT Monte Carlo Reactor Physics Code*”, Inter. Conf. on Mathematics, Computational Methods & Reactor Physics (2009).

15. T. Yamamoto, M. Akiba, S. Morooka, K. Shirakawa and N. Abe, "Thermal Hydraulic Performance of Tight Lattice Bundle," *JSME International Journal*, **49**, no. 2, pp. 334-342 (2006).

16. W. Liu, M. Kureta, H. Yoshida, A. Ohnuki and H. Akimoto, "An Improved Critical Power Correlation for Tight-Lattice Rod Bundles," *Journal of Nuclear Science and technology*, **44**, no. 4, pp. 558-571 (2007).

17. M. Kureta and H. Akimoto, "Critical Power Correlation for Axially Uniformly Heated Tight-Lattice Bundle," *Nuclear Technology*, **143**, pp. 89-100 (2003).

18. W. Liu, M. Kureta and H. Akimoto, "Critical Power in 7-Rod Tight Lattice Bundle," *JSME International Journal*, **47**, no. 2, pp. 299-305 (2004).

19. B.W. Letourneau, A. C. Peterson, K. J. Coeling, M. E. Gavin, S. J. Green, "Critical heat flux and pressure drop tests with parallel upflow of high pressure water in bundles of twenty 0.25-and 0.28-inch diameter rods ," WAPD-TM-1013 (1975).

Attachment 5

For NEUP Project # 11-3023: Self-sustaining thorium boiling water reactors

Self-sustaining thorium-based RBWR core design

The objective of this task is to search for the optimal design for the RBWR-Th core -- a reduced-moderation BWR which is fuel-self-sustaining. Except for the initial fuel loading, it is charged with only fertile fuel and discharges only fission products, recycling all actinides. The RBWR-Th is a variant of the RBWR-AC core proposed by Hitachi, which arranges its fuel in a hexagonal tight-lattice, has a high outlet void fraction, axially segregates seed and blanket regions, and fits within the ABWR pressure vessel. The RBWR-Th shares these characteristics but replaces depleted uranium with thorium as the primary fertile fuel, eliminates the internal blanket while elongating the seed region, and eliminates absorbers from the axial reflectors.

The sensitivity of important RBWR-Th core performance parameters to change in each one of a dozen design variables was established. The design variables of the sensitivity studies include the length of the seed and blanket zones, fuel rod diameter, lattice pitch, the number of pins per assembly, concentration distribution of the recycled transfertile (TRF) isotopes in the seed, amount of depleted uranium (DU) in the seed makeup, coolant mass flow rate, and simulated depletion cycle length. The performance of the RBWR-Th core was found to be highly sensitive to the pitch-to-diameter ratio and to the thermal-hydraulic (TH) modeling assumptions.

The results of the tradeoff studies were used to arrive at two optimized bounding core designs. When using the same TH correlations as assumed for the Hitachi RBWR-AC core design, comparable performance can be achieved but the RBWR-Th core features significantly lower linear heat generation rate, more uniform axial power distribution, significantly smaller peak burnup and larger safety margins against critical heat flux and loss of flow scenarios. However, using the more conservative TH assumptions developed in this project, power had to be reduced to 81.5% of the nominal and the core volume had to be significantly increased; this led to reduced flow stability than the less conservative cases, although it is still permissible. Additionally, Zircaloy-2 will not maintain its integrity over the entire RBWR-Th fuel life, so advanced cladding materials will be required.

1. Introduction

The RBWR-Th core design is based upon the RBWR-AC designed by Hitachi,[1] a reduced-moderation BWR that employs axial seed and blanket segregation for fuel-self-sustaining operation within an ABWR pressure vessel. The RBWR-Th substitutes depleted uranium with thorium as the primary makeup fuel, eliminates the internal blanket while elongating the seed region, and eliminates absorbers from the upper axial reflectors.

The reduced-moderation BWR core concepts, referred to by Hitachi as the Resource-renewable BWR (RBWR), were initially pursued by Hitachi in an attempt to design hard spectrum BWRs to provide missions traditionally assigned to liquid metal cooled reactors – fuel sustainability or TRU transmutation

with unlimited recycling.[1,2] The study reported herein is for fuel self-sustaining designs. By using a small pitch to diameter ratio (P/D=1.13), a triangular lattice and very high exit void fraction, the neutron energy spectrum is significantly harder than that of a conventional BWR. Figure 1 shows a typical neutron energy spectrum for the RBWR-Th, compared against those of a typical BWR and a typical Sodium Fast Reactor (SFR)[20], and Figure 2 shows the spectrum of neutrons which cause fission, while Table 1 tabulates the fraction of fissions induced by thermal, epithermal and fast neutrons. As more than 60% of the RBWR-Th fissions are caused by neutrons between 0.625 eV and 0.1 MeV, these designs can be classified as intermediate spectrum reactors.

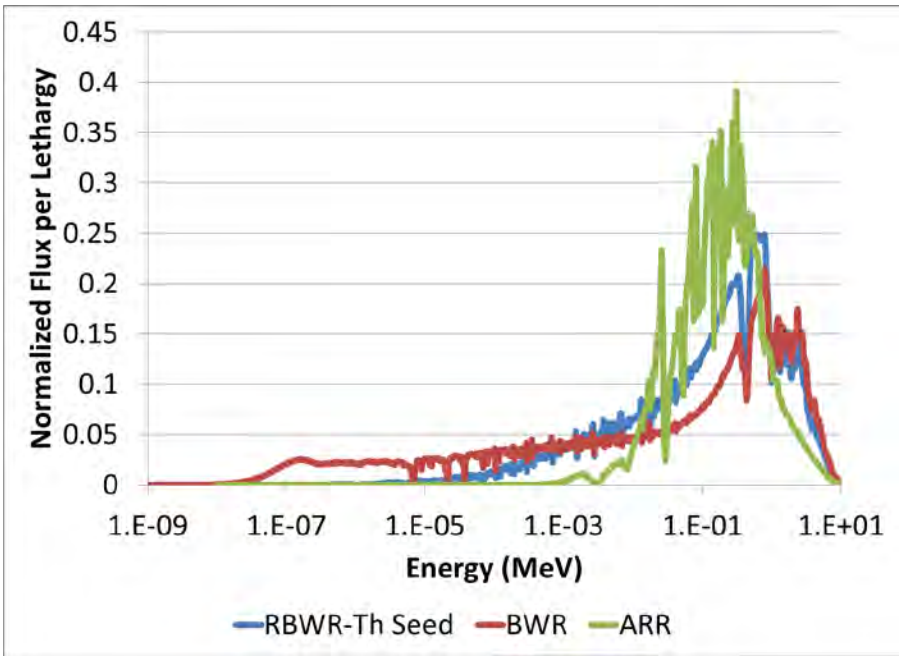

Figure 1. Neutron energy spectrum for the RBWR-Th, compared against that of a BWR and a self-sustaining SFR. The units are arbitrary.

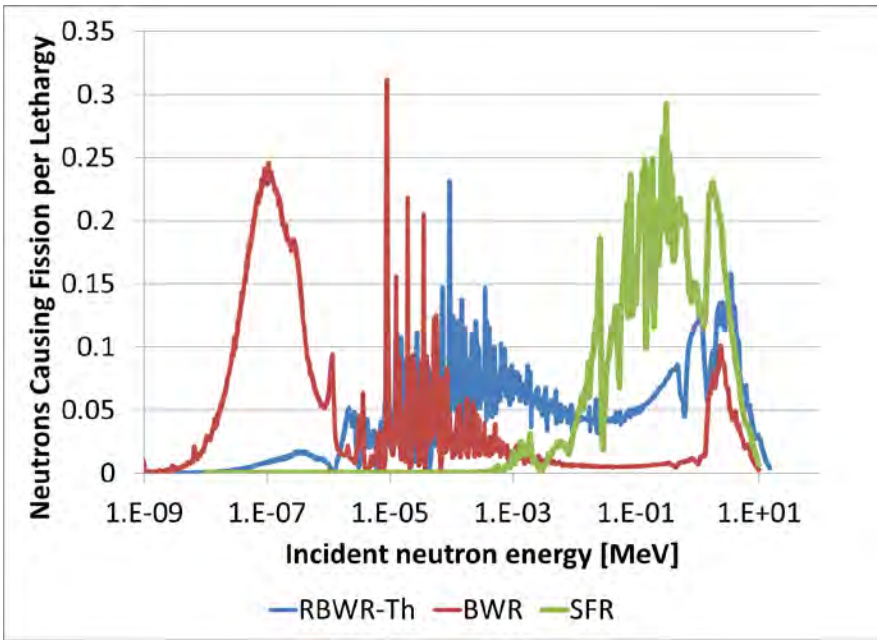

Figure 2. Spectrum of neutrons that cause fission for a typical RBWR-Th, compared against that of a BWR and a self-sustaining SFR (ARR). The units are arbitrary.

Table 1. Fraction of fissions caused by neutrons in the thermal, intermediate and fast energy ranges.

Reactor	<0.625 eV	0.625 eV - 0.1 MeV	>0.1 MeV
BWR	60.2%	28.4%	11.4%
ARR	0.0%	27.9%	72.1%
RBWR-AC	10.9%	39.3%	49.8%
RBWR-ThH	3.2%	60.6%	36.2%
RBWR-ThM	3.7%	62.7%	33.7%

The incentives for considering thorium-based rather than DU-based RBWR core design were several concerns regarding the Hitachi RBWR-AC core that were expressed in a recent EPRI sponsored independent evaluation of the Hitachi core designs [3]: uncertainty in the void reactivity feedback; possibly too small margin against critical heat flux; weak neutronic coupling between the two axial seed segments; and insufficient margin for fuel survivability.[3] The very strong axial heterogeneity of the RBWR-AC core was dictated by the need to maximize the negative leakage component of fuel voiding reactivity effect so as to overcome its large positive spectrum hardening reactivity component.

As shown in Figure 2, ^{233}U has a much flatter fuel reproduction factor with energy than ^{239}Pu. Also, the ^{232}Th fast fission cross section has a higher threshold and lower value than that of ^{238}U. Therefore, the spectral component of void reactivity in a Th-^{233}U fueled RBWR core is negative and there is no need to design the core to have enhanced leakage probability from the seed. This enables use of a single relatively long seed region thereby avoiding many of the above expressed concerns regarding the U-Pu core design.

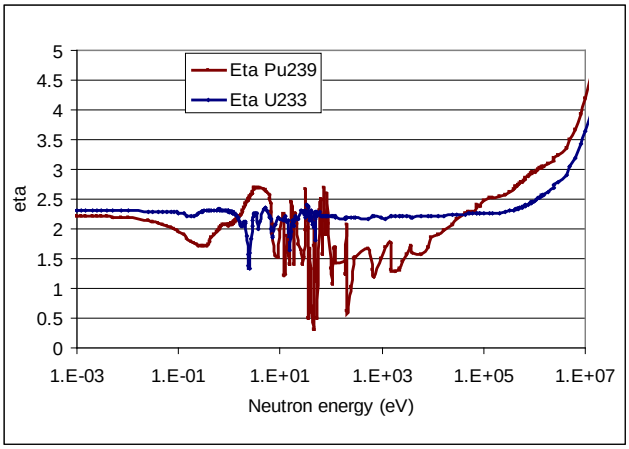

Figure 3. Fuel reproduction factor vs. energy for ^{233}U and ^{239}Pu.

The search for an acceptable RBWR-Th core design was evolutionary. A preliminary study of the thorium-fed RBWR-Th core concept feasibility was reported in reference 4 and results of a more thorough tradeoff study on the RBWR-Th core design using pure thorium feed were summarized in references 5 and 6. Reference 7 reported that the void coefficient of reactivity is too negative, making it practically impossible to design the RBWR-Th core to have adequate shutdown margin and suggested the addition of some DU to the seed makeup fuel in order to make the void coefficient of reactivity (VCR) less negative. Reference 8 updated the thermal-hydraulics model and added in the pressure drop constraint.

This paper aims to summarize the final self-sustaining RBWR-Th core designs arrived at, using a mix of thorium and DU feed fuel. Section 2 comments on the unique physics of the RBWR systems; Section 3 establishes the study methodology and design approach; Section 4 summarizes the results of the tradeoff studies; Section 5 documents the assembly radial enrichment study; Section 6 details the design parameters and the performance characteristics of the optimal core designs; Section 7 comments about the feasibility of the designs; and Section 8 summarizes the conclusions of this study.

2. RBWR-Th Physics

The RBWR-Th requires 3-D modeling techniques in order to adequately predict its performance. Although the single seed region makes it more axially uniform compared to the RBWR-AC, the water density varies significantly from the bottom of the seed to the top of the seed, as seen in Figure 4. This leads, in turn, to a strong axial variation in one-group microscopic cross sections (Figure 5 and Figure 6). The fission cross sections at the bottom of the seed are typically 2 or 3 times higher than those at the top of the seed; this is not adequately captured using 2-D cross sections.

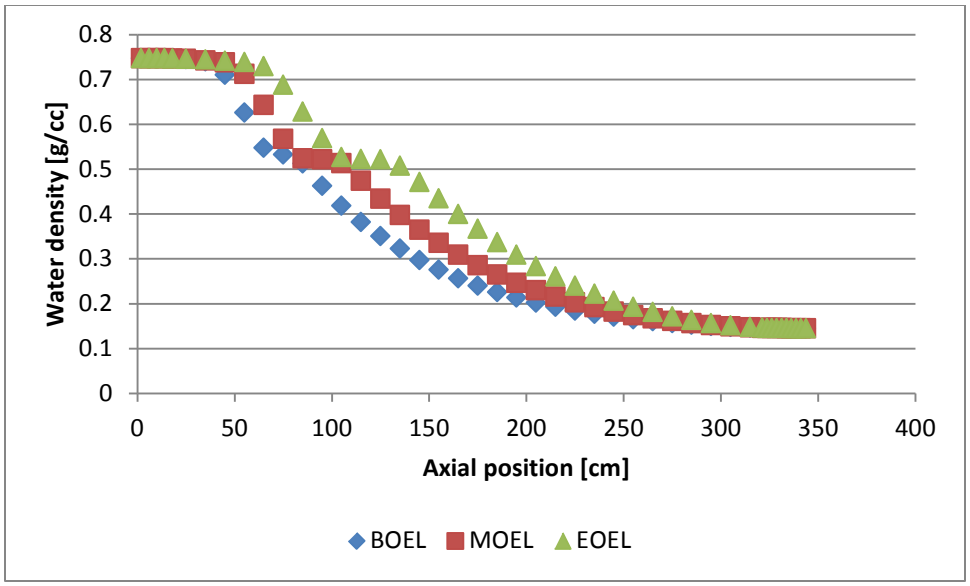

Figure 4. Water density vs. height for the RBWR-Th using MIT-recommended T/H correlations.

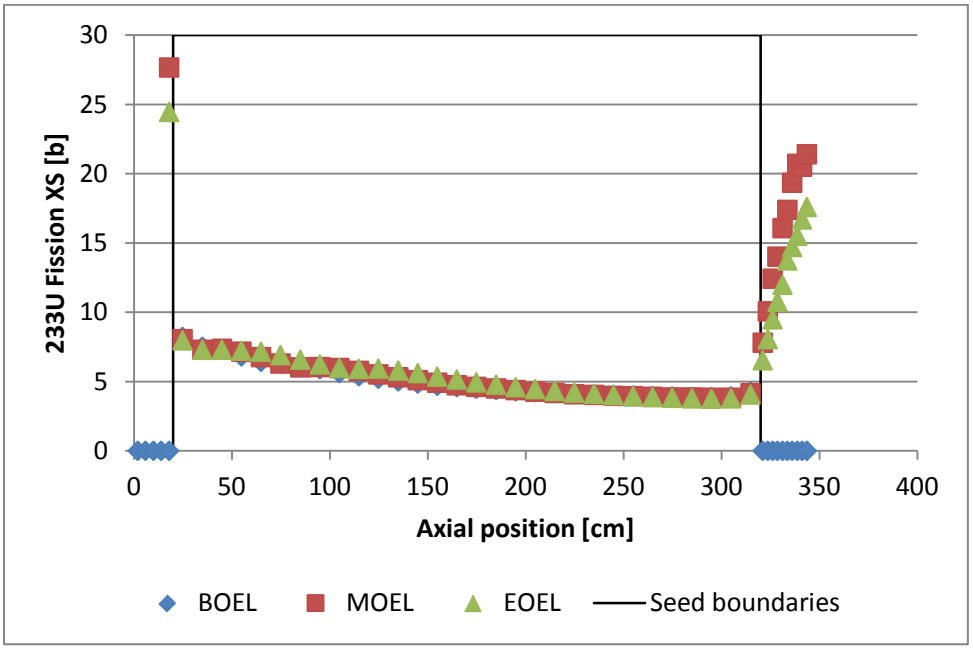

Figure 5. ^{233}U fission cross section vs. height for the RBWR-Th using MIT-recommended T/H correlations. The plot is zoomed in slightly to show variation in the seed values; the cross sections in the lower blanket are cut off somewhat.

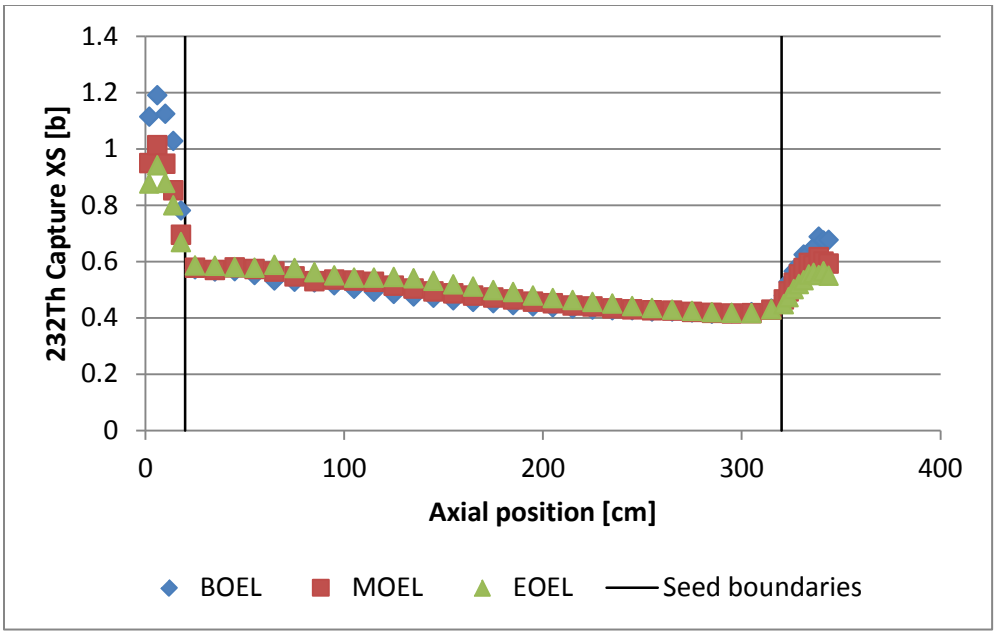

Figure 6. ^{232}Th radiative capture cross section vs. height for the RBWR-Th using MIT-recommended T/H correlations.

In the RBWR-AC design, the middle of the upper reflector also contained boron carbide pins, which are unnecessary for the RBWR-Th. Short axial blankets are added in order to reduce the axial leakage. The axial geometry is shown in Figure 7.

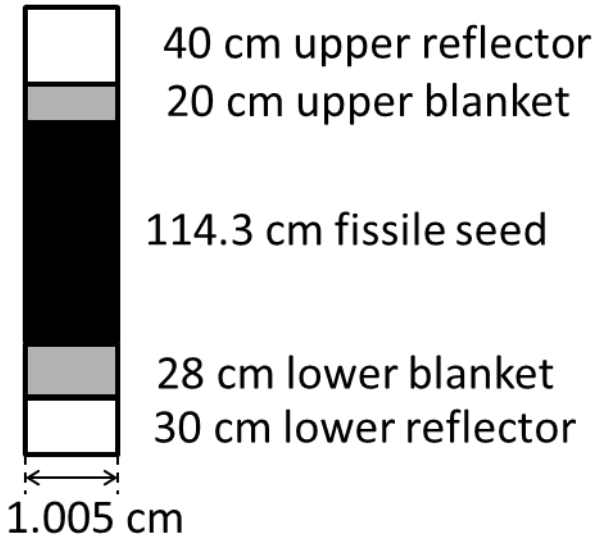

Figure 7. Axial cutaway of an RBWR-Th pin. The length of each fuel region is variable; shown is the optimized design using the Hitachi T/H correlations.

As shown in Figure 8, the average spectrum for the RBWR-AC is significantly softer than that of the RBWR-Th. However, this is misleading; the large internal blanket significantly softens the flux in the RBWR-AC. As shown in Figure 9, the spectrum in the seeds for all three designs is nearly identical.

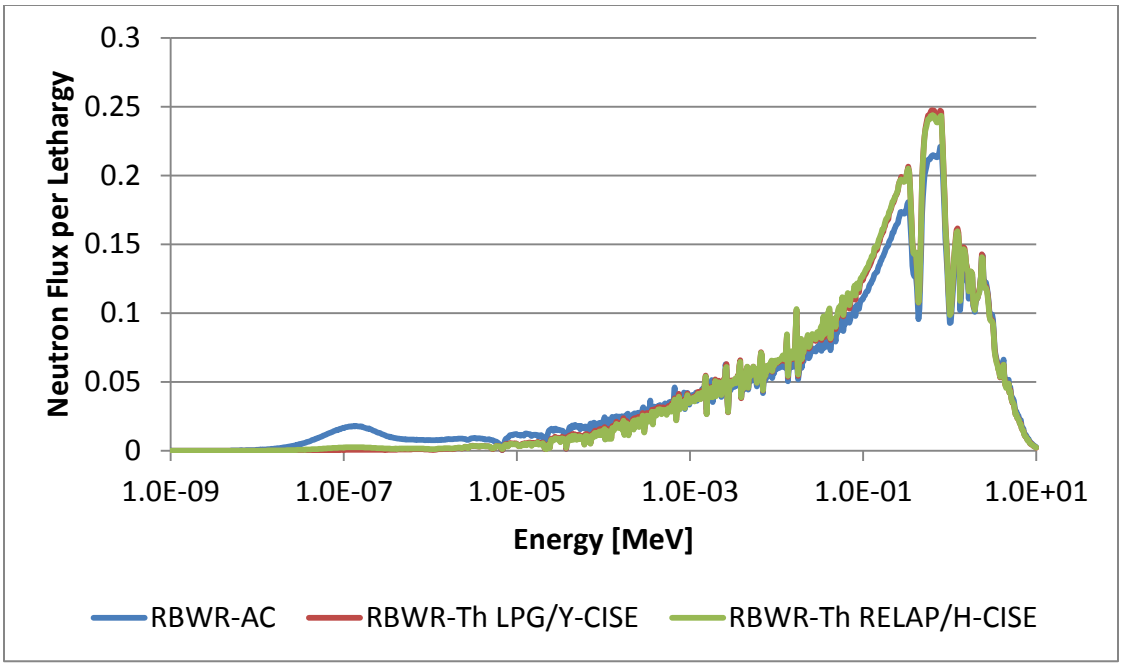

Figure 8.Neutron flux spectrum for the three self-sustaining RBWRs, averaged over the entire fuel length. The units are arbitrary.

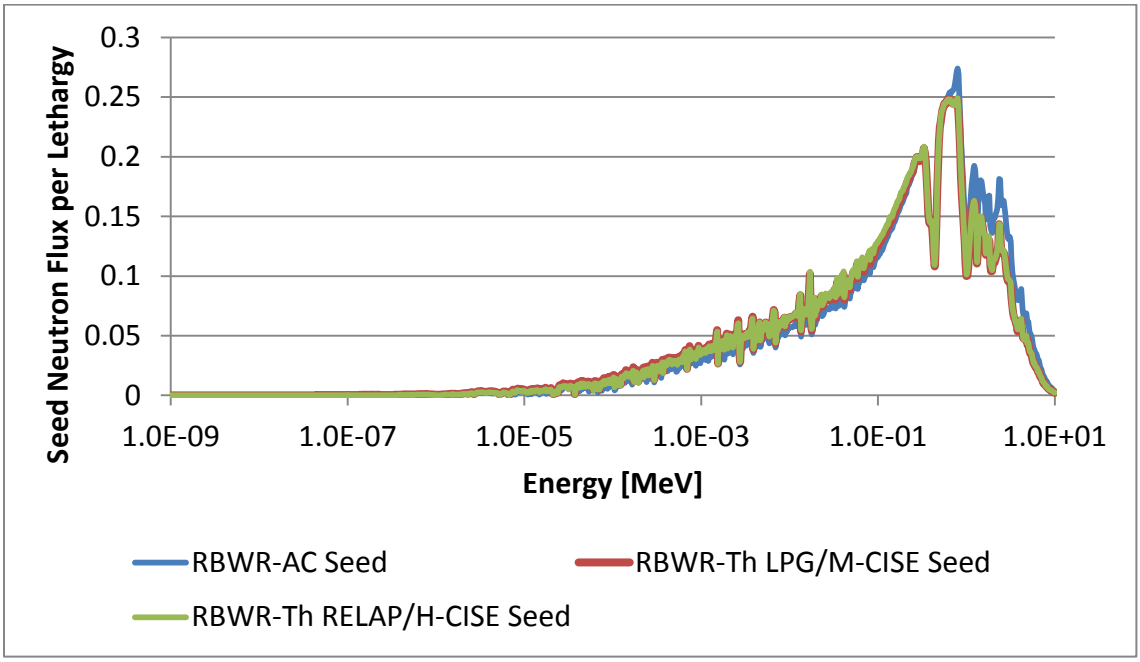

Figure 9. Neutron flux spectrum for the three self-sustaining RBWRs, averaged only over the seeds. The units are arbitrary.

3. Methodology

3.1. Equilibrium search methodology

The MocDown code, which couples neutronics with thermal hydraulics and depletion calculations, was used to simulate an axially finite, radially infinite assembly unit cell for each of the core variations studied and search for its equilibrium composition.[9] It uses MCNP5.1.60 for neutron transport, PATHS

for thermal hydraulic and ORIGEN2.2 for transmutation calculations.[10,11,12] A Monte Carlo technique is used to analyze a 3-D fuel assembly unit cell instead of deterministic 2-D lattice codes in order to accurately capture the axial heterogeneity of the RBWR cores. A three-assembly unit cell is used rather than a single assembly unit cell in order to preserve the periodic boundaries based around the Y-shaped control blade; an illustrative three-assembly unit cell is shown in Figure 10. The water between the assembly cans and the control blade was assumed to be liquid density water for the design using the MIT-recommended T/H correlations, while it was assumed to be boiling for the design using the Hitachi T/H correlations; the impact of this assumption is discussed in Section 4.2.

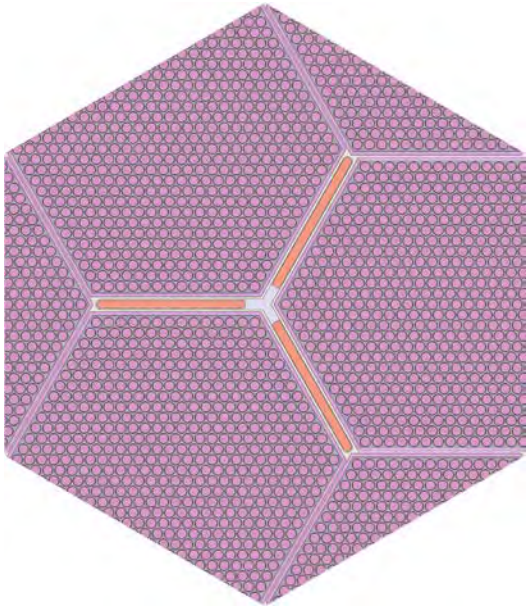

Figure 10. A horizontal cut through a 3-assembly unit cell consisting of 547 fuel pins with a Y-shaped graphite follower inserted.

MocDown's accelerated equilibrium search strategy is utilized in this study, which is detailed in the second attachment.[9,27] The isotopic ∞-norm convergence criterion was 3e-6, while the neutronics convergence criterion was 100 pcm. The recycling scheme that was utilized is shown in Figure 11.

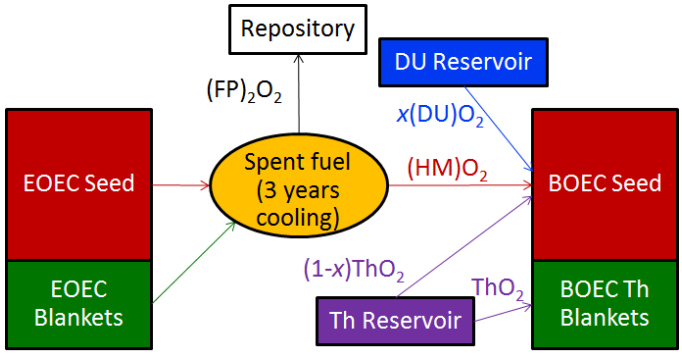

Figure 11. Fuel recycling scheme used in the RBWR-Th.

The PATHS steady-state thermal hydraulics module of the PARCS code was used to provide neutronically consistent water densities.[11,27] Designs were considered in which the coolant cross section area in the fission gas plenum of the RBWR designs was larger than in the active core region; therefore, the PATHS calculations were performed in two steps. The enthalpy and pressure was held constant at the interface. For the assembly level, a form loss of 29.6 was used to account for the orifice plate at the inlet to the

core, and a form loss of 7.93 was used for the lower tie plate. It was also assumed that spacer grids would be located every 50 cm, with form losses of 1.67 at each grid location. Finally, a form loss of 1.22 was applied at the exit for the upper tie plate. The water densities from PATHS are used in the next iteration of the MCNP calculation; the coupling would continue until the ∞-norm of the water densities was within 2% while using a relaxation coefficient of 0.5 (Figure 12).

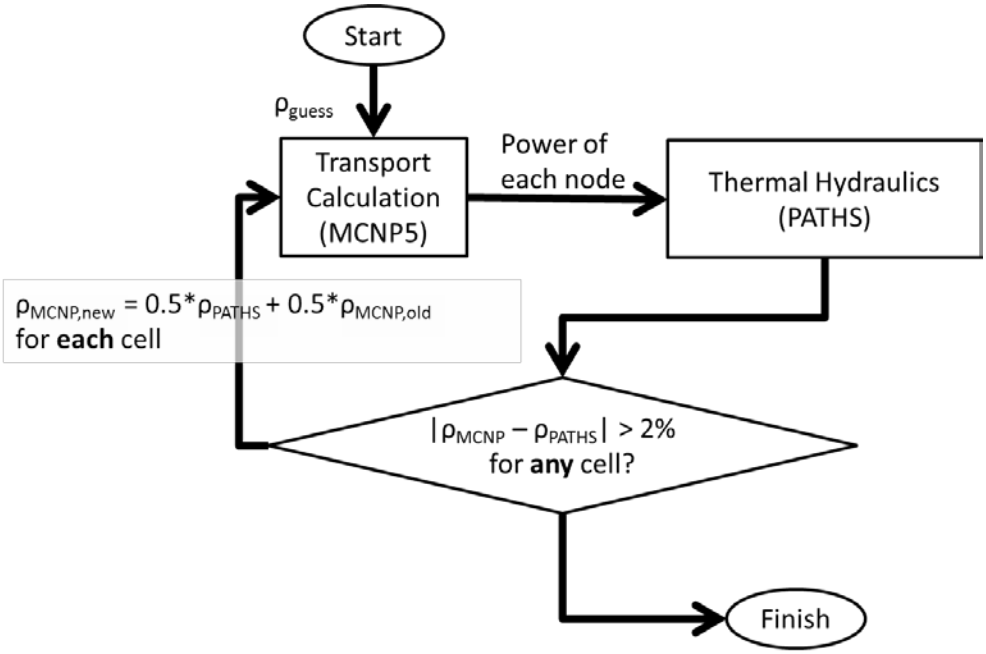

Figure 12. Water density update scheme with relaxation.

The core was assumed to be made of five fuel batches. The linear reactivity model was used to evaluate the core-average reactivity. A linear fit was created for the inverse of the radially infinite multiplication factor variation with burnup, discarding the first two points (corresponding to 0.6 MWd/kgHM) over which non-linearity is introduced by the buildup of xenon and samarium. It was observed that the k progression was insignificantly affected by the depletion time (Figure 13), so the achievable discharge burnup was calculated by lengthening or shortening the cycle length while using the same k regression until a critical cycle was identified. The following relation was used to estimate the core multiplication factor:

$$k_{\text{full core}} = \frac{5}{\sum_{i}^{5}\left(k^{-1}\right)_i} - L_{core}$$

where $(k^{-1})_i$ is the linearly fitted inverse multiplication factor for the *i*-th batch, and L_{core} is the full core radial leakage probability. The full core radial leakage probability was determined to be 1.8% from the full core analyses.

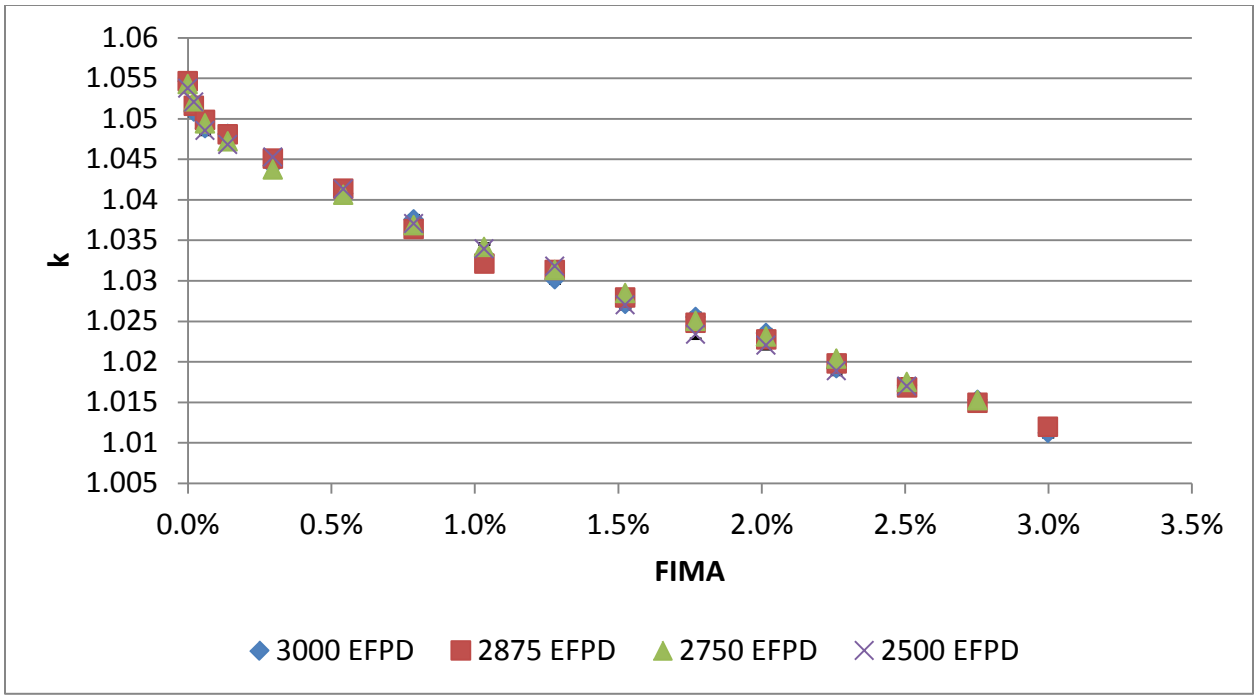

Figure 13. Sample k progression observed during the pin model tradeoff studies. Error bars are shown, but less than 55 pcm.

A detailed assembly-level analysis determined that a scheme of seven gradually varying enrichment groups would be necessary to keep the peak pin power within 120% of the average (Section 5).[8] However, in order to reduce the computational burden for the equilibrium calculation, only two radial enrichment zones were used: a radial blanket, and an enriched zone. The size of the radial blanket depended on the number of pins used in the assembly. The two schemes used in this paper are shown in Figure 14.

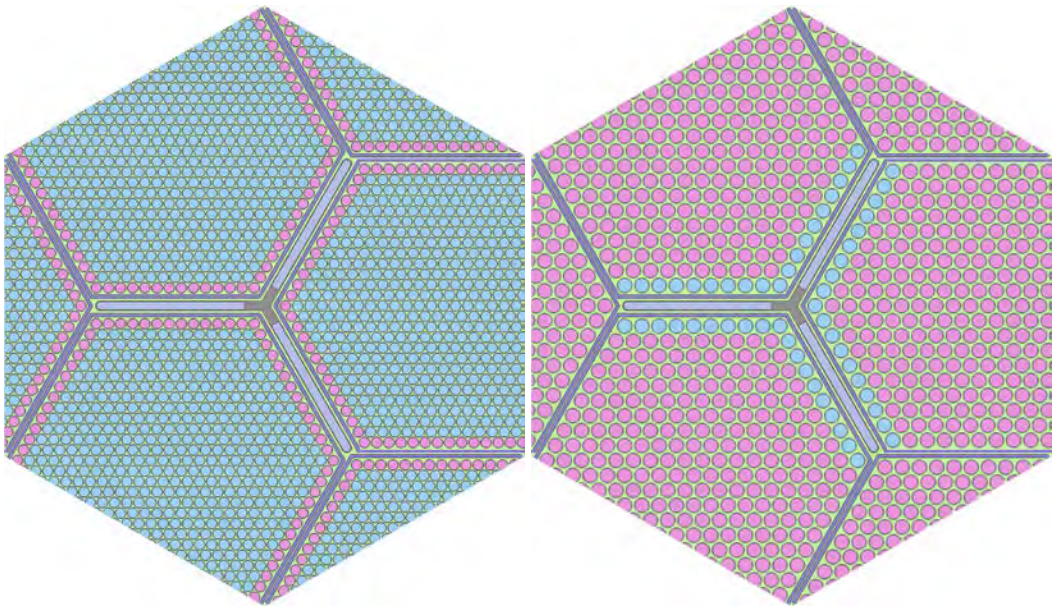

Figure 14. Radial enrichment schemes used in the equilibrium analyses for the 547 pin case (left) and the 271 pin case (right). The pins nearest to the control blade are charged with only thorium and depleted uranium.

3.2. Design variables

The following design variables were considered for the studies:

1. seed region length,
2. outer axial blanket region lengths,
3. internal blanket region length
4. axial isotopic charge distribution,
5. coolant mass flow rate,
6. atom fraction of depleted uranium (DU) in the seed makeup,
7. fuel pin pitch-to-diameter ratio (P/D),
8. number of pins per assembly,
9. core power
10. cycle length
11. void fraction correlation,
12. CPR correlation,
13. bypass flow density, and
14. follower material.

The void fraction correlation, the CPR correlation, and the bypass flow density are not design variables but rather modeling assumptions. They are included in this analysis to quantify the sensitivity of the RBWR-Th to the T/H assumptions, which have significant experimental uncertainties for tight lattice bundles.[13,28]

3.3. Design constraints and assumptions

The tradeoff studies were to abide by the following constraints:

1. Charge only fertile material
2. Recycle all transfertile (TRF) material

3. Maintain a fissile inventory ratio (FIR) of unity at equilibrium
4. Fit within an ABWR pressure vessel
5. Use the Hitachi RBWR assembly dimensions
6. Operate in cycles of at least 12 months
7. Assure pressure drop through core ≤ 0.3 MPa
8. Possess negative coefficients of reactivity for fuel temperature, coolant void, and power
9. Maintain criticality
10. Avoid coolant dryout: MCPR ≥ 1.3
11. Suppress density wave oscillations: DR ≤ 0.8
12. Have sufficient shutdown margin to shut down the core at any point in the cycle

Here, MCPR is the minimum critical power ratio and DR is the decay ratio of the core response to two-phase density wave oscillation (DWO) perturbations.

3.4. Full core simulation methodology

The PARCS nodal diffusion code was used to simulate a full core.[14,26] The SerpentXS code was used to generate cross sections using a three-assembly unit cell that was simulated in Serpent2 from the results of the assembly level tradeoff analysis.[15,16] It should be noted that Serpent2 is still in beta version but was used due to its drastically improved memory utilization and running times. In Serpent2 three-assembly model, the full 7 enrichment zones were used (Section 5).

The SerpentXS code was primarily used as a buffer code to autonomously run multiple branch cases in Serpent at different burnup points. The GenPMAXS code using axial discontinuity factors (ZDFs) was used to generate homogenized macroscopic cross sections from the Serpent output.[17,18,26] Ten different branches were used, with four different depletion histories (denoted with an asterisk):

1. Reference branch*
2. 85% flow branch
3. 70% flow branch*
4. 115% flow branch
5. 130% flow branch*
6. Uniform 1200 K fuel temperature branch
7. Uniform 600 K fuel temperature branch
8. Control rod inserted*
9. Control rod inserted + 70% flow
10. Control rod inserted + 130% flow
11. Shut down conditions (room temperature, liquid density water, control rod inserted, all ^{233}Pa and ^{135}Xe forced to decay to ^{233}U and ^{135}Cs)

A full-core model was created in PARCS, and an equilibrium state was reached by depleting the core and shuffling the fuel until the maximum local burnup difference between cycles was less than 0.1 GWd/t. At each depletion step, thermal hydraulic coupling was performed by PATHS.[12] It was observed that tightening the convergence criteria affected the results, particularly for the power normalization, so an under-relaxation coefficient of 0.1 was used, and the convergence criteria for the outer iterations was tightened from the default of 10^{-6} to 10^{-7}.[12]

Since PARCS does not track isotopes, no explicit recycling could be modeled at the full-core level. The fresh assembly composition was taken from the equilibrium assembly unit cell analysis, but the equilibrium core is not guaranteed to be self-sustaining (unlike in the assembly-level analysis).

3.5. Reactivity coefficients

The void coefficient of reactivity (VCR) was calculated using equation (1) by running two single coupled neutronics-T/H steps at BOEC and EOEC using the full core model at 100% and 85% of the flow rate:

$$\mathrm{VCR} = \frac{\frac{1}{k_{100\%\ \mathrm{flow}}} - \frac{1}{k_{85\%\ \mathrm{flow}}}}{\alpha_{100\%\ \mathrm{flow}} - \alpha_{85\%\ \mathrm{flow}}} * 1000 \qquad (1)$$

where α is the void fraction for each flow rate. The 1000 multiplier converts the units to pcm / % void.

3.6. Shutdown Margin

The shutdown margin was quantified at BOEC by fully inserting all control rods except the center one into the equilibrium core. Thermal hydraulic feedback was removed; the water densities were set to room temperature, and the fuel temperatures were uniformly set to 300 K. The shutdown margin was quantified as the negative reactivity of the subcritical core (i.e. $\frac{1}{k_{shutdown}} - 1$). Since the shutdown branch removed the ^{135}Xe and replaced the ^{233}Pa inventory with ^{233}U (Section 3.4), this would provide a conservative value which would account for decay.

4. Results of Tradeoff Study

The sensitivity of important RBWR-Th core performance parameters to change in each one of a dozen design variables was established. These results are briefly summarized in Table 2. All except the effects of the internal blanket, the bypass region density, and the follower material are quantified in detail for a pin model in Reference 19.

The design variables that most directly influence the discharge burnup are the ones that affect the H/HM ratio -- i.e. P/D, coolant flow rate, and void fraction correlation. Tightening the P/D dramatically improves the achievable burnup with small impacts on the MCPR, but it also increases the pressure drop significantly. Lowering the mass flow rate improves the pressure drop and the discharge burnup, but it worsens the MCPR. For a fixed P/D, the coolant mass flow rate was the dominant factor in maximizing the discharge burnup. It was observed that increasing the seed length reduces the discharge burnup slightly, but also reduces the required mass flow rate to meet the MCPR constraint. Since lower flow rates promote more breeding, the longer seeds result in a higher discharge burnup up to the upper limit (3 m). Similarly, using more pins per assembly improves the wetting of the fuel pins, which permits a lower mass flow rate at the cost of higher pressure drop. Adding axial blanket regions reduce the axial leakage and improve breeding, but if too long, then the extra breeding is cancelled out by the additional HM mass. The blanket length which maximizes discharge burnup varies between 20 cm and 30 cm, depending on the void fraction correlation used. Adding DU to the seed makeup stream has small or negligible effects on most neutronic parameters aside from the VCR and the shutdown margin; it is necessary to use about 1/3 DU in the seed makeup in order to shut down the reactor, due to the strong negative void feedback from a pure Th-^{233}U system.[7] Using a graded axial enrichment is necessary for a pure Th-^{233}U system in order to flatten the axial power profile,[6] but for a mixed Th/DU system, the graded axial enrichment scheme reduced the MCPR, so it was not used.

Table 2. Results of the tradeoff study. The + or – in the parentheses in the header row indicates which value is desired to meet the constraints. Within the table, a + indicates that an increase in the variable on the left column results in an increase of the metric in the top row.

Variables	MCPR (+)	Discharge BU (+)	VCR (-)	Shutdown Margin (+)	Pressure Drop (-)
Seed length	+	-	+	-	+
Outer blanket lengths		+ [note 1]	+	-	+
Internal blanket length [note 2]		-	-		
Axial enrichment (moving fissile from bottom to top)	* [note 3]	* [note 3]		+	-
Coolant flow rate	+	-			+
Makeup DU $^{a}/_{o}$			+	+	
P/D	+	-	-	-	-
Number of pins per assembly	+		-	+	+
Power	-	-	+	+	+
Depletion time		+		+	
Void fraction correlation (LPG to RELAP)		+	+	-	
CPR correlation (from Y-CISE to H-CISE)	+				
Bypass region density (from liquid density to boiling)		+		-	
Follower material (graphite to void)		+			

Note 1: The effect of blanket length on burnup length is not monotonic; lengthening the blankets increases the discharge burnup when there are very short blankets, but adding too much blanket decreases the average discharge burnup. The peak discharge burnup occurs with blankets that are between 20 cm and 30 cm each.

Note 2: Since the total core height was limited, increasing the internal blanket was accomplished by removing a portion of seed from the center and replacing it with blanket material.

Note 3: Any deviation from uniform enrichment (whether it is moving fissile material to the top or to the bottom) reduces the MCPR and the burnup.

4.1. Internal blanket effects

For an intermediate (not optimized) design, the total fuel length was held constant at 162.3 cm, with 28 cm for the lower blanket and 10 cm for the upper blanket, and the seed was split into two equally sized sections. The length between the seed sections was varied from 0 to 20 cm. The Hitachi T/H correlations were used, and a mass flow rate of 9.4 kg/s/assembly was used.

Although it would be ideal to compare discharge burnups of the different designs, the cases with the internal blankets were not critical for any length of time. Therefore, the EOC k_{eff} values from the core

model are compared after being depleted for 1000 effective full power days (EFPD) in Figure 15. Additionally, VCRs are compared in Figure 16. While the internal blanket is very effective at reducing the VCR, it is not necessary for a primarily thorium system, and decreasing the DU feed fraction can reduce the VCR by a comparable amount without penalizing the burnup.

Since the VCR is reduced in these cases, using an internal blanket would add the option of denaturing the design through adding more DU. Such a design would have a much lower burnup, though, while also having a higher peak LHGR.

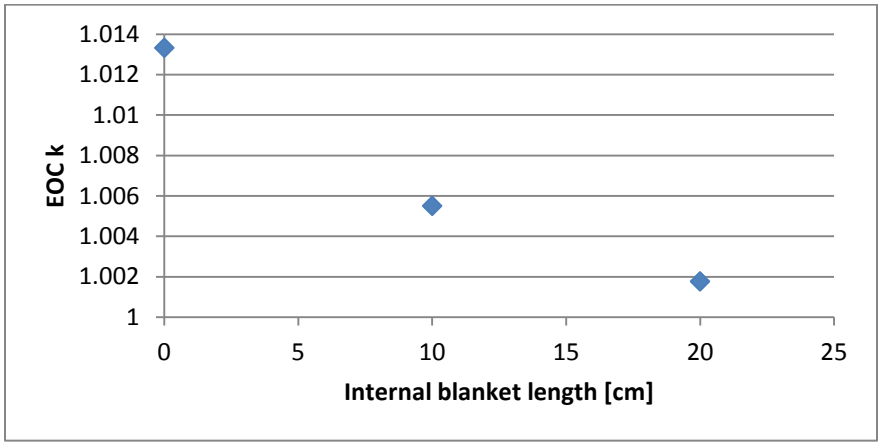

Figure 15. EOC batch-averaged k vs. internal blanket length after 1000 EFPD depletion time.

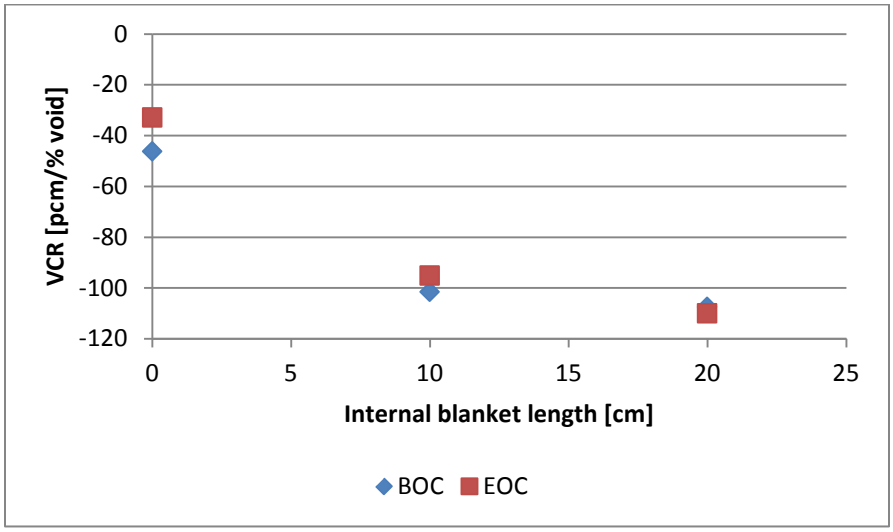

Figure 16. Batch-averaged void coefficients vs. internal blanket length at BOC and after 1000 EFPD depletion time.

4.2. Bypass region density

In order to provide bounding analyses, the cases using the MIT-recommended T/H correlations (which feature more water in the assembly) used liquid density water in the bypass, while the cases with the Hitachi correlations assumed that the water in the bypass was boiling with the same density as the coolant within the assembly cans (which is consistent with the Hitachi analyses). Using the boiling bypass increases the discharge burnup; for the design using the MIT-recommended correlations, the average discharge burnup increases from 49.3 MWd/kgHM to 69.4 MWd/kgHM. In terms of EOC reactivity, the multiplication factor increased by 877 pcm.

4.3. Control rod follower material

The follower material was examined to see if a different choice could promote better breeding. A follower is necessary in order to displace the water in the bypass channel; however, graphite also moderates the neutrons. In order to remove the moderation without increasing parasitic absorbtion, the follower in the design using the MIT-recommended T/H correlations was replaced with a fill gas (modelled as void). The design using the Hitachi T/H correlations still used the graphite follower in order to maintain another layer of similarity to the RBWR-AC design.

When the follower in the design using the MIT-recommended correlations is replaced with graphite, the average discharge burnup decreases from 49.3 MWd/kgHM to 45.1 MWd/kgHM.

4.4. Guidance for the optimal designs

Although it was desired to preserve the ABWR full power, the design based off of the MIT-recommended correlations was not able to be critical at equilibrium while meeting the pressure drop and MCPR constraints at full power. It was observed that if the power was derated, the required mass flow rate could be reduced more proportionally than the power, thereby increasing the average void fraction. Additionally, by reducing the power and extending the cycle length, more ^{233}Pa decays to ^{233}U during the cycle, which improves the burnup slightly. The pressure drop is also reduced, which could enable a tighter P/D ratio, which would further improve burnup. The discharge burnup vs. P/D at the maximum achievable power is shown in Figure 17.

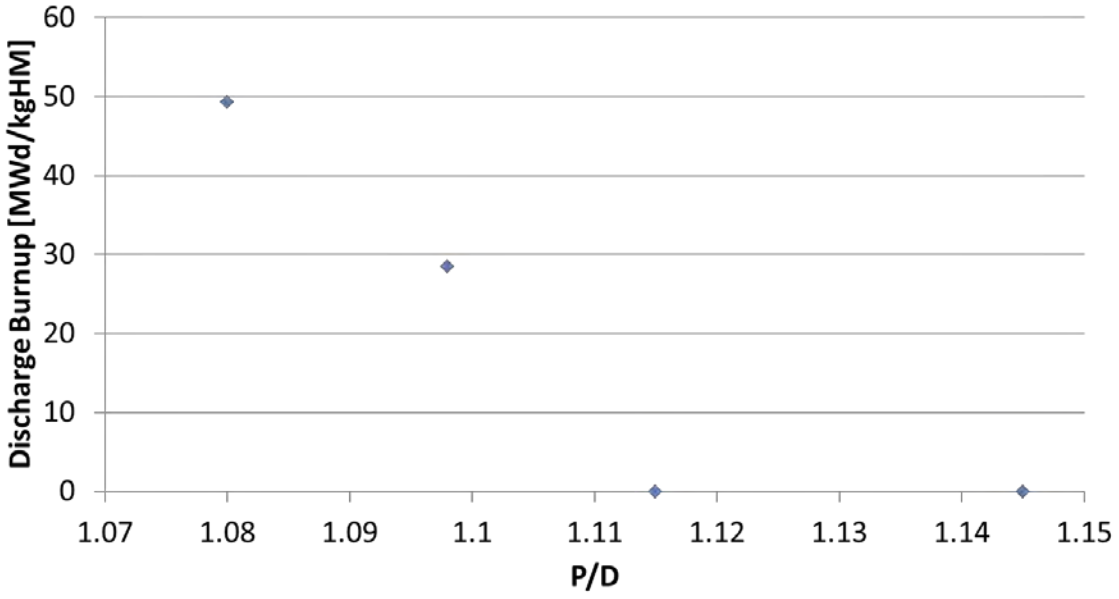

Figure 17. P/D vs. discharge burnup at maximum achievable power with the lowest permissible flow rate for the design using the MIT-recommended T/H correlations.

Since the DU feed fraction had a negligible impact on most performance metrics aside from the VCR and shutdown margin, the DU fraction was adjusted last in order to guarantee a slightly negative void coefficient. Since the equilibrium analysis was performed at an assembly level and the radial leakage from the full core model would make the void coefficient more negative, the target void coefficient was slightly positive. The dependence of the VCR on burnup and DU fraction for the two equilibrium designs

is shown in Figure 18 and Figure 19; it should be noted that the color scaling in the two figures is not conserved.

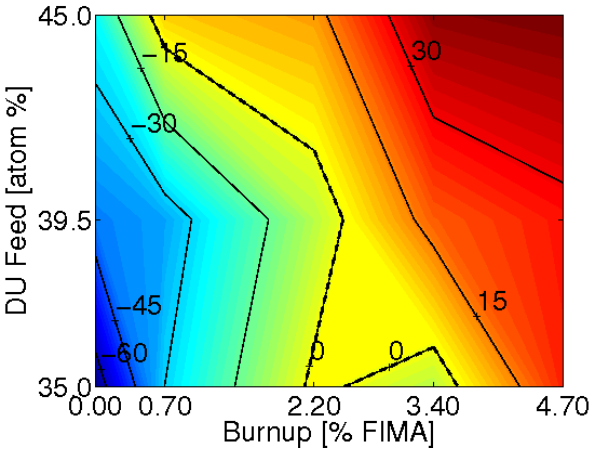

Figure 18. VCR dependence on burnup and DU feed in pcm/% void for the design using the MIT-recommended T/H correlations. The uncertainty at each point was between 5 and 8 pcm/% void. The contours at are intervals of 15 pcm/% void.

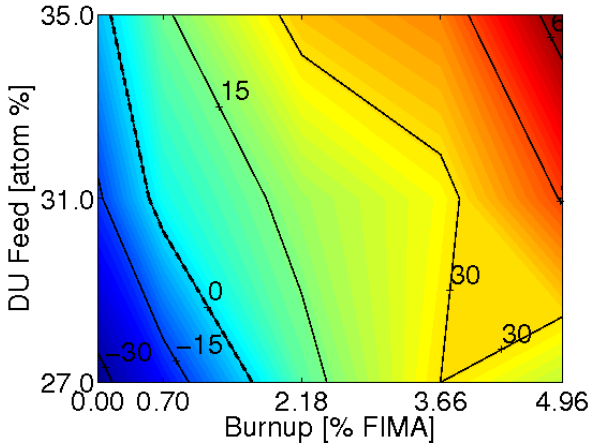

Figure 19. VCR dependence on burnup and DU feed in pcm/% void for the design using the Hitachi T/H correlations. The uncertainty at each point was between 6 and 8.5 pcm/% void. The contours at are intervals of 15 pcm/% void.

For the design using the MIT-recommended T/H correlations, the design process was as follows:

1. Maximize the seed length and the number of pins per assembly to reduce the required flow rate
2. Reduce the power
3. Reduce the flow rate and P/D until pressure drop and MCPR limit are barely met
4. Adjust DU fraction until the VCR is barely negative and the core may be shut down

For the design with the Hitachi T/H correlations, the design process was slightly different. The outlet quality was limited to < 40% in order to maintain two-phase flow stability, so the flow rate could not be reduced beyond a certain point. The presented design uses lowest flow rate that could be used at full power, and uses the same number of pins per assembly as the RBWR-AC in order to reduce the pressure

drop. Due to fuel survivability concerns (Section 7.2), the P/D was not reduced to increase the discharge burnup.

5. Assembly radial enrichment study

Although the control blade follower and the bypass region are relatively small, they introduce radial heterogeneities and extra moderation into the assembly model. The extra moderation results in larger pin powers near the assembly periphery if a uniform radial enrichment is used, as seen in Figure 20.

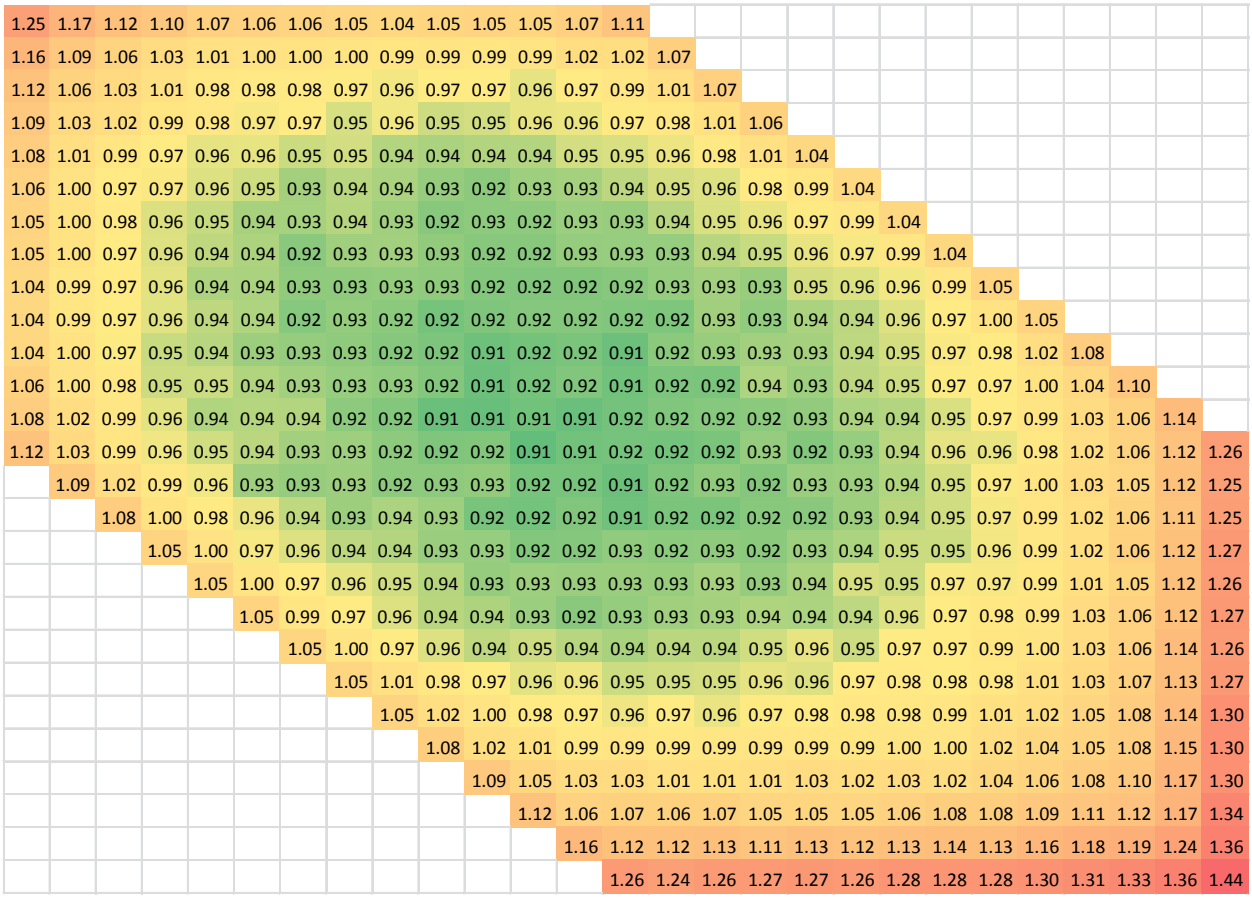

Figure 20. Pin powers for a fresh assembly with 547 uniform pins. The control blade is located at the bottom right of the figure.

In order to reduce the peak pin power to below 120% of the average, some TRF material was moved from the assembly periphery to the center in graded amounts. The equilibrium composition from the two enrichment zones in the equilibrium analysis were divided in to seven enrichment zones. This had an added benefit to the burnup: by having the enrichment gradually increased towards the center of the assembly, more of the fissile fuel was exposed to a harder flux. Compared to the simple two-enrichment group model for the design using the MIT-correlations, the achievable discharge burnup was increased from 49.3 MWd/kgHM to 51.2 MWd/kgHM. These schemes are shown in Figure 21, with Table 3 as a legend. The corresponding power peaking maps are presented in Figure 22 and Figure 23.

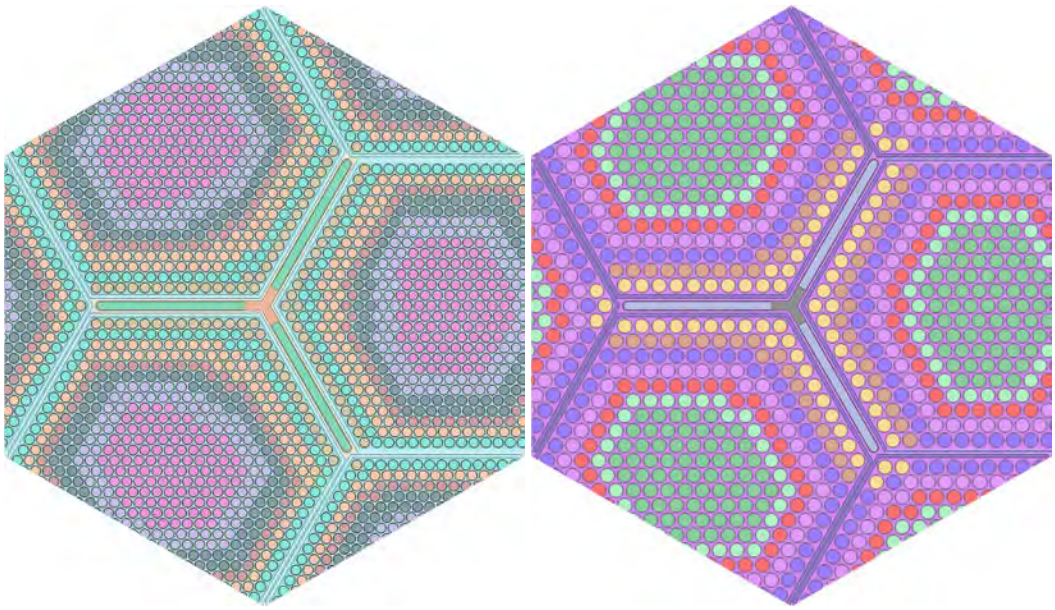

Figure 21. The 7 enrichment zones used to flatten the power in the RBWR-Th three-assembly unit cell using 547 pins per assembly (left) and 271 pins per assembly (right).

Table 3. Key for Figure 21.

	Group color	# of pins	BOEL TRF moles per pin / average moles per pin (%)
547 pins per assembly	Tan	29	19.40%
	Teal	78	54.50%
	Peach	93	90.00%
	Red	62	104.70%
	Dark Grey	92	115.00%
	Lavender	86	122.50%
	Magenta	107	130.00%
271 pins per assembly	Tan	23	40.00%
	Brown	19	60.00%
	Blue	48	77.50%
	Purple	44	100.00%
	Red	38	115.00%
	Light Green	32	120.00%
	Dark Green	67	130.00%

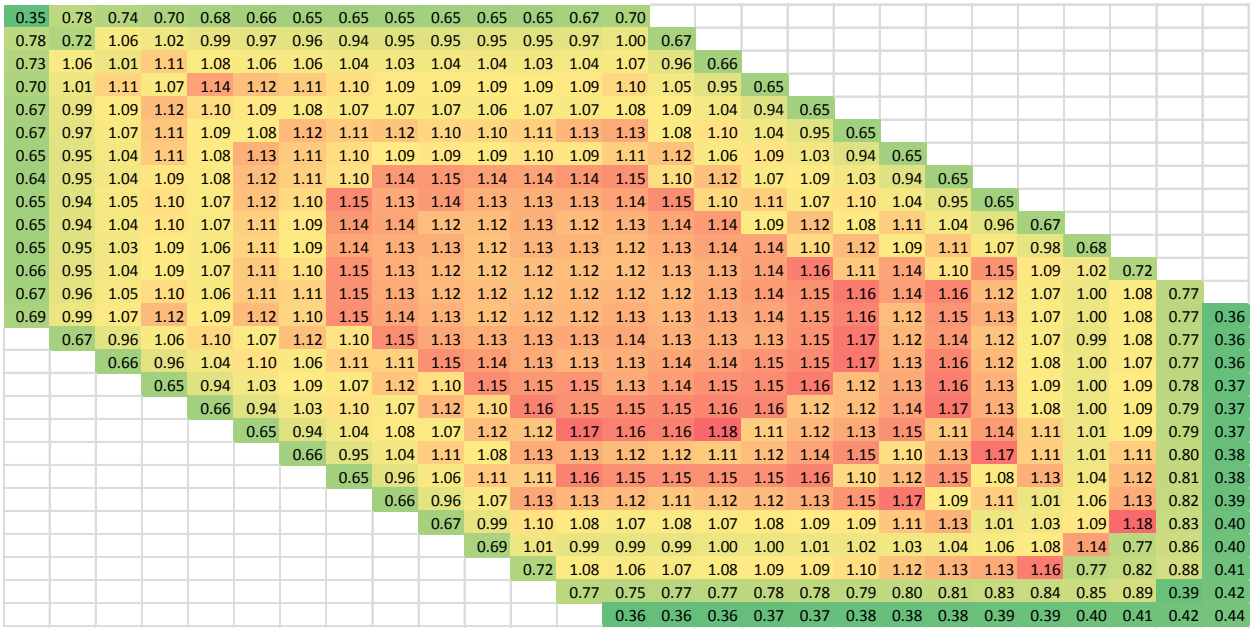

Figure 22. Pin powers for a fresh assembly using the MIT-recommended T/H correlations and 547 pins with the 7-group radial enrichment scheme. The control blade is located at the bottom right of the figure.

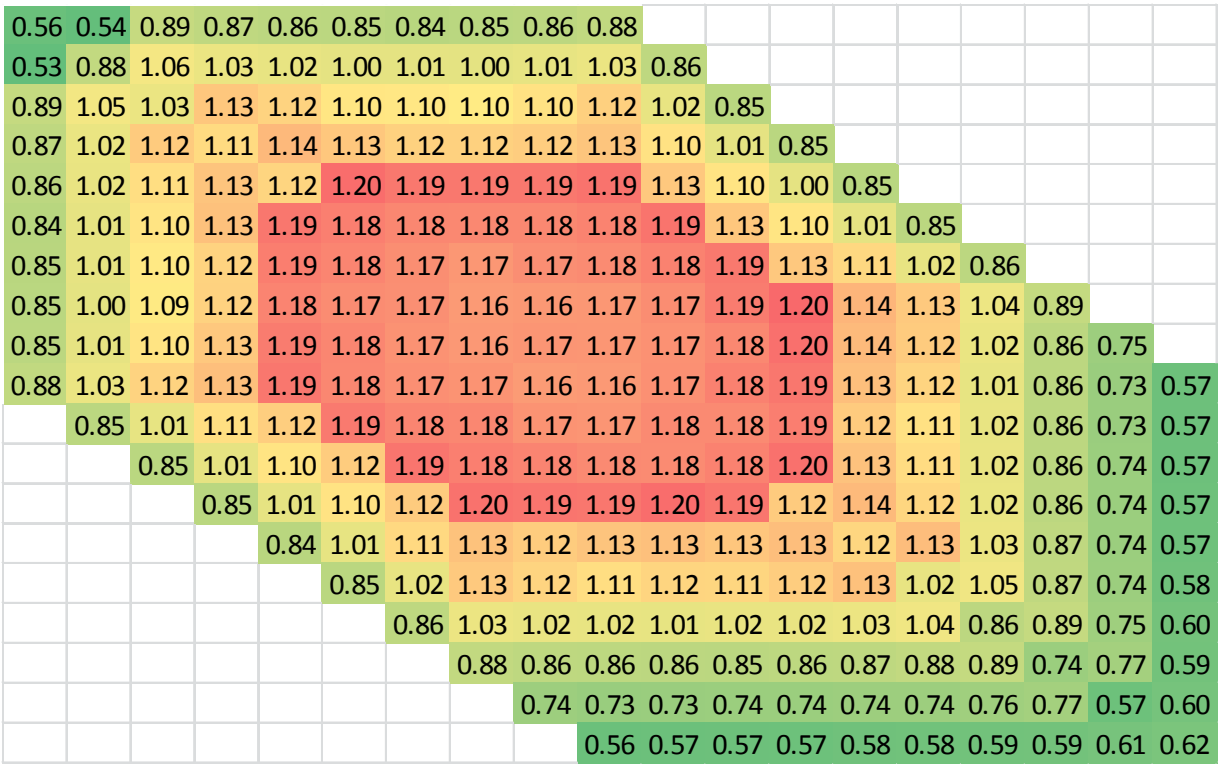

Figure 23. Pin powers for a fresh assembly using the Hitachi T/H correlations and 271 pins with the 7-group radial enrichment scheme. The control blade is located at the bottom and right edges of this figure.

Another radial enrichment scheme was investigated in which the DU that was fed in the core was fed into separated DU/Pu pins, while the thorium was fed into Th/^{233}U pins. An 8 enrichment group scheme was created, shown in Figure 24 and Table 4, with a graded enrichment scheme.

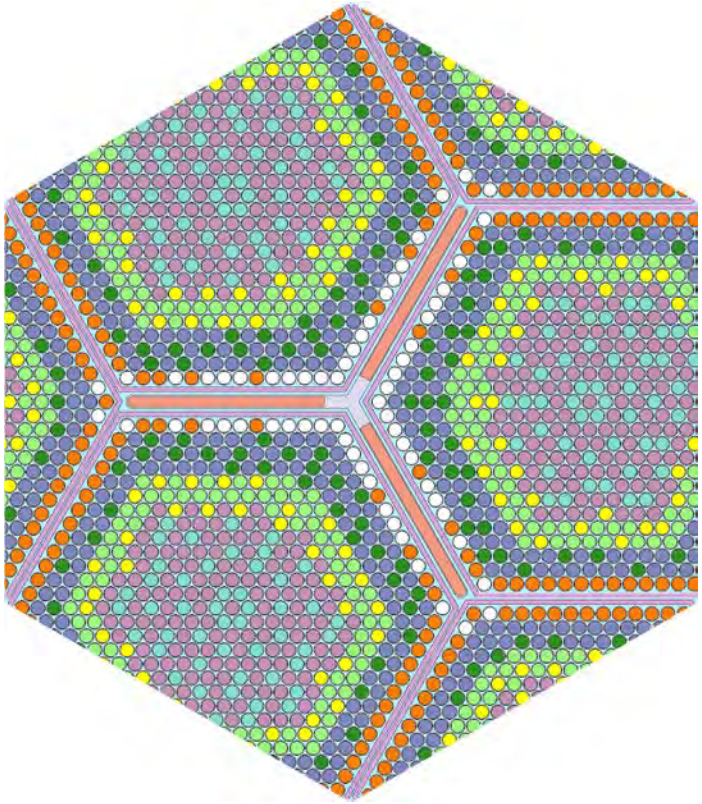

Figure 24. 8-enrichment group scheme using segregated DU/Pu and Th/^{233}U pins.

Table 4. Legend for Figure 22.

Makeup Material	Color	Enrichment (% of average)	Fraction of total TRU/TRTh in group
Th	Orange	30.0%	14.3%
	Blue	80.0%	30.3%
	L. Green	120.0%	21.3%
	Purple	134.6%	34.1%
DU	White	20.0%	14.2%
	D. Green	80.0%	27.0%
	Yellow	120.0%	26.4%
	L. Blue	135.4%	32.4%

As shown in Figure 25, the power of all of the DU/Pu pins was significantly higher than that of the Th/^{233}U pins. It is not feasible to design a scheme in which the highest powered DU/Pu pin has less than 120% of the average power.

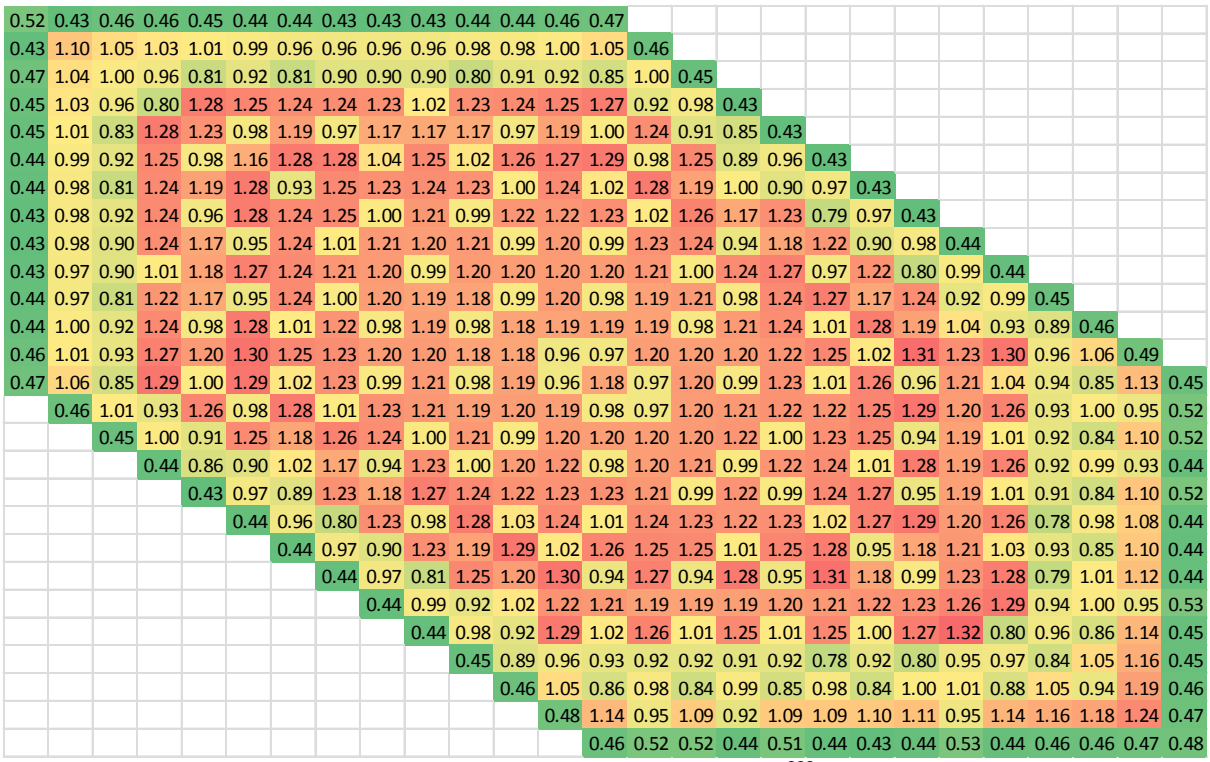

Figure 25. Pin power peaking map using segregated DU/Pu and Th/^{233}U pins. The control blade is on the bottom and right edges of this figure.

6. Optimal core designs

Using the Hitachi-modified CISE4 critical power correlation and the Chexal-Lelouche (RELAP) void fraction correlation, similar performance to the RBWR-AC could be attained while using a single seed. In order to have the most similar comparison possible, the water in the inter-assembly bypass region was assumed to be boiling. Another design was created using the MIT-recommended thermal hydraulic correlations (LPG for void fraction, and Y-CISE for critical power).[14] In order to provide a lower bound on the performance of the RBWR-Th, the inter-assembly bypass flow was assumed to be liquid density water. The design using the MIT-recommended thermal-hydraulic correlations is called the RBWR-ThM, while the design using the Hitachi thermal-hydraulic correlations is designated the RBWR-ThH.

In order to improve breeding, for the Y-CISE and LPG case, the follower was replaced with an inert gas (modelled as void) within the stainless steel sheath. For the design using the same correlations as Hitachi, the graphite follower was kept in order to have another level of similarity to the RBWR-AC.

The design information of each RBWR-Th design, as well as the RBWR-AC design and a CR=1.0 metal-fuelled Advanced Recycling Reactor (ARR),[20] is summarized in Table 5. The performance is summarized in Table 6, and the seed discharge isotopics are summarized in Table 7.

Table 5. ARR, RBWR-AC and RBWR-Th design information.

Parameter	Units	ARR	RBWR-AC	RBWR-ThM	RBWR-ThH
Coolant	-	sodium	light water	light water	light water
Blanket configuration	-	-	parfait	parfait	parfait
Fuel form	-	metal	oxide	oxide	oxide
Core thermal power	MWth	1000	3926	3200	3926
Core electric power	MWe	400	1356	1104	1356
# of assemblies	#	151	720	720	720
Core HM mass (BOEC)	t	16.7	140	354	153
Core TRF mass (BOEC)	t	2.4	16.7	48.9	18.9
TRF/HM core avg at BOEC	w/o	14.6%	11.9%	13.8%	12.4%
Assembly area	cm^2	193	338	338	338
Core volume	m^3	3	32	84	40
Core flow rate	kg/s	6138	7222	5525	6358
Specific power	MWe/t	24	10	3	9
Power density	Wth/cm^3	289	123	38	99
Upper blanket length	cm	-	7	25	20
Upper seed length	cm	101.6	28	300	114.3
Internal blanket length	cm	-	52	-	-
Lower seed length	cm	-	19.3	-	-
Lower blanket length	cm	-	28	20	28
Total fuel length (seed + blanket)	cm	101.6	134.3	345	162.3
Seed length	cm	101.6	47.3	300	114.3
Fuel pin OD	cm	0.808	1.005	0.740	1.005
Fuel pin pitch	cm	0.889	1.135	0.799	1.135
Fuel pin P/D	-	1.10	1.13	1.08	1.13
Hydraulic diameter	cm		0.41	0.22	0.41
Heated diameter	cm		0.44	0.23	0.44
Pins per assembly	-	271	271	547	271

Table 6. ARR, RBWR-AC and RBWR-Th performance metrics.

Metric	Units	ARR	RBWR-AC	RBWR-ThM	RBWR-ThH
Pressure Drop	MPa		0.14	0.29	0.13
Outlet quality	%	-	35.0	39	39.5
Maximum LHGR	Wth/cm	389	472	45	261
# of batches	#	3	5	5	5
Average discharge burnup	GWd/t	73.0	45	50.1	48.9
Fuel residence time	EFPD	1222	1651	5123	1906
Cycle length	EFPD	370	380	1110	413

Metric	Units	ARR	RBWR-AC	RBWR-ThM	RBWR-ThH
Cycle reactivity swing	%dk	-0.6*	1.5	1.9	2.0
VCR (BOEC/EOEC)	pcm/% void	-	-24/-14	-4/-2	-4/-2
Shutdown margin	% Δk			3	1.9
FTCR (BOEC/EOEC)	pcm/K	-0.39/-0.35	-3.1/-3.4		

*The ARR gains reactivity over the course of the cycle.

Table 7. Discharge isotopics from the seed(s) of each design.

Mass fraction [%]	ARR	RBWR-AC	RBWR-ThM	RBWR-ThH
TRF / HM	15.2%	34.0%	16.3%	17.7%
fissile / HM	10.5%	16.8%	10.0%	10.9%
Pa / TRF	0.0%	0.0%	60.0%	0.3%
nonfertile U / TRF	0.0%	0.5%	1.5%	54.0%
Np / TRF	0.6%	0.4%	33.8%	1.3%
Pu / TRF	96.3%	92.2%	3.8%	40.4%
Am / TRF	2.6%	4.8%	0.6%	2.9%
Cm / TRF	0.4%	2.1%	0.0%	1.1%
Cf / TRF	0.0%	0.0%	60.0%	0.0%
^{232}U / U nonfertile		0.0%	0.3%	0.4%
^{233}U / U nonfertile		0.0%	57.0%	57.6%
^{234}U / U nonfertile		18.8%	27.4%	27.0%
^{235}U / U nonfertile		62.5%	7.7%	7.6%
^{236}U / U nonfertile		18.8%	7.5%	7.4%
fissile U / total U	0.03%	0.2%	19.5%	15.2%
^{238}Pu / Pu	1.1%	3.6%	9.0%	6.5%
^{239}Pu / Pu	66.4%	40.9%	48.1%	48.7%
^{240}Pu / Pu	27.5%	42.9%	34.4%	34.1%
^{241}Pu / Pu	2.7%	6.6%	4.4%	6.1%
^{242}Pu / Pu	2.3%	6.0%	4.0%	4.6%
fissile Pu / total Pu	69.1%	47.5%	52.5%	54.8%

The BOC and EOC radial power profile for the RBWR-ThH design is shown in Figure 26. The radial power peaking factor is 1.27 for this case, which is considered acceptable. The relative axial power profile for a fresh assembly for the RBWR-ThH is shown in Figure 27, while the relative axial power profile for the RBWR-AC is shown in Figure 28. It is clear that elongating the seed region provides a much more even power distribution over a longer fuel section. As the two cores have the same total power, same number of fuel pins and similar radial peaking factor, The RBWR-Th core features much lower peak LHGR and therefore peak fuel temperature than the RBWR-AC.

BOC

												1.14	1.14	1.17	1.14	1.13	1.10	1.08	1.07	1.06	1.06	1.05	1.03	0.88	0.75	0.61
											1.25	1.23	1.22	1.20	1.20	1.18	1.17	1.15	1.15	1.14	1.14	1.08	0.99	0.88	0.75	0.61
										1.26	1.27	1.26	1.26	1.25	1.25	1.21	1.20	1.15	1.14	1.12	1.11	1.02	0.87	0.75	0.67	
									1.25	1.24	1.23	1.25	1.24	1.25	1.24	1.20	1.19	1.17	1.16	1.14	1.10	0.97	0.79	0.66		
								1.16	1.26	1.23	1.23	1.25	1.24	1.22	1.24	1.20	1.18	1.16	1.14	1.08	0.95	0.87	0.80	0.64		
							1.13	1.21	1.21	1.21	1.22	1.23	1.25	1.22	1.19	1.20	1.18	1.15	1.08	1.03	0.90	0.66	0.63			
						1.09	1.21	1.20	1.20	1.18	1.20	1.21	1.23	1.18	1.15	1.13	1.11	1.08	0.99	0.88	0.83	0.64				
					1.08	1.16	1.20	1.20	1.18	1.20	1.20	1.19	1.19	1.17	1.13	1.13	1.10	0.97	0.94	0.66	0.64					
				1.14	1.14	1.14	1.18	1.17	1.17	1.17	1.18	1.17	1.15	1.15	1.12	1.06	1.05	0.88	0.84	0.63						
			1.01	1.12	1.13	1.12	1.15	1.16	1.11	1.08	1.08	1.07	1.05	1.04	1.02	0.97	0.90	0.72	0.61							
		0.92	1.09	1.10	1.12	1.11	1.08	1.12	1.09	1.08	0.97	1.04	1.03	1.03	0.98	0.90	0.76	0.64								
	0.85	0.90	1.02	1.04	1.07	1.07	1.07	1.06	1.02	0.98	0.98	0.98	0.98	0.90	0.90	0.69	0.65									
	0.79	0.83	0.94	0.96	0.96	0.97	0.96	0.95	0.95	0.96	0.95	0.94	0.93	0.76	0.77	0.69										
0.63	0.73	0.78	0.80	0.86	0.88	0.84	0.83	0.83	0.86	0.83	0.83	0.81	0.80	0.68	0.68											
	0.58	0.66	0.65	0.67	0.66	0.72	0.73	0.75	0.72	0.74	0.72	0.72	0.72	0.53												
						0.65	0.64	0.67	0.65	0.64	0.65	0.54	0.59	0.54												

EOC

												1.14	1.13	1.13	1.12	1.10	1.10	1.11	1.10	1.09	1.09	1.07	1.05	1.01	0.90	0.71
											1.13	1.14	1.14	1.14	1.14	1.12	1.12	1.11	1.11	1.12	1.11	1.10	1.07	0.94	0.90	0.71
										1.16	1.15	1.15	1.15	1.14	1.14	1.13	1.11	1.12	1.12	1.11	1.09	1.09	1.00	0.81	0.80	
									1.16	1.15	1.14	1.15	1.15	1.13	1.13	1.14	1.13	1.13	1.13	1.11	1.08	1.04	0.93	0.81		
								1.16	1.15	1.14	1.14	1.16	1.15	1.12	1.13	1.13	1.14	1.13	1.12	1.11	1.07	0.94	0.81	0.72		
							1.14	1.14	1.14	1.15	1.15	1.14	1.14	1.15	1.15	1.13	1.12	1.12	1.10	1.07	0.93	0.81	0.83			
						1.09	1.10	1.11	1.08	1.09	1.10	1.09	1.08	1.08	1.09	1.10	1.09	1.07	1.04	0.96	0.84	0.81				
					1.08	1.06	1.08	1.09	1.09	1.08	1.08	1.08	1.06	1.06	1.06	1.06	1.05	1.00	0.97	0.94	0.81					
				1.05	1.06	1.05	1.10	1.11	1.11	1.11	1.11	1.08	1.08	1.08	1.04	1.05	1.02	0.97	0.91	0.81						
			1.02	1.05	1.06	1.06	1.10	1.10	1.11	1.08	1.08	1.07	1.08	1.08	1.04	1.02	0.99	0.90	0.80							
		1.03	1.05	1.06	1.06	1.10	1.10	1.09	1.08	1.08	1.07	1.08	1.08	1.04	1.02	0.95	0.90	0.78								
	0.96	0.97	0.98	1.00	1.04	1.05	1.04	1.03	1.04	1.03	1.05	1.02	1.03	1.01	0.96	0.88	0.80									
	0.84	0.88	0.93	0.94	0.93	0.94	0.95	0.95	0.96	0.96	0.96	0.94	0.92	0.91	0.76	0.70										
0.63	0.74	0.78	0.87	0.89	0.88	0.88	0.88	0.89	0.88	0.89	0.89	0.88	0.86	0.76	0.71											
	0.63	0.68	0.70	0.72	0.72	0.82	0.84	0.85	0.87	0.87	0.83	0.83	0.82	0.73												
						0.73	0.75	0.75	0.75	0.75	0.75	0.75	0.75	0.73												

Figure 26. Radial power map for the RBWR-ThH core.

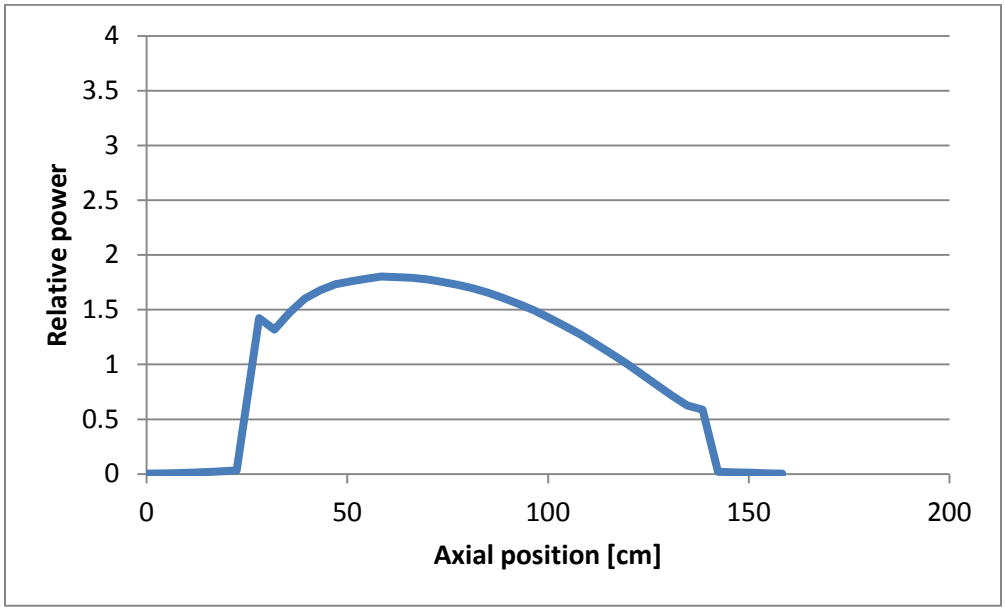

Figure 27. Relative axial power distribution for an RBWR-ThH fresh fuel from assembly level analysis.

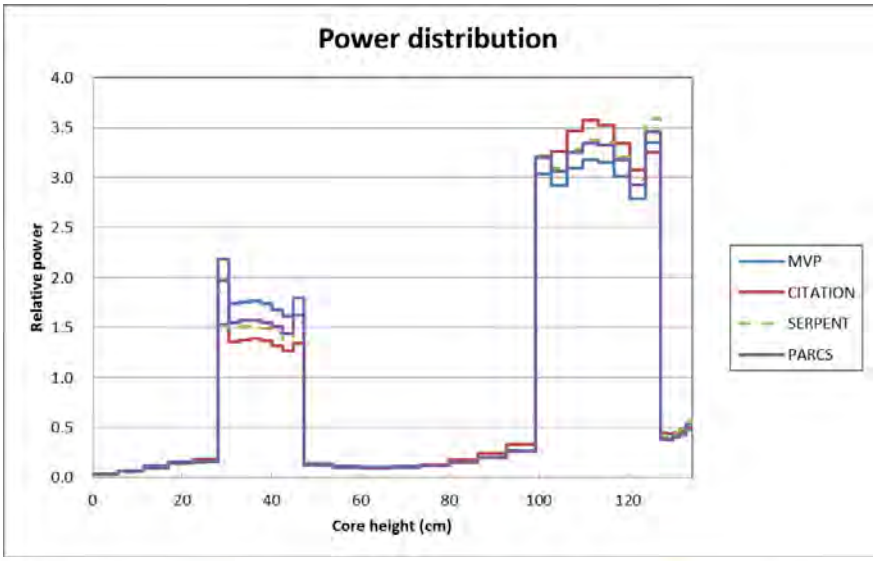

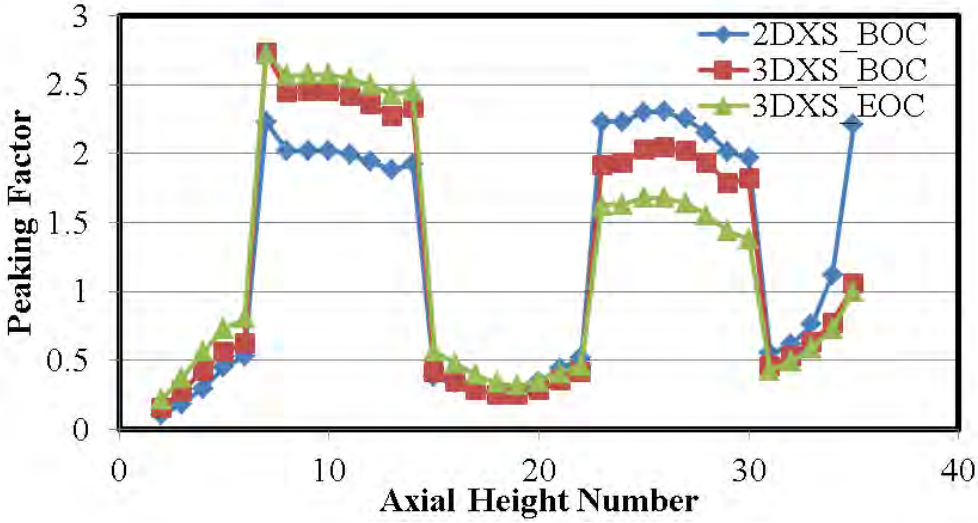

Figure 28. Relative axial power distribution for an RBWR-AC fresh fuel assembly (top) and full core average (bottom).

6.1. Partial rod insertion benchmark

Since the branching scheme selected in Section 3.4 only has fully withdrawn or fully inserted control rods, it was desired to benchmark the Serpent/PARCS code system for partially inserted rod cases. Since Serpent cannot model a full core, the 3-assembly unit cell (Figure 14) for the RBWR-ThM case was used. The control rod was inserted through 2/3rds of the seed. Table 8 shows the differences in k_{eff} between the two codes, and Figure 29 compares the axial power profiles.

Table 8. k_{eff} values in PARCS and Serpent for 2/3rd inserted control rod

Code	k_{eff}
PARCS	1. 01972
Serpent	1.01899

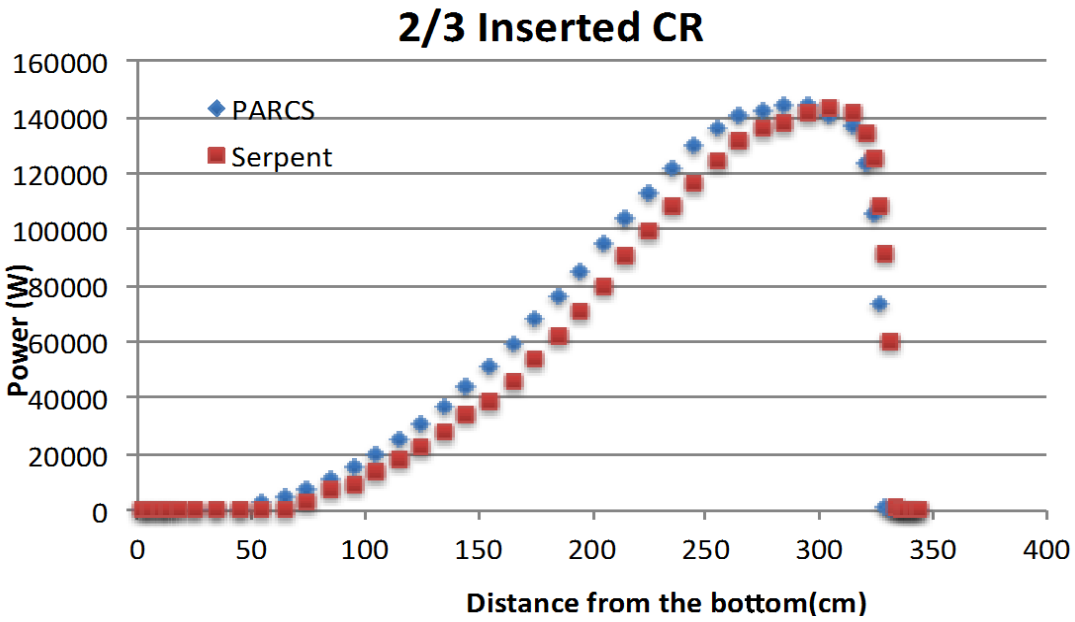

Figure 29. Axial Planar Power Profile difference between Serpent and PARCS for the rodded case.

6.2. Control rod & fuel management scheme

In order to determine the optimal control rod (CR) map during the equilibrium cycle, the following approach was used:

- Definition of the CR Banks: number of the control rod banks (15) and location in the core
- Definition of the CR step dimensions and the position of the full inserted CR: from the bottom to the end of the upper reflector
- Definition of the max and min withdrawn value of the CR in the core: defined with the same proportion as UM for RBWR-AC model
- Definition of the CR composition
- Use of the SEARCH command within PARCS[14] for the CR withdrawn height imposing k-eff equal to 1
- Done for each depletion step by using as reference power shape the one of the step before, starting with the reach for the equilibrium cycle at BOC

The CR banks are mapped radially using the same grouping as Hitachi, and the banks were moved in the same order during the depletion. The most significant change was the height of each control rod withdrawal as the present designs are significantly different from the Hitachi RBWR-AC, since they utilize only one seed. The methodology has been used for this project for the first time for this design and has been optimized for the EOC power map and discharge average burn-up. The k_{eff} values along the cycle obtained with CR inserted are shown in Figure 30.

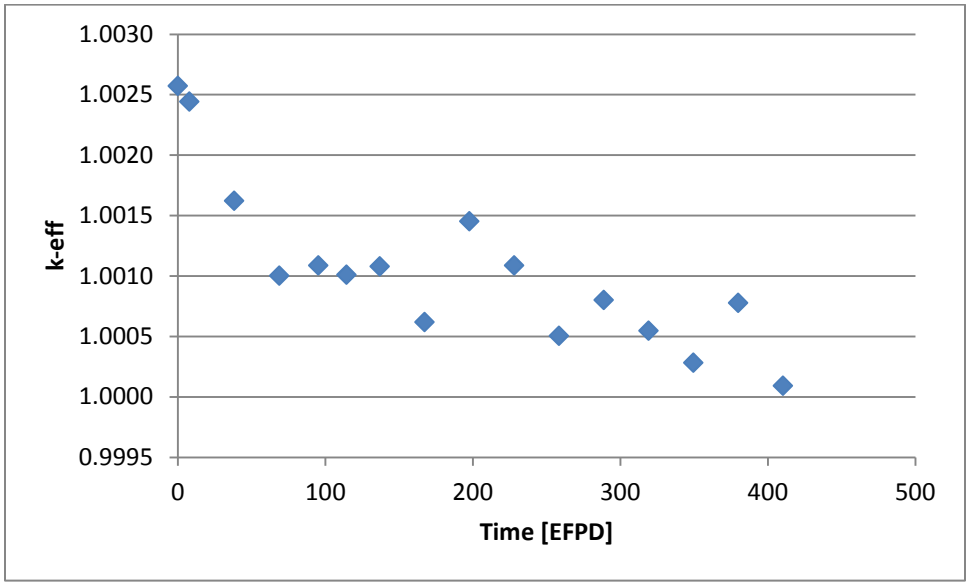

Figure 30. k_{eff} vs. time in cycle for the RBWR-ThH.

7. Designs feasibility

7.1. Safety and stability analysis

Due to similar assembly reactivity swings and average cycle burnup of the RBWR-Th and RBWR-AC designs, it is expected that the RBWR-Th design will have similar assembly average power and burnup distribution in the core. Hence, the Hitachi RBWR-AC core radial power and burnup distribution and orificing scheme were assumed for the safety analysis of the RBWR-Th that was performed before results were obtained from the RBWR-Th full core analysis. The middle of life (MOL) axial power shape from RBWR-Th single assembly calculations was used for the core average axial power shape in TRACE.

Both of the RBWR-Th breeder designs feature mass flow rates that are less than half of the ABWR. Therefore, they are expected to be more susceptible to decrease in core flow rate accident scenarios. However, unlike Hitachi RBWRs, the maximum LHGR of both RBWR-Th breeder designs are lower than the 394 W/cm of the ABWR and 472 W/cm of the RBWR-AC (Table 6). Therefore, the performance of RBWR-Th design with Hitachi correlations (RBWR-ThH) is expected to be better than the Hitachi RBWRs for loss flow scenarios. The RBWR-Th with MIT correlations (RBWR-ThM) is designed with very high pressure drop. The very high pressure drop along with tighter lattice could prevent core reflood in the event of reaching post critical heat flux (post-CHF) regimes. To assess the performance of the RBWR-Th reactor under loss of flow scenarios, the total pump trip accident is modeled. The sequence for the total pump trip accident is listed in Table 9. The sequence of events also includes complete loss of feedwater flow at 1.85 seconds after the pump trip.

Table 9. Sequence of the Pump Trip Accident Event

Time (s)	Event
0	Trip of all RIPs initiated

1.22	Reactor scram
1.85	Feed water flow pump trip
1.97	Turbine Trip initiates bypass operation
20	End of Simulation

Since the specific core kinetics of the RBWR-Th designs were not quantified at the time of the safety analysis, a simulation with zero power coefficient is performed. This is expected to be conservative as both designs are expected to have a negative Doppler coefficient and a small negative void coefficient. The peak cladding temperature (PCT) of 752 and 683 K is obtained for the designs using the Hitachi correlations and the MIT-recommended correlations, respectively. These values are representative of the differences in LHGR for each design. The conventional ABWR design PCT is 800 K during such transient,[21] higher than of the two RBWR-Th designs. The results of this transient simulation imply that the lower LHGR more than offsets the lower core thermal capacity compared to ABWR. The core fluid volume of the ThH and ThM are 1.3 and 2.3 times higher than of the RBWR-AC.

The loss of coolant accident (LOCA) simulations of main steam line break were performed by Hitachi and MIT for the RBWR-AC and yielded satisfactory results. Therefore, with lower LHGR and larger core fluid volume relative to RBWR-AC, it is expected that both RBWR-Th designs have acceptable performance during LOCAs. The shorter core resulting in faster SCRAM times combined with smaller void coefficient has been shown to improve performance in ABWR vessel for over cooling, increase in water inventory and increase in pressure accident scenarios.[29] Thus, it is expected that both RBWR-ThM and ThH designs will have satisfactory response to design basis accidents.

The higher core void fraction and much higher exit quality of RBWR-ThM and ThH compared to ABWR raise concerns about the system stability. Table 10 gives a qualitative performance of the two designs relative to the ABWR.

Table 10. Summary of Parameters Governing the Differences between ABWR and RBWR-ThM/ThH Stability Performance (+/- means more/less stable; * means either possibility).

Parameters	ABWR	ThM	ThH	Effect
Fuel Height (m)	3.7	3.45	1.65	+
Pressure Drop (kPa)	130	180	100	*
Core Exit Quality (%)	14.5	39	39	-
Spacer Grid Span (cm)	~50	30	30	-
Fuel Height to Core Outer Diam. Ratio	~0.7	~0.65	~0.3	-
Fuel Time Constant (sec)	6	~4	~5	-
Peak Heat Flux (kW/m^2-s)	1365	157	708	+
Subcooling (°C)	10	5	5	*
Effective Delayed N Fraction x 10-3	6-5	< less	< less	-
Coolant Average Void Fraction (%)	~40	~65	~65	-
Void coefficient (PCM/% void)	-130 to -70	-15 to 0	-25 to -10	+
Inlet Orificing	15-20	30-70	30-70	+

The main difference between RBWR-ThM and ThH in terms of stability performance is the fuel height, which tends to have a large impact on stability. The global mode of perturbation was found to be the most limiting mode at hot full power (HFP) conditions for the ABWR and RBWR reactors.[22] Assuming each design will have a negative void coefficient of reactivity, the void coefficient where each design reaches the decay ratio limit of 0.8 at 100% flow and 95% flow rate has been calculated using the STAB code. These bounding void coefficients are listed in Table 11. It is noted that the value of 0.8 is the current limit for ABWRs,[21] however, this value is often occurs away from rated power and flow rate.

Table 11. The Void Coefficient (pcm/%void) required to achieve Decay Ratio of 0.8 for a Global Mode Perturbation.

Design	RBWR-ThM		RBWR-ThH	
Flow	100%	95%	100%	95%
BOL	-8	-1	-135	-123
MOL	-55	-49	-168	-151
EOL	-78	-72	-150	-138

As listed in Table 11, assuming the equilibrium core operates with the MOL axial power shape, there is sufficient margin for stable operation at 100% power and flow for both designs. The longer RBWR-ThM core design has much smaller margin to stability than the shorter RBWR-ThH design. The ThH design can operate with void coefficients similar to the conventional ABWR as the stabilizing effect of shorter length is countered by the higher void fraction.

It is noted that an increase in power from 3200 MWth to 3500 MWth while keeping the power to mass flow rate ratio is, in principle, possible for RBWR-ThM design. However, this increase requires changes in ABWR pumps and challenges the design stability performance.

7.2. Fuel performance analysis

In assessing the fuel performance of the RBWR-Th, two separate cases have been considered. For each of these cases, which are referred to based on the void fraction correlation used in their design, ThM and ThH, an average and 130% peaked power pin have been assessed. Due to the lack of power history information at the time of this analysis, both cases make use of the conservative assumption that the average pin power remains constant throughout irradiation. The application of a constant average pin power history is conservative due to a higher end of life power than of a typical operating fuel rod. The higher power results in high end of life fuel temperatures and Fission Gas Release (FGR) compared to typical operating fuel rods. While the average pin power is held constant, the applied axial power shape is varied based on data provided from assembly level Monte Carlo neutronic evaluations. The resulting EOL axial burnup profiles are illustrated in Figure 31, with peak local burnups of 76.3 and 80.4 MWd/kgHM, for the RBWR-ThM and RBWR-ThH case. In addition to the application of axial power shaping, a single axial specific fast neutron flux shape (normalized to specific power) was applied. The resulting local axial cladding fast fluences can be seen in Figure 32 to challenge and even exceed experimentally examined cladding samples that mark the bounds of Zircaloy-2 operational experience.[23,24] In short, the RBWR-Th will require its cladding to withstand fluences that are rarely experienced by BWR fuel.

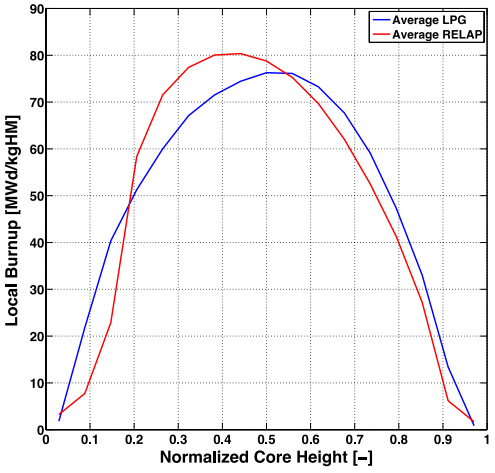

Figure 31. End of life axial burnup profile for the average power pin of the RBWR-ThM and RBWR-ThH case.

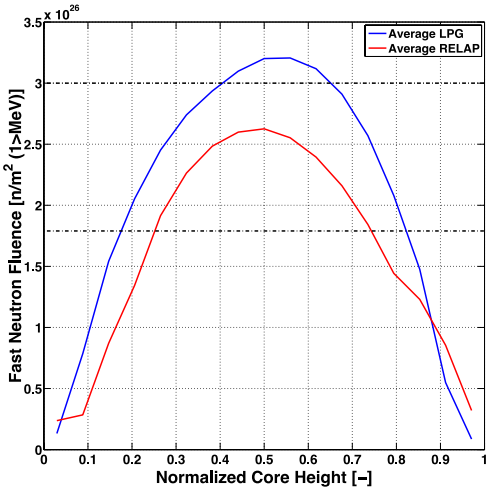

Figure 32. Axial fast neutron fluence profile of the average of the RBWR-ThM and RBWR-ThH cases compared with experiments that mark the boundary of Zircaloy-2 experience.[23,24]

Due to low LHGR of an average RBWR-THM fuel pin, the peak centerline fuel temperature remains low, with the 130% peaked case remaining below 800K. As a result of the low fuel temperatures and the decreased diffusion of fission gases through ThO_2-based fuels, neither of the simulated RBWR-ThM pins experience FGR of more than 6.5%. The low FGR, in turn, ensures that the plenum pressures for the RBWR-ThM fuel remain well below the coolant pressure.

The much higher LHGR of the RBWR-ThH case results in much higher peak centerline fuel temperatures. The maximum temperature for the 130% peaked case is found to be 1840K. While this temperature is over 1000K hotter than of the RBWR-ThM case, the margin to melting (approximately for both cases 3400K) remains very generous. The high temperatures seen in the 130% peaked RBWR-ThH case lead to high calculated FGR values, with an EOL pin average 38.4%. This high FGR results in high plenum pressures which can potentially exceed the coolant pressure of 7.14 MPa and, therefore, the no cladding lift-off criterion. To mitigate this possibility, the cold plenum length of the RBWR-ThH pin was extended to 40cm (assuming identical fuel pin and plenum diameters). The addition of this extra gas volume along with the conservative power history assumption successfully assuaged potential plenum pressure concerns. The maximum fuel temperatures, FGRs, and plenum pressures for each of the RBWR-Th fuel rods are summarized in Table 12. Neither case challenged the 1% cladding hoop strain limit.

Table 12. Maximum fuel temperature, FGR, and plenum pressure for the average and 130% peaked RBWR-THM and RBWR-THH pins.

Case	Maximum Temperature [K]	FGR [%]	Plenum Pressure [MPa]
Average RBWR-ThM	722	0.503	2.81
130% RBWR-ThM	794	6.28	5.25
Average RBWR-ThH	1426	6.24	2.66
130% RBWR-ThH	1840	38.4	6.64

Due to the harder spectrum of the RBWR-Th cores compared to typical BWRs, Zircaloy-2 cladding is expected to experience accelerated oxidation and hydrogen pickup much earlier in life. Inspection of Figure 33 and Figure 34 show this transition to occur prior to 20 MWd/kgHM for both cases. Of particular interest is that the cladding hydrogen content is expected to exceed the practical 600 ppm(wt) at 28 and 32 MWd/kgHM for the RBWR-ThM and RBWR-ThH cores, respectively.

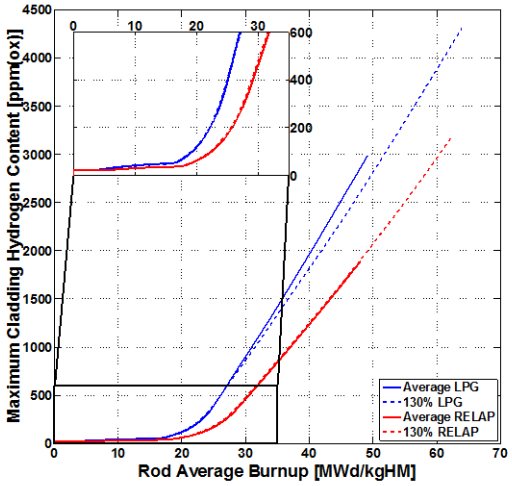

Figure 33. Maximum cladding hydrogen content for the average and 130% peaked RBWR-ThM and RBWR-ThH pins.

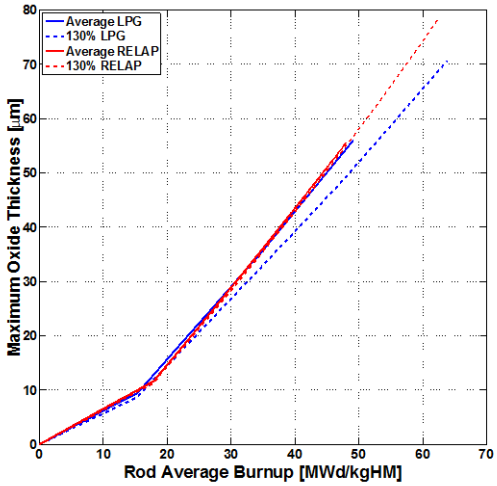

Figure 34. Maximum cladding oxidation thickness for the average and 130% peaked RBWR-ThM and RBWR-ThH pins.

Applying Equation (2) to the cladding hydrogen content for the two RBWR-Th cores provides an understanding of how the accident margins evolve through the fuels' residence time. For both cases, the ECR margin, shown in Figure 35, rapidly degrades following the onset of accelerated corrosion behavior and is completely eliminated prior to EOL.

$$ECR_{Allowed} = \begin{cases} 18 - 0.03H; & H < 400 \\ 18 - 0.01H; & 400 \le H < 600 \\ 0; & 600 \le H \end{cases} \quad (2)$$

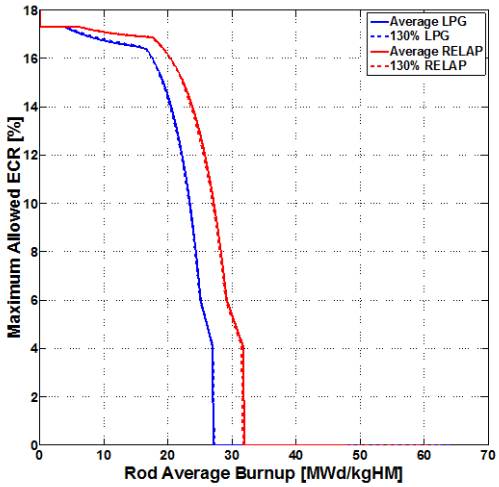

Figure 35. Maximum allowable ECR for Zircaloy-2 during a transient or LOCA for the average and 130% peaked RBWR-ThM and RBWR-ThH pins, based on cladding hydrogen content.

Because Zircaloy-2 is not expected to have any ECR margin by the time the RBWR-Th cores reach their average discharge burnup, it is most likely that an advanced alloy will be required for their fuel cladding. One such alloy, GNF-Ziron, has demonstrated the potential to experience a delay in the onset of hydrogen pickup acceleration, though not in oxidation acceleration.[25] To understand how such a delay will affect the EOL accident margins of the RBWR-Th fuel a sensitivity study was performed wherein the accelerated hydrogen pickup is delayed for a 130% peaked pin. Because the available Ziron corrosion data do not indicate the exact delay it may afford, the fluence at which accelerated hydrogen pickup begins was varied from 1.0 to 5.0 $x10^{26}$ n/m^2 (>1MeV). The resulting allowable ECR margins over the course of irradiation are displayed in Figure 36.

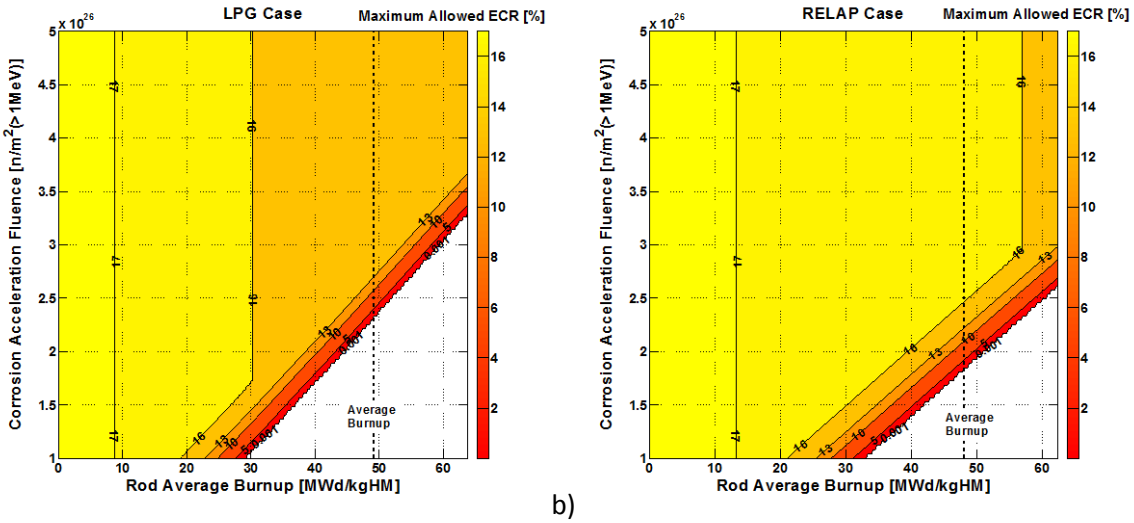

Figure 36. Comparison of allowable ECR values up to 130% of the average EOL burnup, given a delay to the accelerated hydrogen pickup behavior shows that a substantial delay is required to achieve non-zero margins for an average EOL burnup for the (a) RBWR-ThM and (b) RBWR-ThH cases.

The lower average LHGR of the RBWR-Th in comparison to the ABWR, with which all ABWR designs share safety systems, will allow for increased efficacy of emergency cooling. Therefore, it is assumed that the maximum EOL operational ECR of the cladding will provide the necessary margin required of each case. The cladding oxide thickness can be used to calculate the operational ECR, which is then compared against Figure 36 to determine the necessary delay in hydrogen pickup acceleration. This comparison reveals that an advanced cladding material for the RBWR-Th must provide 150, 260, 100, 180% delays in accelerated hydrogen pickup behavior for the average and 130% peaked pins of the RBWR-ThM and RBWR-ThH cases, respectively.

While the RBWR-Th fuel benefits greatly from relatively low LHGRs and the stability of ThO_2-based fuels, resulting in high margins to melting and manageable FGR, the hydrogen uptake behavior of Zircaloy-2 results in eliminated accident margins. The expected acceleration in hydrogen uptake behavior early in life is due to the high fast neutron fluences to the cladding. To mitigate this loss of accident margins, the RBWR-Th is expected to require an advanced cladding which significantly delays accelerated hydrogen pickup behavior.

8. Conclusions

The performance of the RBWR-Th core was found highly sensitive to the pitch-to-diameter ratio and, in particular, to the thermal-hydraulic (TH) modeling assumptions. When using the same TH correlations as assumed for the Hitachi RBWR-AC core design, the RBWR-ThH core features slightly lower power density and specific power; higher discharge burnup while maintaining a significantly lower peak burnup; significantly lower peak linear heat generation rate; more uniform axial power distribution; larger safety margins against critical heat flux and loss of flow scenarios; and lower fast neutron fluence. However, using the more conservative TH assumptions developed in this project, the power of the RBWR-ThM had to be reduced to 81.5% of the nominal and the core volume had to be significantly increased; this led to reduced flow stability than the less conservative cases, although it is still permissible.

The RBWR-ThM has approximately one third of the power density and specific power of the RBWR-ThH, but has a slightly higher discharge burnup and therefore more than three times the cycle length. The void feedback of the two RBWR-Th designs is not quite as negative as would be desired for licensing;

however, the atom fraction of DU in the seed can be decreased slightly to accommodate this with a minimal impact on other parameters.

Both RBWR-Th designs have larger margin in loss of flow transients than the RBWR-AC or the ABWR; however, the RBWR-ThM design (which assumes the most conservative T/H correlations) has a much narrower allowable VCR range compared to the RBWR-AC, RBWR-ThH, or the ABWR. Additionally, Zircaloy-2 will not maintain its integrity over the neutronically designed fuel life of all the RBWRs; advanced cladding materials will have to be developed.

Compared with the ARR, the RBWR-Th designs feature much lower discharge burnup and specific power. Combined with the lower thermal efficiency, this leads to much higher required reprocessing capacity per GWeY.

9. Nomenclature

∞-norm	Absolute value of the maximum difference between iterations
ε	Convergence criterion
ABWR	Advanced BWR
ARR	Advanced Recycling Reactor, a fuel-self-sustaining metal-fuelled sodium-cooled fast reactor
BOEC	Beginning of equilibrium cycle
BOL	Beginning of fuel life (i.e. freshly loaded)
BU	burnup
CHF	Critical heat flux; for boiling water reactors, dryout.
CPR	Critical power ratio
CZP	Cold zero power
DU	Depleted uranium
ECR	Equivalent cladding reacted
EOEC	End of equilibrium cycle
EOL	End of fuel life (i.e. at discharge)
FGR	Fission gas release
FIMA	Fissions per initial metal atom
FIR	Fissile inventory ratio
H-CISE	A critical power correlation for use with the RBWRs which was modified from the CISE-4 correlation for BWRs; it predicts higher CPRs than the MFP-CISE correlation or the M-CISE correlation. The recommended MCPR limit for this correlation is 1.3.
H/HM	Hydrogen to heavy metal ratio.
HFP	Hot full power
HM	Heavy metals (actinides)

LHGR	Linear heat generation rate
LOCA	Loss of coolant accident
LPG	Liao, Parlos, and Griffith void fraction correlation
M-CISE	A critical power correlation for use with the RBWRs which was modified from the CISE-4 correlation for BWRs; it predicts lower CPRs than the MFP-CISE correlation or the H-CISE correlation, but it has a larger factor of experimental uncertainty. The recommended MCPR limit for this correlation is 1.5.
MCPR	Minimum critical power ratio
MOL	Middle of fuel life
N	Number density
pcm	percent milli or “milli-percent”; 10-5
PCT	Peak cladding temperature
RBWR	Resource-renewable BWR
RBWR-AC	DU-fueled fuel-self-sustaining RBWR designed by Hitachi
RBWR-Th	RBWR primarily fueled by Th, with some DU for reactivity feedback control
RBWR-ThM	RBWR-Th designed using the MIT-recommended T/H correlations (LPG for void fraction, Y-CISE for CPR) and with an inlet density inter-assembly bypass region.
RBWR-ThH	RBWR-Th designed using the same T/H correlations as Hitachi used for the RBWR-AC (RELAP for void fraction, H-CISE for CPR) and with an interassembly bypass region in which the coolant was the same density as within the assembly.
RELAP	RELAP5, a USA safety analysis code which uses the Chexal-Lellouche void fraction correlation. This correlation is referred to as the RELAP void correlation within this document.
T/H	Thermal hydraulic
TRF	Transfertile (TRU + transthorium)
TRU	Transuranium
VCR	Void coefficient of reactivity
Y-CISE	A critical power correlation for use with the RBWRs which was modified from the CISE-4 correlation for BWRs; it predicts higher CPRs than the M-CISE correlation but lower CPRs than the H-CISE correlation. There is less experimental uncertainty than the M-CISE correlation, but it has a more narrow range of applicability; additionally, larger inter-assembly power peaking is assumed. The recommended MCPR limit for this correlation is 1.3.

10. Acknowledgements

This research was performed using funding received from the U.S. Department of Energy Office of Nuclear Energy’s Nuclear Energy University Programs. This research is based upon work partially supported by the U.S. Department of Energy National Nuclear Security Administration under Award Number DE-NA0000979.

References

1. R. Takeda, J. Miwa, K. Moriya, “BWRs for Long-Term Energy Supply and for Fissioning Almost All Transuraniums,” *Proceedings of Global 2007*, Boise, Idaho, USA (2007).
2. International Atomic Energy Agency Report, "Status of advanced light water reactor designs." IAEA TECDOC-1391, p 436 (2004).
3. EPRI Report, “Technical Evaluation of the Hitachi Resource-Renewable BWR (RBWR) Design Concept,” EPRI Report number 1025086 (2012).
4. F. Ganda, F. Arias, J. Vujic, E. Greenspan, “Self-Sustaining Thorium Boiling Water Reactors,” Sustainability, Vol. 4, No. 10, 2472—2497 (2012).
5. J. E. Seifried, G. Zhang, C. R. Varela, P. M. Gorman, E. Greenspan, J. L. Vujic, “Self-Sustaining Thorium-Fueled BWR,” Proceedings of INES-4, Tokyo, Japan (2013).
6. G. Zhang, J. E. Seifried, J. L. Vujic, E. Greenspan, “Variable Enrichment Thorium-Fueled Boiling Water Breeder Reactor,” Proceedings of the 2013 American Nuclear Society Annual Meeting, Vol. 108, pp. 846—848, Atlanta, Georgia, USA (2013).
7. P. Gorman, G. Zhang, J. Seifried, C. Varela, J. Vujic, E. Greenspan, “The fuel-self-sustaining RBWR-Th core concept and parametric studies,” Proceedings of ICAPP 2014, Charlotte, North Carolina, USA (2014).
8. P. Gorman, S. Bogetic, J. Hou, J. Seifried, G. Zhang, J. Vujic, E. Greenspan, “Thorium Fuelled Resource-Renewable BWR (RBWR) Design Update,” Proceedings of the 2014 American Nuclear Society Winter Meeting, Vol. 111, pp. 299-303, Anaheim, California, USA (2014).
9. J. E. Seifried, P. M. Gorman, J. L. Vujic, E. Greenspan, “Accelerated Equilibrium Core Composition Search Using a New MCNP-Based Simulator,” Proceedings of SNA&MC 2013, Paris, France (2013).
10. X-5 Monte Carlo Team, “MCNP — A General Monte Carlo N-Particle Transport Code, Version 5, Volume II: User’s Guide” Technical Report LA-CP-03-0245, LANL, Los Alamos, NM, USA (2003).
11. A. Wysocki, Y. Xu, B. Collins, A. Manera, T. Downar, “PATHS: PARCS Advanced Thermal Hydraulic Solver,” University of Michigan (2012).
12. A. Cross, “A User’s Manual for the ORIGEN2 Computer Code,” Technical Report TM-7175, ORNL, Oak Ridge, TN, USA (1980).
13. K. Shirvan, Y. Wu, M. S. Kazimi, “Thermal Hydraulic Recommendation Update for the Resource Renewable BWR (RBWR),” Massachusetts Institute of Technology (2014).
14. T. Downar, Y. Xu, V. Seker, “PARCS v3.0 U.S. NRC Core Neutronics Simulator User Manual”, University of Michigan (2010).
15. B. Herman, “SerpentXS Documentation,” Massachusetts Institute of Technology (2011).
16. J. Leppänen, “Serpent – A Continuous-Energy Monte Carlo Reactor Physics Burnup Calculation Code,” VTT Technical Research Centre of Finland, http://montecarlo.vtt.fi (2013).
17. A. Ward, Y. Xu, T. Downar, “GenPMAXS – v6.1.2ucb, Code for Generating the PARCS Cross Section Interface File PMAXS”, University of Michigan (2013).
18. Hall, A. Xu Y., Ward A., Downar T., Shirvan K., Kazimi M., “Advanced Neutronics Methods for Analysis of the RBWR-AC,” Proceedings of the 2013 American Nuclear Society Annual Meeting, Vol. 108, pp. 771–774, Atlanta, Georgia, USA (2013).
19. P. Gorman, J. Vujic, E. Greenspan, “Tradeoff Studies for the fuel-self-sustaining RBWR-Th core,” Accepted for publication in Nuclear Technology,
20. Hoffman, E.A., Yang, W.S., Hill, R.N., Preliminary Core Design *Studies for the Advanced Burner Reactor over a Wide Range of Conversion Ratios*. 2006, U. S. Department of Energy, Office of Nuclear Energy, Science and Technology
21. GE, “ABWR Design Control Document/Tier 2”, Availablefrom NRC.gov, (2007).

22. K. Shirvan et al., “Stability and Safety analysis of Tight Lattice Breeding LWR,” Proceedings of ICAPP, 14276, 2014.
23. S. VALIZADEH et al., "Effects of Secondary Phase Particle Dissolution on the In-Reactor Performance of BWR Cladding," J. ASTM Intl., Vol. 8, No. 2 (2011).
24. S. MAHMOOD et al, "Post-Irradiation Characterization of Ultra-High-Fluence Zircaloy-2 Plate," Zirconium in the Nuclear Industry: 12th International Symposium, ASTM STP 1354, (2000).
25. “Application of GNF-Ziron to GNF Fuel Designs,” NEDO-33353, Global Nuclear Fuels, Revision 0, (2010).
26. “The SERPENT/PARCS/PATH core simulator,” Attachment 1.
27. “The MocDown/PATHS Assembly Unit Cell Design Tool,” Attachment 2.
28. “Void fraction and critical power correlations for the RBWRs,” Attachment 4.
29. K. Shirvan, M.S Kazimi, “SAFETY ANALYSIS OF BWR-HD: AN OPTIMIZED BOILING WATER REACTOR WITH HIGH POWER DENSITY,” Nuclear Technology, 184, 2013.

Attachment 6

For NEUP Project # 11-3023: Self-sustaining thorium boiling water reactors

TRU-burning Thorium-fuelled Reduced Moderation Boiling Water Reactors (RBWR-TR) Design

The objective of this task is to search for the optimal fuel assembly design for the RBWR-TR core -- a reduced-moderation BWR which is to incinerate TRU from LWR spent fuel using thorium as the fertile fuel. It recycles all actinides unlimited number of times. The RBWR-TR is a variant of the RBWR-TB2 core proposed by Hitachi, which arranges its fuel in a hexagonal tight lattice, has a high outlet void fraction, axially segregates seed and blanket regions, and fits within the ABWR pressure vessel. The RBWR-TR shares these characteristics but replaces depleted uranium with thorium as the fertile fuel, eliminates the internal axial blanket while elongating the seed region, and eliminates absorbers from the axial reflectors.

The sensitivity of important RBWR-TR core performance parameters to change in each one of a dozen design variables was established. The design variables of the sensitivity studies include the length of the seed and blanket zones, fuel rod diameter, lattice pitch, the number of pins per assembly, amount of LWR transuranic waste (TRU) in the seed makeup, coolant mass flow rate, and simulated depletion cycle length.

The results of the tradeoff studies were used to create optimized core designs for full-core analysis. The final design incinerates TRU at a slightly higher rate per GWeY and discharges significantly less plutonium of a smaller fissile fraction than the reference ABR and RBWR-TB2 while meeting all the design constraints. However, due to significantly lower discharge burnup the RBWR cores require significantly larger reprocessing and fuel fabrication capacity per GWeY than the reference ABR.

1. Introduction

The RBWR-TR core design is based upon the RBWR-TB2 designed by Hitachi,[1] a reduced-moderation BWR that employs axial seed and blanket segregation for continuous burning of LWR transuranic waste (TRU). The discharge fuel from the RBWR-TR is recycled, and a mixture of natural thorium and reprocessed LWR TRU is added to maintain the fuel inventory. The RBWR-TR differs from the RBWR-TB2 in that it uses thorium rather than depleted uranium as the fertile component of the makeup fuel, and it eliminates the internal blanket while elongating the seed region and the outer blankets.

Reduced-moderation BWR core concepts, referred to by Hitachi as the Resource-renewable BWR (RBWR), were initially pursued by Hitachi in an attempt to design hard spectrum BWRs to provide missions traditionally assigned to liquid metal cooled reactors – fuel sustainability or TRU transmutation with unlimited recycling.[2,3] As the RBWR-TB2 and RBWR-TR use water coolant, although of low density, their spectrum is softer than that of the reference CR=0.5 TRU-burning Advanced Burner Reactor (ABR), which is a metal-fuelled sodium fast reactor,[14] although harder than of a typical BWR, as shown in Figure 1. The spectrum of neutrons causing fission is shown in Figure 1 and tabulated in Table 1; since 44.0% of the fissions are from neutrons between 0.625 eV and 0.1 MeV and 41.6% of the fissions are induced by neutrons below 0.625 eV, the RBWR-TR can be classified as an epithermal reactor. For comparison, a BWR has 60.2% of its fissions caused by neutrons below 0.625 eV, and the reference ABR has 77.9% of its fissions caused by neutrons above 1.0 MeV.

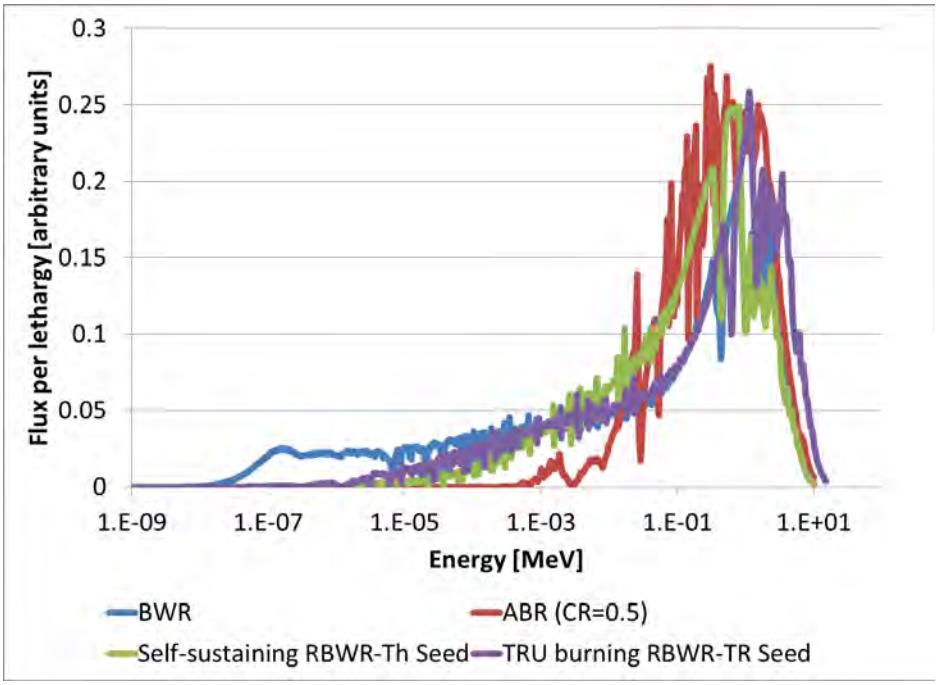

Figure 1. Neutron energy spectrum for the RBWR-TR and RBWR-Th (Attachment 5), compared against that of a BWR and the reference ABR. The units are arbitrary.

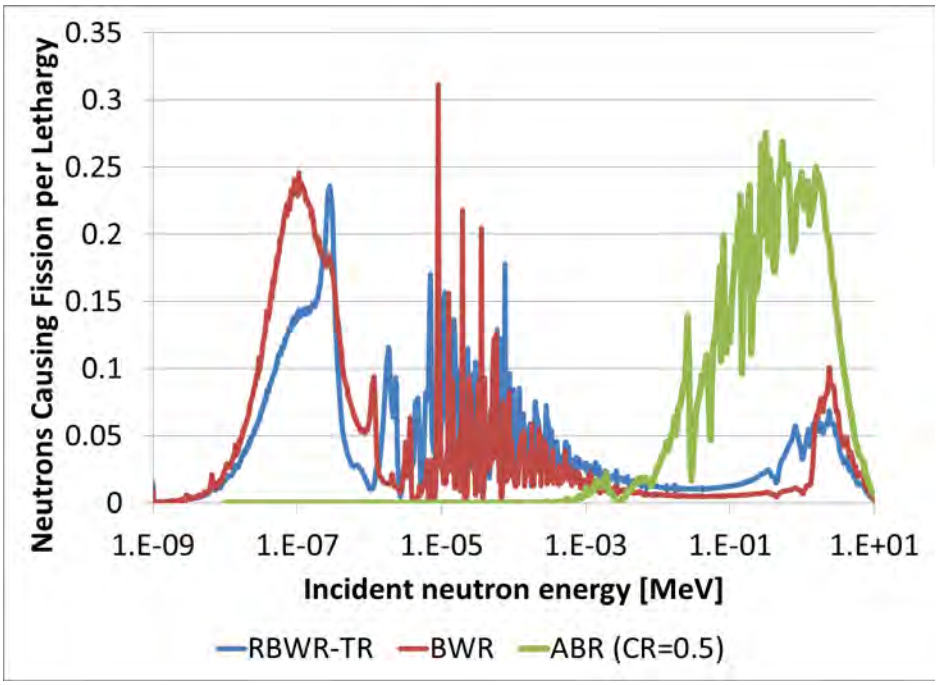

Figure 2. Spectrum of neutrons that cause fission in the RBWR-TR compared against the reference ABR. The units are arbitrary.

Table 1. Fraction of fissions caused by each incident neutron energy range.

Reactor	<0.625 eV	0.625 eV - 0.1 MeV	>0.1 MeV
BWR	60.2%	28.4%	11.4%
ABR	0.0%	22.1%	77.9%
RBWR-TR	41.6%	44.0%	14.4%

There were several concerns regarding the RBWR-TB2 core that provided incentive to examine a thorium-based counterpart: uncertainty in the void reactivity feedback, possibly too small margin against critical heat flux, weak neutronic coupling between the two axial seed segments, and insufficient margin for fuel survivability.[4] The very strong axial heterogeneity of the RBWR-TB2 core was dictated by the need to maximize the negative leakage component of fuel voiding reactivity effect so as to overcome its large positive spectrum hardening reactivity component. In addition, since depleted uranium was used as the blanket material and as the makeup fuel, the transmutation rate was reduced by breeding extra ^{239}Pu from the fertile ^{238}U.

As shown in Figure 3, ^{233}U has a much flatter fuel reproduction factor with energy than ^{239}Pu. Also, the ^{232}Th fast fission cross section has a higher threshold and lower value than that of ^{238}U. Therefore, the spectral component of void reactivity in a Th-^{233}U fueled RBWR core is negative and there is no need to design the core to have enhanced leakage probability from the seed. This enables use of a single relatively long seed region thereby avoiding many of the concerns about the U-Pu core design.

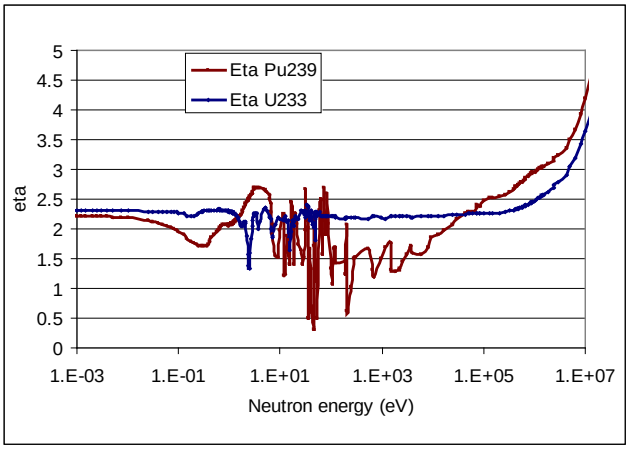

Figure 3. Fuel reproduction factor vs. energy for ^{233}U and ^{239}Pu

This paper summarizes the TRU-burning RBWR-TR design and analysis. Section 2 describes the unique physics of the RBWR-TR; Section 3 establishes the study methodology and design approach; Section 4 summarizes the results of the tradeoff studies; Section 5 describes the results of the assembly physics study; Section 6 details the design parameters and the performance characteristics of the optimal core designs; Section 7 comments about the feasibility of the designs in terms of a brief safety and stability analysis and fuel performance analysis; and Section 8 summarizes the conclusions of this study.

2. RBWR-TR Physics

The RBWR-TR requires 3-D modeling techniques in order to adequately predict its performance. Although the single seed region makes it more axially uniform compared to the RBWR-TB2, the water density varies significantly from the bottom of the seed to the top of the seed, as seen in Figure 4. This, in turn, leads to strong axial variation in the one-group cross sections (Figure 5 and Figure 6). The fission cross sections at the bottom of the seed are typically 2 or 3 times higher than those at the top of the seed; this is not adequately captured using 2-D cross sections.

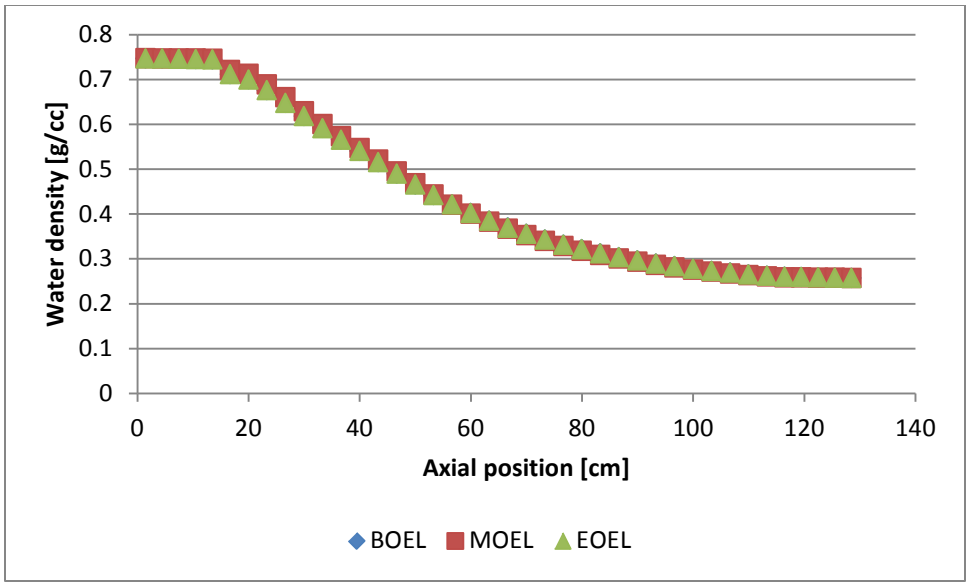

Figure 4. Water density vs. height for the RBWR-TR

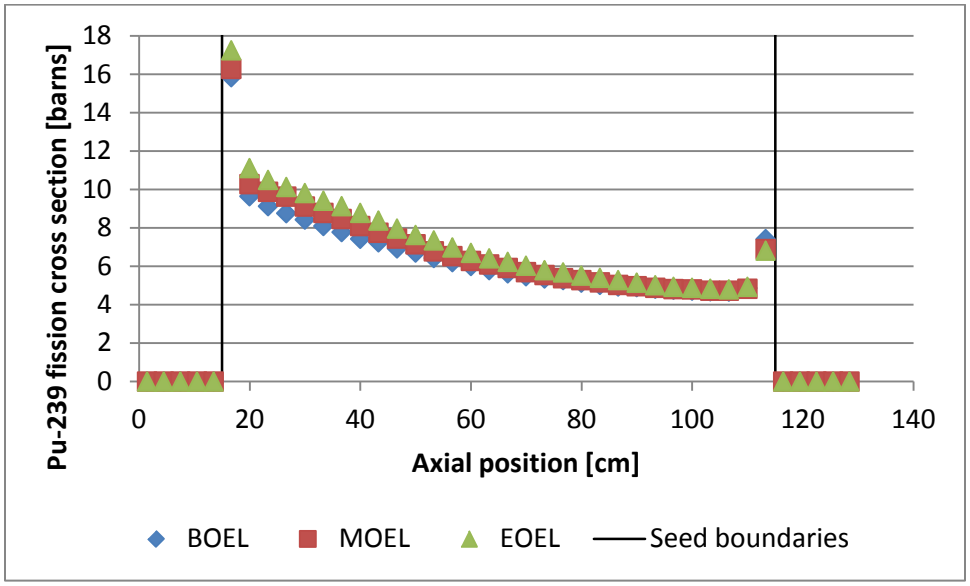

Figure 5. ^{239}Pu fission cross section vs. height for the RBWR-TR

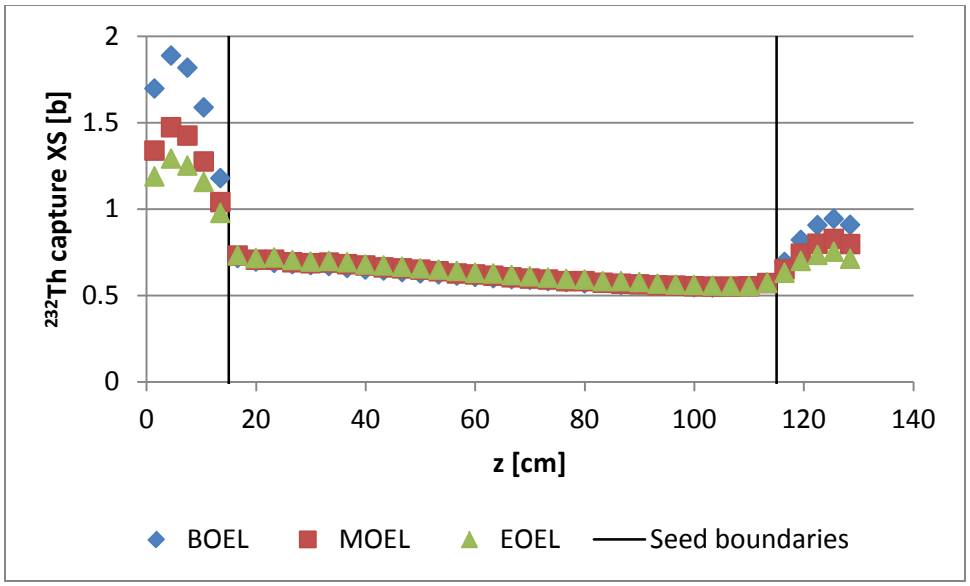

Figure 6. ^{232}Th radiative capture cross section vs. height for the RBWR-TR

In the RBWR-TB2 design, the middle of the upper reflector also contained boron carbide pins, which are unnecessary for the RBWR-Th. Short axial blankets are added in order to reduce the axial leakage. The axial geometry is shown in Figure 7.

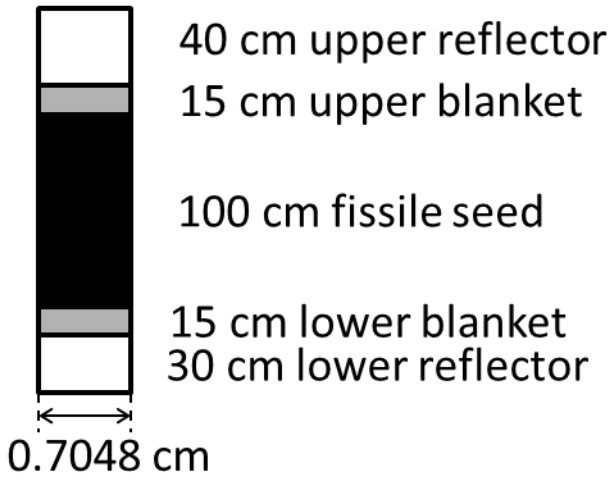

Figure 7. Axial cutaway of an RBWR-TR pin. The length of each fuel region is a design variable

As shown in Figure 8, the average spectrum for the RBWR-TB2 is significantly softer than that of the RBWR-TR, despite that the RBWR-TR has significantly lower flow rate. This is due to the large internal blanket that significantly softens the flux in the RBWR-TB2. As shown in Figure 9, the spectrum in the seed of the TR is slightly softer.

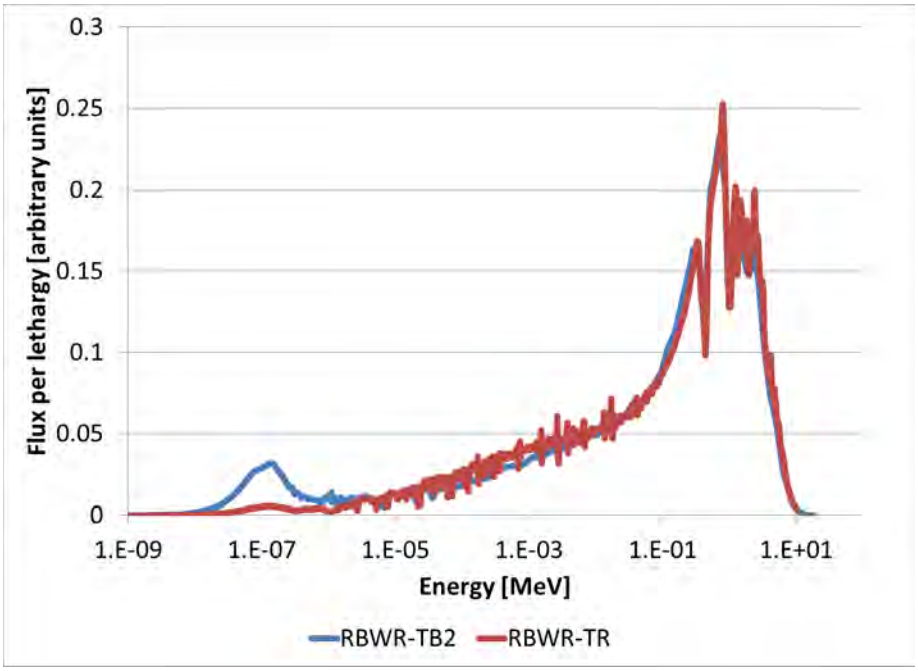

Figure 8. Neutron flux spectrum for the TRU-burning RBWRs, averaged over the entire fuel length. The units are arbitrary.

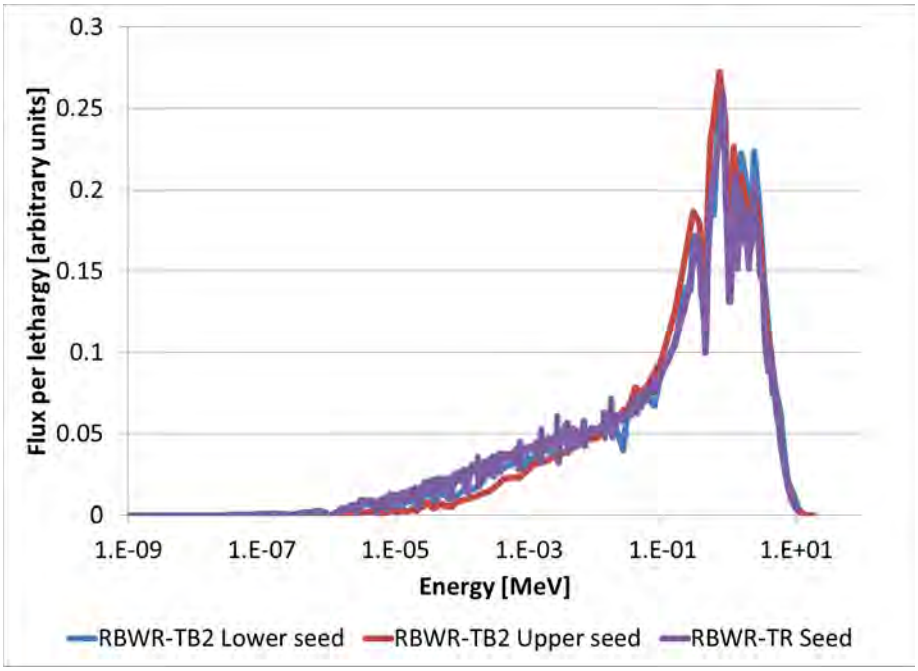

Figure 9. Neutron flux spectrum for the TRU-burning RBWRs, averaged only over the seed sections. The units are arbitrary.

3. Methodology

3.1. Equilibrium search methodology

The MocDown code, which couples neutronics with thermal hydraulics and depletion calculations, was used to simulate an axially finite, radially infinite assembly unit cell for each of the core variations studied and search for its equilibrium composition.[5] It uses MCNP5.1.60 for neutron transport, PATHS for thermal hydraulic coupling, and ORIGEN2.2 for transmutation.[6,7,8] A Monte Carlo technique is used to analyze a 3-D fuel assembly unit cell instead of deterministic 2-D lattice codes in order to accurately capture the axial heterogeneity of the RBWR cores. A three-assembly unit cell is used rather than a single assembly unit cell in order to preserve the periodic boundaries based around the Y-shaped control blade; an example three-assembly unit cell is shown in Figure 10. For this analysis, it was assumed that the water between the assemblies was not boiling.

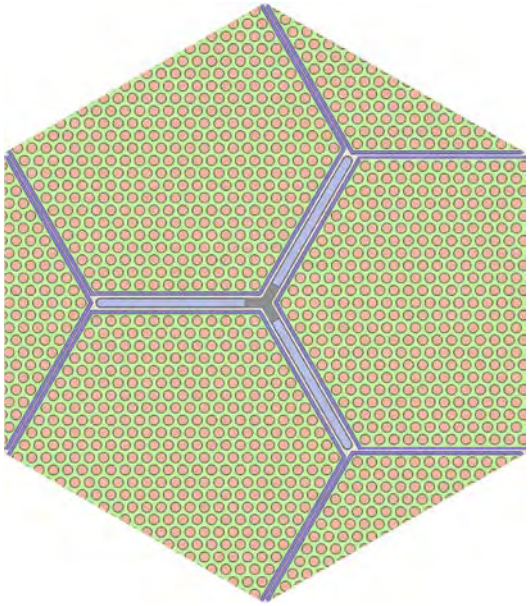

Figure 10. A horizontal cut through a 3-assembly unit cell consisting of 397 fuel pins with a graphite follower of fully withdrawn Y-shaped control blades.

MocDown's accelerated equilibrium search strategy is utilized in this study, which is detailed in Attachment 2.[5,16] The isotopic ∞-norm convergence criterion was 3e-6, while the neutronics convergence criterion was 100 pcm.

The PATHS steady-state thermal hydraulics module of the PARCS code was used to provide neutronically consistent water densities.[7,16] Since designs were considered in which the coolant cross section area in the fission gas plenum of the RBWR designs is larger than in the active core region, the PATHS calculations were performed in two steps. The enthalpy and pressure was held constant at the interface. Form losses were used to account for the orifice plate at the inlet to the core. It was also assumed that spacer grids would be located every 50 cm. The water densities from PATHS are used in the next iteration of the MCNP model; the coupling would continue until the ∞-norm of the water densities was within 2% while using a relaxation coefficient of 0.5. The RELAP void fraction correlation and the M-CISE critical power correlation with an MCPR limit of 1.5 were selected for use in this model.[9,17]

The core was assumed to be made of four fuel batches. The linear reactivity model was used to evaluate the core-average reactivity. A linear fit was created for the inverse of the radially infinite multiplication factor variation with burnup, discarding the first two points (corresponding to 0.6 MWd/kgHM) over which non-linearity is introduced by the buildup of xenon and samarium. Unlike in the self-sustaining designs, it was observed that the k progression was significantly affected by the depletion time, so the achievable discharge burnup was calculated by lengthening or shortening the cycle length iteratively until the full core end of cycle (EOC) multiplication factor was barely critical. The following relation was used to calculate the batch-averaged core multiplication factor:

$$k_{\text{full core}} = \frac{4}{\sum_{i}^{4}\left(k^{-1}\right)_i} - L_{core}$$

where $(k^{-1})_i$ is the linearly fitted inverse multiplication factor for the *i*-th batch, and L_{core} is the full core radial leakage probability. The full core radial leakage probability was estimated to be 1.8% for the

tradeoff studies based off preliminary full core analyses; this value was later corrected to 1.3% for the final design.

3.2. Design variables

The following design variables were considered for the tradeoff studies:

1. fuel pin pitch-to-diameter ratio (P/D),
2. number of pins per assembly,
3. seed region length,
4. axial blanket region lengths,
5. atom fraction of LWR TRU in the seed makeup,
6. coolant mass flow rate, and
7. depletion time.

These design variables were selected because of their effect on the heavy metal loading, the axial leakage probability, the H/HM ratio, and flow conditions. The effects of changing the void fraction correlation were not considered, as the spacing between pins was sufficiently large that the RELAP correlation is considered reliable.[9] As shown in Section 3, there is a considerable benefit to performance when using a larger flow rate, so only the MIT-modified CISE4 (M-CISE) critical power correlation was used, which is considered more limiting than the Hitachi-modified CISE4 correlation (H-CISE).[9]

3.3. Design constraints and assumptions

The tradeoff studies were to abide by the following mission constraints:

1. Recycle all actinides
2. Fit within an ABWR pressure vessel
3. Provide the full ABWR thermal power
4. Maintain criticality
5. Possess negative coefficients of reactivity for fuel temperature, coolant void, and power
6. Operate in cycles as close to 12 months as possible
7. Have sufficient shutdown margin to shut down the core at any point in the cycle
8. Remain compatible with ABWR pumps (pressure drop through core ≤ 0.3 MPa, core flow rate ≤ 120% ABWR flow rate)
9. Avoid coolant dryout: MCPR ≥ 1.5
10. Suppress density wave oscillations: DR ≤ 0.7

Here, MCPR is the minimum critical power ratio and DR is the decay ratio of the core response to two-phase density wave oscillation (DWO) perturbations. While it was desirable to maximize the discharge burnup of the fuel in order to improve the economics, the primary objective was to maximize the TRU fission efficiency and TRU consumption. The TRU fission efficiency is defined as the fraction of fissions that are caused within TRU isotopes; that is, TRU consumption per unit core power. The TRU fission efficiency is defined as in (2):

$$\text{TRU fission efficiency} = \frac{\text{net mass of TRU consumed}}{\text{mass of fissioned actinides}} \tag{2}$$

3.4. Full core simulation methodology

The PARCS nodal diffusion code was used to generate a full core model.[10] The SerpentXS code was used to generate cross sections based off a three-assembly unit cell that was generated in Serpent2 from the

results of the assembly level tradeoff analysis.[11,12] It should be noted that Serpent2 is still in beta version for now, but this version was still used due to the drastically improved memory utilization and running times.

The SerpentXS code was primarily used as a buffer code to autonomously run multiple branch cases in Serpent at different burnup points. The GenPMAXS code was modified to account for axial discontinuity factors (ZDFs) in addition to the typical assembly discontinuity factors (ADFs), and generated homogenized macroscopic cross sections from the Serpent output.[13] Ten different branches were used, with four different depletion histories (denoted with an asterisk):

1. Reference branch*
2. 85% flow branch
3. 70% flow branch*
4. 115% flow branch
5. 130% flow branch*
6. Uniform 1200 K fuel temperature branch
7. Uniform 600 K fuel temperature branch
8. Control rod inserted*
9. Control rod inserted + 70% flow
10. Control rod inserted + 130% flow
11. Shut down conditions (room temperature, liquid density water, control rod inserted, all ^{233}Pa and ^{135}Xe forced to decay to ^{233}U and ^{135}Cs)

A full-core model was created in PARCS, and an equilibrium state was reached by depleting the core and shuffling the fuel until the maximum local burnup difference between cycles was less than 0.1 GWd/t. At each depletion step, thermal hydraulic coupling was performed by PATHS.[13] It was observed that tightening the convergence criteria affected the results, particularly for the power normalization, so an under-relaxation coefficient of 0.1 was used, and the convergence criteria for the outer iterations was tightened from the default of 10^{-6} to 10^{-7}.[13]

Since PARCS does not track isotopes, no explicit recycling could be modeled at the full-core level. The fresh assembly composition was taken from the equilibrium assembly analysis.

3.5. Reactivity coefficients

The void coefficient of reactivity (VCR) was calculated using equation (1) by running two single coupled neutronics-T/H steps at BOEC and EOEC using the full core model at 100% and 85% of the flow rate:

$$\mathrm{VCR} = \frac{\frac{1}{k_{100\%\ \mathrm{flow}}} - \frac{1}{k_{85\%\ \mathrm{flow}}}}{\alpha_{100\%\ \mathrm{flow}} - \alpha_{85\%\ \mathrm{flow}}} * 1000 \qquad (1)$$

where α is the void fraction for each flow rate. The 1000 multiplier converts the units to pcm / % void.

3.6. Shutdown Margin

The shutdown margin was quantified at BOEC by fully inserting all control rods except the center one into the equilibrium core. Thermal hydraulic feedback was removed; the water densities were set to room temperature, and the fuel temperatures were uniformly set to 300 K. The shutdown margin was quantified as the negative reactivity of the subcritical core (i.e. $\frac{1}{k_{shutdown}} - 1$). Since the shutdown

branch removed the ^{135}Xe and replaced the ^{233}Pa inventory with ^{233}U (Section 3.4), this would provide a conservative value which would account for decay.

3.7. Fuel recycling scheme

After every cycle in the equilibrium analysis calculation, the fuel was allowed to cool for three years. All actinides above thorium in the cooled fuel were then collected, and redistributed evenly among the seed cells for the fresh fuel. Since the amount of actinides at the end of cycle is less than the amount at beginning of cycle, makeup fuel is added until the number of moles matches the number of moles used for the fresh fuel during the previous cycle. The makeup fuel is a mixture of thorium and reprocessed LWR SNF; the balance between the two components is left as a design variable. The composition of the LWR SNF was taken from Reference 4, and is summarized in Table 2. The fuel recycling scheme is shown in Figure 11.

Table 2. TRU feed vector from reprocessed LWR SNF.[4]

Isotope	$^{w}/_{o}$
Np-237	7.24%
Pu-238	2.71%
Pu-239	45.70%
Pu-240	23.53%
Pu-241	10.41%
Pu-242	5.43%
Am-241	3.17%
Am-242	1.36%
Cm-244	0.45%

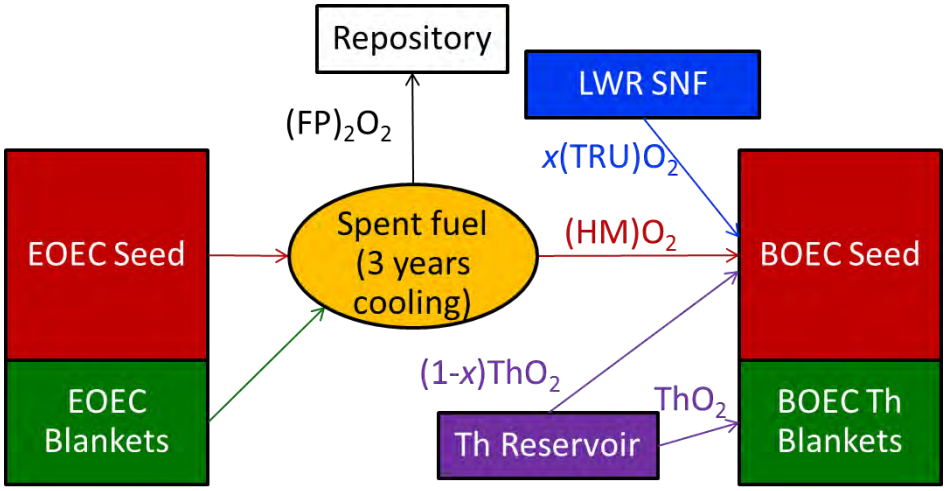

Figure 11. Schematics of RBWR-TR fuel recycling

4. Results of Tradeoff Study

The results are summarized in Table 3. Most of the same trends from the self-sustaining study[18] are observed; however, the primary goal is not to maximize the discharge burnup, but to maximize the TRU fission efficiency. As the spectrum shifts more into the intermediate range, less ^{233}U breeds into the system, while the fission cross section of the TRU isotopes increases. Therefore, unlike in the self-sustaining design,[18] there is significant benefit to using a more thermal spectrum. Also unlike in the self-

sustaining designs, lengthening the depletion time reduces the void coefficient of reactivity (VCR), since the inventory of Pu isotopes decreases with burnup, rather than remaining constant. Lengthening the seed increases the TRU fission efficiency because it increases the total TRU inventory; lengthening the blankets increases the ^{233}U production, which penalizes the TRU fission efficiency. Changing the number of pins per assembly without changing the H/HM ratio has a negligible impact on the TRU fission efficiency.

Table 3. Results of the tradeoff study. The + or – in the parentheses in the header row indicates which value is desired to meet the constraints. Within the table, a + indicates that an increase in the variable on the left column results in an increase of the metric in the top row.

Variables	MCPR (+)	Discharge BU (+)	VCR (-)	Shutdown Margin (+)	Pressure Drop (-)	TRU Fission Efficiency (+)
Seed length	+	-	+	-	+	+
Blanket lengths		+		-	+	-
Coolant flow rate	+	-	-		+	+
Makeup TRU $^{a}/_{o}$		+	+			+
P/D	+	-	-		-	+
Number of pins per assembly	+			+	+	
Depletion time		+	-	+		-

The constraints that were the most limiting for the RBWR-TR were the negative VCR constraint and the constraint that the reactor must operate in sufficiently long cycles. As shown in Table 2, with the exception of the seed length, the variables that improved the VCR also worsened the burnup; however, although shorter seeds improved the burnup, it shortened the cycle length.

5. Assembly enrichment study

A detailed assembly-level analysis was performed to determine the pin power peaking within an assembly. The interassembly bypass region was assumed to be liquid density water; if the bypass region is assumed to be boiling, then the maximum peak power would be slightly lower. The results for a uniform enrichment at BOEL are shown in Figure 10. Although it was desired to keep the maximum pin power within 120% of the average, it was deemed acceptable for several reasons. First, the power profile will flatten as the assembly burns; second, the thermal margins are sufficient to prevent violating any constraints even with this slight penalty. The most limiting constraint is the fuel performance due to peak fast fluence (Section 7.2), and with a uniform radial enrichment, it becomes possible to rotate the fuel assembly between reloads, thereby enabling a flatter fast fluence profile at discharge. Such effects were not accounted for in any analysis, however.

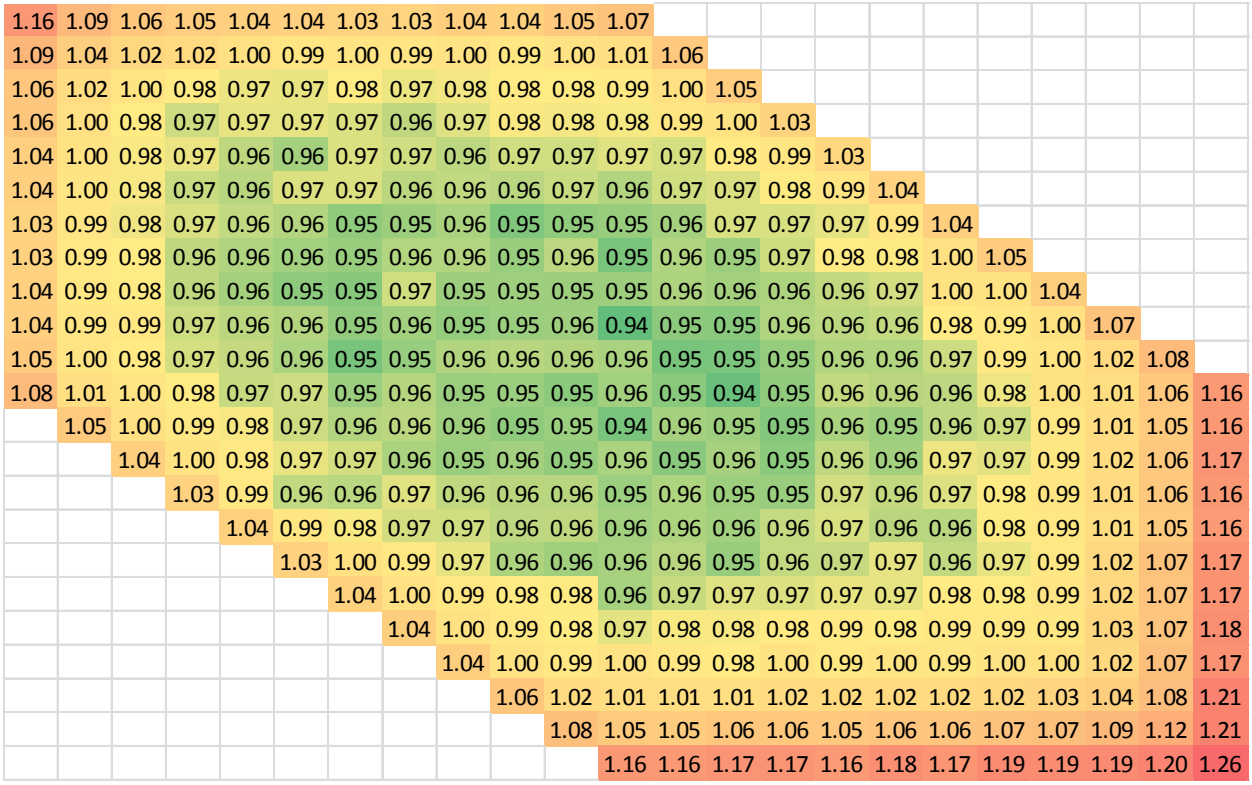

Figure 12. Pin power peaking within an assembly at BOEL using a uniform radial enrichment.

6. Optimal core design

The tradeoff study indicated that for TRU transmutation there is a clear benefit to using a softer spectrum than for fuel sustainability. The P/D was confined to ≤1.34 due to the range of validity of the M-CISE critical power correlation,[10] and the mass flow rate was capped at 120% of the ABWR nominal flow rate that is the upper limit of the existing ABWR pumps. The core height was made slightly longer than the minimum required by the MCPR in order to increase the cycle length. Small axial blankets were added to the top and bottom of the seed to boost the reactivity of the core. The TRU feed fraction was adjusted so as to provide negative void feedback. Unlike in the self-sustaining designs,[9] the fraction of the feed which was TRU significantly impacted the cycle length and the TRU fission efficiency; Figure 7 shows that the VCR varies proportionally to the TRU feed fraction but is nearly constant in the cycle after a significant dip for fresh fuel. The cycle length and TRU fission efficiency dependence on the feed fraction are shown in Figure 8 and Figure 9.

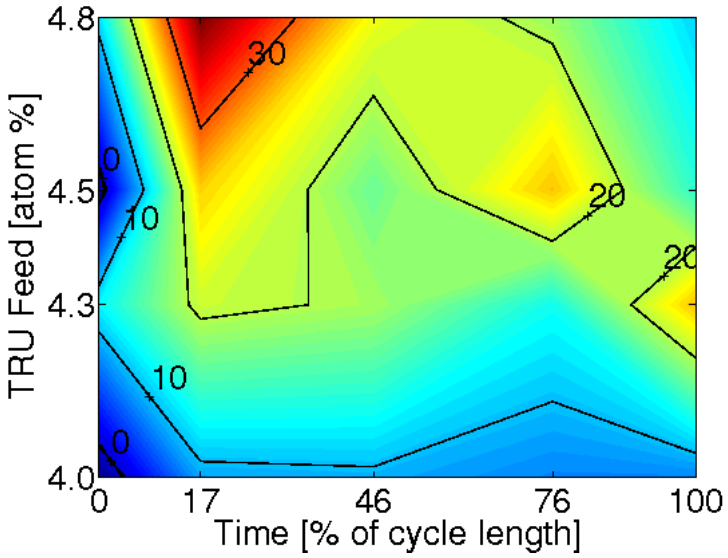

Figure 13. VCR in pcm/% void for the optimized design on TRU feed fraction and time. Each of the four cases are critical, but have different cycle lengths and burnups; in order to have a fair comparison, the x-axis is normalized by the cycle length. The uncertainties in each data point are between 7 and 9 pcm / % void.

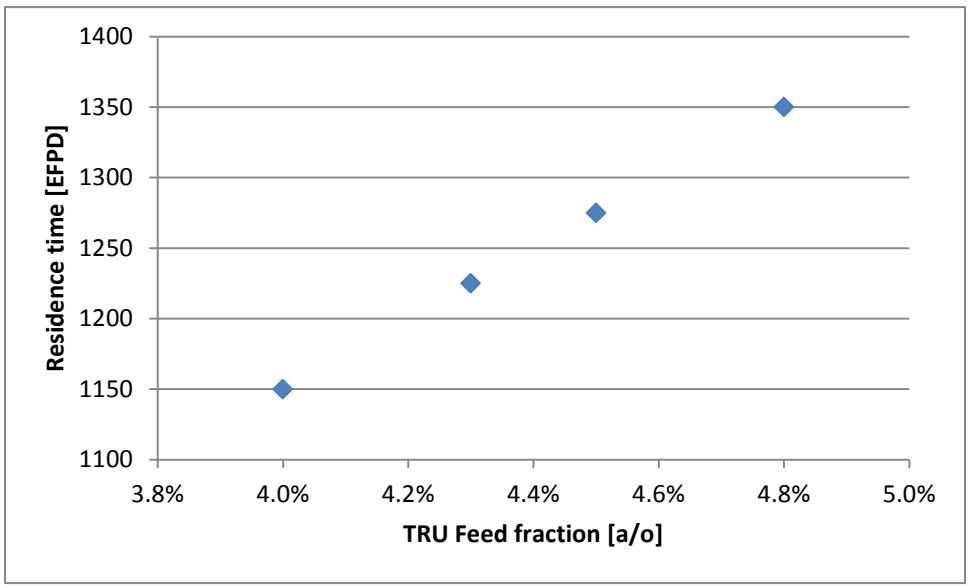

Figure 14. Achievable residence time vs. TRU feed fraction for the optimized design.

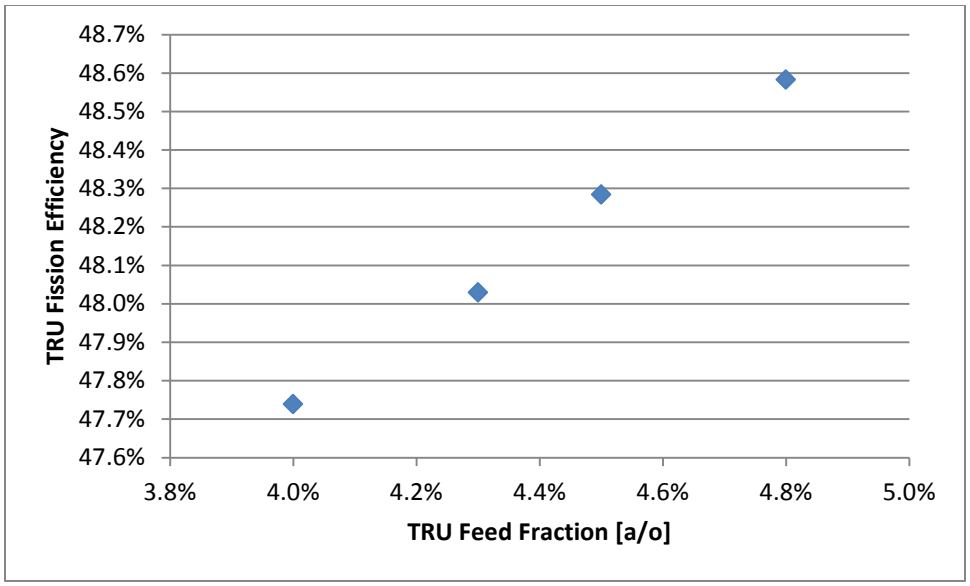

Figure 15. TRU fission efficiency vs. TRU feed fraction for a critical cycle for the optimized design.

Guided by the tradeoff studies in Section 3 and the above "two-at-a-time" studies, the optimized core was designed. Table 3 defines the selected design and compares it to the Hitachi RBWR-TB2[1] and the reference ABR,[14] while Table 4 compares the performance metrics. Table 5 summarizes the average discharge isotopics of the RBWR-TR. Figure 16 shows the k_{eff} evolution with time in cycle. The control rod management strategy is described in Section 6.1 of Attachment 5. Figure 17 shows the relative axial power profile of the RBWR-TR based off of assembly level analyses, while Figure 18 shows the relative axial power profile of the full RBWR-TB2 core. It is clear that the elongation of the seed and elimination of the internal blanket make the linear heat rates of the RBWR-TR much more even and of a smaller peak value than in the RBWR-TB2. Moreover, the RBWR-TR LHGR change over the cycle is much smaller and more stable than of the RBWR-TB2.

The ABR outperforms both RBWR designs in terms of specific power and burnup, but the RBWR-TR incinerates slightly more TRU per GWe-yr.

The RBWR-TR features a much lower fissile Pu/Pu ratio than either of the depleted uranium fed designs. The RBWR-TR discharge fuel contains much less transfertile material (TRF) per mass than the ABR, and much less fissile material per mass as well. However, since no DU is added to the RBWR-TR feed, the uranium discharged from the RBWR-TR is considered highly enriched.

Unfortunately, the presented RBWR-TR design has a slightly positive VCR. As shown in Figure 13 through Figure 15, this could be eliminated by using less TRU in the feed, which will slightly reduce the TRU fission efficiency and the cycle length. From the trends shown in these figures, it is expected that the RBWR-TR with a negative VCR would still incinerate at least as much TRU per GWe-yr as the RBWR-TB2 while maintaining a reasonable burnup and cycle length.

Table 4. Design information for the RBWR-TR compared with the RBWR-TB2 and the reference ABR.

Parameter	Units	ABR (CR=0.5)	RBWR-TB2	RBWR-TR
Coolant	-	sodium	light water	light water
Blanket configuration	-	n/a	parfait	parfait
Fuel form	-	metallic	oxide	oxide
Core thermal power	MWth	1000	3926	3926
Thermal efficiency	MWe/MWth	40%	34.5%	34.5%
Core electric power	MWe	1000	1356	1356
# of assemblies	#	144	720	720
Core HM mass (BOEC)	t	9.5	73	88
Core TRF mass (BOEC)	t	3.1	23.9	20.5
TRF/HM core avg at BOEC	w/o	32.6%	32.6%	23.3%
# of batches	#	6	4	4
Assembly area	cm^2	193	338	338
Core volume	m^3	-	25	32
Core flow rate	t/hr	2.0E+04	2.4E+04	6.3E+04
Outlet quality	%	n/a	36%	13.2%
Specific power	MWe/t	42	18	15
Power density	Wth/cm^3	303	158	124
Upper blanket length	cm	-	2	15
Upper seed length	cm	101.6	22	100
Internal blanket length	cm	-	56	-
Lower seed length	cm	-	22.1	-
Lower blanket length	cm	-	7	15
Total fuel length (seed + blanket)	cm	101.6	110	130
Seed length	cm	101.6	44.5	100
Fuel pin OD	cm	0.623	0.724	0.705
Fuel pin pitch	cm	0.806	0.941	0.944
Fuel pin P/D	-	1.293	1.30	1.34
Hydraulic diameter	cm		0.60	0.66
Heated diameter	cm		0.65	0.70
Pins per assembly	-	324	397	397

Table 5. RBWR-TR performance metrics compared with the RBWR-TB2 and the reference ABR.

Metric	Units	ABR (CR=0.5)	RBWR-TB2	RBWR-TR
Pressure Drop	MPa		0.06	0.15
Maximum LHGR	Wth/cm	327	470	189
Average discharge burnup	GWd/t	132	65	55
TRU fission efficiency	%	44.3	45	48
Fuel residence time	EFPD	1326	1215	1250
Cycle length	EFPD	221	304	313
VCR (BOEC/EOEC)	pcm/% void	-	-42/-35	+2/+4[1]
Shutdown margin	% Δk			3.5

Table 6. Average discharge isotopics of the RBWR-TB2 and the RBWR-TR.

Mass fraction [%]	ABR (CR=0.5)	RBWR-TB2	RBWR-TR Seed only	RBWR-TR Seed+Blanket
TRF / HM	31.5%		26.6%	20.5%
fissile / HM	14.2%		12.1%	9.4%
Pa / TRF	0.0%	0.0%	0.2%	0.2%
nonfertile U / TRF	0.1%	0.0%	37.0%	37.8%
Np / TRF	1.5%	1.4%	2.4%	2.4%
Pu / TRF	87.8%	87.8%	47.7%	47.1%
Am / TRF	7.6%	8.0%	7.0%	6.9%
Cm / TRF	3.1%	2.8%	5.7%	5.6%
Cf / TRF	0.0%	0.0%	0.0%	0.0%
^{232}U / U			0.4%	0.4%
^{233}U / U			50.9%	52.4%
^{234}U / U			28.9%	28.1%
^{235}U / U			10.7%	10.3%
^{236}U / U			9.1%	8.7%
fissile U / total U	0.06%		61.5%	62.7%
^{238}Pu / Pu	4.1%	7.6%	19.1%	19.1%
^{239}Pu / Pu	41.3%	29.0%	17.6%	17.6%
^{240}Pu / Pu	38.0%	45.7%	33.6%	33.6%
^{241}Pu / Pu	5.1%	6.2%	10.8%	10.8%
^{242}Pu / Pu	11.5%	11.5%	18.9%	18.9%
fissile Pu / total Pu	46.4%	35.2%	28.4%	28.4%

[1] A positive VCR is not acceptable. A design modification is presently being worked out that will make the RBWR-TR core VCR negative. The required design changes are not expected to significantly vary the conclusions related to the overall performance of this core.

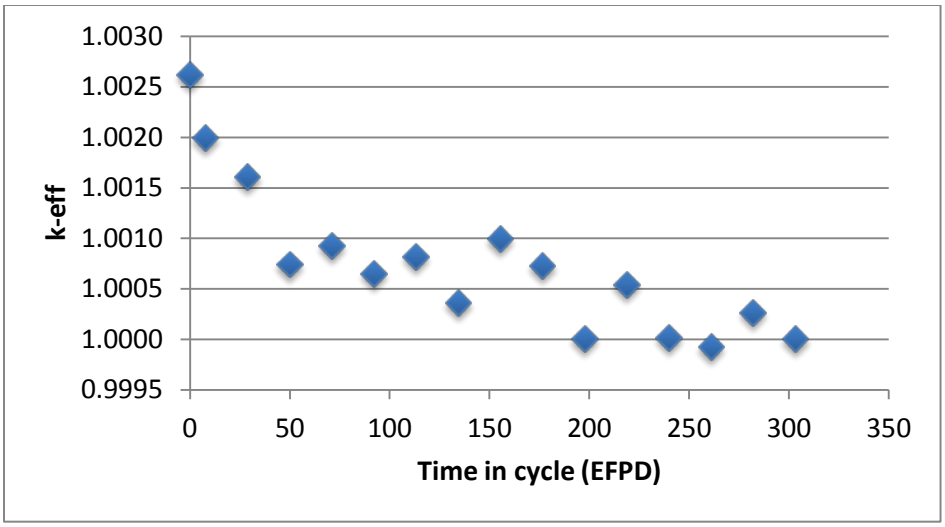

Figure 16. k_{eff} vs. time in cycle.

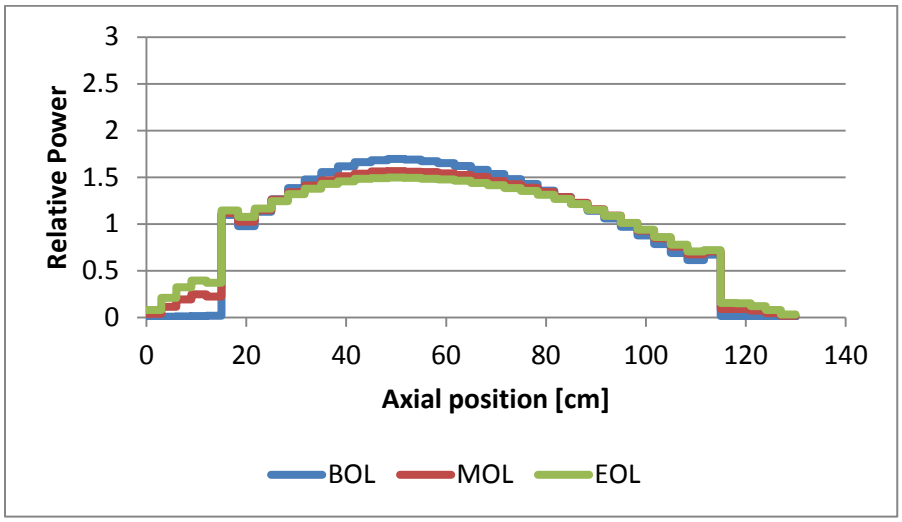

Figure 17. Relative power profile for the RBWR-TR based on the assembly analysis.

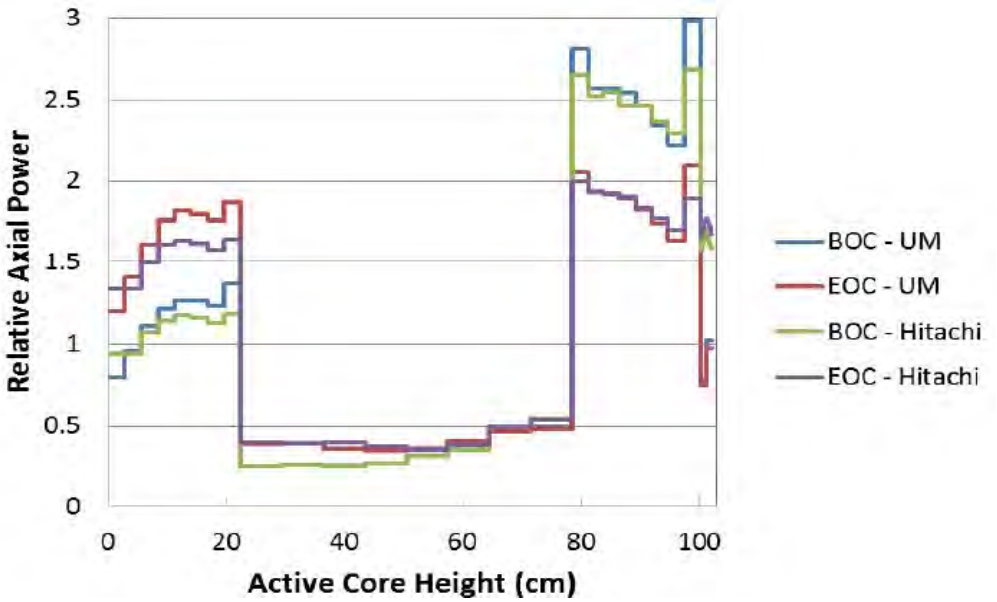

Figure 18. Relative power profile of the full RBWR-TB2 core.

7. Designs feasibility

7.1. Safety and stability analysis

The HITACHI RBWR-AC core radial power and burnup distribution and orificing scheme was also used for the safety analysis of RBWR-TR. The middle of life (MOL) axial power shape from RBWR-TR single assembly calculations were used for the core average axial power shape.

The RBWR-TR burner design does not differ significantly from ABWR in terms of operating conditions. The geometry still features tighter rod spacing with shorter core. The void coefficient of reactivity is also very small. Section 7.1 of Attachment 5 has already discussed the benefits of shorter core height and smaller void coefficient for safety response except for loss of flow transients. The all pump trip transient was simulated to assess the burner design performance. The peak clad temperature of 681 K was calculated, which is lower than a conventional ABWR, as well as the RBWR-ThH design, mainly due to lower LHGR and higher MCPR margin. Similarly, its performance during LOCA is expected to be satisfactory as the total mass of water in the vessel has not decreased significantly compared to a conventional ABWR.

The shorter core height, higher inlet orificing and lower void coefficient while operating at similar core average void fraction (in the fuel area) compared to ABWR, makes the RBWR-TR have better response to the stability modes. While both safety and stability of the RBWR-TR are expected to be superior compared to ABWR, the main area of concern is its potential to operate with positive void coefficient, which is world-wide scrutinized in licensing processes.

7.2. Fuel performance analysis

Similar to the self-sustaining RBWR-Th, the fuel performance assessment of the RBWR-TR will evaluate an average and 130% peaked power pin. Both cases make use of the conservative assumption that average pin power remains constant throughout irradiation, while the axial power shapes are varied based on neutronic evaluations. The resulting axial burnup profile is illustrated in Figure 19, with a peak local burnup of 88.1 MWd/kgHM.

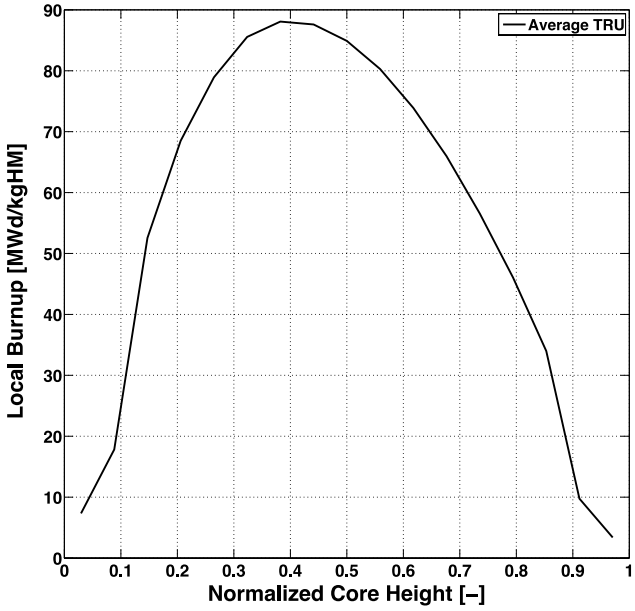

Figure 19. End of life axial burnup profile for the average power pin of the RBWR-TR.

In comparison to the self-sustaining RBWR-Th, the RBWR-TR has a softer neutron spectrum, which results in a lower cladding fast neutron fluence. While the EOL cladding fluence is significantly lower than the RBWR-Th, average RWBR-TR pins can be expected to challenge the bounds of Zircaloy-2 operational experience, shown in Figure 20.

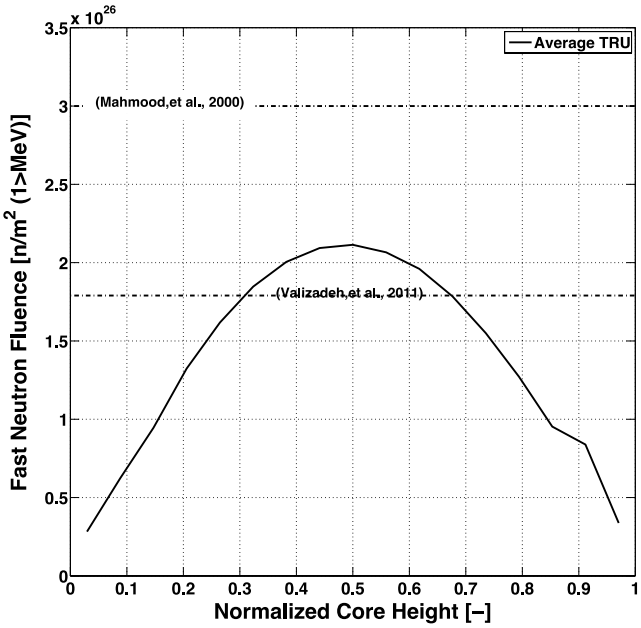

Figure 20. Axial fast neutron fluence profile of the average of the RBWR-TR compared with experiments that mark the boundary of Zircaloy-2 experience.[20,21]

With an average LHGR ~15% lower than that of the RBWR-Th design using the Hitachi T/H correlations, the RBWR-TR fuel maintains a comfortable margin to the melting temperature of approximately 3400K, with a 130% peaked pin maximum centerline temperature of 1630K. Similarly, a 130% peaked pin FGR of 35% dictates a 40cm (assuming identical fuel pin and plenum diameters) cold plenum length to assure plenum pressure remains below the 7.14 MPa coolant pressure.

The maximum fuel temperatures, FGRs, and plenum pressures for the average and 130% peak RBWR-TR pins are summarized in Table 7. Additionally, neither case challenged the 1% cladding hoop strain limit.

Table 7. Maximum fuel temperature, FGR, and plenum pressure for the average and 130% peaked RBWR-TR pins.

Case	Maximum Temperature [K]	FGR [%]	Plenum Pressure [MPa]
Ave. RBWR-TR	1288	2.26	2.26
130% RBWR-TR	1626	34.6	5.96

Thanks to the softer spectrum of the RBWR-TR, the oxidation and hydrogen pickups, shown in Figure 21 and Figure 22, transition to accelerated behavior much later than the RBWR-Th. However, the accelerated behavior does begin at 25 MWd/kgHM and the cladding hydrogen content exceeds the practical 600 ppm(wt) by 45 MWd/kgHM.

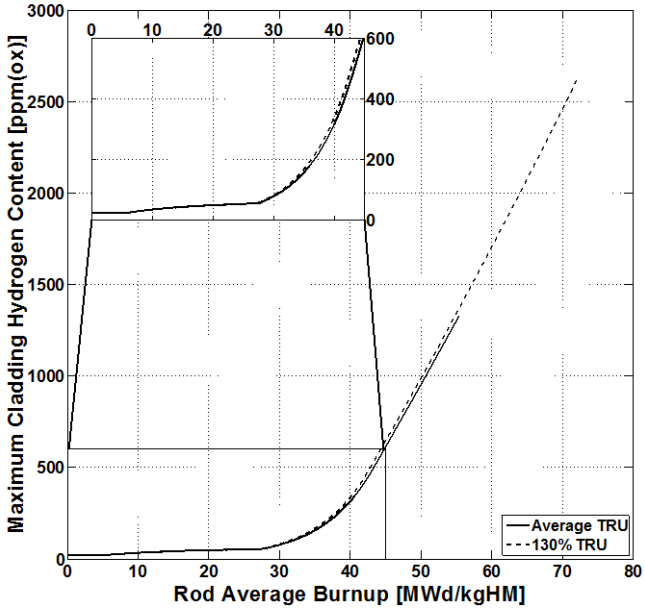

Figure 21. Maximum cladding hydrogen content for the average and 130% peaked RBWR-TR pins.

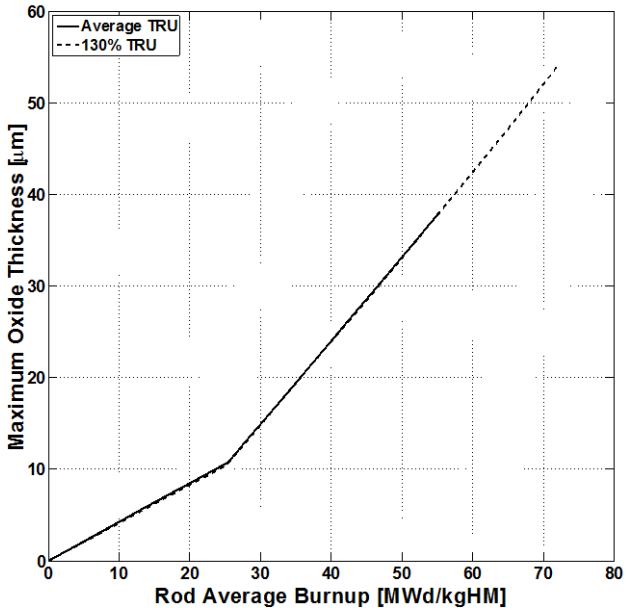

Figure 22. Maximum cladding oxidation thickness for the average and 130% peaked RBWR-TR pins.

Applying Equation (3) to the cladding hydrogen content, shown in Figure 23, results in the allowable margin rapidly deteriorating after the onset of accelerated corrosion behavior. As with the RBWR-Th, the ECR margin is completely eliminated prior to EOL.

$$ECR_{Allowed} = \begin{cases} 18 - 0.03H; & H < 400 \\ 18 - 0.01H; & 400 \le H < 600 \\ 0; & 600 \le H \end{cases} \quad (3)$$

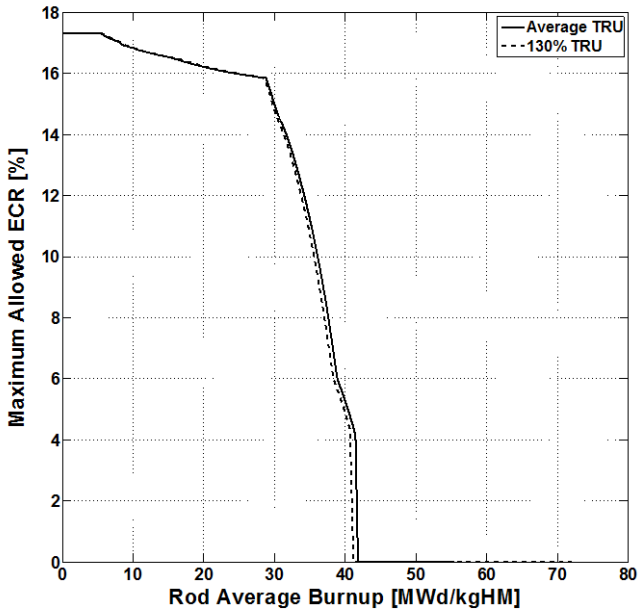

Figure 23. Maximum allowable ECR for Zircaloy-2 during a transient or LOCA for the average and 130% peaked RBWR-TR pins, based on cladding hydrogen content.

As with the RBWR-Th, the potential benefits of an advanced cladding material were explored. The resulting allowable ECR margins throughout the irradiation of a 130% peaked pin with delayed hydrogen pickup acceleration varied from 1.0 to 5.0 x10^{26} n/m^2 (>1MeV) are presented in Figure 24.

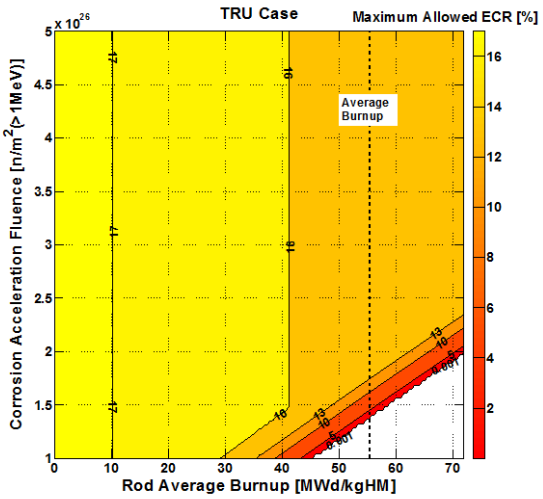

Figure 24. Comparison of allowable ECR values up to 130% of the average EOL burnup, given a delay to the accelerated hydrogen pickup behavior shows that a substantial delay is required to achieve non-zero margins for an average EOL burnup for the RBWR-TR.

Using the operational ECR calculated from the oxide thickness during steady state irradiation with the information presented in Figure 24, the necessary delay in accelerated hydrogen pickup behavior for the average and 130% peaked pin were found to be 50 and 120%, respectively. Available data,[19] which is very limited, suggests that the new Ziron cladding material may be able to provide the delay required for an average pin. This provides a promising example that future cladding development will be overcome the current challenges presented to Ziracloy-2 in the RBWR-TR.

As expected, the expected fuel performance of the RBWR-TR is very similar to that of the RBWR-Th. Fuel temperatures and FGR are predicted to remain well within tolerable limits. Despite its softer neutron spectrum, the RBWR-TR is still expected not to have any remaining ECR margin at EOL if Zircaloy-2 is employed as a fuel cladding. However, the RBWR-TR will require less ambitious advancements in cladding performance than its breeding counterpart, with the possibility of the currently under development material Ziron meeting its needs.

8. Conclusions

It is possible to design a thorium-based reduced moderation BWR core for LWR TRU transmutation with unlimited recycling. The optimal RBWR-TR core design features significantly higher water-to-HM volume ratio, smaller void fraction and, hence, smaller uncertainty in thermal-hydraulic correlations and softer spectrum, than of the self-sustaining RBWR core designs. Relative to the analogous DU-fuelled RBWR-TB2, the performance of the thorium-fuelled RBWR-TR features some improvement in TRU fission efficiency, slightly lower power density and specific power; somewhat lower discharge burnup but a significantly lower peak burnup; significantly lower peak linear heat generation rate; more uniform and stable axial power distribution; larger safety margins against critical heat flux at steady-state operation; lower fast neutron fluence and improved fuel survivability; smaller throughput of Pu and MA, lower (fissile Pu)/Pu ratio, higher ^{238}Pu/Pu ratio; but recycles significant amount of ^{233}U.

Compared to the reference ABR, the RBWR-TR, like the RBWR-TB2, has roughly one third of the discharge burnup, power density, and specific power. It requires a larger reprocessing capacity, but can operate in longer cycles with a comparable reactivity swing. The RBWR-TR discharges much less plutonium and has a significantly smaller fissile-to-total mass of plutonium, but it discharges a significant

quantity of fissile uranium as well. Overall, the fuel cycle cost will be greater for the RBWR-TR and RBWR-TB2 than for the ABR, but the capital cost of the RBWRs is expected to be lower than the ABRs.

Although the presented RBWR-TR design did not meet the VCR constraint, it is shown that a design in which the VCR is negative is feasible and would perform similarly. There would be a penalty on the achievable burnup and the TRU consumption rate, but it would still be able to outperform the RBWR-TB2. If the void coefficient were made negative, then the RBWR-TR would likely have more favorable safety margins than the ABWR. Although the RBWR-TR could not be made using Zircaloy-2 cladding, Ziron remains a promising candidate.

9. Nomenclature

∞-norm	Absolute value of the maximum difference between iterations
ε	Convergence criterion
ABR	Advanced Burner Reactor, a sodium-cooled fast reactor with a wide range of conversion ratios. The metal-fuelled CR=0.5 variant was chosen as a reference for this study.
ABWR	Advanced BWR
BOEC	Beginning of equilibrium cycle
BOL/BOEL	Beginning of equilibrium fuel life (i.e. fresh fuel)
BU	burnup
CPR	Critical power ratio
CR	Conversion ratio
CZP	Cold zero power
DU	Depleted uranium
ECR	Equivalent cladding reacted
EOEC	End of equilibrium cycle
EOL/EOEL	End of equilibrium fuel life (i.e. discharge fuel)
FGR	Fission gas release
H-CISE	A critical power correlation for use with the RBWRs which was modified from the CISE-4 correlation for BWRs; it predicts higher CPRs than the MFP-CISE correlation or the M-CISE correlation. The recommended MCPR limit for this correlation is 1.3.
H/HM	Hydrogen to heavy metal ratio.
HFP	Hot full power
HM	Heavy metals (actinides)
LHGR	Linear heat generation rate
M-CISE	A critical power correlation for use with the RBWRs which was modified from the CISE-4 correlation for BWRs; it predicts lower CPRs than the MFP-CISE correlation or the H-CISE correlation, but it has a larger factor of experimental uncertainty. The recommended MCPR limit for this correlation is 1.5.
MCPR	Minimum critical power ratio

N	Number density
pcm	percent milli or “milli-percent”; 10-5
RBWR	Resource-renewable BWR
RBWR-AC	DU-fueled fuel-self-sustaining RBWR designed by Hitachi
RBWR-TB2	TRU-burning RBWR fed with a mix of DU and LWR SNF designed by Hitachi
RBWR-Th	Fuel self-sufficient RBWR primarily fueled by Th, with some DU for reactivity feedback control
RBWR-TR	TRU-burning RBWR fed with a mix of LWR SNF and Th
RELAP	RELAP5, a USA safety analysis code which uses the Chexal-Lellouche void fraction correlation. This correlation is referred to as the RELAP void correlation within this document.
T/H	Thermal hydraulic
TRF	Transfertile (TRU + transthorium)
TRU	Transuranium
VCR	Void coefficient of reactivity

10. Acknowledgements

This research was performed using funding received from the U.S. Department of Energy Office of Nuclear Energy’s Nuclear Energy University Programs.

11. References

1. T. Hino, M. Ohtsuka, R. Takeda, J. Miwa, Y. Ishii, and K. Moriya, “Core Designs of RBWR (Resource-renewable BWR) for Recycling and Transmutation of Transuranium Elements - an Overview,” Proceedings of ICAPP 2014, Charlotte, North Carolina, USA (2014).
2. R. Takeda, J. Miwa, K. Moriya, “BWRs for Long-Term Energy Supply and for Fissioning Almost All Transuraniums,” *Proceedings of Global 2007*, Boise, Idaho, USA (2007).
3. International Atomic Energy Agency Report, "Status of advanced light water reactor designs." IAEA TECDOC-1391, p 436 (2004).
4. EPRI Report, “Technical Evaluation of the Hitachi Resource-Renewable BWR (RBWR) Design Concept,” EPRI Report number 1025086 (2012).
5. J. E. Seifried, P. M. Gorman, J. L. Vujic, E. Greenspan, “Accelerated Equilibrium Core Composition Search Using a New MCNP-Based Simulator,” Proceedings of SNA&MC 2013, Paris, France (2013).
6. X-5 Monte Carlo Team, “MCNP — A General Monte Carlo N-Particle Transport Code, Version 5, Volume II: User’s Guide” Technical Report LA-CP-03-0245, LANL, Los Alamos, NM, USA (2003).
7. A. Wysocki, Y. Xu, B. Collins, A. Manera, T. Downar, “PATHS: PARCS Advanced Thermal Hydraulic Solver,” University of Michigan (2012).
8. A. Cross, “A User’s Manual for the ORIGEN2 Computer Code,” Technical Report TM-7175, ORNL, Oak Ridge, TN, USA (1980).
9. K. Shirvan, Y. Wu, M. S. Kazimi, “Thermal Hydraulic Recommendation Update for the Resource Renewable BWR (RBWR),” Massachusetts Institute of Technology (2014).
10. T. Downar, Y. Xu, V. Seker, “PARCS v3.0 U.S. NRC Core Neutronics Simulator User Manual”, University of Michigan (2010).
11. B. Herman, “SerpentXS Documentation,” Massachusetts Institute of Technology (2011).

12. J. Leppänen, “Serpent – A Continuous-Energy Monte Carlo Reactor Physics Burnup Calculation Code,” VTT Technical Research Centre of Finland, http://montecarlo.vtt.fi (2013).
13. A. Ward, Y. Xu, T. Downar, “GenPMAXS – v6.1.2ucb, Code for Generating the PARCS Cross Section Interface File PMAXS”, University of Michigan (2013).
14. Hoffman, E.A., Yang, W.S., Hill, R.N., Preliminary Core Design Studies for the Advanced Burner Reactor over a Wide Range of Conversion Ratios. 2006, U. S. Department of Energy, Office of Nuclear Energy, Science and Technology.
15. “The SERPENT/PARCS/PATH core simulator,” Attachment 1.
16. “The MocDown/PATHS Assembly Unit Cell Design Tool,” Attachment 2.
17. “Void fraction and critical power correlations for the RBWRs,” Attachment 4.
18. “Self-sustaining Thorium-fuelled Reduced Moderation Boiling Water Reactors (RBWR-Th) Core Design,” Attachment 5.
19. “Application of GNF-Ziron to GNF Fuel Designs,” NEDO-33353, Global Nuclear Fuels, Revision 0, (2010).
20. S. VALIZADEH et al., "Effects of Secondary Phase Particle Dissolution on the In-Reactor Performance of BWR Cladding," J. ASTM Intl., Vol. 8, No. 2 (2011).
21. S. MAHMOOD et al, "Post-Irradiation Characterization of Ultra-High-Fluence Zircaloy-2 Plate," Zirconium in the Nuclear Industry: 12th International Symposium, ASTM STP 1354, (2000).

Attachment 7

For NEUP Project # 11-3023: Self-sustaining thorium boiling water reactors

Stability and Safety analysis of RBWR

The objective of this task is to perform stability and safety analysis of two RBWR-Th breeder designs, one using the MIT recommended correlation and other using the same correlations as HITACHI, and one burner design – RBWR-TR also using the same correlations as HITACHI and to compare the performance of the thorium-based designs to analogous HITACHI RBWR-AC and TB2 design as well as a conventional ABWR. The stability analysis was performed in frequency domain with point kinetics. The safety analysis was performed by simulating the all pump trip accident scenario, which it is expected to be one of the most limiting design basis accidents. The safety analysis utilized an enhanced TRACE ABWR plant model that is capable of effectively simulating the thermal hydraulic performance of tight lattice assemblies under accident conditions. During the transient, all of the three UCB designs experienced peak cladding temperature that is lower than RBWR-AC/TB2 and even lower than an ABWR, mainly due to operating with significantly lower peak linear heat generation rate.

I. INTRODUCTION

For the next generation of breeder/burner reactors, University of California Berkley (UCB) has proposed a LWR tight-lattice fuel design based on the Resource-Renewable Boiling Water Reactor (RBWR) design by HITACHI. The UCB design introduces Thorium instead of Uranium as the fuel matrix to promote breeding/burning while ensuring negative void coefficient of reactivity. The main motivation behind development of these concepts are to build upon existing LWR technology, specifically, the Advanced BWR (ABWR) technology, while fast non-LWR technology undergoes further development. ABWRs are the only Gen III+ plant built in the world, and the vessel and containment structures proposed for the UCB designs are the same as the ABWR design. Nevertheless, the UCB designs are different from the ABWR, in terms of core geometry and operating conditions. Table I lists the key design parameters for an ABWR core and the three UCB RBWR designs.

The first two UCB designs are breeder reactors with a conversion ratio of 1.0, similar to the HITACHI's RBWR-AC design. Each design is based on a certain void fraction (LPG or RELAP) and critical power (Y-CISE or H-CISE) correlation. The RBWR-Th Y-CISE/LPG, uses the MIT recommended correlations, while the RBWR-Th H-CISE/RELAP uses the same correlations as HITACHI. As implied by the lower power rating of the Y-CISE/LPG design, the MIT recommended correlations are more conservative than the correlations used by HITACHI (e.g. lower critical power and void fraction with MIT correlations). It is noted that a 300 MWTH increase in power, while keeping the power to mass flow rate ratio, was possible for RBWR-Th with MIT correlations. However, this increase requires changes in ABWR pumps. As listed in Table I, both of the breeder designs are rated at around three times the outlet quality of an ABWR. The rod-to-rod gap is also significantly narrower and the pins are arranged in a hexagonal configuration to further reduce the H/HM ratio. The third UCB design, RBWR-TR, is a burner reactor, where its operating conditions are very similar to an ABWR. Though, its fuel geometry is in hexagonal configuration and its H/HM ratio is lower compared to an ABWR. RBWR-TB2 is the analogous burner design by HITACHI that operates at much lower H/HM ratios compared to RBWR-TR.

Table I The ABWR vs. UCB RBWR design specifications.

Parameters	ABWR	RBWR-Th Y-CISE/LPG	RBWR-Th H-CISE/RELAP	RBWR-TR
Reactor thermal power (MW)	3926	3200	3926	3926
Core flow rate (kg/s)	14500	4530	6358	17395
Core Pressure Drop	0.21	0.28	0.10	0.12
Core inlet temperature (^{o}C)	274.3	278.3	278.3	278.3
Core Average Void fraction (%)	36	43	57	38
Core Exit Quality (%)	14	38.7	39.5	
Number of fuel assemblies	872	720	720	720
Bundle Type	Square	Hexagonal	Hexagonal	Hexagonal
Maximum linear power (kW/m)	44	3.7	22.4	18.3
Fuel rod OD (mm)	10.3	7.4	10.05	7.05
Fuel rod pitch (mm)	12.95	7.99	11.35	9.44
Active fuel rod height (m)	3.71	345	162.3	120
Number of fuel rods	92	547	271	397
Assembly inner dimension (mm)	133	194.4	194.4	194.4
MCPR	1.3	1.37	1.25	1.5
Void coefficient (pcm/% void)	-120	-20>&<0	-20>&<0	-20>&<0

Even though all three designs feature shorter active fuel length, their maximum linear heat generation rate (LHGR) is smaller than an ABWR, since there are higher number of pins in the core of similar volume. The shorter core will result into better two-phase stability as well as reducing the time needed to SCRAM. The smaller maximum LHGR will also lower the expected peak cladding temperature (PCT) upon core uncovery or reaching post-dryout heat transfer regime. The axial power profiles of each design at beginning of life (BOL) and end of life (EOL) are shown in Figure 1. The axial power profile dictates the single phase to two phase boundary, which is important in the stability analysis. These axial profile shapes are obtained by 3D single assembly calculations.

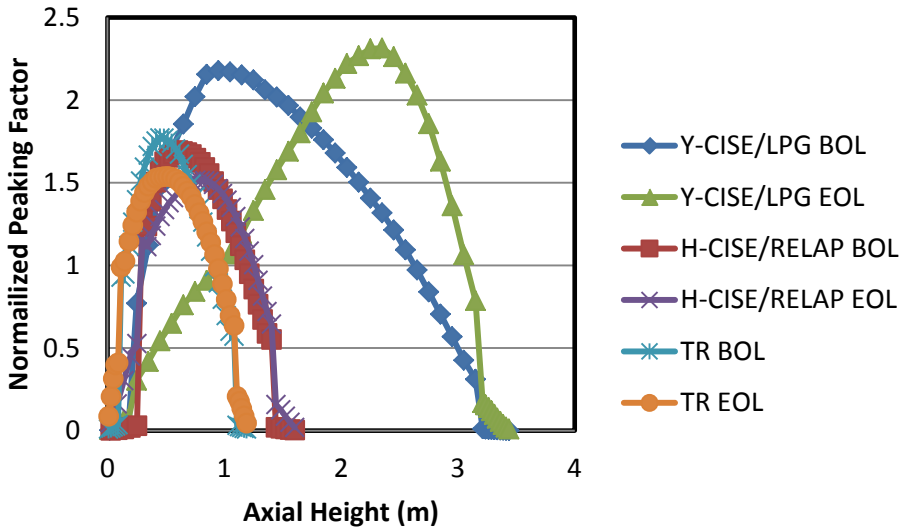

Figure 1. The normalized axial power profile of the UCB designs listed in Table I.

In addition to the fuel length and LHGR rating and shape, the difference in reactivity coefficients, fuel rod dimensions, core mass flow rate, feed water mass flow rate and power-to-flow ratio of the UCB designs will affect their safety and stability performance compared to an ABWR. These expected differences in transient behavior, motivates the evaluation of the stability and safety performance of these reactors. For such evaluation, this work will build upon the capability of proven tools and methods applicable to an ABWR and extend their range of applicability to be able to model the three UCB Thorium based RBWR designs.

In absence of equilibrium core physics data, simplifications and assumptions has been made in this work to analyze the safety and stability performance of the RBWR-Th designs. For stability, MIT in-house frequency domain code, STAB, is used.[1] The point kinetics model within STAB is informed by the 3D single assembly level calculations for the UCB designs. For the core radial power and inlet orificing distribution, the HITACHI RBWR design values are assumed for the UCB design. This is expected to be valid since the UCB breeder and burner designs have similar reactivity swings to their analogous HITACHI designs. For safety analysis, similar assumptions are made but the model development and evaluation is performed in NRC's system code, TRACE,[2] discussed in more detail in Section III.

II. STABILITY

Any BWR type system will have susceptibility to two phase flow oscillations of the density wave type. A widely used industry approach to evaluating the stability margin of a BWR system nowadays is through coupling of a core neutronics model with a system wide thermal hydraulics model to address in

the time domain the response of the system to perturbations. This approach can be taken using a coupled TRACE/PARCS analysis. However, it requires a final equilibrium core model of the designs that could be coupled to TRACE, and that is currently not available. The other method that was widely used in the past, is the frequency domain approach, where the kinetic behavior of a nuclear reactor is lumped using reactivity feedbacks and the characteristics of the Laplace transformation of the equations describing the propagation of perturbations in the core are used to assess the reactor's hypothetical response. This is the approach followed here through the STAB code[1].

II.A Methodology

There are three oscillation modes in BWR stability analysis that are commonly investigated. They are core-wide in phase or global instability, regional-wide out-of-phase instability and single channel thermal hydraulic without feedback instability. The modes' decay ratio is the main parameter that are calculated in a stability analysis. The MIT in house code STAB is based on the linearization and Laplace-transformation of the mass, momentum and energy equations along with the constitutive relations. It is capable of performing analysis for these three modes of oscillation. The STAB code also uses simple input file format that can easily be modified. The core can be modeled by 3 channels: high, medium and low powered regions. The void fraction correlation used in STAB is the Homogenous Equilibrium Model (HEM), therefore overestimating the void fraction. Similar to the void feedback, the fuel temperature is modeled as a lumped geometry, both for fuel heat transfer and kinetics feedback. The structures of the core are also modeled using simple lumped parameters resulting into more stable numerical schemes and solution characteristics than the system level codes.

The single channel thermal hydraulic instability is an instability that might develop in a single assembly due to its flow perturbation. In this case, neutronic feedback and flow fluctuations introduced in other assemblies can be neglected. Unlike PWRs, a BWR channel box prevents radial cross flow among assemblies. It has been shown that the hottest single channel in the core is more susceptible to instability than the other assemblies. The oscillations are of density wave type where the pressure drop characteristic delays the response at the exit to changes of the inlet velocity and that will result into oscillations in the flow in the channel.

The coupled neutronic regional out-of-phase instability has been observed in several BWRs across the world during startups. The out-of-phase term comes from the fact that half of the core changes its power in the exact opposite direction as the other half. However, the total flow rate remains constant as does the pressure drop across the core. This type of instability occurs at a constant total core flow rate. Typical regional STAB analysis divides each half of the core into three radial regions distinguished by power level. About $1/5^{th}$ of the assemblies are high powered and $1/5^{th}$ are low powered and the rest are considered middle powered. It has been shown that the three power region modelling is enough to capture the stability of the system accurately. Unlike the single channel instability analysis, in this case, the neutronic feedback is applied in the calculations. The neutronic coefficients are taken from the respective design's single assembly calculations. The kinetic parameters such as the neutron time constant and the six group delayed neutron fractions and their respective yields are used as inputs into STAB.

The coupled neutronic core-wide in-phase instability has also been observed in low flow and natural circulation conditions. In this case, the oscillations due to two phase flow density fluctuation and the reactivity provided by the void coefficient are in-phase. The core is not the only component in the whole reactor system that can affect the core-wide in-phase instability. In addition to the core, the riser, separators, downcomer are accounted for in the loop model of the ABWR. In this mode, the pressure drop across the core is not constant, but the pressure drop in the vessel does remain constant.

The in-phase has been shown to be the most limiting instability for RBWR type cores and is the focus of this analysis.

II.B Stability Performance of HITACHI RBWR Designs

This section summarizes the stability analysis performed on HITACHI designs, since such analysis will give useful insights to the stability performance of the UCB designs. The void fraction correlation used in STAB is the HEM, therefor overestimating the void fraction. This will be conservative for a purely thermal hydraulic instability. However, the overestimation of the void fraction might not be conservative for the modes of stability with strong changes in the neutronic feedback. Therefore, we have extended STAB to also be capable of using the Bestion, RELAP5 and LPG drift flux void fraction correlations.[3] Previous study,[4] investigated the performance of many void fraction models for tight lattice geometries against limited experimental data. The evaluation indicated that the Bestion model overestimates the tight lattice assembly void fraction, though has the most simple formulation that renders its implementation within the STAB code's characteristics equations very easy. The RELAP5 correlation was recommended for use for the wide range of conditions for an RBWR type reactor while the LPG provided the best estimate model at hydraulic diameters less than 5 mm, which underestimated the void fraction by about 10% compared to the RELAP5 model.[4] The sensitivity studies showed that the core in-phase is the most limiting mode of instability, regardless of void fraction correlation. The effect of void fraction correlation was found to be small and the HEM model provided the most conservative approach in STAB.[3]

However, the coupled neutronics-thermal hydraulic simulations performed in TRACE/PARCS showed the much stronger effect on stability.[5] A 5% decrease in void fraction prediction reduced the decay ratio of RBWR-TB2 design for a core in-phase perturbation from ~0.6 to ~0.3. The void fraction in the core also effected the calculated void coefficient significantly. However, the magnitude of the effect depends on the fuel composition and H/HM ratio. According to STAB analysis supported by coupled simulations, the RBWR showed more stability to physical perturbations with smaller void coefficients. The magnitude, not the sign, mainly controls the stability. The designs that exhibited small positive void coefficient resulted in more stable performance compared to assuming a large negative coefficient.[5]

The axial void fraction profile is also a function of core residence time. For RBWR HITACHI designs, at the same flow rate, the average void fraction of the core from BOC to EOC is increased by 5%, which has significant impact on stability performance of the system. The power profile also changes the single phase to two phase boiling boundary. The change in boiling boundary at such high qualities showed significant impact on the stability performance of the system, simulated with both TRACE/PARCS and STAB tools.

The HITACHI BWR orificing map is divided into 5 groups, where most of the orifices with high loss coefficients are situated mostly toward the core periphery. This is somewhat different than a conventional BWR, where there are only two orificing groups, where the group with the higher loss coefficient is strictly in the periphery. Since the HITACHI RBWRs operate with very high outlet qualities, the complex orifcing map allows uniform distribution of quality in the core, which is needed to accommodate for sufficient critical power margin. However, such unconventional orificing map created regional out-of-phase instabilities with very high decay ratios within the orificing groups.[5] This was investigated using the detailed TRACE/PARCS simulations, where all 720 assemblies in the core are explicitly modeled. STAB code is only capable of simulating upto to three regions and not able to resolve such instabilities.

Overall, the HTIACHI RBWR designs were found to be stable at rated power and flow conditions, with RBWR-AC showing much better stability performance compared to RBWR-TB2, mainly due to lower void coefficient of reactivity and smaller void fraction. However, when deviating slightly from the rated

conditions, the RBWR-TB2 performance was considered undesirable and further work on design modification and analysis was recommended.

II.C UCB RBWR Stability Analysis

Similar to HITACHI RBWRs, the higher core void fraction and much higher exit quality of RBWR-Th with MIT and RBWR-Th with HITACHI correlations, compared to an ABWR, raise concerns about the system stability. Table II shows the qualitative performance of the two designs relative to an ABWR. Based on the discussion in section IIB, it is expected that the RBWR-Th design with HITACHI models to perform similar to RBWR-AC due to similarity of the core geometry and operating conditions. The RBWR-Th with MIT correlations smaller void fraction and void coefficient could offset the negative effect from larger core height relative to RBWR-AC. The RBWR-TR design is not listed in Table II, since it has an advantage in terms of expected stability performance to an ABWR in key areas. RBWR-TR design's height and void coefficient are significantly smaller than the ABWR, which introduces a large stabilizing effect while operating with similar void fraction.

Table II. The summary of parameters governing the differences between ABWR and RBWR-ThM/ThH stability performance (+/- means more/less stable; * means either possibility).

Parameters	ABWR	RBWR-Th Y-CISE/LPG	RBWR-Th H-CISE/RELAP	Effect
Fuel Height (m)	3.7	3.45	1.65	+
Pressure Drop (kPa)	130	180	100	*
Core Exit Quality (%)	14.5	39	39	-
Spacer Grid Span (cm)	~50	30	30	-
Fuel Height to Core Outer Diam. Ratio	~0.7	~0.65	~0.3	-
Fuel Time Constant (sec)	6	~4	~5	-
Peak Heat Flux (kW/m^2-s)	1365	157	708	+
Subcooling (°C)	10	5	5	*
Effective Delayed N Fraction x 10-3	6-5	< less	< less	-
Coolant Average Void Fraction (%)	~40	~65	~65	-
Void coefficient (PCM/% void)	-130 to -70	-15 to 0	-25 to -10	+
Inlet Orificing	15-20	30-70	30-70	+

The single channel thermal hydraulic perturbation of the breeder designs at 100% and 95% flow rate for BOL and EOL, can be seen in Table III. The RBWR-TR decay ratio could not be calculated in STAB since it was below 0.1, exhibiting very stable behavior. For this mode of instability, the hot assembly peaking factor of 1.3 was assumed, based on the full core calculations of the HITACHI RBWR designs.[5] Table III shows that at BOL, the hot assembly of RBWR-Th design with MIT correlations will have unacceptable performance, while RBWR-Th design with HITACHI correlations will have high risk to density wave oscillations. The decay ratio is drastically reduced with EOL LHGR profile for the RBWR-Th design with MIT correlations. Similar trend with less drastic (but significant) magnitude is observed for the RBWR-Th design with HITACHI correlations. As seen, from Figure 1, the LHGR profile of the RBWR-Th design with MIT correlation widely differs at BOL and EOL. This relative difference is also more significant compared to the difference in LHGR profile of the RBWR-Th design with HITACHI correlations.

The downward peak LHGR profile provides a more stabilizing effect compared to the upward peak. It is noted that for both designs, the HEM model was used, which is more conservative for the RBWR-Th design with MIT correlations compared to RBWR-Th design with HITACHI correlation.

Table III. The decay ratios of the RBWR-Th breeder designs for the sing channel thermal hydraulic perturbation.

Time	Core Flow (%)	RBWR-Th Y-CISE/LPG	RBWR-Th H-CISE/RELAP
BOL	100	1.22	0.65
BOL	95	1.31	0.73
EOL	100	0.38	0.37
EOL	95	0.42	0.40

The global mode of perturbation was found to be the most limiting mode at hot full power (HFP) conditions for the ABWR and RBWR reactors.[3] Assuming each design will have a negative void coefficient of reactivity, the void coefficient where each design reaches the decay ratio limit of 0.8 at 100% flow and 95% flow rate has been calculated using the STAB code. These bounding void coefficients are listed in Table IV. It is noted that the value of 0.8 is the current limit for ABWRs[6], however, this value is often occurs away from rated power and flow rate.

Table IV. The void coefficient (pcm/%void) required to achieve decay ratio of 0.8 for a global mode perturbation.

Design	RBWR-Th Y-CISE/LPG		RBWR-Th H-CISE/RELAP	
Flow	100%	95%	100%	95%
BOL	-8	-1	-135	-123
MOL	-55	-49	-168	-151
EOL	-78	-72	-150	-138

As listed in Table IV, assuming the equilibrium core operates with the MOL axial power shape, there is sufficient margin for stable operating at 100% power and flow for both designs. The longer Y-CISE/LPG design shows to be much more unstable than shorter H-CISE/RELAP design. The H-CISE/RELAP design can operate with void coefficients similar to the conventional ABWR as the stabilizing effect of shorter length is countered by the higher void fraction. RBWR-TR exhibited very low decay ratios for the coupled analysis. Assuming -120 pcm/%void of reactivity (similar to an ABWR), the perturbation decay ratio of 0.23 was calculated for RBWR-TR with the in-phase mode simulation. The shorter core height, higher inlet orificing and lower void coefficient while operating at similar core average void fraction (in the fuel area) compared to ABWR, makes RBWR-TR burner design to have superior responses to the stability modes.

III. SAFETY

This section provides the safety assessment of the UCB design using the enhanced TRACE tool.[5]

III.A Methodology

A reference ABWR TRACE input deck was obtained from University of Michigan.[3] The core model in the ABWR deck consisted of three rings, six azimuthal sectors, and 16 separate channels of uniform radial peaking with no neutronic feedback modeling. The desired model for safety analysis will require 720 separate channels, and thus, such modification has been made. Furthermore, the control system modeled in the deck was separated from the components and played no role in the steady-state test simulation run. The ABWR deck also did not have steam separators and safety relief valves, which are critical in performing transient simulations. The deck also contains explicit modeling of all the four steam lines and ten internal reactor pumps in the ABWR design. Figure 2 shows the improved ABWR TRACE model with added safety and relief valves and steam separators. These valves were modeled with spring and relief set pressure in accordance to GE ABWR design control document available from NRC.[6] The feedwater, pump and turbine controller were also added.

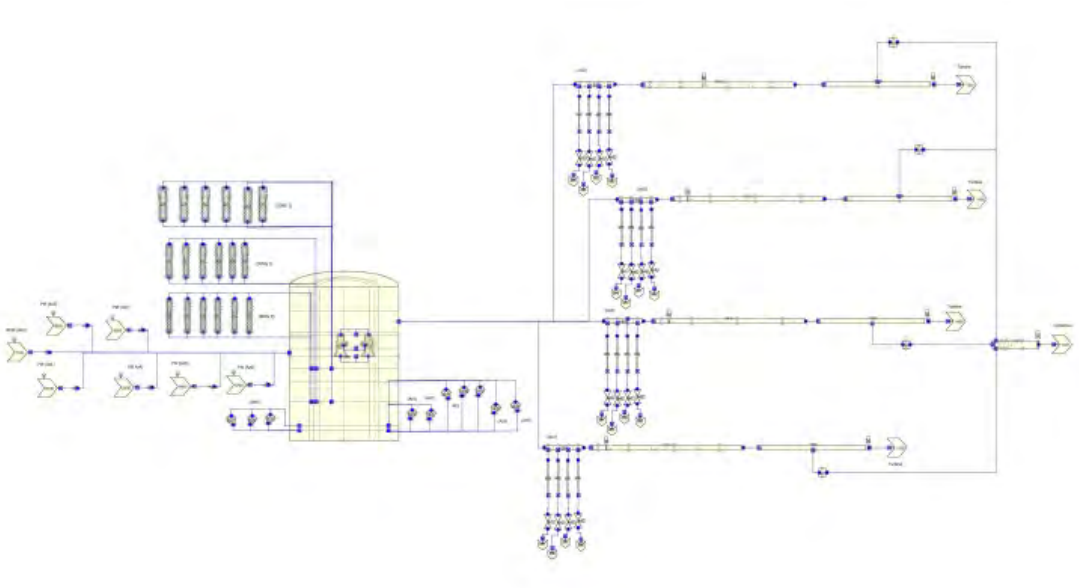

Figure 2. The improved ABWR TRACE deck layout.

Similarly, the operating parameters such as reactor power, flow rate and inlet temperature were adjusted to the NRC ABWR specifications. A simplified point kinetics model with fuel and void feedback was also coded in the TRACE input deck. The assumed void coefficient at hot full power conditions was -120 pcm/%void. The ABWR model performance was assessed for selected transients and agreed well with the published results.[3] In order to simulate the UCB RBWR designs, the axial power profile, inlet temperature, pumps flow rate and core geometry of the 720 channels in TRACE were adjusted accordingly to the specification of each design as listed in Table I and shown in Figure 1.

In order to quantify the Minimum Critical Power Ratio (MCPR), three critical power correlations were added within TRACE source code. All correlations are based on modifications to the CISE-4 CP correlation, one representing a HITACHI recommendation (H-CISE), the other is a more conservative M-CISE correlation, and even more conservative correlation with limited range of applicability, Y-CISE. This step was necessary as the CP models within TRACE diverge at UCB design rated conditions.

According to the TRACE documentation,[2] the role of critical quality in post CHF analysis is limited and requires additional modeling. The current method as shown by Figure 3, primarily relies on the CHF temperature as the method to determine which post heat transfer regime will be assumed and for calculating the magnitude of the heat transfer correlation during the transition from inverted annular film boiling to dispersed flow film boiling. The CHF temperature is calculated from the 1995 AECL-IPPE

CHF lookup tables. The application of local CHF values especially with very high peaking factors in the second fissile zone of the RBWR is very questionable. The mechanism of reaching boiling crisis has been experimentally found by JAEA double humped experiments at RBWR type conditions to be dryout.[7] The inclusion of dryout instead of CHF temperature is not compatible with the interpolation post-CHF model for film boiling. Additionally, in case of core uncovery toward the bottom of the core or during low power or pressure operating conditions, the local CHF consideration will be more appropriate than dryout.

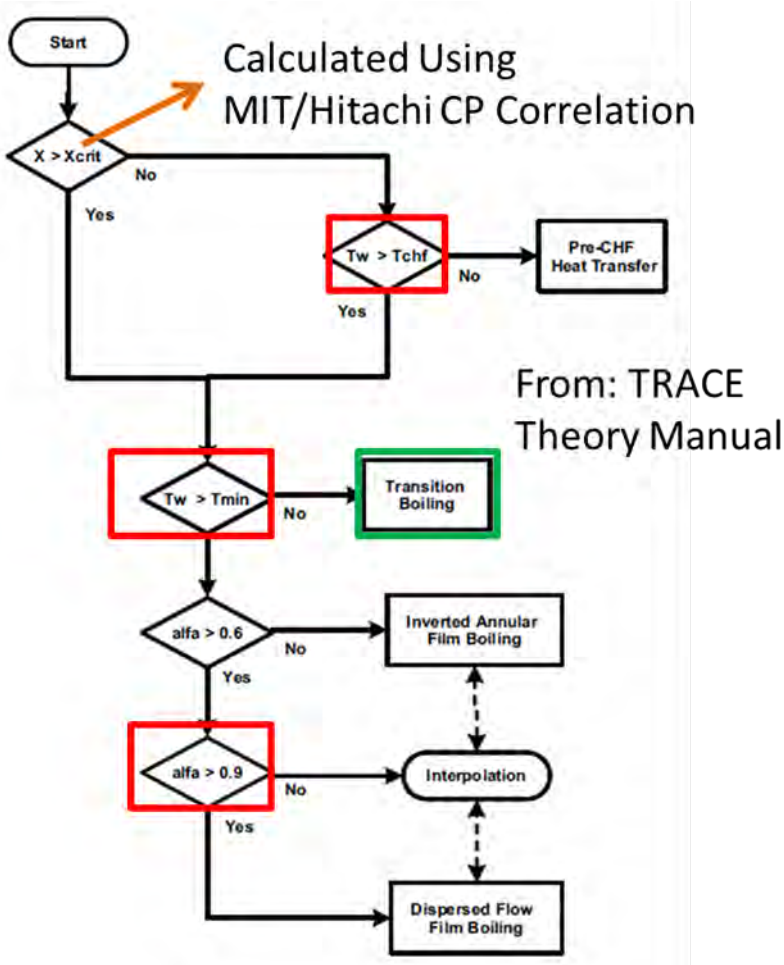

Figure 3. The post CHF wall heat transfer logic diagram implemented in TRACEv5.[2]

In order to calculate the minimum film boiling temperature for determination of post-CHF heat transfer, TRACE chooses the maximum temperature between quench temperature and film boiling temperature calculated by the Groeneveld-Steward model.[2] In TRACE, the quench temperature is assumed to be 725 K. The data shows the Groeneveld-Steward model is able to effectively capture the shape and magnitude of the quench temperature for pressures between 5-7 MPa, but for low pressures it underpredicts the quench temperature by ~100 K. The RBWR minimum film boiling temperature at operating conditions is ~650 K. For this work, the quench temperature is assumed to be 650 K to consistently model at ~7 MPa where the current safety analysis is restricted. Further considerations are required in order to accurately model the safety performance of RBWR type reactors at low pressure (~<2 MPa) accident scenarios, which is not covered in this work.

Limited loss of flow experiments were performed at the JAEA 37 rod test facility at prototypical RBWR steady state operating conditions.[7] The tests showed that the measured post-CHF temperature is higher than the common models such as TRAC, which is also used in TRACE. Since outlet qualities of these tests are well over 40% with void fraction in excess of 80%, it is postulated that film boiling is initiated instead of transition boiling, therefore, smaller than expected heat is transferred from the wall to the fluid. The heat transfer logic was changed accordingly to represent such a modeling feature.

The new developed TRACE post CHF wall heat transfer model for the RBWR was validated against the JAEA tests database. In order to predict the time when dryout occurs, the MIT critical power correlation was used. The validation study resulted in a great agreement between the TRACE RBWR model and the experimental data in terms of peak cladding temperature, quench temperature, and time when dryout occurs and is recovered. A sample result with direct comparison to experimental data is shown in Figure 4. As shown, the time when dryout starts is almost identical to the experimental data as well as the peak cladding temperature. The TRACE v5 critical power correlations predicts a 1000 ratio meaning the operating conditions of the tests are beyond their range of applicability. Interestingly, in this small test, the CHF lookup tables within TRACE predicted that the bundle will not reach post-CHF conditions.

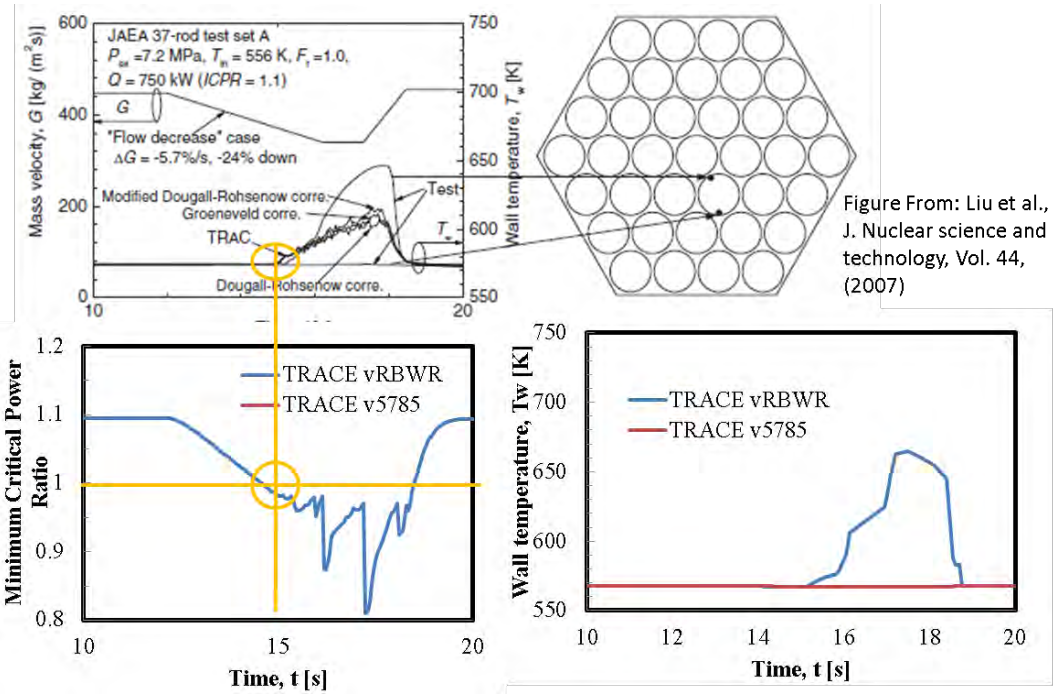

Figure 5. The comparison of JAEA experimental data[7] to the base TRACE (v5785) and improved TRACE (vRBWR).

III.B Safety Performance of HITACHI RBWR Designs

This section summarizes the safety analysis of the HITACH RBWR designs, which will provide more insights into the UCB RBWRs' safety performance. The RBWR-AC safety performance was published by HITACHI in the 1990s and ongoing.[8] The study pointed out that the RBWR-AC will most likely perform very well in most transients, while the total pump trip transient and loss of coolant being the most limiting. In fact, both transients performed worse than the ABWR. Recent study on safety performance of various accident using the described TRACE model, yielded that pump trip would be the most limiting accident. Therefore, the performance of both RBWR-AC and TB2 using different CPR

correlations at both BOC and EOC of their equilibrium cycle were assessed during the total pump trip transient.[5] The calculated PCT for both RBWR-AC and TB2 were higher than the ones reported for ABWR (720 vs. 640^{o}C) for all assumed CPR correlations, though well below the 1204^{o}C safety limit. The sensitivity studies also showed that the magnitude of void coefficient is very important driver of PCT, as even small positive void coefficients could push the PCT to unacceptable temperatures. It is important to note that even though the performance of RBWR-AC and TB2 were satisfactory, both reactors exhibited insufficient margin to CP using the MIT recommended CP correlation during steady state operation.

III.C UCB Designs Safety Analysis

Chapter 15 licensing safety analysis of an ABWR is divided into 8 different categories[6] that cover range of conditions that a reactor may face during transient operation. The following is the list of each category followed by a qualitative discussion of how the UCB designs will perform compared to an ABWR.

- Increase in reactor pressure: The generator load rejection without bypass is typically the limiting transient for BWRs under this category. The main concern within this category is whether the reactor pressure vessel is able to safely handle pressure rises due to power increased induced by collapse of the voids in the core from the pressure increase due to a turbine trip or other postulated sequence of events. Previous work has shown that the relative magnitude of the power increase is strongly dependent on the void coefficient of reactivity and the core volume.[3] The less negative and smaller the core volume that is occupied by voids, the smaller the observed power increase. The magnitude of pressure increase has been observed to be mainly the function of added void fraction in the core that is a weak function of power at high qualities.[3] Judging by the satisfactory performance of the HITACHI RBWR designs, it is expected that the UCB design will perform the same or better than the ABWR, since they all feature shorter cores and less negative void coefficient.
- Decrease in reactor coolant inventory: The main steam line break and feedwater line break accidents are limiting transients for an ABWR under this category. The core LHGR and reflood flow rate are the main controlling parameters in this class of accidents when comparing designs of similar vessel volume, water inventory and power rating. The UCB RBWR designs have slightly less mass of water present in an ABWR vessel and are rated at the same or lower total power. The experimental data on reflood flow rates in tight lattices showed that it is similar to regular BWR assembly geometries.[7] The UCB RBWR designs LHGR is significantly lower than an ABWR, as listed in Table I. Therefore, it is expected that the designs perform similar or better in this class of accidents.
- Decrease in reactor coolant system flow rate: The total pump trip accident is the limiting accident scenario under this category for an ABWR. The detailed quantitative assessment of the UCB designs will be performed in this section. However, due to smaller LHGR, it is expected that the UCB design to perform the same or better than the ABWR in this category.
- Decrease in reactor coolant temperature: The loss of feedwater heating is an example of a transient often considered for an ABWR under this category. The concern under this category is similar concern as for the increase in reactor coolant pressure category, where reactor power increase is due to positive reactivity induced by reduction in coolant temperature. The increase in power could cause prolonged dryout, resulting in fuel failures. The time scale of the accident in this category is significantly longer than the increase in pressure category. Since all the three UCB designs have smaller void reactivity coefficients and margin to CP, it is expected that they will perform the same or better in this accident scenario. Though, as implied by the stability

assessment of the two breeder UCB designs in Section II, those designs could undergo flow and power oscillations with very high decay ratios induced by such transients, which requires future investigations with coupled code analysis.

- Increase in reactor coolant inventory: The feedwater controller failure, where feedwater flow rate is suddenly increased is one such accident. The performance of an ABWR under this category is very similar to the increase in reactor coolant pressure category. Due to smaller void reactivity coefficient, the UCB designs are expected to perform similar or better than an ABWR. The larger feedwater to core flow ratio of the UCB breeder designs compared to an ABWR could result into larger relative increase in core flow for a given controller failure. However, the void worth has been significantly reduced and the margin to critical power significantly improves with increase in coolant mass flow rate at the ~40% rated outlet quality of the UCB breeder designs.
- Reactivity and power distribution anomalies: This category of accidents includes control rod withdrawal error at variety of power conditions. Traditionally, the control rod ejection has been the limiting transient from a fuel performance point of view under this category. However, the ABWR control rod drives(CRD) are licensed to eliminate rod ejection scenarios from licensing analysis.[6] Therefor, the concern for consequences of such reactivity and power anomalies are not significant for an ABWR. The HITACHI and UCB RBWR CRD have not been built, tested and licensed, therefore, at this moment it cannot be determine if the rod ejection accident will be included in the design basis analysis. The expected control rod worth of the UCB design is similar to an ABWR and therefore, it is not expected that the UCB designs performance will be more limiting that an ABWR under this category. Though ,detailed stability analysis needs to be performed on oscillations induced by asymmetric withdraw of CRDs for the two breeder designs.
- Anticipated Transient Without SCRAM (ATWS): Typically, a failure or a transients discussed in the previous categories are analyzed by assuming the core fails to SCRAM under this category. The core two phase flow stability under this category is closely monitored. The RBWR-TR design is expected to perform similar or better than an ABWR, since it is expected to perform similar or better in other categories as well as stability performance. The two breeder design require more detailed stability analysis in order to confidently discuss their expected performance under ATWS events. It is noted that the HITACHI RBWR designs also require such future investigation, as these concerns are not limited to the UCB breeder designs.
- Radioactive release from subsystems and component: The failure of component such as the off-gas systems in an ABWR is expected to result in similar consequences for the UCB designs, since they are designed with the identical such components. Other concern, under this category, is the release of fission gases upon mishandling of assemblies. The total amount of fission gas released depends on the total mass of burned fuel and fraction of gases released to rod plenum. The fuel performance analysis of the UCB design showed that the relative release of gases is not significantly different than an ABWR.[9] Even though the LHGR is significantly lower, the higher maximum peak burnup results in large athermal release of fission gases. The rod average burnup and fuel loading of the RBWR-Th with HITACHI correlation and RBWR-TR design are similar to an ABWR assembly. Therefore, the two design are expected to perform similarly under this category. For the RBWR-Th with MIT correlations, while the average assembly discharge burnup will be similar to an ABWR, the assembly fuel loading is 2.5 times an ABWR assembly. Therefore, higher than normal levels of fission gases will be released for such design and further assessment needs to be performed under this category, especially investigating the fuel handling of such heavy assemblies of the RBWR-Th with MIT correlations.

The all pump trip transient is likely the most limiting design basis transient for an RBWR core as it produced the highest cladding peak temperature of all the other transients analyzed by HITACHI and MIT/BNL using their system code packages.[3,8] Specifically, this is an accident limiting for RBWR type reactors due to increased sensitivity to mass flow rate decrease as RBWR has almost half the mass flow rate/mass flux of an ABWR. Table V lists the sequence of events for the all pump trip transient. The sequence of events also includes complete loss of feedwater flow at 1.85 seconds after the pump trip. In this transient, transition boiling is reached in a standard ABWR and if the fuel has a burnup of less than 20 MWD/kg its cladding temperature cannot exceed 873 K above 60 seconds. Otherwise, fuel rods with greater burnup than 20 MWD/kg, are assumed to fail. For an ABWR, the peak cladding temperature was 800 K within the core and less than 0.2% of the fuel rods higher than 20 MWD/kg entered transition boiling, which would not result in significant releases from less than about 100 fuel rods.[5] Due to the reduction in the amount of moderation in the core of the RBWR designs, almost all the assemblies in the equilibrium cycle remain at above average power rating above 20 MWD/kg. Therefore, significant fuel failures needs to be assumed upon core uncovery, which may or may not affect the offsite dose calculation as typically very conservative assumptions are used in such calculations.

Table V. The total pump trip sequence of events.

Time (s)	**Event**
0	Trip of all RIPs initiated
1.22	Reactor scram
1.85	Feed water flow pump trip
1.97	Turbine Trip initiates bypass operation
20	End of Simulation

The HITACHI RBWR-AC and RBWR-TB2 core radial power and burnup distribution and orificing scheme were used for the safety analysis of the analogous UCB designs. Due to similar assembly reactivity swings and average cycle burnup, it is expected that the UCB designs to have similar assembly average power and burnup distribution in the core. The middle of life (MOL) axial power shape from 3D single assembly calculations was used for the core average axial power shape in TRACE. Both of the breeder designs feature mass flow rates that are less than half of the ABWR, while the burner design has similar flow rates. Therefore, the breeder designs are expected to be more susceptible to decrease in core flow rate accident scenarios. However, unlike HITACHI RBWRs, the maximum LHGR of both breeder designs are lower than ABWR as listed in Table I. Therefore, the performance of breeder designs with HITACHI correlations is expected to be better than the HITACHI RBWRs for loss flow scenarios. The RBWR-Th with MIT correlations is designed with very high pressure drop. The very high pressure drop along with tighter lattice could prevent core reflood in the event of reaching post critical heat flux (post-CHF) regimes.

Since the specific core kinetics of the UCB designs are unknown, a simulation with zero power coefficient is performed. This is expected to be conservative as both designs are expected to have a negative Doppler coefficient and a small negative void coefficient. Figure 6 shows the total reactor power during the all pump trip simulation. Since the power coefficient is assumed to be zero, the reactor power stays constant until the SCRAM point. The SCRAM worth is taken to be the same as an ABWR, which is conservative compared to RBWR-AC and TB2 SCARM worth.

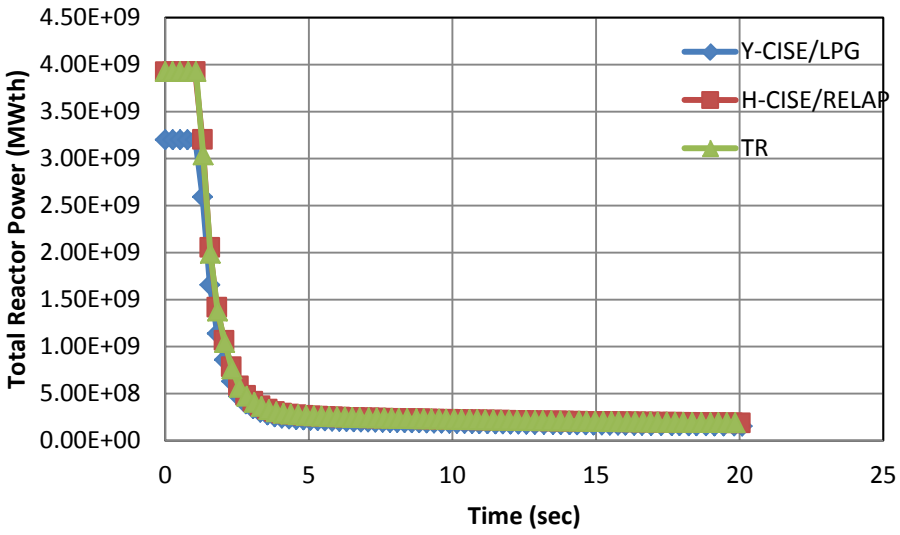

Figure 6. The total reactor power level during the all pump trip transient.

Figure 7 shows the inlet mass flow rate to the separator during the all pump trip simulation. The RBWR-TR design has the largest relative decrease in mass flow rate which results in the fastest reflood (e.g. negative mass flow rate) compared to the breeder designs.

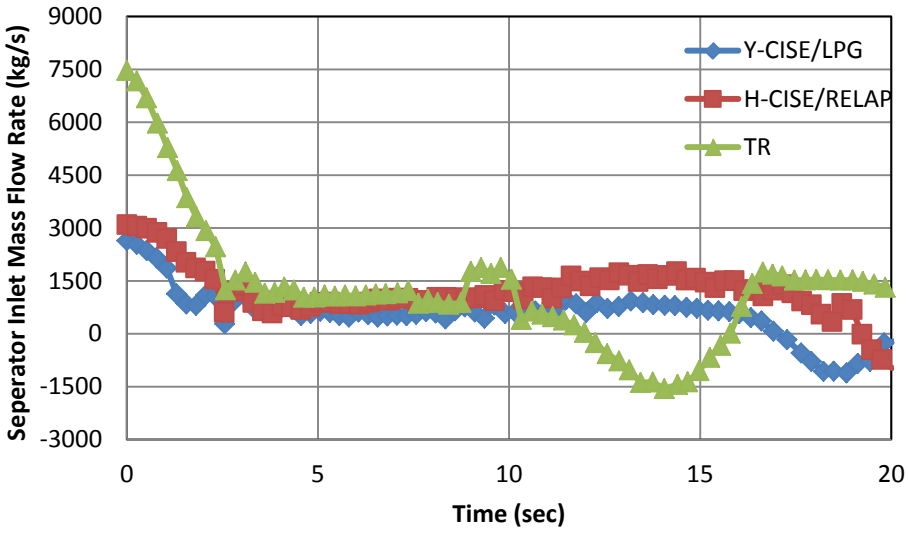

Figure 7. The separator inlet mass flow rate during the all pump trip transient.

Figure 8 shows the PCT during the all pump trip simulation. The PCT of 752 K and 683 K is obtained for RBWR-Th breeder designs with MIT and HITACHI correlations, respectively. These values are representative of the differences in rated peak LHGR for each design. The conventional ABWR design PCT is 800 K during such transient,[6] higher than the two breeder designs. The simulation of this transient implies the lower LHGR more than offsets the lower core thermal capacity compared to an ABWR. It is noted that the core fluid volume of the Y-CISE/LPG and H-CISE/RELAP are 1.3 and 2.3 times higher than RBWR-AC. The RBWR-TR design experiences a PCT of 681 K, which is also lower than an

ABWR PCT. Similar to the breeder design, the significantly lower LHGR contributes to its superior performance compared to RBWR-TB2 and ABWR.

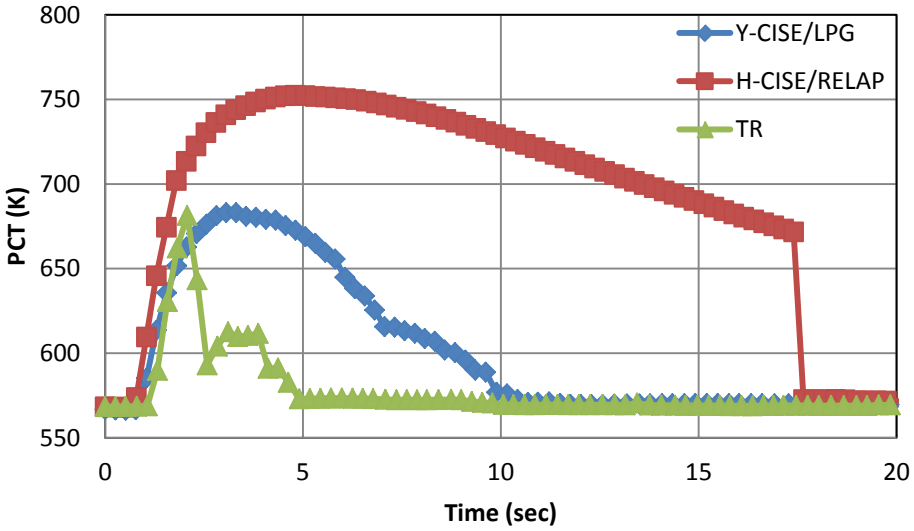

Figure 8. The PCT during the all pump trip transient.

IV. CONCLUSIONS

This work extended the capability of tools used for stability and safety assessment of conventional BWRs to be able to evaluate the performance of the UCB RBWR designs. In absence of equilibrium core physics parameters, the stability analysis was limited to frequency domain with point kinetics and course spatial discretization. The safety analysis was also limited to point kinetics and utilized the HITACH RBWR core radial power distributions.

It was found that the RBWR-Th breeder design with HITACHI used correlations should have sufficient margin to density wave oscillation at its operating power and flow rates. Furthermore, in terms of stability performance, it is expected that the design with HITACHI used correlation to behave similar to HITACHI's RBWR-AC. The breeder design with MIT recommended correlations exhibited unstable behavior with its BOL power distribution, as further redesign is recommended. Both designs require further investigations in their stability performance using higher fidelity time domain tools. The RBWR-TR burner design exhibited higher levels of stability compared to the ABWR and its stability performance is expected to be satisfactory. This is not the case for RBWR-TB2, where similar to AC, more comprehensive stability assessment is required.

The qualitative safety performance of the UCB designs under Chapter 15 licensing safety analysis was discussed. The RBWR-TR is expected to perform better or similar in all categories compared to an ABWR. Other than potential issues regarding unstable behavior during transients, the RBWR-Th with HITACHI used correlation is expected to also perform similar or better than an ABWR. Besides the mention stability issues, the RBWR-Th with MIT used correlation could also perform poorly in fuel handling accidents due to the 2.5 times the mass of fuel loading. The simulation of the all pump trip accident for all three designs were performed using an enhanced TRACE ABWR plant model. All three UCB designs experienced PCT that is lower than an ABWR, mainly due to the significantly lower peak LHGR during an all pump trip accident, where it is expected be one of the most limiting design basis accidents. Both RBWR-AC and RBWR-TB2 resulted in PCT higher than an ABWR.[5]

Overall, in terms of stability and safety, mainly due to lower LHGR, the performance of the UCB RBWR designs with HITACHI used correlations are expected to be similar or superior to RBWR-AC and RBWR-TB2 designs. The RBWR-Th design with MIT recommended correlation requires further redesign and investigation on details of its stability and safety performance. It is noted that while both safety and stability of RBWR-TR burner design are expected to be similar or superior even compared to an ABWR, the main area of concern is its potential to operate with positive void coefficient, which is world-wide scrutinized in licensing processes. The RBWR-TR smaller fuel diameter compared to conventional BWR requires further investigation as well.

ACKNOWLEDGMENTS

This work was funded by DOE NEUP grants.

REFERENCES

1. K. Shirvan, M.S Kazimi, “STABILITY ANALYSIS OF BWR-HD: AN OPTIMIZED BOILING WATER REACTOR WITH HIGH POWER DENSITY,” Nuclear Technology, 184, 2013
2. US NRC, “TRACE V5.0: Theory Manual,” Division of Safety Analysis, Washington DC, 2012.
3. K. Shirvan, et al., “*Stability and Safety Analysis of Tight Lattice Breeding LWR,”* ICAPP Charlotte, NC, 2014.
4. K. Shirvan, N. Andrews, M. Kazimi, “Best Estimate Void Fraction and Critical Power Correlations for Tight Lattice BWR Bundles,” ICAPP 2013, Korea, (2013).
5. T. Downar et al., “Transient Safety Analysis of Fast Spectrum TRU Burning LWRs with Internal Blankets,” DOE NEUP Final Report, 89536, 2015.
6. GE, “ABWR Design Control Document/Tier 2”, Availablefrom NRC.gov, (2007).
7. W. Liu, M. Kureta, H. Yoshida, H. Tamai, A. Ohnuki and H. Akimoto, " Critical Power Characteristics in 37-rod Tight Lattice Bundles under Transient Conditions," Journal of Nuclear Science and technology, 44, no. 4, pp. 1172-1181 (2007).
8. R. Takeda, M. Aoyama, M. Moriwaki, S. Uchikawa, O. Yokomizo, K. Ochiai, "General Features of Resource-Renewable BWR (RBWR) and Scenario of Long-term Energy Supply," *Proc. of International Conference on Evaluation of Emerging Nuclear Fuel Cycle Systems*, p. 938 (1995).
9. A. Mielosyzk, M.S. Kazimi, “Fuel Performance Analysis of a (ThU)O2 Fueled Reduced Moderation Boiling Water Reactor,” Nuclear Technology, Accepted, 2015.

Attachment 8

For NEUP Project # 11-3023: Self-sustaining thorium boiling water reactors

Comparison of Reduced-moderation Boiling Water Reactor and Sodium-cooled Fast Reactor Technologies

This objective of paper is to compares (1) a thorium fueled self-sustaining Reduced-moderation Boiling Water Reactor core design (RBWR-SS) with a couple of previously designed self-sustaining uranium-based reactors – the Hitachi designed RBWR-AC and the ANL designed Sodium-cooled Fast Reactors (ARR); and (2) a thorium fueled BWR core designed for transmutation of LWR TRU (RBWR-TR) with uranium-based transmuting cores – the Hitachi designed RBWR-TB2 and the ANL designed ABR. Core design parameters along with fuel cycle performance characteristics are compared. The overall performance of the thorium-based RBWR and their uranium-based RBWR counterparts is similar. Relative to the uranium-based cores, the major differences are that the thorium-based RBWR cores have significantly longer seed (driver) fuel without central axial blanket and, therefore, significantly lower peak linear heat generation rate; more stable axial power distribution along with larger safety margins. All the RBWR cores have lower discharge burnup than the SFR of comparable TRU fission efficiency and therefore require a larger fuel recycling capacity per unit of electricity generated. This results in a higher fuel cycle cost and less favorable waste characteristics. The discharged plutonium from RBWR cores have fewer fissile plutonium but high ^{238}Pu/Pu ratio such that it is less attractive for weapon-use compared with SFR's discharged fuel.

1. Introduction

The Reduced-moderation Boiling Water Reactor (RBWR) concept was proposed by Hitachi for achieving the same missions traditionally assigned to Sodium-cooled Fast Reactor (SFR) – either fuel self-sustaining or transmutation of TRU elements from LWR's Used Nuclear Fuel (UNF) by using the more mature and well-commercialized Advanced BWR (ABWR) technology [1]. The RBWR designs proposed by Hitachi include: the RBWR-AC – a fuel self-sustaining core, and the RBWR-TB2 – a LWR TRU transmutation core [2]; both use depleted uranium as the fertile fuel. In an attempt to resolve certain safety related concerns regarding these designs [1], a preliminary conceptual design of a couple of thorium fueled RBWR cores – RBWR-SS[1] for fuel self-sustaining and RBWR-TR for LWR TRU transmutation, was undertaken at the University of California Berkeley in collaboration with the University of Michigan Ann Arbor, MIT, and BNL [3-7]. All four RBWR designs feature an intermediate spectrum with a closed fuel cycle.

The objective of this paper is to interactively compare the performance metrics of the four RBWR cores and to evaluate these cores with their SFR equivalents – the Advanced Recycling Reactor (ARR) and the Advanced Burner Reactor (ABR) [8,9]. The methodology used by recent Fuel Cycle Evaluation and Screening (FCE&S) Campaign [10] is applied for part of this comparison.

[1] In previous publications we have referred to this core as the RBWR-Th. In this write-up RBWR-Th refers to either RBWR-SS or RBWR-TR,

The methodology, including comparison metrics and assumptions, is briefly described in section 2; sections 3 and 4 summarize the basic design parameters and fuel cycle characteristics; sections 5, 6, and 7 compare the nuclear waste, proliferation resistance and fuel cycle cost while section 8 compares the different technologies using the E&S metric.

2. Methodology

2.1 Computation methods

The performance of the RBWR-SS [11] and RBWR-TR [12] cores reported in this write-up are based on the estimation deduced from fuel assembly unit cell calculations carried out at the University of California Berkeley using the MocDown code system [13] Detailed information about the computational methodology is given in [11,12].

The performance of the RBWR-AC and RBWR-TB2 designs used for the present comparison is that reported by Hitachi [2] and reproduced at University of Michigan Ann Arbor based on multi-group deterministic calculations using the SerpentXS/PARCS/PATH code system described in Attachment 1.

The ABR and ARR were designed by Argonne National Laboratory (ANL) [8] using the ANL developed deterministic suit of fast reactor codes DIF3D/REBUS-3 supplemented by the ETOE-2/MC2-2/SDX multi-group cross-section generating codes. The discharge composition used for the equilibrium fuel cycle analysis was provided by ANL [14].

For the fuel cycle analysis, the fresh fuel from the equilibrium cycle was depleted up to the average discharge burnup to track the isotopes which were not included in the neutronics model. The one-group cross-sections used in ORIGEN2.2 were updated from the neutronics models. Then, the waste characteristics (like atomic density, radioactivity, decay heat) of the discharged fuel were calculated with ORIGEN2.2 accounting for 879 fission products and 128 actinides.

2.2 Metrics for comparison

The comparison metrics are divided into 3 parts: core design parameters; core and fuel cycle performance characteristics and waste characteristics. An overall technology evaluation based on the methodology developed by the E&S Campaign is applied to related technologies.

The core design parameters include the thermal/electrical power, fuel form, core dimensions and intra-assembly design. The fuel cycle performance characteristics compared in this study pertain to the equilibrium cycle and include fuel loading, specific power, power density, peak linear heat generation rate, average discharge burnup, reprocessing capacity, cycle length, burnup reactivity swing and fuel composition at charge, discharge, and after 5-years cooling. The fuel cycle cost of the RBWR and SFR designs was quantified accounting for both front-end and back-end activities.

The waste characteristics include radioactivity of the used nuclear fuel and high level waste at short term (10 years) and long term (100,000 years) after fuel discharge; inhalation toxicity; ingestion toxicity and proliferation resistance related characteristics – plutonium

throughput, fissile plutonium fraction, ^{238}Pu fraction, specific decay heat and spontaneous fission rate.

Finally, a high-level comparison of the different reactor technologies was conducted using the evaluation criteria developed by the Nuclear Fuel Cycle Evaluation and Screening (FCE&S) campaign [10] of US DOE. The primary objective on this undertaking was to find whether the fuel cycle of RBWRs is as promising as the FCE&S campaign claimed for the SFR fuel cycle.

2.3 Assumptions

The major assumptions and constraints used for fuel self-sustaining designs and TRU transmutation RBWR core designs are summarized in Attachments 5 and 6 [11,12]. Additional assumptions used for this fuel cycle analysis are: a thermal efficiency of 34.5% for the RBWRs and 40% for the SFRs; 5-years cooling of the discharged fuel before recycling; 1% of the discharged heavy metal is lost during recycling and ends up in the waste stream together with the fission products.
For the fuel cycle analysis of the transmuting reactors, a 2-tier system was assumed – Tier-1 consists of PWRs while Tier-2 is composed of either RBWR or SFRs. An equilibrium state is assumed such that the amount of TRU generated from Tier-1 PWRs is equal to the TRU consumed by Tier-2 reactors. All TRU transmuting cores were designed to recycle all (99%) of their HM and have conversion ratio of 0.5 approximately. In principle, ABR cores can accommodate even smaller conversion ratios [8].

3. Basic core design parameters

3.1 Fuel self-sustaining cores

Table 1 compares the main design parameters of the three self-sustaining cores while Figure 1 compares these cores average neutron spectra. The two RBWR cores were designed to fit within the ABWR pressure vessel and deliver its nominal power of 1356 MWe. The makeup fuel for the RBWR-SS is a mix of natural thorium and depleted uranium in oxide form while the RBWR-AC makeup fuel is only depleted uranium dioxide. There are two design variants for RBWR-SS in [11] based on different void fraction and critical power correlations. The RBWR-SS design examined in this paper is based on Hitachi recommended critical power correlation (H-CISE) – the modified BWR CISE4 correlation – and the RELAP void fraction correlation [15]. Both RBWR cores have similar intra-assembly parameters including P/D ratio and the outer diameter of fuel pin but the RBWR-SS has a longer driver fuel without central axial blanket. The RBWR-AC spectrum has a significantly larger thermal component than the RBWR-SS. This is may be due to the fact that nearly half of the RBWR-AC fissions occur in the lower seed (driver) fuel section where the coolant density is relatively high. The 52cm long internal blanket between the two driver fuel regions also contributes to spectrum softening [11].

The ARR designed by ANL is a small module reactor with nominal electrical power of 400 MWe. Its fuel is the ternary metallic alloy U-10wt%Zr-TRU that has a theoretical density of 15.7 g/cc and a smear density of 75% to accommodate the fuel swelling with burnup. The low-swelling ferritic martensitic steel HT9 is selected as the structural and cladding material. Unlike the control blades in RBWR designs, ARR uses control assemblies composed of B_4C with HT9 ducts. The ARR features a much harder neutron spectrum than the RBWRs.

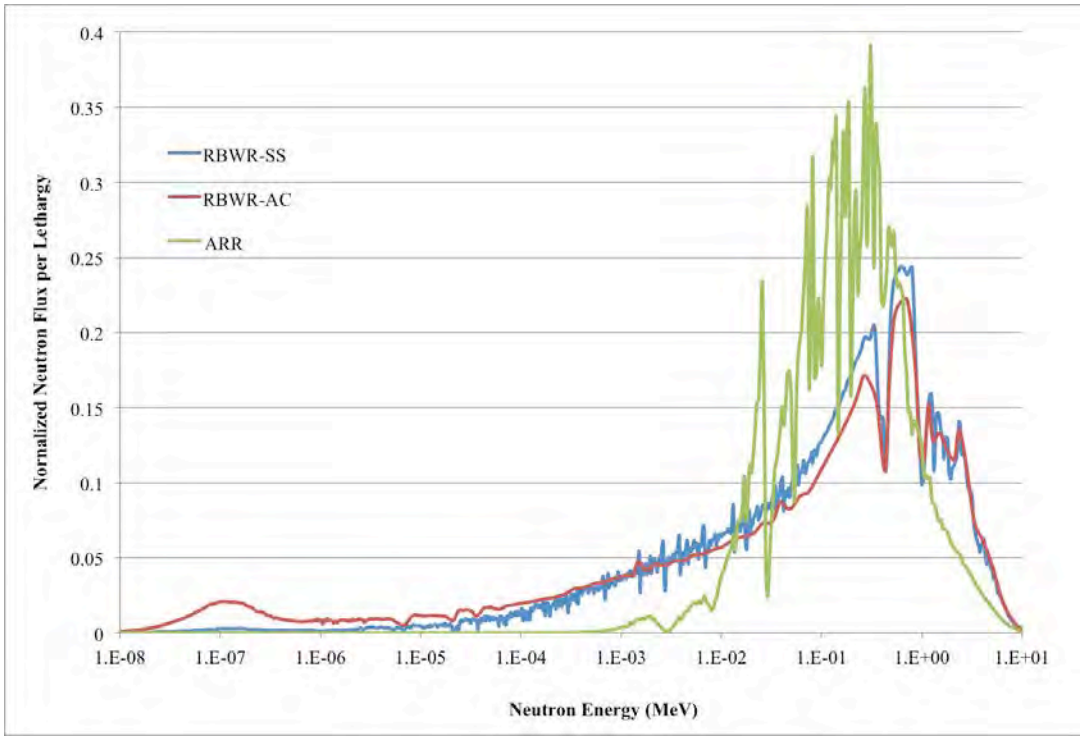

Fig. 1. Core average spectra of RBWR-SS, RBWR-AC, and ARR

Table 1 Main design parameters of RBWR-SS, RBWR-AC, and ARR

Parameters	RBWR-SS	RBWR-AC	ARR
Reactor power, MWt/MWe	3926/1356	3926/1356	1000/400
Fuel form	Th-U Oxide	U Oxide	U-10Zr-TRU Metallic
Feed fuel	Thorium+DU	DU	DU
Coolant	Light Water	Light Water	Sodium
Cladding	Zircaloy	Zircaloy	HT9
Pressure drop, MPa	0.13	0.14	N/A
Coolant flow rate, kg/sec	6358	7222	~5729
Void fraction correlation	RELAP	RELAP	N/A
Critical power ratio correlation	H-CISE	H-CISE	N/A
Outlet void fraction	89%	81%	-
Fuel lattice type	hexagonal	hexagonal	hexagonal
Control rod type	Y-shape	Y-shape	Assembly-type
Equivalent core height, cm	162.3	134.3	101.6
upper/lower blankets, cm	20/28	7/28	-
internal blankets, cm	-	52	-
upper/lower driver, cm	114.3/-	28/19.3	101.6/-
RPV diameter, m	7.1	7.1	3.2
Pin pitch-to-diameter ratio	1.13	1.13	1.10
Fuel pin OD, cm	1.005	1.005	0.808
Pins per assembly	271	271	271
Fuel smeared density	89.90%	89.90%	75%
Number of fuel assembly	720	720	151

3.2 TRU transmuting cores

The RBWR-TB2 core was designed by Hitachi to incinerate TRU from LWR UNF and its counterpart RBWR-TR was designed at UC Berkeley. The main difference between RBWR-TR and RBWR-TB2 is the fertile material mixed with LWR TRU in the makeup fuel: depleted uranium for the RBWR-TB2 versus thorium for the RBWR-TR . The basic design parameters of these two cores are compared in Table 2 and their spectra are compared in Fig. 2. The design of the two cores is similar with two exceptions: the RBWR-TR design has (1) a significantly higher coolant flow rate and therefore lower average void fraction and (2) a longer driver without internal blanket. Despite of the higher core average void fraction the RBWR-TB2 core features a softer spectrum than RBWR-TR (Fig. 2) because the 56cm internal blanket in RBWR-TB2 design significantly softens the neutron spectrum [12].

The modular ABR used for this comparison was designed by ANL and features a significantly harder neutron spectrum than the RBWR counterparts (Fig. 2). Its design parameters are deduced from [8] and the detail composition of its discharged fuel was provided by ANL [14].

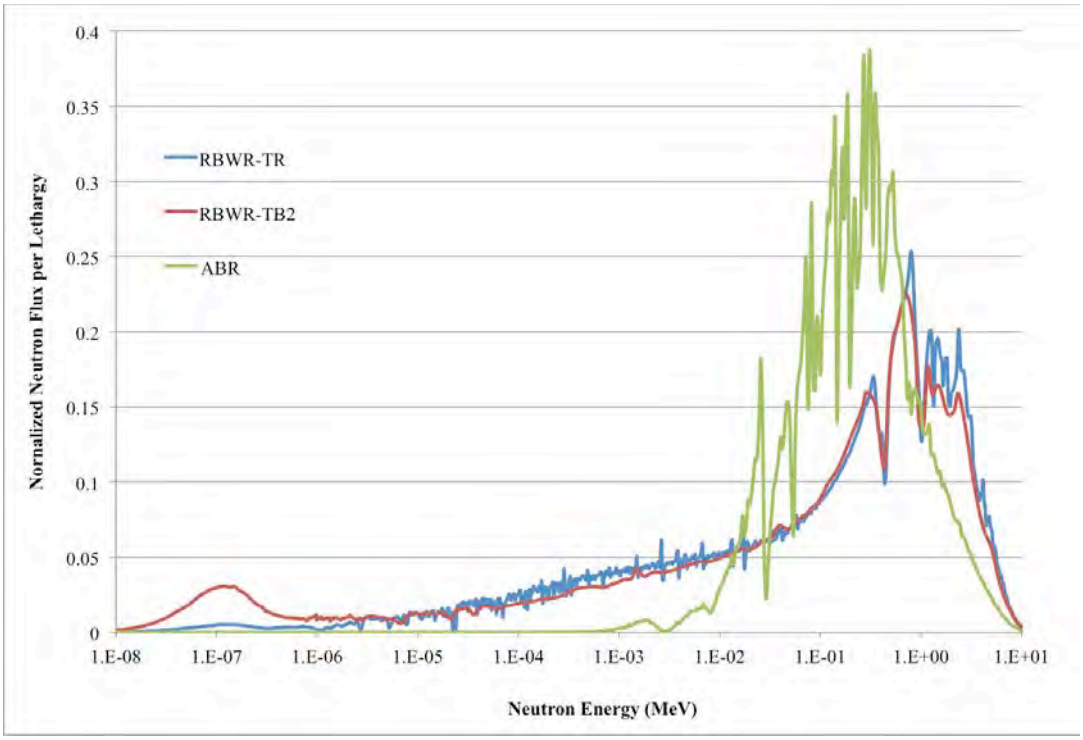

Fig. 2. Core average spectra of RBWR-TR, RBWR-TB2 and ABR

Table 2 Main design parameters of RBWR-TR, RBWR-TB2 and ABR

Parameters	RBWR-TR	RBWR-TB2	ABR
Reactor power, MWt/MWe	3926/1356	3926/1356	1000/400
Fuel form	Th-U Oxide	U Oxide	U-10Zr-TRU Metallic
Feed fuel	Thorium+LWR's TRU	DU+LWR's TRU	DU+LWR's TRU
Coolant	Light Water	Light Water	Sodium
Cladding	Zircaloy	Zircaloy	HT9
Pressure drop, MPa	0.15	0.06	N/A
Coolant flow rate, kg/sec	17395	6667	~5599
Void fraction correlation	RELAP	RELAP	N/A
Critical power correlation	M-CISE	H-CISE	N/A

Outlet void fraction	69%	80%	-
Fuel lattice type	hexagonal	hexagonal	hexagonal
Control rod type	Y-type	Y-type	Assembly-type
Equivalent core height, cm	130.0	102.5	101.6
upper/lower blankets, cm	15/15	2/-	-
internal blankets, cm	-	56	-
upper/lower driver, cm	100	22.4//22.1	101.6/-
RPV diameter, m	7.1	7.1	3.1
Pin pitch-to-diameter ratio	1.34	1.30	1.29
Fuel pin OD, cm	0.705	0.724	0.623
Pins per assembly	397	397	324
Fuel smeared density	89.9%	89.9%	75.0%
Number of fuel assembly	720	720	144

4. Fuel cycle characteristics

4.1 Fuel self-sustaining cores

Fig. 3 shows a schematic view of the RBWR-SS, RBWR-AC, and ARR fuel cycles considered. It is assumed that the recycled uranium (RU) and thorium (RTh) are recovered and recycled together with transuranium (TRU) for RBWR-AC and trans-thorium (TransTh) for RBWR-SS. Electro-chemical reprocessing is assumed for both RBWR and ARR discharged fuel based on the experience of SFR development in the US. The fission products and heavy metal loses are sent to geologic repository.

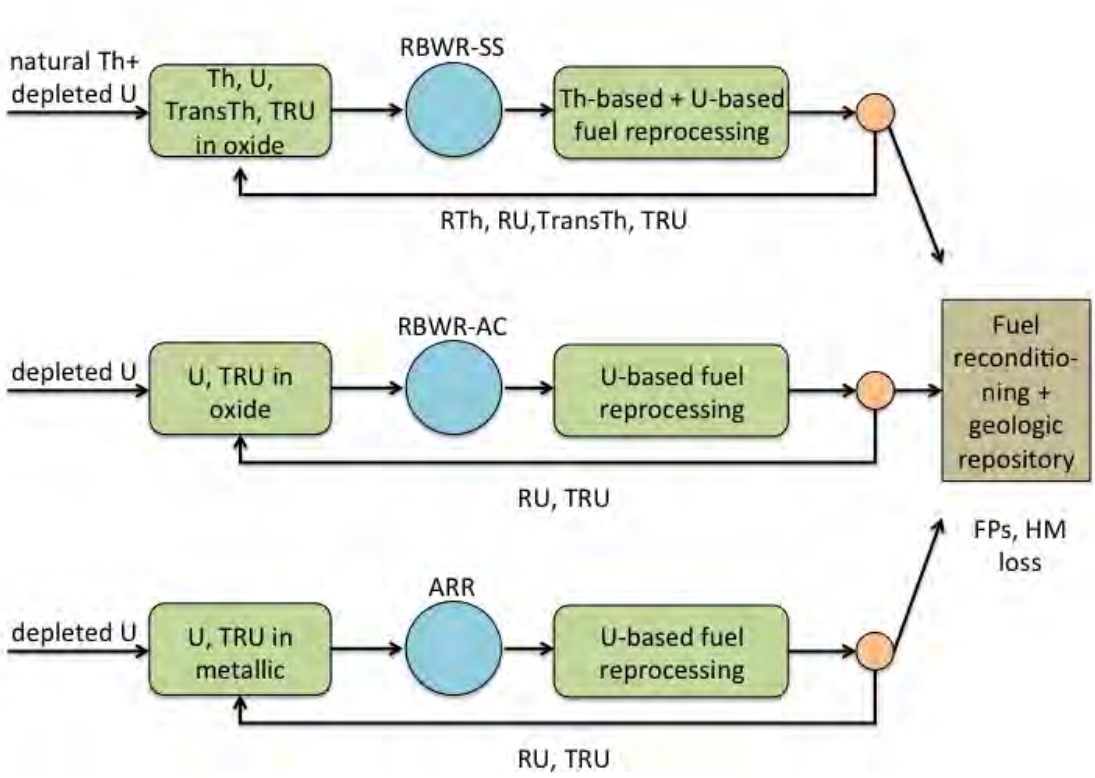

Fig. 3. Schematic view of the RBWR-SS, RBWR-AC, ARR fuel cycles

Table 3 tabulates the performance characteristics of the three cores for an equilibrium cycle. The RBWR-SS and RBWR-AC have very similar performance in terms of average discharge burnup, fuel inventory, cycle length and reprocessing capacity per unit of electricity generated. Compared with the RBWRs, the ARR design features higher average discharge burnup and thus smaller reprocessing capacity. The specific power of ARR is about two times those of the RBWRs. The RBWR-SS design has the lowest TRU fraction out of the three designs but the total fraction of trans-fertile (TransTh + TRU) in the HM of the RBWR-SS is approximately the same as of the RBWR-AC and ARR.

Table 3 Performance characteristics of RBWR-SS, RBWR-AC, ARR at equilibrium cycle

Parameters	RBWR-SS	RBWR-AC	ARR
Capacity Factor, %	90	90	85
Average discharge burnup, GWD/t	48.8	45	73.0
Specific power, MWt/t	25.7	27.3	59.7
Power density, W/cc	61.1	73.8	122.4
Peak LHGR, W/cm	261	472	389
Number of batches	4.6	4.2	3/3/4.5
Fuel inventory in core, t	153.0	144.0	16.7
Charge fuel mass per batch, t	33.6	33.9	4.8
Fuel residence time, EFFD	1901	1651	1110/1110/1665
Cycle length, EFPD	412	389	370
Burnup reactivity swing, %Δk/k	-1.9	-1.5	0.1
TRU transmutation efficiency[2]	-1%	0%	0%
Reprocessing capacity, kg/GWeYr	21664.2	23483.9	12500.0
Pu	1037.8	2717.7	1643.6
TRU	1170.8	2943.7	1711.3
Charge mass fraction, %			
- Th232	65.4	-	-
- TransTh[3]	6.8	-	-
- U238	22.5	87.5	86.3
- TRU	5.4	12.5	13.7
Discharge mass fraction, %			
- Th232	62.4	-	-
- TransTh	6.9	-	-
- U238	20.8	82.9	78.5
- TRU	5.4	12.6	13.7
- FPs	4.6	4.6	7.8
Fuel mass at time of recycle, %			
- Th232	62.4	-	-
- TransTh	6.9	-	-
- U238	20.8	82.9	78.5
- TRU	5.4	12.5	13.7
- FPs	4.6	4.6	7.8

[2] TRU fission efficiency is defined as the ratio between the amounts of TRU consumed over one cycle and HM fed at beginning.

[3] TransTh includes all the nuclides bred from thorium.

Table 4 shows the fuel compositions of the three cores after 5 years cooling; these compositions are used for the later fuel cycle analysis.

Table 4 Discharge fuel compositions of RBWR-SS, RBWR-AC, ARR after 5 years' cooling

Nuclide	RBWR-SS	RBWR-AC	ARR
TH-232	65.36	0.00	0.00
PA-231	0.04	0.00	0.00
PA-233	0.00	0.00	0.00
U-232	0.02	0.00	0.00
U-233	4.32	0.00	0.00
U-234	1.83	0.03	0.03
U-235	0.50	0.09	0.30
U-236	0.50	0.03	0.39
U-238	21.78	86.72	84.43
Np-237	0.15	0.07	0.17
Pu-238	0.32	0.39	0.20
Pu-239	2.49	5.72	9.43
Pu-240	1.73	4.74	3.94
Pu-241	0.25	0.64	0.38
Pu-242	0.23	0.65	0.32
Am-241	0.25	0.54	0.25
Am-242m	0.01	0.02	0.01
Am-243	0.10	0.19	0.08
Cm-244	0.07	0.13	0.06
Cm-245	0.03	0.04	0.01
Cm-246	0.02	0.02	0.01

4.2 TRU transmuting cores

Fig. 4 shows a schematic view of the RBWR-TR, RBWR-TB2, and ABR fuel cycles considered. These three cores are designed to incinerate TRU recovered from LWR UNF and operate on a closed fuel cycle. The first stage consist of a typical PWR fed by 4.5% ^{235}U enriched UOX fuel that is burned up to 50 MWd/kg followed by 10-years cooling. The TRU recovered from the PWR (composition shown in table 5) is used to feed the second stage cores – either one of the RBWRs or the ABR after mixing with thorium (RBWR-TR) or depleted uranium (RBWR-TB2). There are approximately two PWRs per one RBWR of identical electrical power since the support ratio of these RBWR cores is 2 approximately.

Table 5 Composition of TRU extracted from LWR's SNF at discharge burnup of 50 MWd/kg with 10-year Cooling [16]

Isotope	Weight Percent
^{237}Np	4.7%
^{238}Pu	2.2%
^{239}Pu	47.3%
^{240}Pu	22.8%
^{241}Pu	8.4%
^{242}Pu	6.8%

^{241}Am	5.6%
^{243}Am	1.6%
^{244}Cm	0.5%

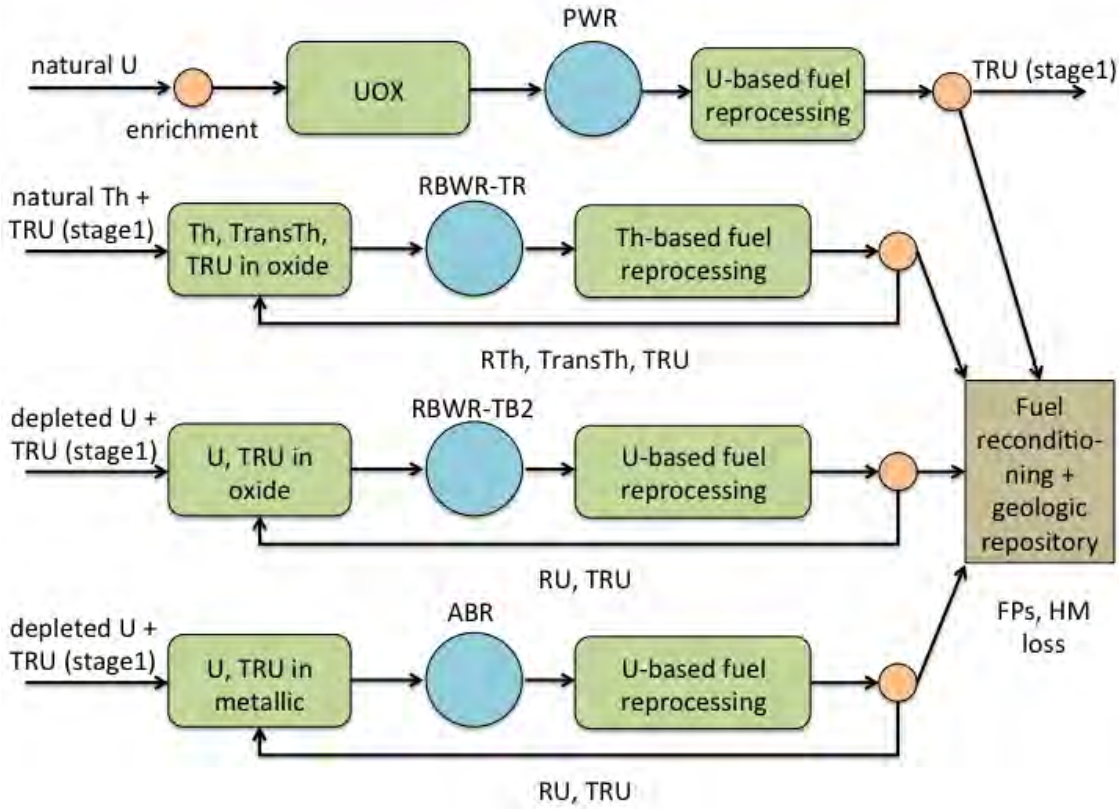

Fig. 4. Schematic view of the RBWR-TR, RBWR-TB2 and ABR fuel cycles

Table 6 compares the performance characteristics of the three TRU transmutation cores. The two RBWR designs feature a similar performance; the most notable differences are the lower TRU fraction in the charge fuel and significantly lower LHGR of the RBWR-TR core. Both cores have smaller burnup and therefore require higher fuel reprocessing and fabrication capacity than the ABR. All three designs have comparable TRU transmutation rate as they all feature a TRU conversion ratio of ~0.5. For this reason they all have a support ratio of about 2; about one third of their total fuel cycle power is generated from stage 2. As the RBWR-TR is operated on a thorium fuel cycle it breeds no plutonium from ^{238}U. As result, the RBWR-TR charge fuel requires only ~15% TRU fraction which is less than half the ~33% requires by both the RBWR-TB2 and ABR. The discharged fuel composition after 5 years cooling is shown in table 7; it is used for later fuel cycle analysis.

Table 6 Performance characteristics of RBWR-TR, RBWR-TB2 and ABR at equilibrium cycle

Parameters	RBWR-TR	RBWR-TB2	ABR
Capacity Factor, %	90	90	85
Average discharge burnup, GWD/t	55.0	65.0	131.9
Specific power, MWt/t	43.8	53.8	105.8
Power density, W/cc	76.3	96.7	130.4
Peak LHGR, W/cm	189	470	327
Number of batches	4	4	6/6/7
Fuel inventory in core, t	89.7	73.0	9.5

Charge fuel mass per batch, t	22.4	18.3	1.7
Fuel residence time, EFFD	1250	1215	1326/1326/1547
Cycle length, EFPD	313	304	221
Burnup reactivity swing, %Δk/k	-2.0	-2.5	-2.9
TRU transmutation rate, kg/GWeYr	453.6	455.3	396.8
TRU transmutation efficiency	48%	44%	45%
Power Fraction, %			
Stage 1 (PWR)	64.4	64.5	61.4
Stage 2	35.6	35.5	38.6
Reprocessing capacity, kg/GWeYr			
SNF from 1st stage	14098.4	14117.0	13435.8
SNF from 2nd stage	6844.7	5777.9	2673.8
Pu from 2nd stage	628.3	1503.8	646.1
TRU from 2nd stage	827.1	1726.8	736.0
Charge mass fraction, %			
- Th232	78.2	-	-
- TransTh	7.4	-	-
- U238	-	67.3	66.7
- TRU	14.4	32.7	33.3
Discharge mass fraction, %			
- Th232	75.7	-	-
- TransTh	7.4	-	-
- U238	-	63.9	59.6
- TRU	12.2	30.0	27.6
- FPs	4.7	6.1	12.8
Fuel mass at time of recycle, %			
- Th232	75.7	-	-
- TransTh	7.5	-	-
- U238	-	64.0	59.7
- TRU	12.1	29.9	27.5
- FPs	4.7	6.1	12.8

Table 7 Discharge fuel composition of RBWR-TR, RBWR-TB2 and ABR after 5 years cooling

Nuclide	RBWR-TR	RBWR-TB2	ABR
TH-232	79.62	0.00	0.00
PA-231	0.05	0.00	0.00
PA-233	0.00	0.00	0.00
U-232	0.03	0.00	0.00
U-233	4.13	0.00	0.00
U-234	2.22	0.13	0.17
U-235	0.80	0.06	0.04
U-236	0.68	0.03	0.07
U-238	0.00	67.95	68.17
Np-237	0.49	0.49	0.46
Pu-238	1.84	2.10	1.14
Pu-239	1.72	8.12	11.42

Pu-240	3.33	12.70	10.53
Pu-241	0.93	1.58	1.42
Pu-242	1.82	3.23	3.19
Am-241	0.80	1.89	1.27
Am-242m	0.04	0.07	0.06
Am-243	0.64	0.82	1.07
Cm-244	0.59	0.57	0.66
Cm-245	0.27	0.18	0.21
Cm-246	0.18	0.07	0.11

5. Nuclear waste analysis

Radioactivity of the UNF and High Level Waste (HLW) was quantified at short term (10 years) and long term (100,000 years) after the fuel is discharged from the cores. 1% of the recycled heavy metals are assumed to get into the HLW stream. ORIGEN 2.2 is used for the decay calculation. In addition to radioactivity, the inhalation toxicity and ingestion toxicity of UNF+HLW are calculated by considering different types of radiation on different parts of the human body. The values of the activity were weighted by the inhalation and ingestion conversion factors (207 fission products and 91 actinides in [17]). Effective inhalation/ingestion coefficients were applied for a typical adult member of the public with median aerodynamic (diameter = 1 μm) radionuclides being inhaled into the blood stream via the lungs. The typical values of inhalation/ingestion coefficients are shown in Table 8. In general, the alpha-emitters heavy metals tend to contribute more radiation damage than most low atomic mass elements (like FPs) that are mostly beta-emitters. The actinides inhaled through lungs are far more hazardous than ingested via stomach [18].

Table 8 Effective inhalation/ingestion coefficients

Dose Conversion Factor (Sv/Bq)	Inhalation	Ingestion
FPs	1.E-5 ~1.E-4	1.E-7 ~ 1.E-6
Actinide	1.E-10 ~ 1.E-8	1.E-10 ~ 1.E-8

5.1 Fuel self-sustaining cores

Fig. 5 displays the radioactivity of SNF+HLW at 10 years and 100,000 years after discharge. In the short term (10 years from discharge), fission products contribute most of the activity for RBWR cores and ARR. Both the ARR and the RBWR-AC are fueled by uranium, and the difference between the ARR and the RBWR-AC is mainly due to the different thermal efficiencies (34.5% for RBWR core vs. 40% for ARR). Between the two RBWR cores, the relatively higher activity of RBWR-SS is primarily attributed to ^{90}Sr, which is generated from the thorium-based fuel cycle 3 times as many as from the uranium fuel cycle per unit of electricity [18].

In the long term (100,000 years from discharge), the waste streams from the two RBWR cores have higher radioactivity than the ARR because of the lower average discharge burnup and therefore higher recycling throughput of the RBWR cores. Between the RBWRs, thorium fuel cycle has much higher long-term activity than the uranium fuel cycle since the long-life ^{233}U lost in the waste stream decays into highly radioactive nuclides such as ^{209}Pb, ^{213}Bi, ^{217}At, ^{221}Fr, ^{225}Ra, ^{225}Ac, and ^{229}Th. The trans-uranium actinides undergo substantial decay by 100,000 years.

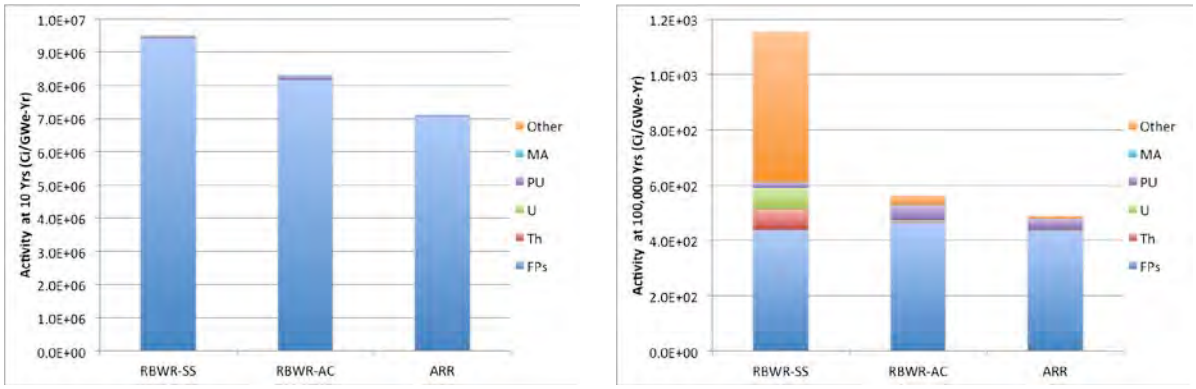

Fig. 5. Radioactivity of the waste stream from RBWR-SS, RBWR-AC and ARR at 10 years (left) and 100,000 years (right)

The inhalation toxicity and ingestion toxicity of the waste streams are compared in fig. 6 and fig. 7. ^{238}Pu, ^{244}Cm, ^{240}Pu, and ^{241}Am are the predominant contributors to inhalation toxicity at 10 years, which is highly demonstrated in the RBWR-AC as more minor actinides are lost via fuel reprocessing. Since the RBWR-SS is fueled by the mixture of depleted uranium and natural thorium, few TRU elements are lost in the waste and the inhalation toxicity of RBWR-SS at 10 years is lower than that of RBWR-AC. The ^{233}U lost from the RBWR-SS contributes very small fraction of the inhalation toxicity. However, at 100,000 years, ^{238}Pu, ^{244}Cm, ^{240}Pu, and ^{241}Am decays out while ^{229}Th – a strong alpha-emitter with half-life of 7340 years – becomes the major contributor to the inhalation toxicity of RBWR-SS. The ARR exhibits the lowest inhalation toxicity at both 10 and 100,000 years due to its high discharge burnup and absence of ^{233}U from uranium fuel cycle.

As the ingestion conversion factors of fission products are generally larger than their inhalation coefficients by a factor of 100, fission products dominate the ingestion toxicity in short term. The comparison of ingestion toxicity shows similar results as the radioactivity at 10 years. As fission products decay out before 100,000 years, heavy metals in the waste stream become the main contributors. The thorium fuel cycle used by the RBWR-SS generates more hazardous nuclides including ^{229}Th, so the total value of RBWR-SS is much higher than those of the RBWR-AC and the ARR.

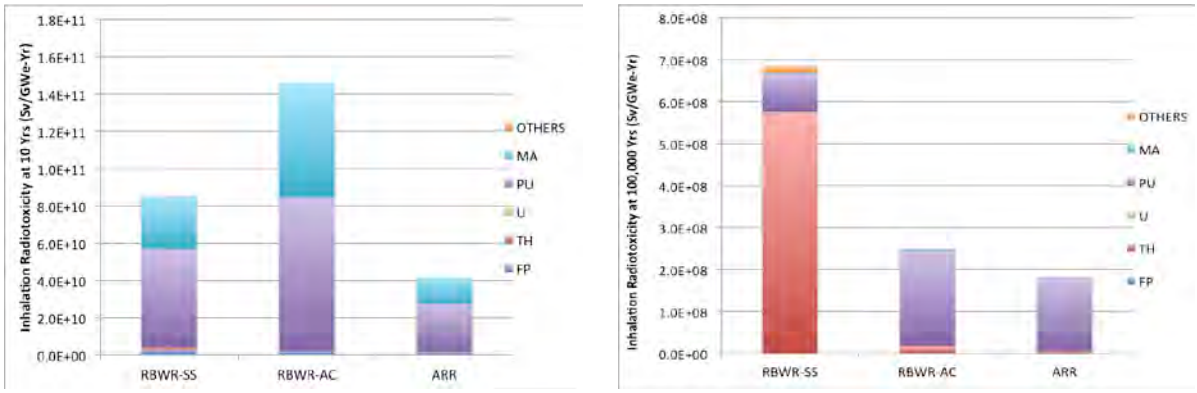

Fig. 6. Inhalation toxicity of the waste stream from RBWR-SS, RBWR-AC and ARR at 10 years (left) and 100,000 years (right)

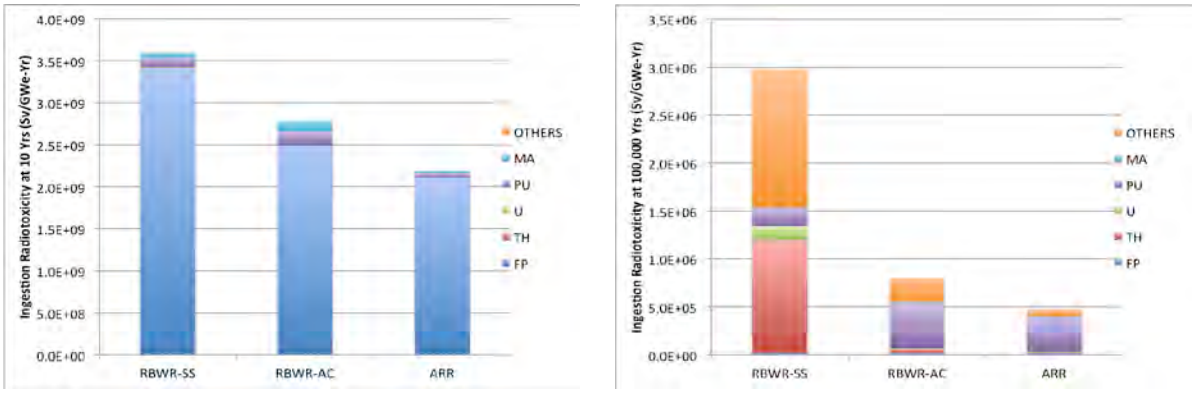

Fig. 7. Ingestion toxicity of the waste stream from RBWR-SS, RBWR-AC and ARR at 10 years (left) and 100,000 years (right)

5.2 TRU transmuting cores

Fig. 8 shows the radioactivity of TRU burner systems at 10 years and 100,000 years. As two thirds of the power is generated from the PWR, the differences between the PWR-RBWR systems and the PWR-ABR system are small. At 100,000 years, the waste from the PWR-RBWR(TR) has a higher radioactivity since the actinides lost from the thorium fuel cycle are more radioactive than those from the uranium fuel cycle.

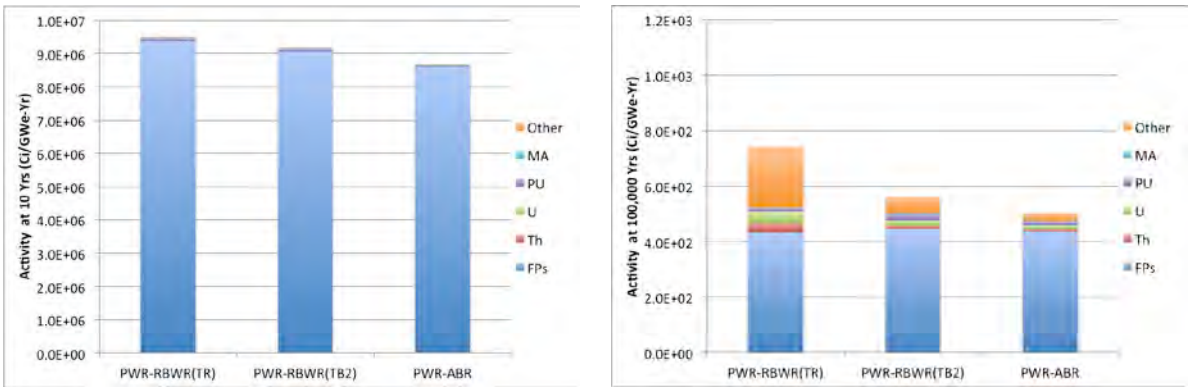

Fig. 8. Radioactivity of the waste stream from RBWR-TR, RBWR-TB2 and ABR at 10 years (left) and 100,000 years (right)

Fig. 9 shows the inhalation toxicity at 10 years and 100,000 years. The fuel discharged from the PWR has much lower Plutonium and MA contents than the fuel discharged from the second stage. As a result, FPs, Plutonium, MA in the discharge fuel from the first stage contribute only few percent of total inhalation toxicity for the two-stage system. The major inhalation toxicity at 10 years comes from the second stage where the discharge fuel has a large fraction of ^{238}Pu and ^{244}Cm. Because of this, the inhalation toxicity of TRU transmuting systems is generally higher than that for fuel self-sustaining systems. In addition, the reprocessing capacities of both the RBWR-TR and the RBWR-TB2 are about three times that for the ABR system such that the ABR features the least inhalation toxicity of the three TRU transmutation systems at 10 years. At 100,000 years, the PWR-RBWR(TR) system has a higher inhalation toxicity due to the hazardous decay daughters of ^{233}U.

Fig. 10 shows the ingestion toxicity of TRU transmutation systems at 10 years and 100,000 years. At 10 years, fission products still dominate the ingestion toxicity so there are no significant differences between the three systems. At 100,000 years, even though only one third of the power is from the thorium fueled RBWR-TR, the hazardous nuclides from thorium fuel cycle results in a larger ingestion toxicity than the two uranium fueled systems.

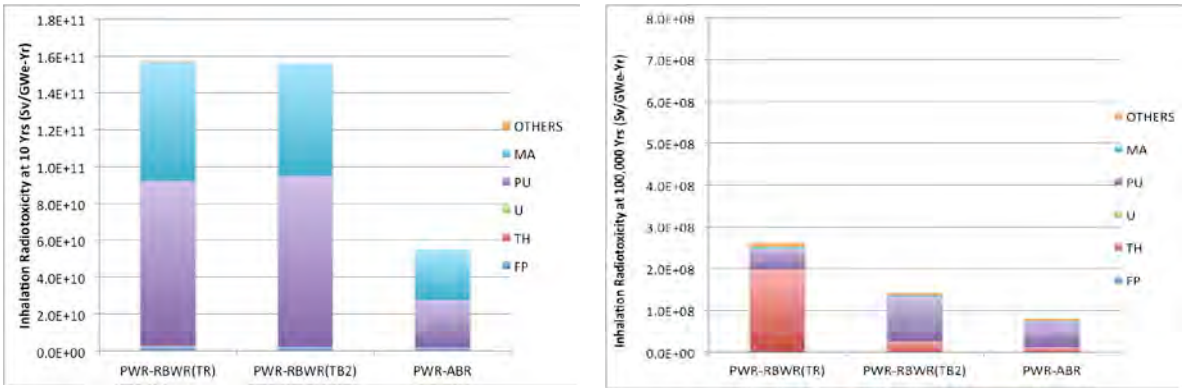

Fig. 9. Inhalation toxicity of the waste stream from RBWR-TR, RBWR-TB2 and ABR at 10 years (left) and 100,000 years (right)

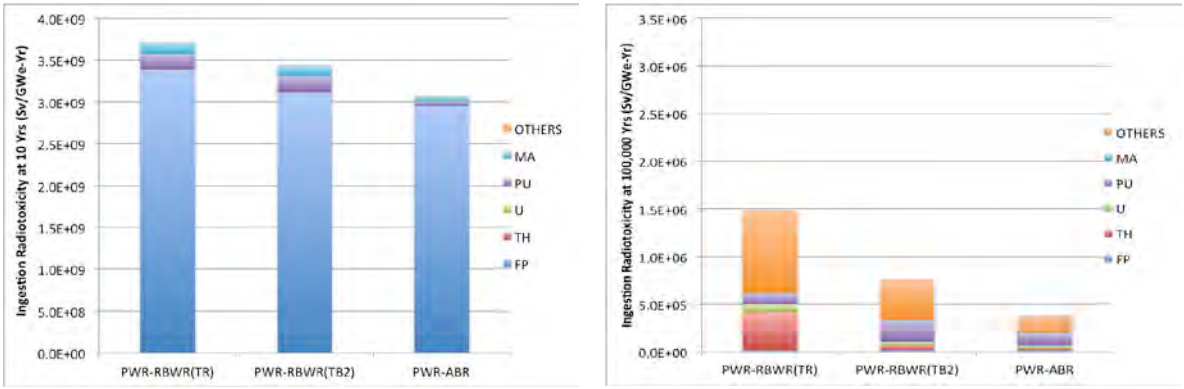

Fig. 10. Ingestion toxicity of the waste stream from RBWR-TR, RBWR-TB2 and ABR at 10 years (left) and 100,000 years (right)

6. Proliferation resistance

The proliferation resistance is mainly evaluated based on the fissile plutonium fraction, specific decay heat of discharged plutonium, spontaneous fission rate, plutonium inventory, ^{238}Pu/Pu ratio, and ^{232}U/^{233}U ratio. ^{238}Pu, ^{240}Pu, and ^{242}Pu have high spontaneous neutron generation which significantly reduces the nuclear explosive yield; ^{238}Pu has a large decay heat to further complicate the design of an explosive device [19]. Although the effectiveness of plutonium for weapon purposes varies significantly with its isotopic composition, it is usually not realistic to apply plutonium for weapon use when the fraction of ^{238}Pu is beyond 2% of the total plutonium [20].

As to the thorium fuel cycle, it seems to be no more proliferation resistant than conventional uranium cycle [21]. ^{233}U extracted from thorium fuel cycle is applicable for weapon use because the critical mass of ^{233}U is close to that of ^{239}Pu while spontaneous fission rate is much lower [22]. Nevertheless, the decay chain of co-product ^{232}U produces penetrating 2.6 MeV gamma rays from ^{208}Tl and makes ^{233}U less desirable as weapon materials due to the significant radiation dose. It is very difficult to separate ^{232}U from ^{233}U considering the close atomic mass. For ^{233}U containing ^{232}U, the buildup in dose rate with time reflects the in-growth of ^{228}Th that ^{232}U and ^{229}Th have half-life times of 68.9 years and 1.9 years, respectively. Then, ^{228}Th decays to ^{208}Tl immediately as the decay daughters of ^{228}Th have short half-life times. After this in-growth, the dose rate from ^{233}U contaminated by 1ppm ^{232}U is about the same as from reactor-grade plutonium [22]. However, to achieve the IAEA criterion for self-protection of 100-rem per hour at 1 meter [22], the level of ^{232}U needs be 2.4% [22]. Despite this, a more recent study [23] by Los Alamos National Laboratory concludes that, in general, dilution with ^{238}U or ^{232}Th increases the bare critical mass and reduces the

attractiveness of the material to a sub-state actor. With >80% ^{238}U or 70% ^{232}Th, the material is unattractive.

6.1 Fuel self-sustaining cores

Table 9 shows the proliferation resistance metrics of the three cores. The ARR has the highest fissile plutonium fraction due to its harder neutron spectrum. The plutonium from the RBWR-SS has the highest ^{238}Pu/Pu ratio and the highest specific decay heat along with highest spontaneous fission rate. The ^{238}Pu/Pu ratio of both the RBWR-SS and the RBWR-AC are above the threshold value of 2% so that the discharged plutonium is considered to be not practical for weapon purpose. The plutonium from ARR does not meet this threshold value after 5-years cooling time. Moreover, as the RBWR-SS is fed with a mixture of thorium and depleted uranium, its plutonium throughput per unit of electricity is smallest among the three designs. However, the RBWR-SS has the potential proliferation issue of ^{233}U. The concentration of ^{232}U in the discharged ^{233}U is 5429 ppm, well above the contamination level that remote production operations would be required to extract ^{233}U on a large scale without incurring large occupational dose [22]. The dilution with ^{238}U adds extra difficulty to extract ^{233}U for weapon-use due to the large critical mass. In fact, the fissile U/U ratio is close to the definition of low enriched ^{233}U fuel – 12% [24]. Overall, the RBWR-SS tends to be more proliferation resistance compared with the ARR.

Table 9 Proliferation resistance metrics of RBWR-SS, RBWR-AC and ARR

Metrics	RBWR-SS	RBWR-AC	ARR
Fissile plutonium fraction at reprocessing, %	55%	52%	69%
^{238}Pu/Pu ratio at reprocessing, %	6.4%	3.2%	1.4%
Specific decay heat of plutonium at reprocessing, W/kg	39.7	22.0	11.2
Spontaneous fission neutrons per kg Pu at reprocessing, n/sec-kg	5.6E+05	5.3E+05	3.3E+05
Tot. plutonium reprocessed, tons/GWe-yr	1.04	2.72	1.64
Pu/^{238}U ratio at reprocessing	23.0%	14.0%	16.9%
^{232}U/^{233}U ratio at reprocessing, ppm	5429	-	-
Fissile U[4]/U ratio at reprocessing, %	17%	-	-
Fissile U/Th ratio at reprocessing	7%	-	-
(Pu+fissile U)/(^{238}U+Th) ratio at reprocessing	10%	14%	17%

6.2 TRU transmuting cores

The proliferation resistance metrics of the fuel discharged from the RBWR-TR, the RBWR-TB2 and ABR are given in table 10. Compared with the fuel self-sustaining designs (table 9), the discharge plutonium from the TRU transmuting cores contains less fissile isotopes due to two reasons: softer neutron spectrum and higher discharge burnup. The plutonium is discharged with a burnup of 50 MWd/kg from the first stage PWRs that have a thermal neutron spectrum and burned up to additional 50-60 MWd/kg in the intermediate-spectrum RBWR cores or to ~130 MWd/kg in the fast-spectrum ABR of the second stage. Due to the higher cumulative burnup, the ^{238}Pu/Pu ratio of TRU transmutation cores is generally higher than those of the fuel self-sustaining cores. The ^{238}Pu/Pu ratio in the fuel discharged from all the TRU transmuting cores is above the 2% threshold that makes the plutonium not practical for weapon-use. Although the RBWR-TR has to reprocess more plutonium per unit of electricity compared with the RBWR-SS, the high specific decay heat of its discharged plutonium complicates the design of explosive device. As the RBWR-TR is not fed with ^{238}U, the fissile U/U ratio is well above the definition of low enriched ^{233}U fuel – 12% [24]. It requires

[4] Fissile uranium includes ^{233}U, ^{235}U, and ^{237}U.

physical-protection to prevent the discharged ^{233}U from potential weapon-use. However, the ratio of fissile uranium over thorium is 6% – well increasing the critical mass and reducing the attractiveness of the fissile uranium [23]. At the same time, the ^{233}U is highly contaminated by ^{232}U so it will feature a large radiation dose.

Table 10 Proliferation resistance metrics of RBWR-TR, RBWR-TB2 and ABR

Metrics	RBWR-TR	RBWR-TB2	ABR
Fissile plutonium fraction at reprocessing, %	27%	35%	46%
$^{238}Pu/Pu$ ratio at reprocessing, %	19.1%	7.6%	4.1%
Specific decay heat of plutonium at reprocessing, W/kg	111.46	46.95	26.94
Spontaneous fission neutrons per kg Pu at reprocessing, n/sec-kg	1.1E+06	8.1E+05	6.5E+05
Tot. plutonium reprocessed, tons/GWe-yr	1.76	4.23	1.67
$Pu/^{238}U$ ratio at reprocessing	Infinite	40.8%	40.6%
$^{232}U/^{233}U$ ratio at reprocessing, ppm	8053	-	-
Fissile U/U ratio at reprocessing, %	63%	-	-
Fissile U/Th ratio at reprocessing	6%	-	-
(Pu+fissile U)/(^{238}U+Th) ratio at reprocessing	17%	41%	41%

7. Fuel cycle cost

The economics of nuclear power plants are usually measured by the levelized electricity cost, which is composed of the capital cost, operation-and-maintenance (O&M) cost, and fuel cycle cost. Due to the large uncertainty in the RBWR and SFR capital and O&M cost, this analysis focuses on the fuel cycle cost, accounting for both front-end and back-end cost components. Due to the high fissile contents in the discharged fuel, aqueous reprocessing and low enriched UOX fabrication technology developed for conventional PWR fuel may not be applicable for RBWRs. This study assumes that the RBWR discharged fuel undergoes electro-chemical reprocessing and remote fuel fabrication, as planned for the SFRs based on the EBR-II project in the US. The nominal values reported in [25] and reproduced in Table 11 are used for the cost of major activities. The costs for innovative reactor technology usually involve large uncertainties due to lack of commercial experience. Nevertheless, sensitivity analysis is beyond the scope of this preliminary comparison.

Table 11. Costs of Major Fuel Cycle Activities [25]

Activities of Fuel Cycle	**Cost**
Natural uranium mining and milling, $/kg U	60
Natural thorium mining and milling, $/kg Th	100
Conversion processes, $/kg U or Th	10
Enrichment, $/SWU	105
LWR UO_2 fuel fabrication, $/kg U	240
UREX aqueous separation, $/kg HM	1,000
Electro-chemical reprocessing & remote fuel fabrication, $/kg HM	5,000
SNF conditioning/packaging/disposal, $/kg HM	1100
RU conditioning, $/kg HM	93
Aqueous HLW conditioning/storage/packaging (FPs+Ln), $/kg FPs	2,000
Geologic repository (HLW FPs+Ln+Tc), $/kg FPs	10,000

7.1 Fuel self-sustaining cores

Fig. 11 compares the fuel cycle cost of the RBWR-SS, the RBWR-AC, and the ARR. About 90% of the total cost of these closed fuel cycles comes from fuel reprocessing and remote fabrication. The capacity for reprocessing and remote fuel fabrication is inversely proportional to the average discharge burnup and, therefore, both RBWR designs have higher fuel cycle cost than the ARR. Of the two RBWR designs, the fuel cycle cost of RBWR-SS is slightly lower than that of RBWR-AC due to the relatively higher average discharge burnup.

Since the RBWR design is based on the well-proven commercial ABWR technology, it is likely that their commercialization will require a smaller investent in R&D and their capital cost may be smaller than of the SFRs. This might partially compensate the higher fuel cycle cost of the RBWRs.

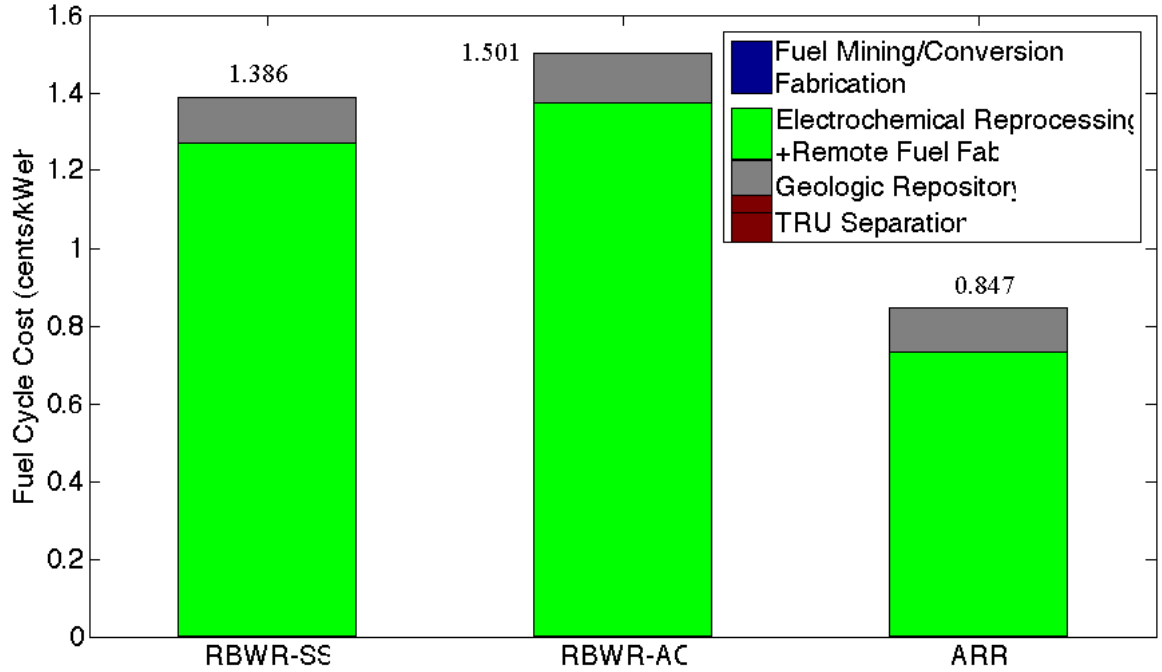

Fig. 11. Fuel cycle costs of RBWR-SS, RBWR-AC, and ARR

7.2 TRU transmuting cores

The fuel cycle costs for the transmuting reactors are compared in fig. 12. These include the cost of activities for both stages of the fuel cycle – PWR and TRU transmuting systems. Compared with the fuel self-sustaining designs (fig.11), the fuel cycle cost of the 2-stage systems is significantly lower. This is primarily because about two thirds of these systems power is generated from PWR and the fuel cycle cost of the PWR is significantly lower. This significantly reduces the capacity required for electro-chemical processing and of TRU-containing fuel fabrication which are about five times more expensive than UREX processing and UOX fuel fabrication (table 11). Moreover, the TRU transmuting reactors tend to discharge their fuel at a high average burnup which further reduces the recycling capacity required for the second stage.

The smaller reprocessing capacity for the ABR, due to its substantially higher average discharge burnup, contributes the lowest fuel cycle cost compared with that of the two RBWR systems. Similarly, the PWR-RBWR(TB2) system has a lower fuel cycle cost than the PWR-RBWR(TR) system due to the difference in Stage 2 discharge burnup. Even though the fuel cycle cost of the PWR-ABR system is lower than of the PWR-RBWR systems, the levelized cost of electricity of the PWR-RBWR

systems is expected to be lower as past economic analyses concluded that the capital cost of SFRs is higher than that of LWRs.

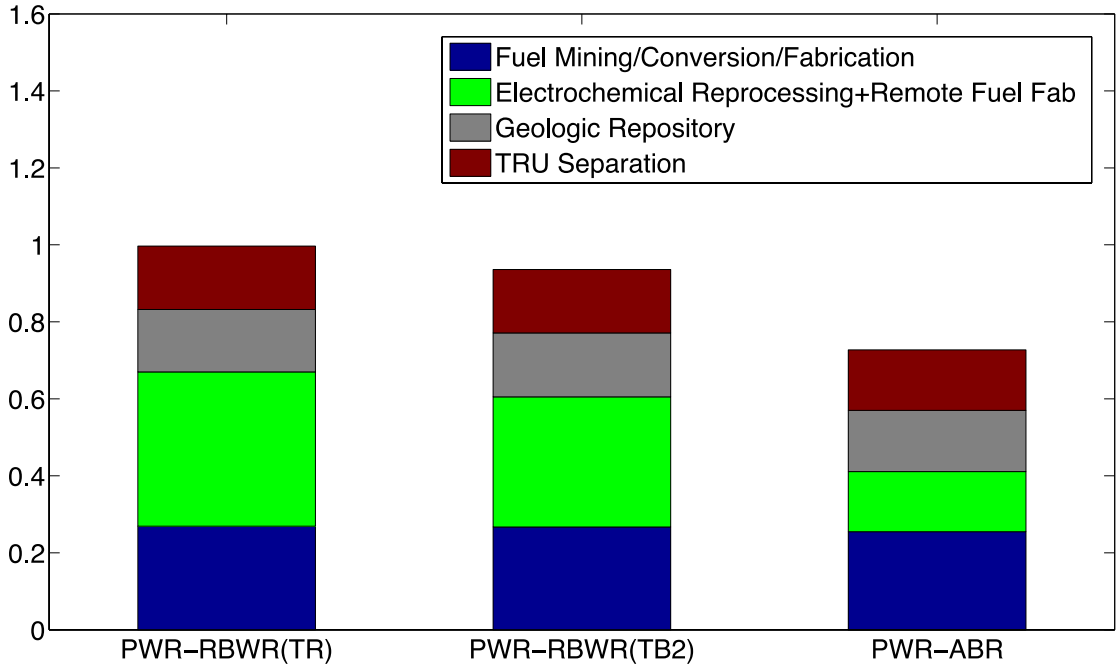

Fig. 12. Fuel cycle costs of RBWR-TR, RBWR-TB2, and ABR

8. Fuel cycle evaluation

The comprehensive fuel cycle evaluation methodology developed by Nuclear Fuel Cycle Evaluation and Screening (FCE&S) campaign [10] is applied to further evaluate the RBWR-based fuel cycles. These criteria include nuclear waste management, environmental impact and resource utilization. Each evaluation criterion is composed of several evaluation metrics defined in [10] appendix A. The detailed impact factors, like water use for uranium enrichment and radiological dose for fuel reprocessing, are summarized in [10] appendix C. To account for uncertainties and differences in calculation approaches, each calculated metric is assigned with a letter score based on a binned approach defined in [10] appendix D such that two systems exhibit same performance for that metric if the calculated metric values fall within the same bin range. This method will help to find whether RBWRs can accomplish the missions previously assigned to SFRs as attractive as the SFRs.

As the fuel cycle metrics were developed to identify the promising fuel cycle options, the different thermal efficiency introduces potential bias over the Evaluation Groups (EG). To avoid this, the FCE&S campaign decided to renormalize the mass flow rate to a uniform thermal efficiency of 33%. Analytical formulas were developed for this re-normalization to modify the mass flow and power sharing between reactors in different stages of the fuel cycle options. The general formulas are defined in [10] appendix D:

$$F_k^n = \frac{\omega_k}{\sum_i \omega_i F_i^o} F_k^o$$

$$M_k^n = \frac{1}{\sum_i \omega_i F_i^o} M_k^o$$

where the superscripts of “n” and “o” indicate the new and original thermal efficiencies, respectively, and the subscript “k” and “i” denotes the stage number,

F_k^n = Power-sharing fraction of k-th stage with new thermal efficiency,

F_k^o = Power-sharing fraction of k-th stage with original thermal efficiency,

M_k^n = Mass data of k-th stage with new thermal efficiency,

M_k^o = Mass data of k-th stage with original thermal efficiency,

ω_k = New to original thermal efficiency ratio of k-th stage ($\frac{\eta_k^n}{\eta_k^o}$),

η_k = Thermal efficiency of stage k reactor.

8.1 Fuel self-sustaining cores

The ARR discussed in previous sections is referred by the FCE&S as Evaluation Group 24 (EG24): "continuous recycle of TRU/U in SFR". It is concluded to be the most promising fuel cycle out of the 40 EGs options examined in terms of nuclear waste and long-term energy sustainability [10]. The mission of the RBWR-AC is the same as of the EG24 while using the ABWR technology. The RBWR-SS is fueled by a mixture of thorium and depleted uranium and may be compared with EG28: "continuous recycle of ^{233}U/Th in SFR."

Since the fuel self-sustaining cores involve only one stage, the mass flow data of the systems are renormalized to a thermal efficiency of 33%. Table 12 compares the evaluation of the RBWR-SS, RBWR-AC, EG24 and EG28 fuel cycles based on the criteria of nuclear waste management, environmental impact, and resource utilization. It found that the RBWR-AC could successfully deliver the same functions previously demonstrated by ARR. It generates a little bit more LLW since it is still accounted as LWR technology, which degrades the evaluation score. The RBWR-AC design is able to support the long-term energy sustainability with high fuel utilization. Since both thorium and uranium fuel cycles are applied for RBWR-SS, the high radioactivity at 100,000 years observed in section 5.1 receives a score of "C", which is between the corresponding scores of EG24 – "B" and EG28 – "D". The nuclear waste management of the RBWR-SS is generally worse than EG24 but better than EG28. RBWR-SS is expected to show same environmental impact as EG24 and the lowest amount of natural uranium required per unit of electricity compared with the RBWR-AC and the ARR. Based on the economics analysis in section 7.1, the fuel cycle cost of fuel self-sustaining SFR is cheaper than those of RBWR designs but the capital cost of the RBWRs may be lower. Also, RBWRs are based on the mature technology of ABWR while commercialization of SFR technology is likely to require significantly more investment in R&D [10].

Fig. 13 compares the score of each of the 40 evaluation groups received by E&S team [10] in terms of benefit they offer versus technological challenge for implementation. EG24 scores a benefit of 0.81 (1.0 means the highest benefit), the highest value out of 40 evaluation groups, and a challenge of 0.32 (1.0 is the least challenging). For comparison, the contemporary once-through LWRs (EG01) scored a benefit of 0.45 and a challenge of 1.0. Another EG of interest is EG22 – continuous recycling of TRU in PWR (the E&S study considered PWR as representative of LWR). It scored a benefit of 0.55 and a challenge of 0.42. It is expected that the fuel self-sustaining RBWR cores will score the benefit of EG24 (0.81) and a challenge somewhat lower than of EG22 (0.42); thorium-based systems score a somewhat lower challenge value (larger challenge) than uranium-based systems. This is due primarily to lack of commercial experience in the reprocessing and recycling of thorium fuel.

Table 12 Evaluation of RBWR-SS, RBWR-AC, and ARR fuel cycle

	Metric	Metric/Bin	Metric/Bin	Metric/Bin	Metric/Bin
		RBWR-SS	RBWR-AC	EG24	EG28
Renormalization Factor		1.045	1.045	1.21	1.21
Nuclear Waste Management	Mass of SNF+HLW disposed, t/GWe-yr	1.26/A	1.37/A	1.34/A	1.58/A
	Activity of SNF+HLW (@100 years), MCi/GWe-yr	1.11/C	0.98/B	1.04/B	1.18/C
	Activity of SNF+HLW (@100,000 years), 10^{-4} MCi/GWe-Yr	12.1/C	5.9/B	6.06/B	30.1/D
	Mass of DU+RU+RTh[5] disposed, t/GWe-yr	0.0/A	0.0/A	0.0/A	0.0/A
	Volume of LLW, m^3/GWe-yr	710.3/D	742.6/D	561.42/C	1168.72/D
Environmental Impact	Land use per energy generated, km^2/GWe-yr	0.08/A	0.08/A	0.082/A	0.086/A
	Water use per energy generated, ML/GWe-yr	23722.9/B	23724.8/B	23717/B	23748/B
	Radiological exposure, Sv/GWe-yr	1.00/B	1.03/B	1.21/B	1.24/B
	Carbon emission - CO_2 released per energy generated, kt CO_2/GWe-yr	33.4/B	35.3/B	24.1/A	50.1/B
Resource Utilization	Natural Uranium required per energy generated, t/GWe-yr	0.38/A	1.12/A	1.37/A	0.00/A
	Natural Thorium required per energy generated, t/GWe-yr	0.69	0.00	0.0	0.0

[5] Depleted Uranium (DU) + Recycled Uranium (RU) + Recycled Thorium (RTh)

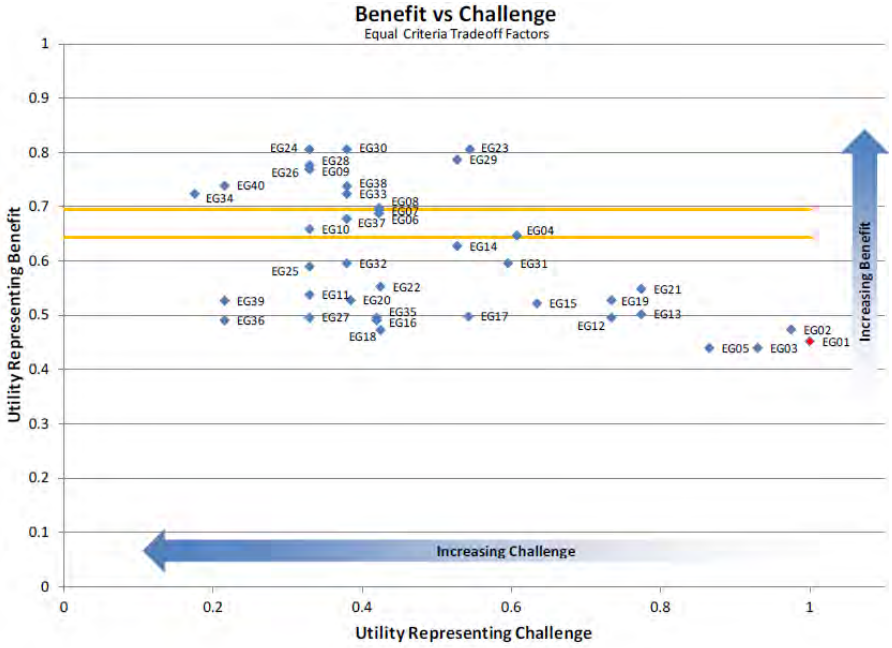

Fig. 13 E&S summary of benefits versus technological challenges of the 40 Evaluation Groups [10]. The PWR-ABR system is EG32; the uranium fueled self-sustaining SFR is EG24; the thorium fueled self-sustaining SFR is EG28.

8.2 TRU transmuting cores

The PWR-ABR system is defined in FCE&S as EG32: “continuous recycle of TRU/U from PWR in SFR burner” [10]. This fuel cycle option is designed to maintain current PWR technology while reducing the amount of nuclear waste from the first stage. It also improves the fuel utilization as the second stage reactors generate additional energy from the LWR UNF. The uranium fueled RBWR-TB2 offers the same functions as the ABR of EG32 by using LWR technology while RBWR-TR is fueled by thorium. The power fraction of the first stage (table 6) is multiplied by the renormalization factor when the thermal efficiency of reactor on the second stage is adjusted to 33%. Table 13 summarizes the evaluation results of the RBWR-TR, the RBWR-TB2, and the ABR two-stage fuel cycles. Both the RBWR-TR and the RBWR-TB2 get very similar scores as EG32 so most functions demonstrated by the ABR could be accomplished by the RBWRs. Some metrics of the RBWR designs are even better than the ABR but this is probably due to the bin range set by FCE&S campaign and the differences are very small. The economics of TRU transmuting RBWRs are improved and close to that of corresponding SFR technology. It is likely that the levelized cost of TRU transmuting RBWRs, after including the capital cost, will be lower than of the SFR technology.

According to the FCE&S report [10], EG32 scored a benefit of 0.6 and a challenge of 0.38. As LWR technology applied, the TRU transmuting RBWRs is expected to score a benefit of EG32 (0.6) and a challenge of EG22 (0.42), a slightly smaller challenge than of the PWR-ABR system.

Table 13 Evaluation of RBWR-TR, RBWR-TB2 and ABR fuel cycle

	Metric	Metric/Bin	Metric/Bin	Metric/Bin
		PWR-RBWR(TR)	PWR-RBWR(TB2)	EG32
Renormalization Factor (stage 1)		1.016	1.016	1.07
Nuclear Waste Management	Mass of SNF+HLW disposed, t/GWe-yr	1.26/A	1.28/A	1.32/A
	Activity of SNF+HLW (@100 years), MCi/GWe-yr	1.06/C	1.03/B	1.08/C
	Activity of SNF+HLW (@100,000 years), 10^{-4} MCi/GWe-Yr	7.4/B	5.6/B	5.19/B
	Mass of DU+RU+RTh disposed, t/GWe-yr	117.5/D	117.5/D	127.15/E
	Volume of LLW, m^3/GWe-yr	688.4/D	670.0/D	579.27C
Environmental Impact	Land use per energy generated, km^2/GWe-yr	0.14/B	0.14/B	0.13/B
	Water use per energy generated, ML/GWe-yr	23829.2/B	23828.4/B	23838/B
	Radiological exposure, Sv/GWe-yr	1.02/B	1.01/B	1.13/B
	Carbon emission - CO_2 released per energy generated, kt CO_2/GWe-yr	45.9/B	44.9/B	41.6/B
Resource Utilization	Natural Uranium required per energy generated, t/GWe-yr	118.4/C	118.6/C	128.5/C
	Natural Thorium required per energy generated, t/GWe-yr	0.2	0.0	0.0

9. Conclusions

This paper compares (1) a thorium fueled self-sustaining Reduced-moderation Boiling Water Reactor core design (RBWR-SS) with a couple of previously designed self-sustaining reactors – the Hitachi designed RBWR-AC and the ANL designed Sodium-cooled Fast Reactors (ARR); and (2) a thorium fueled BWR core designed for transmutation of LWR TRU (RBWR-TR) with the Hitachi designed RBWR-TB2 and the ANL designed ABR. The comparison includes basic design parameters, core performance characteristics, fuel cycle characteristics and overall fuel cycle evaluation.

The overall performance of the thorium fueled RBWR and their uranium fueled RBWR counterparts is similar. Relative to the Hitachi (uranium-based) RBWR cores, the thorium-based cores have significantly longer seed (driver) fuel without central axial blanket and, therefore, significantly lower peak linear heat generation rate; more stable axial power distribution along with larger safety margins; higher short term radioactivity and ingestion radio-toxicity of the HLW, primarily, due to the ~3 times higher yield of ^{90}Sr from fissions of ^{233}U; lower short-term inhalation radio-toxicity due to smaller fraction of Pu and MA in the waste; higher long term radioactivity and radio-toxicity due to decay products of the long-lived ^{233}U; smaller throughput of Pu and MA, lower (fissile Pu)/Pu ratio, higher ^{238}Pu/Pu ratio, higher specific decay heat of the Pu, higher spontaneous fission rate of the Pu, significant amount of recycled ^{233}U. The ^{233}U discharged from RBWR-SS and RBWR-TR is contaminated with significant concentration of ^{232}U whose decay daughters are strong gamma

emitters. This provides certain proliferation resistance but the high $^{233}U/U$ ratio in RBWR-TR requires extra physical protection.

Due to their softer neutron spectra all the RBWR cores feature a significantly lower average discharge burnup than their SFR counterparts. This, along with their smaller thermal efficiency, lead to a significantly larger capacity required for fuel recycling that result in a higher fuel cycle cost and less favorable waste characteristics – higher radioactivity along with higher inhalation and ingestion toxicity. On the other hand, the plutonium discharged from the RBWR cores has a lower fissile/total Pu ratio, a larger $^{238}Pu/Pu$ ratio and, therefore, a higher specific decay heat along with higher spontaneous fission rate making this plutonium of lower attractiveness for weapon-use than the Pu recycled from the SFR.

Relative to the self-sustaining reactors, the TRU transmuting reactors tend to have a higher discharge burnup and therefore smaller recycling capacity and lower fuel cycle cost. Particularly smaller is the fuel cycle cost of a two-stage energy system consisting of PWR and a transmuting reactor; the support ratio is ~2:1. However, the fuel utilization of these 2-stage energy systems is on the order of only 1% of the fuel utilization of the self-sustaining energy systems. The plutonium discharged from the TRU burners has lower fissile plutonium, a larger $^{238}Pu/Pu$ ratio and larger specific decay heat than plutonium from the fuel self-sustaining core. Only the two RBWR out of the three fuel self-sustaining cores satisfy the definition of unattractive plutonium while all the three TRU burners generates unattractive plutonium.

In the overall fuel cycle evaluation the RBWR-based fuel cycles score similarly to SFR-based fuel cycles in terms of nuclear waste management, environmental impact, and resource utilization. However, a thorough technology maturity and economic analysis are needed in order to complete the comparison of the RBWR and SFR technologies.

Acknowledgements
This research was performed using funding received from the DOE Office of Nuclear Energy's Nuclear Energy University Programs. An ongoing project is being funded by Hitachi Ltd. Collaborations with Argonne National Laboratory are appreciated.

References
1. EPRI Report, Technical Evaluation of the HITACHI Resource-Renewable BWR (RBWR) Design Concept, in EPRI Report number 1025086 (2012). 2012.
2. T. Hino, M. Ohtsuka, R. Takeda, J. Miwa, Y. Ishii, Core Designs of RBWR (Resource-renewable BWR) for Recycling and Transmutation of Transuranium Elements - an Overview. in ICAPP. 2014. Charlotte, USA, April 6-9, 2014.
3. P. Gorman, S. Bogetic, J. Hou, G. Zhang, J. Vujic, E. Greenspan, Thorium Fueled Resource-Renewable BWR (RBWR) Design Update, in Anaheim, USA, Transactions of the American Nuclear Society. 2014.
4. C. R. Varela, J. Seifried, J. Vujic, E. Greenspan, Sensitivity of thorium-fueled reduced moderation BWR performance to void fraction correlation. In Atlanta, USA, Transactions of the American Nuclear Society. 2013.
5. G. Zhang, J. Seifried, J. Vujic, E .Greenspan, Variable Enrichment Thorium-Fueled Boiling Water Breeder Reactor. In Atlanta, USA, Transactions of the American Nuclear Society, 2013. 108: p. 846-8.
6. G. Zhang, J. Seifried, J. Vujic, E .Greenspan, Analysis of Local Void Reactivity Coefficients for the RBWR-Th. Transactions of the American Nuclear Society, 2013. 108: p. 849-52.
7. P.M. Gorman, J.L. Vujic, E. Greenspan, Tradeoff Studies for the Fuel-self-sustaining RBWR-Th Core. Nuclear Technology, 2015 (article in press).

8. E.A. Hoffman, W.S. Yang, R.N. Hill, Preliminary Core Design Studies for the Advanced Burner Reactor over a Wide Range of Conversion Ratios. 2006, U. S. Department of Energy, Office of Nuclear Energy, Science and Technology.
9. A.E. Dubberley, K. Yoshida, C.E. Boardman, T. Wu, SuperPRISM Oxide and Metal fuel core designs, in ICONE 8. 2000: MD,USA.
10. R. Wigeland, T. Taiwo, H. Ludewig, M. Todosow, W. Halsey, J. Gehin, R. Jubin, J. Buelt, S. Stockinger, K. Jenni, B. Oakley, Nuclear Fuel Cycle Evaluation and Screening – Final Report. 2014, US DOE.
11. P.M. Gorman, S. Bogetic, J.E. Seifried, G. Zhang, C.R. Varela, M. Fratoni, J.L. Vujic, E. Greenspan, K. Shirvan, Al. Mieloszyk, M. Kazimi, Self-sustaining Thorium-fuelled Reduced Moderation Boiling Water Reactors (RBWR-Th) Design (attachment 5).
12. P.M. Gorman, S. Bogetic, J.E. Seifried, G. Zhang, C.R. Varela, M. Fratoni, J.L. Vujic, E. Greenspan, K. Shirvan, Al. Mieloszyk, M. Kazimi, TRU-burning Thorium-fuelled Reduced Moderation Boiling Water Reactors (RBWR-TR) Design (attachment 6).
13. J.E. Seifried, P.M. Gorman, J.L. Vujic, E. Greenspan, Accelerated Equilibrium Core Composition Search Using a New MCNP-Based Simulator, in Joint International Conference on Supercomputing in Nuclear Applications + Monte Carlo (SNA&MC) Conference. 2013.
14. private communication with Dr. E.A. Hoffman. 2014.
15. K. Shirvan, N. Andrews, M.S. Kazimi, Best Estimate Void Fraction and Critical Power Correlations for Tight Lattice BWR Bundles, in ICAPP. 2013: Jeju Island, Korea. p. Paper No. FA159.
16. T.K. Kim, W. S. Yang, C. Grandy, R. N. Hill, Core design studies for a 1000 MWth Advanced Burner Reactor. Annals of Nuclear Energy, 2009. **36**(3): p. 331-336.
17. K. Eckerman, J. Harrison, H.G. Menzel, C.H. Clement, Compendium of Dose Coefficients based on ICRP Publication 60, in ICRP Publication 119. Ann. ICRP 41. 2012.
18. N. E. Stauff, T.K. Kim, T.A. Taiwo, Variations in Activity, Toxicity and Decay Heat of Nuclear Waste of Various Fuel Cycles, in PHYSOR 2014. 2014: Kyoto, Japan.
19. Z. Xu, M.S. Kazimi, M.J. Driscoll, Impact of high burnup on PWR spent fuel characteristics. Nuclear Science and Engineering, 2005. **151**(3): p. 261-273.
20. B. Pellaud, Proliferation Aspects of Plutonium Recycling. Journal of Nuclear Materials Management, 2002. **31**(1): p. 30-38.
21. D. Greneche, The Thorium Cycle: An Assessment of Its Potentialities with a Focus On Non proliferation Aspects. in 2006 Winter Meeting of the American Nuclear Society. 2006. Albuquerque, NM.
22. J. Kang, F.N. Von Hippel, U-232 and the Proliferation-Resistance of U-233 in Spent Fuel. Science & Global Security, 2001. **9**: p. 1-32.
23. C.G. Bathke, H.R. Trellue, B.B. Ebbinghaus, B.A. Collins, A.W. Prichard, B.W. Smith, An Assessment of the Attractiveness of Material Associated with Thorium Fuel Cycles, in Transactions of the American Nuclear Society. 2014: Anaheim, California.
24. IAEA report, Thorium fuel cycle potential benefits and challenge. 2005.
25. D.E. Shropshire, K.A. Williams, E.A. Hoffman, J.D. Smith, D.J. Hebditch, J.J. Jacobson, J.D. Morton, A.M. Phillips, J.P. Taylor, Advanced Fuel Cycle Economic Analysis of Symbiotic Light-Water Reactor and Fast Burner Reactor Systems. 2009, Idaho National Laboratory.

Attachment 9

For NEUP Project # 11-3023: Self-sustaining thorium boiling water reactors

Technical Gap Analysis and Roadmap Development

The objective of this task is to perform a thorough viability and applicability assessment of the thorium-based RBWR reactor concepts identified along with their associated fuel cycle, a detailed technology gap analysis, and a comprehensive technology development roadmap. Viability issues of the RBWRs identified but were not resolved in this project are identified in Section 1. Future undertakings recommended for resolving these viability issues are suggested in Section 2.

1. Issues/Gap Analysis

The RBWR design described in the previous sections employs a tight lattice cooled by light water to produce a hard enough neutron spectrum to enable the RBWR to perform functions traditionally assigned to fast spectrum reactors -- sustainability (conversion ratio ~1.0) and transmutation of TRU from LWR. The design is essentially a new fuel/reactor core rather than a new reactor and is intended to fit within the pressure vessel of an ABWR. The core design is significantly different from a conventional ABWR (or any other light-water reactor) and the operating parameters and environment present new challenges. The following subsections describe the issues identified to have a technology gap that will have to be further addressed in followup studies.

1.1 Mechanical Design/Fabrication/Performance

The fuel rods, hexagonal assembly lattice and Y-shaped control rods are significantly different from those of an ABWR. The Y–shaped along with thinner thickness of the control rods could make the hydraulic drive designs challenging to ensure proper insertion at all Anticipated Operational Occurrences (AOO). The specific rod diameter and pitch-to-diameter ratio depend on whether the system is intended to be self-sustaining or a burner, and the thermal-hydraulic correlations employed in the design. The smaller cladding thickness of RBWR-Th Y-CISE/LAPG is beyond the current experience base with fabrication of Zircaloy cladding. As shown in Table 1, these parameters tend to be closer to those of a sodium fast reactor than an ABWR. The active length of the fuel rods of one variant of the RBWR core are significantly longer than that of an SFR but not longer than that of the ABWR. The longer non-active fuel length of the RBWR-Th designs compared to ABWR could require different upper assembly and core support structure. Whether grid spacers or wire-wrap are used will affect the mechanical “rigidity” of the assembly under operating, refueling and transportation conditions. On the other hand, the total coolant flow rate has also been reduced while the steam velocity has increased due to higher void fraction and smaller hydraulic diameter.This and the shorter fuel lead to different total forces of vibration and liftoff. These aspects of the RBWR core design have not been addressed in this NEUP project; they will have to be addressed in followup studies.

Table 1 Comparison of Fuel Rod Parameters

	PWR	ABWR	SFR (oxide) Cr=1.0 – 0.5**	RBWR-Th Y-CISE/LPG	RBWR-Th H-CISE/RELAP
Fuel Rod length, cm	458.32	447.0	422.28	345	162.3
Active Height, cm	426.72	381	137.16	300	114.3
Pellet OR, cm	0.4096	0.441			
Gap Thickness, cm	0.0082	0.0082*			
Clad Thickness, cm	0.0572	0.066			
Rod OR, cm	0.475	0.515	0.434-0.329	0.370	0.503
Rod Pitch, cm	1.26	1.295			
Pitch-to-Diameter	1.326	1.257	1.023-1.224	1.08	1.13

* assumed same as PWR

** from ANL-AFCI-189

1.2 Thermal-Hydraulic Performance

The performance and the details of the fuel-self-sustaining RBWR core designs described in this paper are extremely sensitive to the assumed void fraction and CHF correlations as shown in Table 1. There are unacceptable uncertainties in these correlations due to very limited relevant experimental data on void fraction and critical power for the tight lattices. Validation of these correlations for the conditions in an RBWR will require additional experiments including appropriately scaled test sections and grid spacers. Experiments may be required also for determining the axially dependent void fraction along the bypass channels between fuel assemblies.

1.3 Fuel and Cladding Performance and Qualification

Validation/confirmation of the performance of the fuel and cladding under conditions that are atypical for a water-cooled reactor will require irradiation experiments. Issues include fuel pellet swelling, fission product transport/release, fuel pellet chemical/mechanical interaction, clad performance under high fluence of high-energy neutrons and, in particular, hydrogen pickup and corrosion in the neutron and high void water environment. Extrapolation of current knowledge to the conditions in an RBWR implies that use of Zircaloy-2 may not be feasible. Since the neutron spectra are more like those in a fast reactor (Figure 1) an iron-based clad such as HT-9 may need to be employed at the cost of neutronic penalty and cladding qualification. Executing a roadmap for fuel qualification (with high Pu content for the RBWR, and with ThO2 as a host in the RBWR-Th, as well as a new cladding material) would be expected to take a decade or longer.

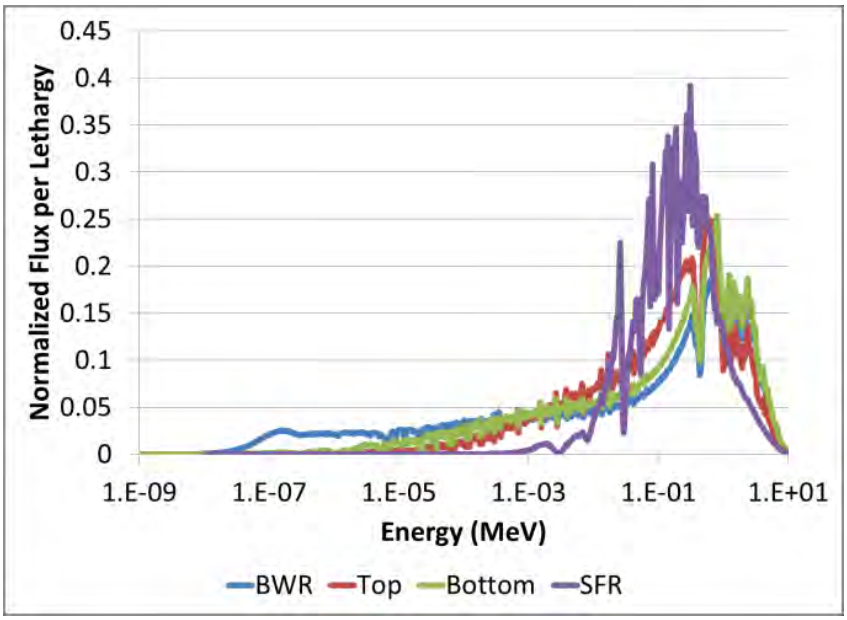

Fig. 1. Spectrum at the top and bottom of the RBWR-Th, along with a typical BWR and SFR for comparison.

1.4 Reactor Physics

The tight-lattice, the use of thorium, the strongly varying water density, the heterogeneous fuel assembly design and intermediate neutron spectrum present challenges for analytic tools, although significant progress has been made as described earlier. The nuclear data for intermediate spectrum tends to be sparse and have greater uncertainties, in particular for thorium and trans-thorium isotopes, than for conventional LWRs or SFRs. Differential and integral experiments (e.g., criticals) may be necessary to improve the quality of data evaluations, benchmark computational tools, confirm design predictions, and reduce uncertainties. There is also a need to demonstrate the stability of the RBWR design by performing more detailed coupled (neutronics/thermal-hydraulics) analysis.

1.5 Out of Core Components

The harder neutron spectrum will increase the heating and radiation induced damage in the in-vessel components and the pressure vessel compared to ABWR. Though, the fluence on the ABWR pressure vessel is orders of magnitude lower than a typical BWRs/PWRs due to large water present between the core barrel and pressure vessel to accommodate for the present of recirculation pumps. Also, the performance of balance-of plant components such as the steam separator need to be confirmed/addressed as the design core outlet steam quality of the RBWR is about three times that of the ABWR. (The total steam flow rate should be the same for similar powered ABWR, but with much less water leaving the core. This means smaller recirculation ratio in the vessel. It also implies that fewer separators may be required and dryers might not be needed.

1.6 Licensing

Licensing of the RBWR variants described earlier (as for any reactor concept) will require validated tools for nuclear, thermal-hydraulic, and mechanical performance of the fuel and core components in steady state and transient/accident conditions. This will generally require both in-core and ex-core experiments to generate the needed data for the computational models, and demonstrate adequate safe performance.

1.7 Reprocessing

Commercial thorium fuel reprocessing and recycling capability will have to be developed. Reprocessing of axially heterogeneous fuel with uranium and thorium involves additional complexities to recycling of the RBWR fuels.

1.8 Economics

Relative to the its sodium-cooled fast reactor counterpart (ARR) the RBWR-Th features less than half the core power density and specific power; ~70% of the discharge burnup; more than twice the Trans-Fertile (TRF) loading and a roughly 70% higher rate of HM reprocessing and TRF discharge per unit of electricity generated. The RBWR-Th discharged plutonium contains significantly less fissile isotopes but discharges a larger amount of americium and curium per unit HM mass as well as per unit of electricity generated. The mass fraction of ^{237}Np discharge by the two cores is comparable.

The RBWR-TR incinerates the same amount of TRU from LWR UNF per unit of electric energy produced as a sodium-cooled Advanced Burner Reactor (ABR) that has a comparable conversion ratio. Relative to the ABR, the RBWR-TR has less than half the discharge burnup, power density, and specific power; requires more TRF loading, HM reprocessing, and TRF discharge per unit electricity generated; can have longer cycles for the same cycle reactivity swing; contains a significantly smaller amount of TRF and fissile plutonium per HM mass discharged; and has a smaller fissile-to-total mass of plutonium.

The comparison of fuel cycle characteristics reported above indicates that the fuel cycle cost of the RBWRs is likely to be higher than that of a similarly performing SFR. However, the capital cost of the ABWRs is presently expected to be lower than that of SFRs and this may compensate for the higher fuel cycle cost of the RBWRs.

A detailed economic analysis is required before the economic viability of the RBWR could be determined.

2. Roadmap

Phase-1: Development of Conceptual Design and Identification of Issues (this NEUP)

Phase-2: Address Key Issues Identified in Phase-1

- Generate experimental data on water-cooled tight lattice(s) to create/confirm correlations for void fraction and critical power
- Differential and integral nuclear experiments may be required:
    - Criticals

    - Improve neutron data for thorium, uranium, and TRU in “intermediate energy” (cross sections, fission product yields, etc.)
- Initiate fabrication and property measurements for fuel(s), clad(s), control rods
- Initial ex-core mechanical testing of fuel assembly/can/control rods
- Irradiate fuel pellets, clad and fuel rod in test reactor with suitably modified spectrum to be prototypic of RBWR conditions
- Bootstrap irradiation program to allow more timely PIE and feedback to design analyses
- Benchmark/validate design tools (nuclear, thermal-hydraulic, fuel performance (nuclear/mechanical)) and quantify uncertainties based on comparisons to measurements
- R&D on reprocessing of Th and TRU-based fuels

Phase-3: Develop Preliminary Design

- Refine conceptual design based on Phase-2 results. Assess key sensitivities affecting performance and cost to identify “optimized design”. Historically, some designs of the RBWR have had positive reactivity coefficients, issues with shutdown margin, etc. which will need to be resolved in this design utilizing the results of the work performed in Phase-2.
- Perform initial transient testing of fuel irradiated in Phase-2
- Initiate interactions with NRC, and identify reactor for full-scale testing of Lead Test Rods and possibly control rods
- Fabricate test articles, irradiate and PIE
- Initiate licensing process for incorporation of new fuel in existing ABWR as a new reload core
- Design, licensing and deployment of scalable prototype reprocessing facility

Phase-3: Design, Licensing and Implementation of First-of-a- Kind RBWR-Th and Reprocessing Facility